Forschungszentrum Jülich

Institut für Festkörperforschung

The Jig-saw Puzzle of Crystal Structures:

Alloys, Superconducting Oxides, Semiconductors, Ionic Conductors, Surface Adsorbates and Magnetic Structures

Jürgen Hauck *Klaus Mika*

Jül-3732

The Jig-saw Puzzle of Crystal Structures:

Alloys, Superconducting Oxides, Semiconductors, Ionic Conductors, Surface Adsorbates and Magnetic Structures

Jürgen Hauck *Klaus Mika*

Berichte des Forschungszentrums Jülich ; 3732
ISSN 0944-2952
Institut fürFestkörperforschung Jül-3732

Zu beziehen durch: Forschungszentrum Jülich GmbH · Zentralbibliothek
D-52425 Jülich · Bundesrepublik Deutschland
☎ 02461/61-6102 · Telefax: 02461/61-6103 · e-mail: zb-publikation@fz-juelich.de

The number of essentially different kinds of constituents in a crystal tends to be small
(Pauling's rule of parsimony, 1929)

Abstract:

The crystal structures of ordered bcc, fcc or primitive cubic alloys A_xB_y and related NaCl, ZnS or CaF_2 derivative structures are characterized by the self-coordination numbers T_1, T_2 of the A atoms with A atoms. Structures with identical T_1, T_2 values for all A atoms are at the corners of T_1, T_2 structure maps and can be analyzed for attractive or repulsive interactions of A atoms. Most observed structures are at the borders of the structure map and can be obtained by different combinations of structural units. The combination mechanisms explain e.g. the shear structures of CuAu II or Nb_2O_5 and the occurrence of vacancies in NaCl related structures like NbO. Many other ordered structures like magnetic ordering, adatoms on metal surfaces, colloids and clusters are analyzed by the same method. The very large numbers of possible structures are reduced to a smaller number of structures at the borders of the structure maps, which are stabilized by enthalpy. The other structures are stabilized by entropy. The T_1, T_2 values of DNA sequences in different areas of the structure map are related with the evolution.

Table of Contents

1 Introduction

Many physical properties like the conductivity of electrons or ions, superconductivity, mechanical strength or thermal properties can be varied in solid solutions. At decreased temperatures the different atoms of the solid solutions are ordered. The variety of materials showing ordering extends from substitutional alloys like $AuCu_3$ to interstitial alloys like Nb_4C_3, $AlFe_3C$ and NbO or semiconducting materials like $CdIn_2Se_4$ or non-metallic compounds like $CaTiO_3$. The Au atoms of $AuCu_3$ which are distributed randomly on all positions of the face-centered cubic (fcc) Cu structure above $\approx 390^0$ C order at decreased temperatures in such a way that the corners of the cube are occupied by Au atoms and the three face centers by Cu atoms. The same ordering is obtained for the NaCl related structure of $Nb_4C_3 \mathrel{\widehat{=}} Nb_4\square C_3$ with Nb on Na positions and an ordering of vacancies $\square$ and C atoms like Au and Cu in $AuCu_3$. A second fcc sublattice containing non-metal atoms is shifted by $a/2$ $a/2$ $a/2$ in $AlFe_3C \mathrel{\widehat{=}} AlFe_3C\square_3$, $NbO \mathrel{\widehat{=}} \square Nb_3\square O_3$, $CaTiO_3 \mathrel{\widehat{=}} CaO_3Ti\square_3$ or $a/4$ $a/4$ $a/4$ in $CdIn_2Se_4 \mathrel{\widehat{=}} \square(CdIn_2)Se_4$.

The ordered phases show different physical properties like superconducting NbO or $Ba(Bi,Pb)O_3$ ($CaTiO_3$ structure), semiconducting $CdIn_2Se_4$ with interesting properties for solar cells or carbides like Nb_4C_3 or $AlFe_3C$ which are used as abrasives or high temperature materials. Many materials with practical relevance are tailored to achieve the desired ordering by the proper substitution.

The ordering of atoms like Au in $AuCu_3$ or Ca in $CaTiO_3$ is related to the interactions between the atoms in the present investigation, to figure out the selection of few structures. The number of observed structures is small compared to the number of all possible structures, which is 2^{n-1} for a unit cell with n possible positions of A and B atoms.

All reduced unit cells of the fcc, bcc (body-centered cubic), pc (primitive cubic) and other lattices with $n \leq 9$ atom positions were determined and the different structures selected numerically in the present investigation. The theoretical structures can be sorted for different aspects like high

symmetry, single coordination numbers or the extent to which Pauling's rules are obeyed (Pauling, 1929). Pauling's rule of parsimony is particularly useful for the selection: "The number of essentially different kinds of constituents in a crystal tends to be small. The polyhedra circumscribed about all chemically identical atoms should, if possible, be chemically similar, and similar in the nature of the sharing of corners, edges and faces with other polyhedra". This explanation is similar to the Wiener-Sohncke principle: "Points are disposed around each point in the same way as around every other" (Wiener, 1863; Sohncke, 1879; Brunner, 1971). We have selected the self-coordination numbers T_i of A atoms with A atoms as parameters. In the fcc lattice each Cu atom with diameter d for example has $T_1 = 12$, $T_2 = 6$ and $T_3 = 24$ nearest, next-nearest and third neighbors at distances $R = d$, $\sqrt{2}d$ and $\sqrt{3}d$. The T_i values are reduced in ordered alloys like $AuCu_3$ to $T_1 = 0$, $T_2 = 6$, $T_3 = 0$ for Au atoms. This structure is characterized by the T_i values of the minority component and the ratio $r = y/x \geq 1$ of A_xB_y, e.g. 0 6 0 ; 3 for $AuCu_3$. The structures of Nb_4C_3, $AlFe_3C$, NbO, $CaTiO_3$ and $CdIn_2Se_4$ are characterized by the same self-coordination numbers of the minority component and the translation of both fcc lattices $a/2$ $a/2$ $a/2$ or $a/4$ $a/4$ $a/4$.

The T_i values can be plotted in two-dimensional T_1, T_2 structure maps. All possible structures are in a range which is limited by straight lines. Most observed structures like 0 6 0 ; 3 for $AuCu_3$ are at a corner at the end of a straight line. Some other structures like $ZrAl_3$ with the self-coordination numbers 0 5 4 ; 3 of Zr atoms (Section 6) are on the line $T_1 = 0$. This structure, which was determined by Brauer (1939), can be assembled from structural elements of the $AuCu_3$ structure (0 6 0 ; 3) and the $TiAl_3$ structure (0 4 8 ; 3) at the corners of the structure map in a similar way as the architecture of Ruddlesden-Popper phases from $CaTiO_3$ and NaCl structural elements (Section 18). The structures at the borders of the structure map were projected in different directions to determine the structural units, which are assembled similar to a jig-saw puzzle. Some structural elements are shown in the compilations of Schubert (1964), Sato and Toth (1965), Ogawa (1974), Pearson (1967/1972), Wells (1984), Hyde and Andersson (1989) and Parthé et al. (1993). All structures on a border of the structure map with different numbers of

structural units form a family of structures, which is named by the authors of the first observed structure like the Ruddlesden-Popper phases. About 5 – 30 structural units were determined for the ordered structures of the different lattices like fcc, bcc, pc, etc., which is a small number compared to the several million possible structures. The interactions between A can be related with the T_i values and vary gradually along a line of the structure map as the number of structural units is varied. The Au atoms of $AuCu_3$ for example are as far apart as possible for an AB_3 alloy with A and B atoms on an fcc lattice indicating repulsive interactions. Structures containing chains or planes of A atoms with attractive interactions are obtained at $T_1 \neq 0$ and minimum T_2 values. Some of these structures were also obtained using different Ising methods like Monte Carlo simulations by assuming different interactions between A and B atoms (Section 11) or by the investigation of homogeneous sphere packing (Section 25).

The combination of structural units similar to a jig-saw puzzle can be useful for the search of new compounds with different physical properties and supports the analysis of these compounds by electron diffraction for example. Only few structural units fit the frame of the jig-saw puzzle, which can be determined by electron diffraction.

The interactions between atoms are related to different atomic radii, electronegativity and number of electrons in a very complex manner (Schubert, 1964/1967; Sato and Toth, 1965; Ogawa, 1974; Villars and Hulliger, 1987; Villars et al., 1989; Carlsson and Meschter, 1994; Ellner and Predel, 1994; Villars, 1994; Pettifor, 1994). These parameters or relative ordering numbers (Section 32) give rise to another type of structure map with sections, where the $AuCu_3$ or $CaTiO_3$ structures for example can be obtained.

2 Analysis of stacking sequences by the one-dimensional Ising model

The use of self-coordination numbers T_i and of T_1, T_2 structure maps can be demonstrated for a linear chain of M and N atoms or sequences of bases adenine, cytosine, guanine and thymine in DNA (Section 26). Close-packed layers with a sequence of M and N layers can be analyzed by the one-dimensional Ising model (Section 15). The different stacking of close-packed layers, c or h gives rise for a linear chain of stacking symbols for a single element M as will be outlined in this section.

In pure metals, the bonding tendencies of the individual atoms should be identical. The same environment can be expected for each metal atom as e.g. strong directional covalent bonds as in gray α-Sn with the diamond structure or a close-packing of spherical metal atoms as in Mg or Cu. Metal atoms with weak bonding behave like tennis balls packed in a basket. The packing consists of coplanar hexagonal layers (Fig.1). Succesive layers are stacked with centers of spheres at A, B or C positions. The different stacking sequences of hexagonal layers can be characterized by the sequence of positions. The periodic sequences AB of two layers and ABC of three layers are called hexagonal close-packed (hcp or h) and cubic close-packed (ccp or c), because of the hexagonal and cubic symmetry, respectively. The hcp and ccp metal structures are usually distinguished by the prototype elements Mg and Cu, the space group and Pearson symbols (Table 1). Most metals (except Eu, U and Np) can be obtained in a close-packed modification (Villars and Calvert, 1986). A few metals crystallize in more complex close-packed structures with a maximum of nine layers (Table 1). These structures can be described unambiguously by the stacking symbols h and c introduced by Pauling and Jagodzinski (Pearson, 1972; Mardix, 1990). This notation describes a layer as h or c type according to whether the layers on each side of it are of the same type, such as for B in ABA, or of different types as for B in ABC (Fig.1). The two-layer hcp sequence AB gets the symbol hh or h, the three-layer ccp sequence ABC the symbol ccc or c. The lanthanides La to Sm, Gd and the actinides Am to Cf crystallize in the ABAC or chch = $(ch)_2$ stacking. Sm, Gd and the heavier lan-

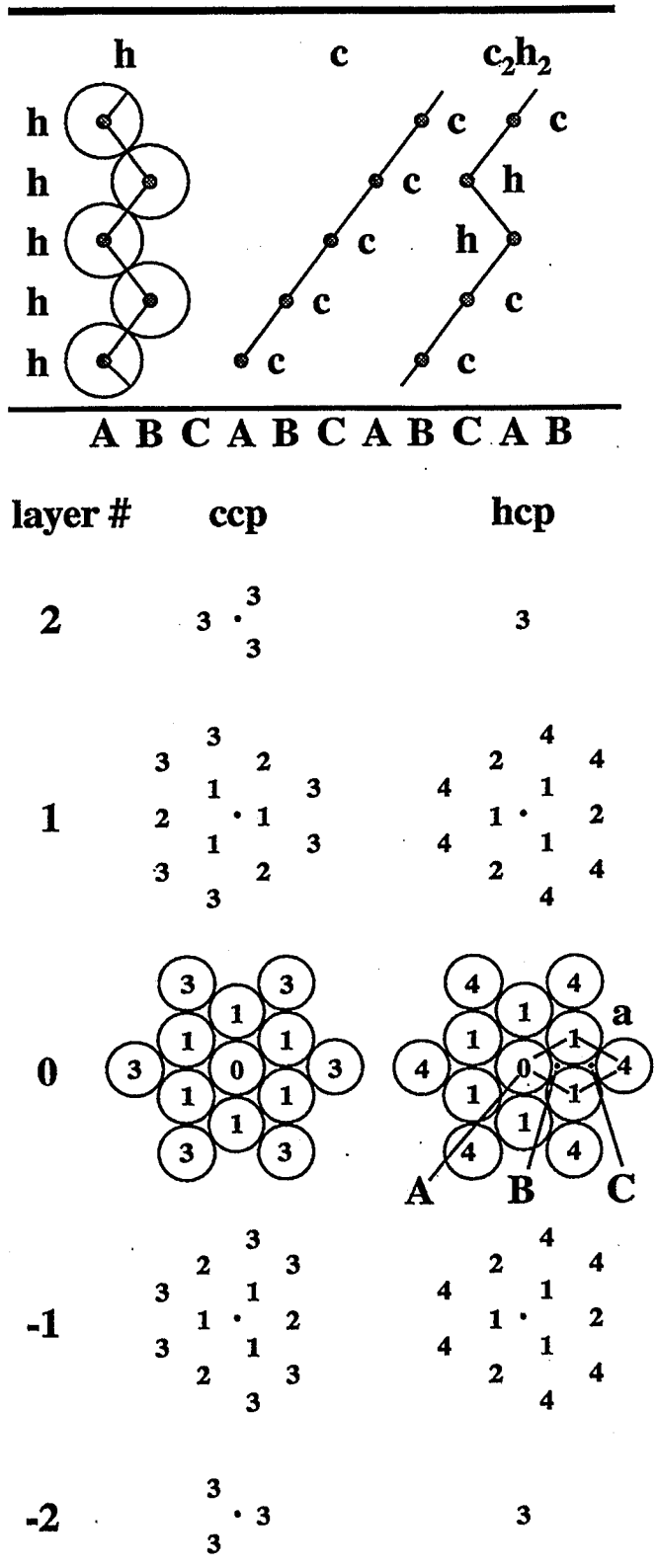

Figure 1: [110] projection (above) of the layer sequence in h, c_2h_2 or c stacking and [001] projection of the different layers with the 12 nearest (1), 6 next-nearest (2) and 24 or 2 third neighbors (3) in ccp or hcp alloys and unit cell with lattice constant a. The metal atoms are at different positions A, B, C in layer # –2, –1, 0, 1, 2, respectively.

thanides Tb to Ho, Tm, Lu can crystallize also in the ABABCBCAC or chhchhchh = $(chh)_3$ stacking. A comparison of the stacking symbols and population data in Table 1 shows the preference of simple sequences hh, ccc, $(ch)_2$, $(hcc)_2$ or $(chh)_3$. Some more complex sequences are found in alloys M_xN_y (Table 1), which are discussed in Section 7.

The stacking sequence can be analyzed by the one-dimensional Ising model. The sequences of layers h and c can be compared with a one-dimensional chain of atoms with $\oplus$ or $\ominus$ spin (Ising, 1925) or M and N atoms (Ducastelle, 1991). The large variety of chains is characterized by the self-coordination numbers (s-CN) of M atoms (or h layers) to construct a structure map (Fig.2).

Each h layer of the sequence chchch e.g. has no nearest h layers ($T_1 = 0$), two next-nearest h layers ($T_2 = 2$) and no third-nearest neighbors of h layers ($T_3 = 0$). The sequence of layers is characterized by the three s-CN values $T_1 = 0$, $T_2 = 2$, $T_3 = 0$ and the total composition y/x = 1 of c and h layers c_xh_y. The notation 0 2 0 ; 1 for the sequence chchch is identical for c and h layers at y/x = 1 and deviates for $y/x \neq 1$ as e.g. 0 0 2 ; 2 for h or 1 1 2 ; 0.5 for c in the hc_2 stacking sequence. The T_i(M) values of the minority component and T_i(N) of the majority component give identical Cowley short-range order parameters α_i (Ducastelle, 1991; Hauck et al., 1988a).

Structure maps with T_i(M) or α_i values as parameters can be obtained by the following procedure:

(1) The coordination numbers of each shell are averaged for structures which have different T_i values. For example the three c in the c_3h_6 chain (ccchhhhhh,c) 1 1 0, 2 0 0 and 1 1 0 are averaged to 1.3 0.7 0 ; 2.

(2) The crystal structures characterized by the coordination numbers T_1, T_2, T_3 and a fixed composition y/x can be plotted as single points in a T_1, T_2, T_3 coordinate system or as projection in the T_1, T_2 plane as outlined for T_1 T_2 T_3 ; 1 structures in Fig.2. All structures with y/x = 1 are found to fall within a triangle, with the three structures 0 2 0 ; 1 (for ch), 1 0 2 ; 1 (for h_2c_2) and 2 2 2 ; (1) ($h_\infty c_\infty$

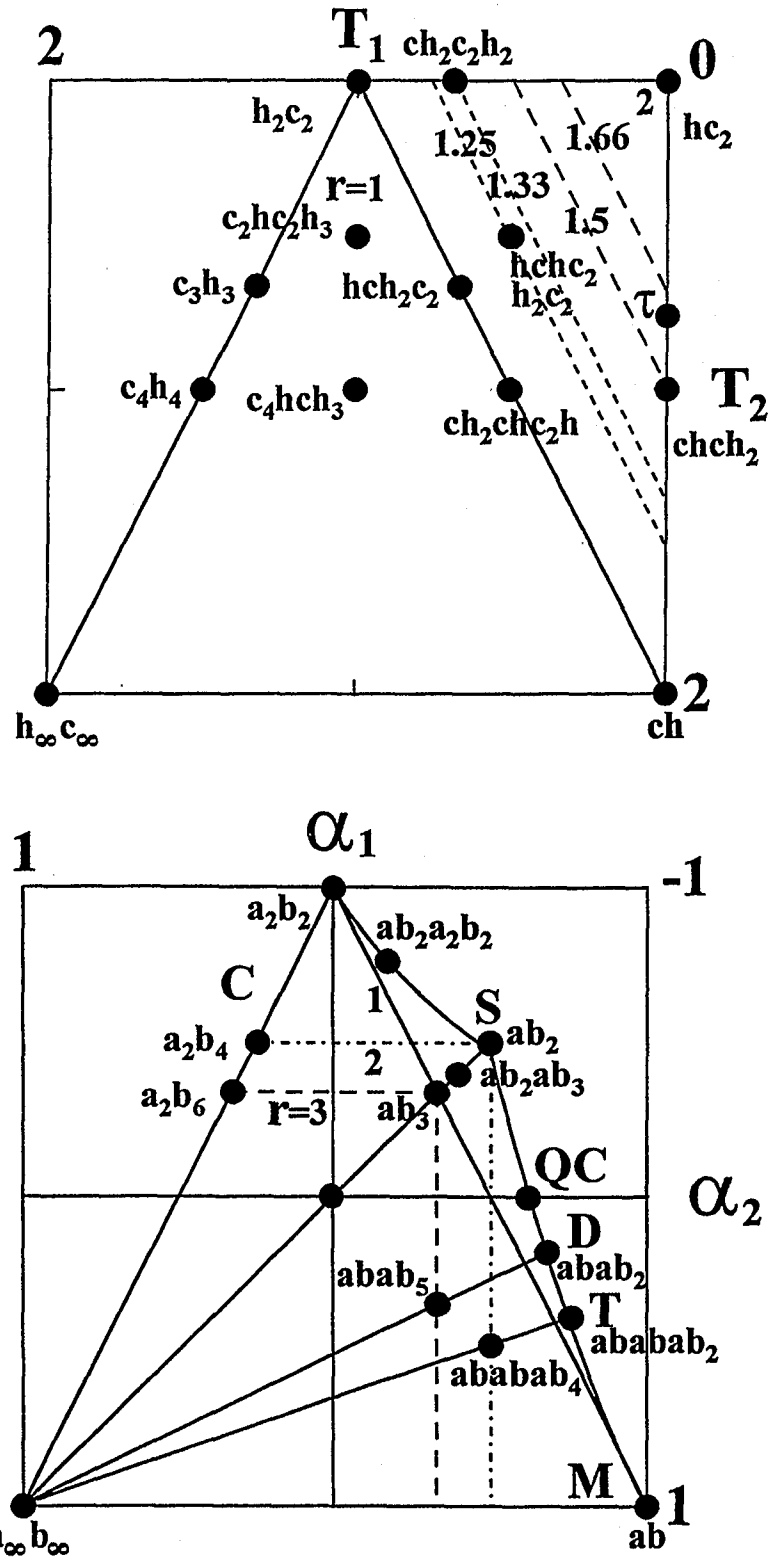

Figure 2: Structure map of a linear chain of c and h or a and b with the self-coordination numbers T_1, T_2 of nearest and next-nearest neighbors (a), or the short-range order parameters α_1, α_2 as axes. Single (S), double (D), triple (T), multi-alternating units (M) or clusters (C) are at straight lines, a quasicrystal at point QC (b).

for segregation of h and c layers) at the corners. The structure 2 2 2 ; (1) with the composition given by (1) in brackets is used to indicate that the structure can only be obtained in the limit of very large stacks and a negligible border between h and c layers.

(3) The sequences at the left-hand border of the structure map as e.g. c_3h_3 or c_4h_4 contain increasing segments h_n and c_n, which are segregated at the lower left-hand corner for $n \rightarrow \infty$. The sequences at the right-hand border of the structure map at y/x = 1 as e.g. hch_2c_2 are a combination of h_2c_2 and hc (= ch) at the upper and lower corners of the border, respectively. The structural units h_2 and c_2 can be combined with h_3 and c_3 at the left hand border and with hc_x or ch_x at the right hand border of the structure map (Table 1). The number of theoretical combinations 2^{n-2}, which is 64 for $n = 8$ for example, is reduced to 16 combinations (13 at the four borders and 3 interior points). The structures at the four borders with the relation between T_1, T_2 and r = y/x values $T_2 = 2T_1 - 2$, $T_2 = 0$, $T_2 = -2T_1 + 2(2 - r)$ and $T_1 = 0$ (Section 22) correspond to four different structure families with a combination of different structural units.

(4) Structures $T_1\ T_2\ T_3$; y/x with different y/x values can be included in the same structure map (Fig.2b) by using Cowley's short-range order parameter α_i (Eqs. (1) and (2) below), which can vary within $-1 \leq \alpha_i \leq 1$. The α_i values can be obtained from the coordination numbers T_i(M) and T_i(N) of M and N atoms or from the T_i(M) and r = y/x values (Hauck et al., 1988a):

$$\alpha_i = 1 - p_i(\mathrm{N})\,\mathrm{y}', \tag{1}$$

$$\mathrm{y}' = \mathrm{y}/(\mathrm{x}+\mathrm{y}), \tag{2}$$

$$T_i(\mathrm{N}) = T_i^{\max} - (T_i^{\max} - T_i(\mathrm{M}))\,\mathrm{x/y}, \tag{3}$$

$$\alpha_i T_i^{\max} = T_i(\mathrm{M}) + T_i(\mathrm{N}) - T_i^{\max}, \tag{4}$$

$$\alpha_i T_i^{\max} = T_i(\mathrm{M}) - (T_i^{\max} - T_i(\mathrm{M}))\,\mathrm{x/y}, \tag{5}$$

$$T_i^{\max} = T_i(\mathrm{M}) + T_i(\mathrm{M,N}). \tag{6}$$

p_i(N) is the probability of finding an N atom in the i-th coordination shell of an M atom. y′ is the fraction of N atoms in M_xN_y. $T_1^{\max} = T_2^{\max} = T_3^{\max} = 2$ are the maximum s-CN values of the linear

chain. T_i(M,N) is the coordination number CN of M atoms with N atoms. The self-coordination numbers T_i(M) and T_i(N) of h and c layers are identical at composition r = 1 but different at other compositions. The area mapped out by the maximum range of α_1, α_2 values is different at different compositions, as outlined for r = 2 and 3 in Fig.2b.

(5) The α_i values are zero for a random distribution of h and c layers, because the mean value of T_i(M) + T_i(N) equals T_i^{max}, which corresponds e.g. to $T_1 = T_2 = T_3 = 2/(r + 1)$ (Fig.2b). Very small α_i values are expected for alloys with very weak interactions and in particular at high temperatures. Positive α_1 values are obtained for attractive interactions of M atoms, i.e. for cluster formation or segregation. The 1 0 2;1 (h_2c_2) structure of Fig.2a consists of double h and c layers. The size of h and c layers is increased e.g. in c_3h_3 or c_4h_4 to complete segregation $h_\infty c_\infty$ of h and c layers in the 2 2 2;(1) structure. Negative α_1 values indicate repulsive interactions between layers, e.g. Coulomb repulsion for alternating layers ch (0 2 0;1) at 50% h (Section 11).

(6) Homometric structures (Patterson, 1944) or homologous structures (Hauck and Mika, 1994) have the same α_i values (Sections 8,9).

(7) The different structural units of one border of the structure map can also be combined randomly or aperiodically. The T_i(h) values 0 0.76 1.24;τ are obtained, for example, if the structural units hc and hc_2 in the ratio $hc_2/hc = \tau \approx 1.62$ vary aperiodically in a Fibonacci sequence (Table 1) (Section 13). The α_i values of the one-dimensional quasicrystal (QC) are on the boundary of the structure map with $\alpha_2 = 0$ (Fig.2b).

Atoms of close-packed structures with diameter $d = 1$ have $T_1 = 6$ nearest neighbors in the same layer at distance $d = a$ (Fig.1) and $T_1 = 6$ neighbors in the two adjacent layers (three in each). The number $T_2 = 6$ of second-nearest neighbors at distance $\sqrt{2}d$ is also identical for all close-packed structures. The atoms of the hh (hcp) structure, however, have $T_3 = 2$ third-nearest neighbors at distance $\sqrt{8/3}d$ (in the next-nearest layers) and 18 fourth-nearest neighbors at distance $\sqrt{3}d$, while atoms of

ccc (ccp) packing have 24 third-nearest neighbors at distance $\sqrt{3}d$ (Fig.1, Table 2). The coordination polyhedra of T_1, T_2 and T_3 neighbors of the hcp structure correspond to CN 12′, CN 6 (octahedron) and CN 2, and the coordination polyhedra of the ccp lattice to CN 12 (cuboctahedron), CN 6 and CN 24″, as shown by Villars (1994). The metal atoms of the sequences ch_n (n = 1, 2, 3, 6), hc_2, h_2c_n (n = 2, 3) and ch_2ch_3 (Table 1) have $M^i = 2$ different values of T_3, T_4 and higher coordination shells. The more complex structures contain three or more metal atoms with different environments. The averaged T_3 and T_4 coordination values of these structures depend on the fraction f of h layers as given by $T_3 = 2f$ and $T_4 = 24 - 6f$.

The hh hexagonal close-packed and the ccc cubic close-packed structures are the only structure types with a single environment for close and distant neighbors of all atoms (M^i=1). These structures have been observed in 673 binary and ternary systems (Villars and Hulliger, 1987). The sequences of layers with two different environments of metal atoms (M^i=2) (Pauling, 1945/1960) (Table 1) have been found in 66 systems. The metal atoms of the other sequences of layers contain three or more different environments. The tendency to small numbers M^i of metal atoms with different environment can be described by Pauling's rule of parsimony: The number of essentially different kinds of constituents in a crystal tends to be small (Pauling, 1929).

The number M^i of metal atoms with different sets of T_i values is often identical to the number of Wyckoff positions, the number of symmetrically different atom positions. For example, the numbers of Wyckoff positions of the Mg, Cu, Sm and Nd structures are identical to M^i, but are larger than M^i as e.g. 5 for the n = 8b, 9b (M^i = 3) structures (Table 1).

The different stacking sequences with n layers in A, B or C positions can be described by hexagonal unit cells with the lattice parameters $a = b = d$ (diameter of atoms) and $c = n\sqrt{2/3}d$ (Fig.1). The smallest unit cell of ccc packing containing only one metal atom is rhombohedral with lattice constants $a = d$ and $\alpha = 60^0$. Usually, the ccc structure is

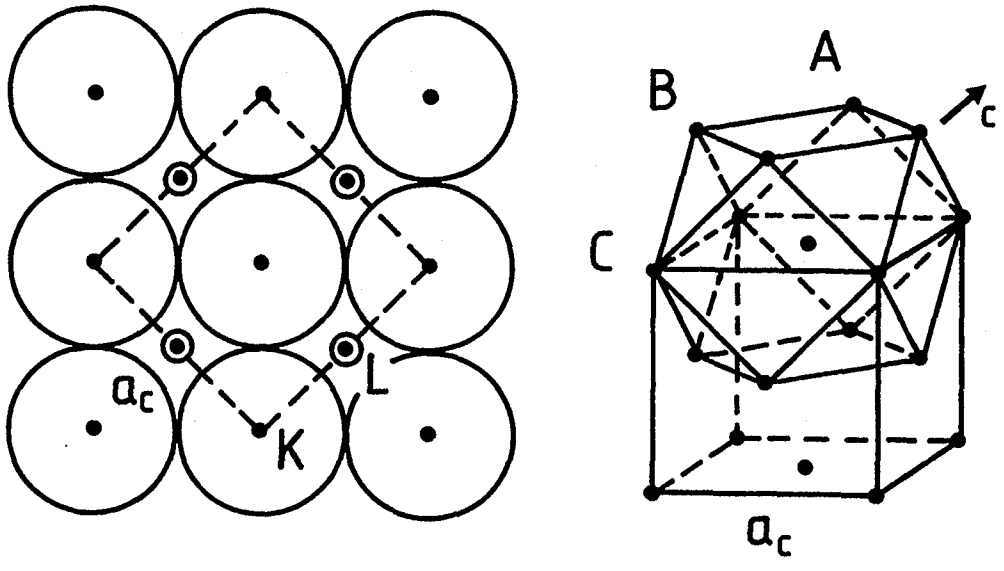

Figure 3: Packing of square layers at K and L positions in face-centered cubic metal structure and relation to ccp stacking of hexagonal layers in ABC position.

described as face-centered cubic lattice containing four metal atoms with lattice constant $a_c = \sqrt{2}d$ (Fig.3). The fcc lattice can also be considered as a stacking of square layers in the K and L positions. The c axis of the rhombohedral cell corresponds to one of the four space diagonals of the cubic cell. The only periodic three-dimensional packing of spheres having close-packed hexagonal layers in four inclined directions is ccc. All other sequences are maintained in one direction only.

A comparison of the close-packed structures shows that the interactions between metal atoms, e.g. in the ccc Cu structure, must be strong enough to stabilize the atoms of the neighboring layers at the proper position. The M atoms of the $hchc_4$ structure must be stabilized in the eighth layer.

A participation of f orbitals is suggested for bonding in lanthanides or actinides with ch, ch_2 or hc_2 stacking sequences and $M_i = 2$ different sets of s-CN values for atoms M and M′ at h or c layers.

An interaction between metal atoms with directional bonding can also be deduced from the distortion of some crystal structures. The ratio c/a

of the lattice constants of the hh hexagonal close-packed structures of Ca and Sr is almost ideal with $c/a = n\sqrt{2/3} \approx 1.63$ for $n = 2$ layers (Sections 15,23). The c/a ratio is slightly decreased to 1.56 for most hcp metals and increased to $c/a = 1.86$ and 1.89 for Zn and Cd, respectively (Pauling, 1945/1960; Laves, 1967; Wyckoff, 1982). The distance between close-packed layers $\sqrt{2/3} \approx 0.8$ is also decreased in cubic close-packed Hg, Po and Te with the rhombohedral angle $\alpha = 71^0 - 103^0$ instead of $\alpha = 60^0$ (Villars and Calvert, 1986).

3 Alloy formation

All metal atoms for $n = 2$ and 3 (hcp and ccp structures) have the same environment ($M^i = 1$) (Table 1). The $n = 4$, 5, 6b, 8a and 9a layer stackings of Table 1 contain $M^i = 2$ metal atoms with different T_i values, the other structures 3, 4 or 5 different sets of T_i values (Table 1). Therefore the structures of the rare earth elements α-Nd ($n = 4$ layers), Tb HP ($n = 6$b) and α-Sm ($n = 9$a) with two different T_i can be formulated as pseudobinary alloys $NdNd'$ ($n = 4$, 8a), $TbTb'_2$ or $SmSm'_2$ ($n = 6$b, 9a) and MN_4 ($n = 5$). Other stacking sequences are pseudoternary e.g. $M^1M^2_2N_3$ ($n = 6$a), $M^1M^2_2N_4$ (7), $M^1M^2_2N_5$ (8b), $M^1M^2N_2$ (8c, 8e, 8f), $M^1M^2_4N_4$ (9b), and $M^1_2M^2_3N_4$ (9c). The population of the different structure types decreases with increasing M^i. Ordered binary and ternary alloys have not been observed with these structures. The MN, MN_2, MN_4 binary alloys e.g. favor other close-packed structures (Section 7).

The M and N atoms of most close-packed M_xN_y alloys are ordered in different hexagonal or square layers with the composition M_xN_y. These structures can be characterized by the type of the hexagonal or square layer and the stacking of these layers as will be outlined in Sections 4 – 7. The separation of M and N atoms in different layers indicates repulsive interactions. Few structures of M_xN_y alloys are composed of two layers with different composition like layers with composition $M_xN_{y'}$ and layers with y'' N atoms ($y = y' + y''$). This indicates repulsive interactions only for M atoms. The attractive interactions between M and N atoms are

increased in M_xN_y compounds with x layers of M atoms and y layers of N atoms (Section 15). The distance between the layers of close-packed metals $\sqrt{2/3} \approx 0.8$ is decreased to ≈ 0.4 in the primitive cubic (pc) lattice of Po and to ≈ 0.2 in the body-centered cubic (bcc) lattice of W as will be outlined in Section 15.

Some ccp alloys can be characterized by sequences of square layers instead of hexagonal layers (Fig.3). The distance between two identical square layers of ccc packing, which is $a_c = \sqrt{2}d$ for cubic Cu, can be increased up to $1.66d$ in In, Ga, La or Ce or decreased to $1.0d$ in Po or $1.15d$ in W. Tungsten has a body-centered cubic structure. The 74% density of the close-packed structures however is reduced by hexagonal or tetragonal distortions, e.g. to 68% for the body-centered cubic structure (Laves, 1967; Pearson, 1972). These strongly distorted structures are considered as different structure types in some compilations (Ho and Douglas, 1968). This is one reason that the population numbers of different structure types are only rough values for comparison. We have taken the maximum values from the compilations of Wyckoff (1982), Pearson (1972) or Villars and Calvert (1986) of experimentally determined crystal structures. The undistorted structures are compared in the present article for the analysis of the self-coordination numbers T_i.

The atoms M and N e.g. of a binary alloy M_xN_y have different sizes and a different tendency to exchange electrons, which gives rise to different bonding. The electron density and the radii of the M and N atoms can be varied by charge transfer between the M and N atoms. Both parameters do not vary independently for most metals (Fig.4). The electronegativity values of the elements can be related to the electron work function and indicate the tendency of a metal to exchange electrons (Pauling, 1945/1960; de Boer et al., 1988; Sutton, 1993). The electronegativity increases with increasing number of electrons to a maximum for the 8b – 10b transition elements. Those elements with an almost filled d shell try to accept electrons to complete the d shell with 10 electrons, while elements with few outer electrons like the 1a and 2a alkali and alkaline earth or the 1b and 2b transition metals with lower electronegativity are ready to donate these electrons. The 1a and 2a metals are then stabilized in the spherical s^2p^6 shell of the noble gases, the 1b and 2b

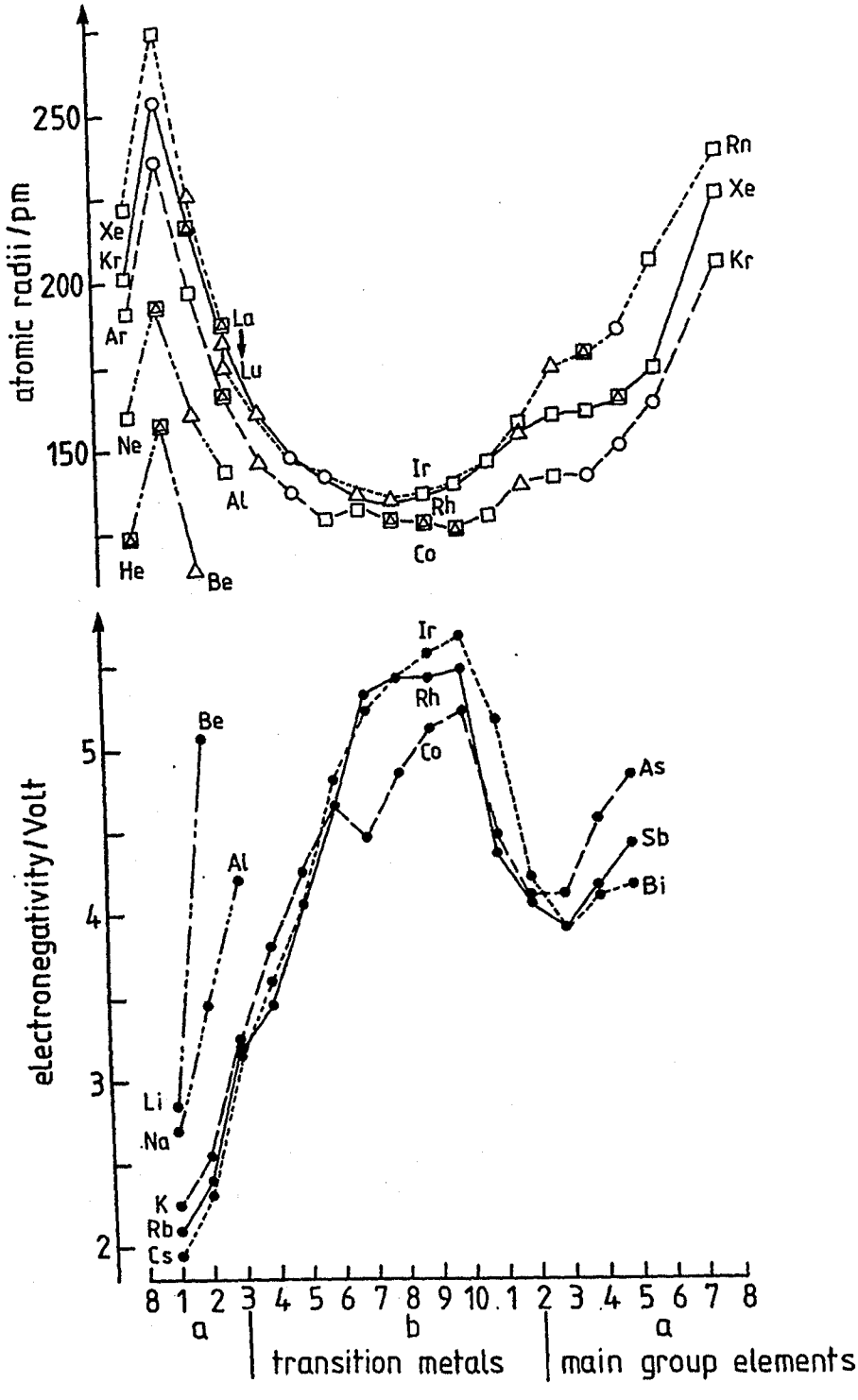

Figure 4: Electronegativity ϕ^* (de Boer et al., 1988) and radii (Schubert, 1967) of 1a – 8a main group and 1b – 10b transition metals with cubic (□) or hexagonal (△) close-packed crystal structures. Some metals (○) are not observed in a close-packed modification.

transition metals in the d^{10} shell with decreased radii. The electronegativity increases again for the 4a – 7a elements because of the tendency to attain the stable s^2p^6 octet of the noble gases. The radii of metal atoms decrease with increasing number of electrons to a minimum for the stable d^{10} electron configuration (Schubert, 1967). Also the radii of the lanthanides La to Lu are decreased slightly as indicated by the arrow in Fig.4 for the same effect of the filling of the inner $4f$ electron shell. The relation between radii and electronegativity indicates the tendency to form spherical metal atoms in alloys.

The interactions between the M metal atoms in M_xN_y alloys can be attractive, as e.g. with segregation, or repulsive. Both interactions can be distinguished by an analysis of the self-coordination numbers T_i of M atoms with M atoms. Analysis of the different ways of sphere packing showed the same number $T_1 = 12$ and $T_2 = 6$ of nearest and next-nearest M atoms. These numbers are reduced on the formation of ordered M_xN_y alloys and can be used to obtain structure maps (Hauck et al., 1988a/1989; Mika and Hauck, 1990).

The derivation of structure maps will be outlined for the simple examples of the square and hexagonal nets of single metal atom layers. The single square or hexagonal two-dimensional layers of M atoms (Figs. 1,3) are the basic units for describing the three-dimensional close-packed metal structures (Beattie, 1967; Lima-de-Faria and Figueiredo, 1969; Beck, 1969).

4 Ordering of atoms in hexagonal and square layers

The hexagonal layer (in h or c position) is the structural unit of the close-packed metals or alloys (see previous section). The M and N atoms of alloys with composition M_xN_y are usually not at different h and c layers but at different positions within the hexagonal layers (Beattie, 1967; Lima-de-Faria and Figueiredo, 1969; Beck, 1969; Parthé et al., 1993).

The self-coordination numbers (s-CN) of nearest, next-nearest and third M atoms within a hexagonal layer were analyzed in a similar procedure as was outlined for the sequence of h and c layers in Section 2. Each metal atom of a hexagonal layer has $T_1^{max} = 6$ nearest, $T_2^{max} = 6$ next-nearest and $T_3^{max} = 6$ third neighbors at distances d, $\sqrt{3}d$ and $2d$, respectively (Table 2). The maximum s-CN values are reduced, if the positions are occupied by different atoms M and N in alloys M_xN_y. The different structures are characterized by the s-CN values T_1, T_2, T_3 of the minority component M and the composition $y/x \geq 1$. Different structures are obtained by variation of the unit cell, the occupation of different positions by M atoms to a maximum of 50% and the determination of the s-CN values of the different M atoms to obtain the averaged values $T_1\ T_2\ T_3\,;y/x$ for the characterization of the structure. The corresponding α_1, α_2 values can be obtained from the T_1, T_2 values by $6\alpha_i = T_i - (6 - T_i)x/y$, as was outlined in Section 2.4. The T_1, T_2 or α_1, α_2 values of the different structures are plotted in the structure maps. The α_1, α_2 structure map (Fig.5b) contains six structures with a single environment at the corners of an irregular pentagon with curved borderlines: 6 6 6;(1), 4 2 2;1, 2 0 2;2, 2 2 6;1, 0 0 6;3, and 0 6 0;2. The 2 2 6;1 and 0 0 6;3 structures are homologous with identical α_i values (Section 9). The T_1, T_2 structure map (Fig.5a) shows the different borders at varied y/x values. The crystal structures existing along the different borderlines can be obtained by a combination of triangles with three and two M or N atoms at the left-hand border (structural units a – c) and triangles with one and two M or N atoms at the right-hand border (structural units e – k) (Fig.6). The 0 6 0;2 structure (structural unit e) for example contains triangles with one M atom and two N atoms at composition MN_2. The dashed areas of the pentagon with the limiting structures 2 0 2;2 and 0 6 0;2 exceed the area at composition $y/x = 1$, because of the impossibility of 3 0 T_3;1 or 0 6 T_3;1 structures at the corners of a structure map as in Fig.2. The hexagonal layers of close-packed structures are those of Fig.6 like 2 2 6;1 (c_2), 0 6 0;2 (e), 0 0 6;3 (k), 0 2 2;3 (f′) and 0 1 4;3 (f′k) (Sections 5–7). The structures at the right-hand border of the map are also common for the ordering of surface atoms or gas atoms at [111] surfaces of ccp metals and are usually characterized by the dimension of the unit cell like (1×1) for the 6 6 6;(1) structure, (2×2) (0 0 6;3) or $(\sqrt{3} \times \sqrt{3})$ (0 6 0;2) (Fig.5)

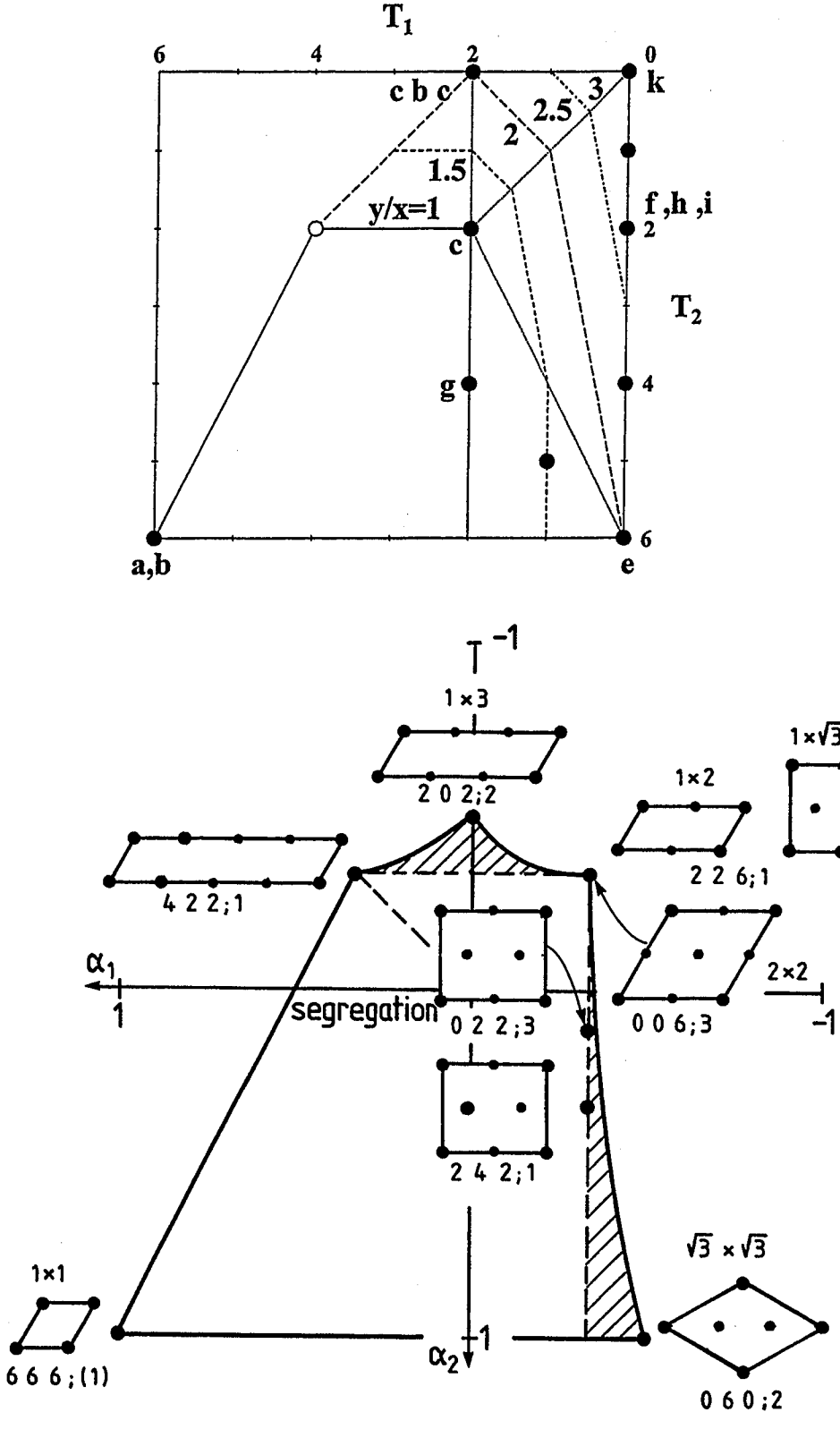

Figure 5: T_1, T_2 (a) and α_1, α_2 (b) structure map of the hexagonal net with different borders for y/x = 1, 1.5, ..., 3. The structures of Fig.6 with structural units a – i and the surface structures $l_1 \times l_2$ are at the borderline (•).

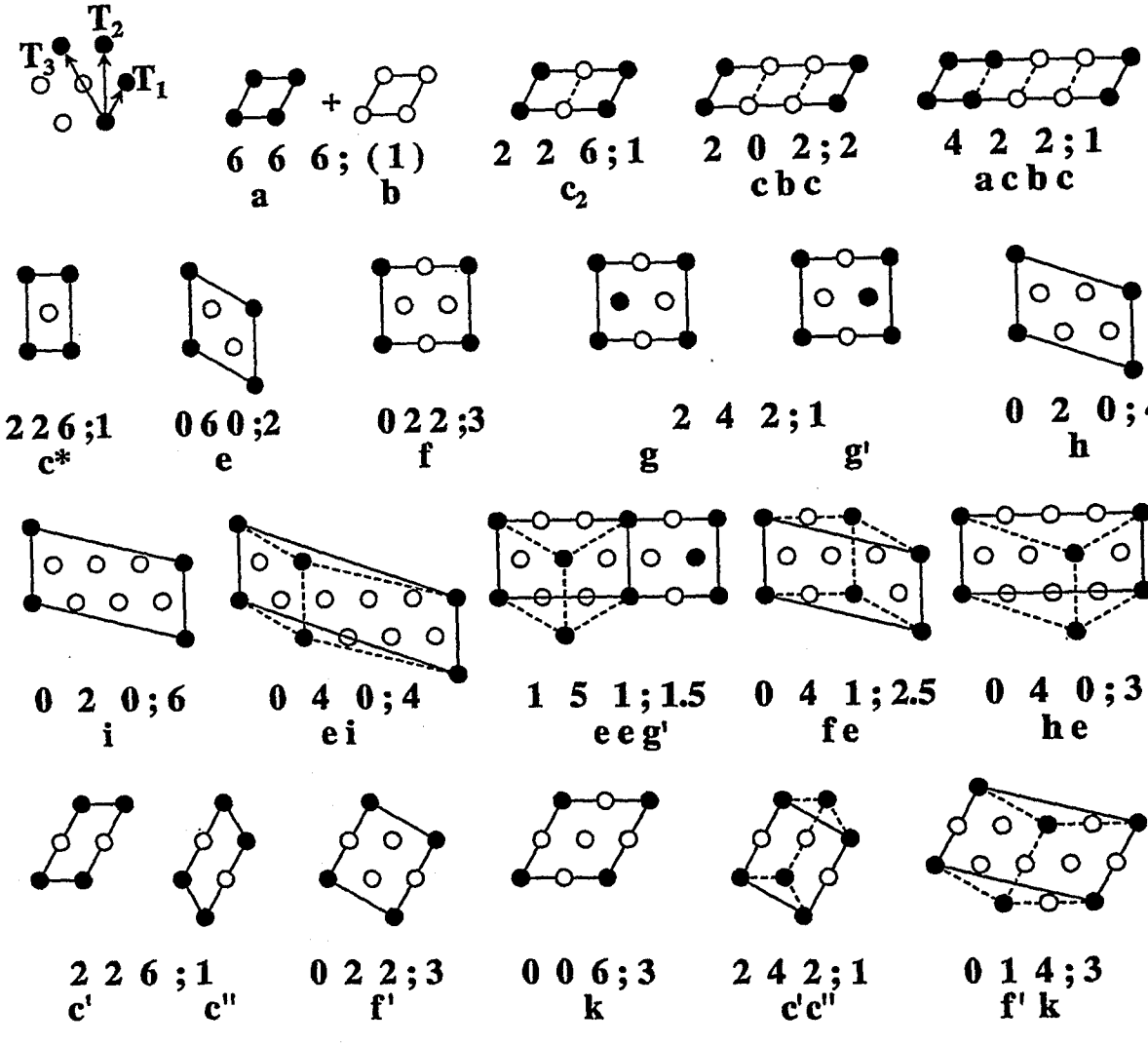

Figure 6: Self-coordination numbers $T_1\ T_2\ T_3$; y/x for the hexagonal net of A atoms in A_xB_y compounds (A = •, B = ○). A atoms with concentration y/x $\geq$ 1 are the minority component. The different structural units a, b, c, etc. are shown by dashed lines.

(Watson et al., 1994).

The metal atoms of the square net have $T_1^{max} = 4$ nearest, $T_2^{max} = 4$ next-nearest and $T_3^{max} = 4$ third neighbors at distances d, $\sqrt{2}d$ and $2d$, respectively (Table 2). The structure map (Fig.7) is similar to the structure map of the chain (Fig.2) with the three structures T_1^{max} T_2^{max} T_3^{max}; (1) (segregation), $T_1^{max}/2$ 0 T_3^{max}; 1 or $T_1^{max}/2$ 0 $T_3^{max}/2$; 1 (attraction) and 0 T_2^{max} T_3^{max}; 1 or 0 T_2^{max} 0; 1 (repulsion) at the corners of the triangle. The T_i values of the three structures at the corners (2 2 2; (1), 1 0 2; 1 and 0 2 0; 1 for the chain and 4 4 4; (1), 2 0 4; 1 and 0 4 4; 1 for the square net) show different relations to the T_i^{max} values. The 0 0 T_3^{max} structure is obtained for y/x = 3 (instead of y/x = 2 for the chain). The M atoms of the square net form chains with $T_1 = 2$ nearest M atoms in the 2 0 4; 1 structure containing two squares c_2 or c* with M atoms in neighboring *cis* positions. The diagonal *trans* positions (t_2 or t_2^*) are occupied in the 0 4 4; 1 structure and a single position (s_4 or s_2^*) in the 0 0 4; 3 structure. The structures at the left- and right-hand borders are combinations of structural units a – c and b, c, s, t (or b*, c*, s*, t*), respectively (Fig.8).

5 Hexagonal close-packed structures

The Mg atom positions of the hexagonal close-packed Mg structure (Table 1) can be substituted by different M and N atoms in M_xN_y alloys. The structures of all possible alloys can be obtained, if the unit cell of the Mg structure is increased in a systematic way (Section 33) (Hauck and Mika, 1999), the metal positions occupied by M atoms to a maximum of 50% and the s-CN values T_1, T_2, T_3 of all M atoms averaged, to characterize the structure by T_1 T_2 T_3; y/x. The s-CN values of the N atoms are different at y/x > 1. The α_i values, which can be obtained from the T_i values (Section 2.4) are identical for M and N atoms in binary M_xN_y alloys. In ternary compounds $M_xN_yR_z$ the α_i values of M, N and R atoms can be different (Section 14).

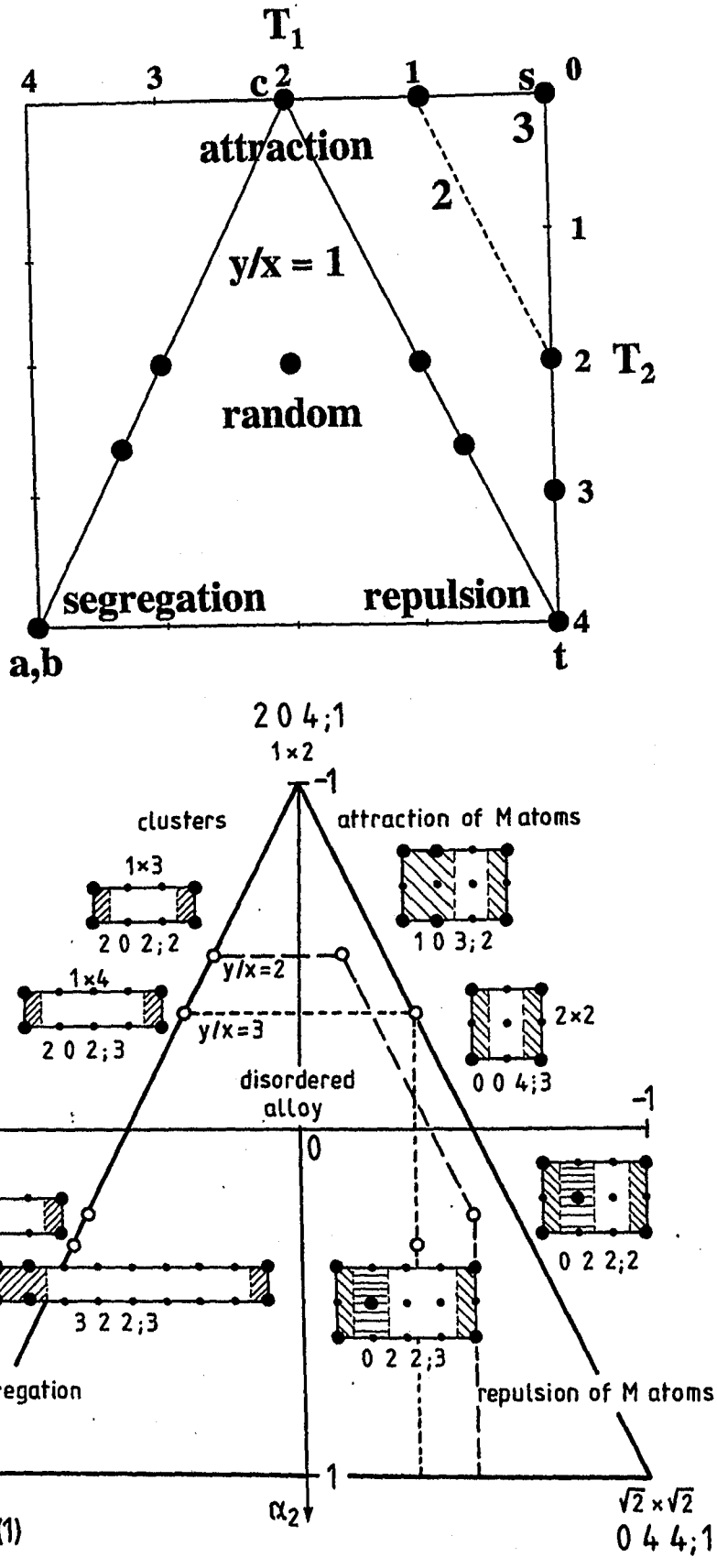

Figure 7: T_1, T_2 (a) and α_1, α_2 (b) structure map of the square net with different borders for y/x = 1, 2, 3. The structures of Fig.8 with structural units a, b, c, s and t (different shading) are at the borderline (•).

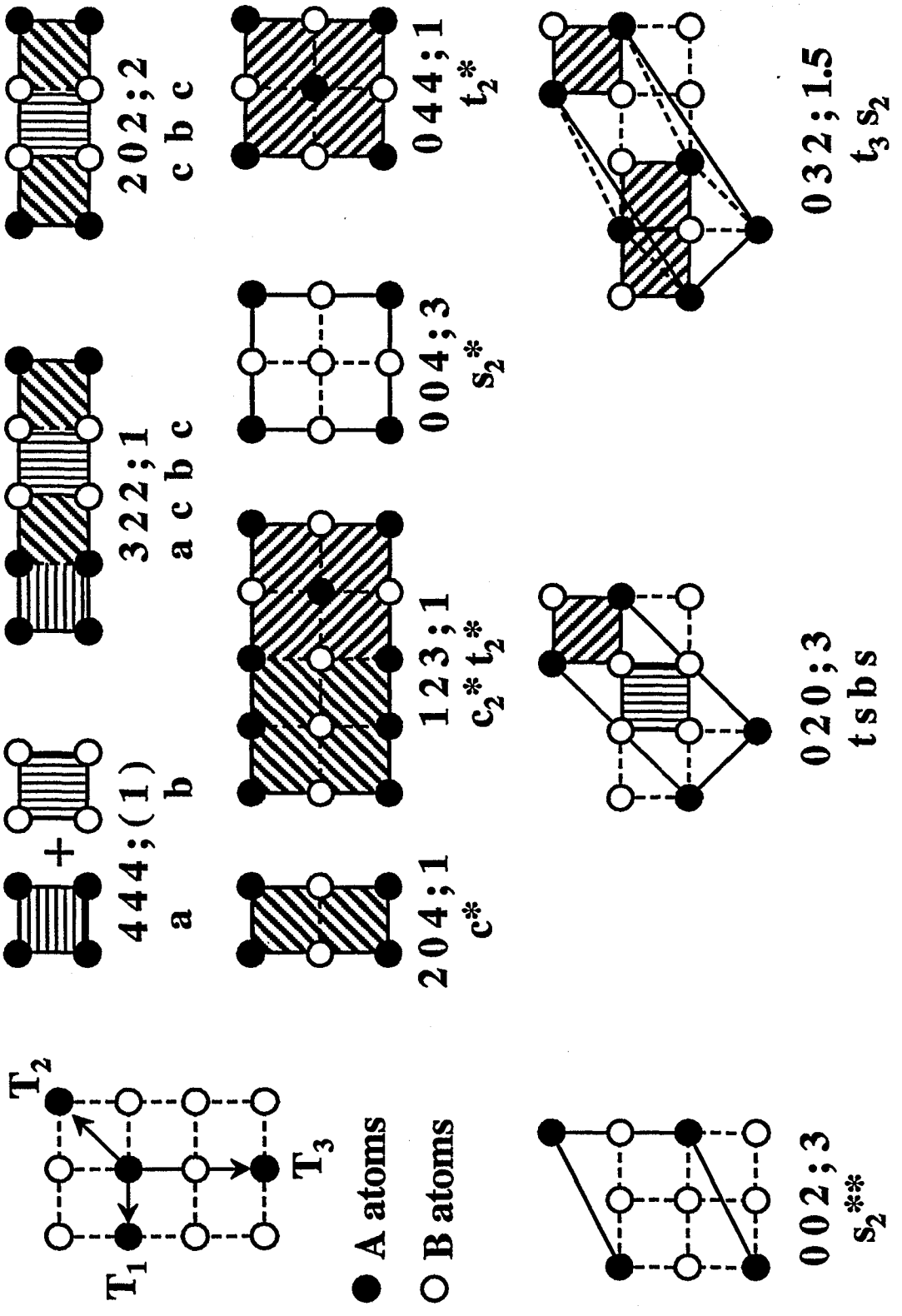

Figure 8: Self-coordination numbers $T_1\ T_2\ T_3$; y/x for the square net of A atoms in A_xB_y compounds (A = •, B = ○). The different structural units a, b, c, etc. are shown by different shading.

The hexagonal close-packed alloys consist of two hexagonal layers in A and B positions with identical environment of 12 nearest, 6 next-nearest and 2 third neighbors at distances d, $\sqrt{2}d$ and $\sqrt{8/3}d$, respectively (Fig.1, Table 2). The maximum α_1, α_2 range of ordered hcp M_xN_y alloy structures with the 12 6 2;(1), 6 0 2;1, 4 4 2;1, 4 6 2;1 (and 0 6 2;3) structures at the corners of a tetragon has the same shape as the y/x = 1 border of the T_1, T_2 structure map (Figs. 9,10). The 5 3 0;1 and 9 3 0;1 structures are also at the corners in the three-dimensional α_1, α_2, α_3 space (Mika and Hauck, 1990). Several structures with a single environment of metal atoms are inside of the structure map (Section 33). The 9 3 0;1 structure with two layers of M atoms followed by two layers of N atoms can be considered as partially segregated sheets of M and N atoms (Table 3). The M atoms of the 6 0 2;1a and 6 0 2;1b structures are clustered in layers and chains, respectively. The M atoms of the remaining structures of Fig.10 are as far apart as possible. The 4 6 2;1 and 0 6 2;3 structures with identical α_i values correspond to the AuCd and $SnNi_3$ structures. These structures are homologous (Section 9). The N atom positions of the 0 6 2;3 MN_3 structure can be occupied by M or M′ atoms to M_2N_2 (= MN) or $MM'N_2$ alloys. These structures have $T_2 = 6$. The other experimental structures are found at lower T_2 values.

The architecture of the different structures built up from structural units is more complicated than for the chain or hexagonal layer. The construction of MN_y alloys (y = 1, 3, 5) by combination of structural units a – o in [120] direction and of MN and MN_3 structures by combination of u, v, x and y units in [220] is shown in Fig.10. The $CdAu_3$ structure e.g. can be obtained by combination of these units in the sequence uv (Table 3). The theoretical structures at the left-hand border of Fig.9 and the LiRh structure consist of alternating layers of M and N atoms. Most of the other structures have layers with identical composition and environment of the M atoms in these layers (Table 3). Therefore these structures can also be described by the type and the stacking sequence of hexagonal layers. Layers of N = Ag or Au atoms are alternating in $SbAg_3$ ($SbAg/Ag_2$) and $SnAu_5$ ($SnAu_2/Au_3$), to obtain the proper composition. All structures which can be obtained by combination of structural units are considered as a structure family with the name of the pioneers simi-

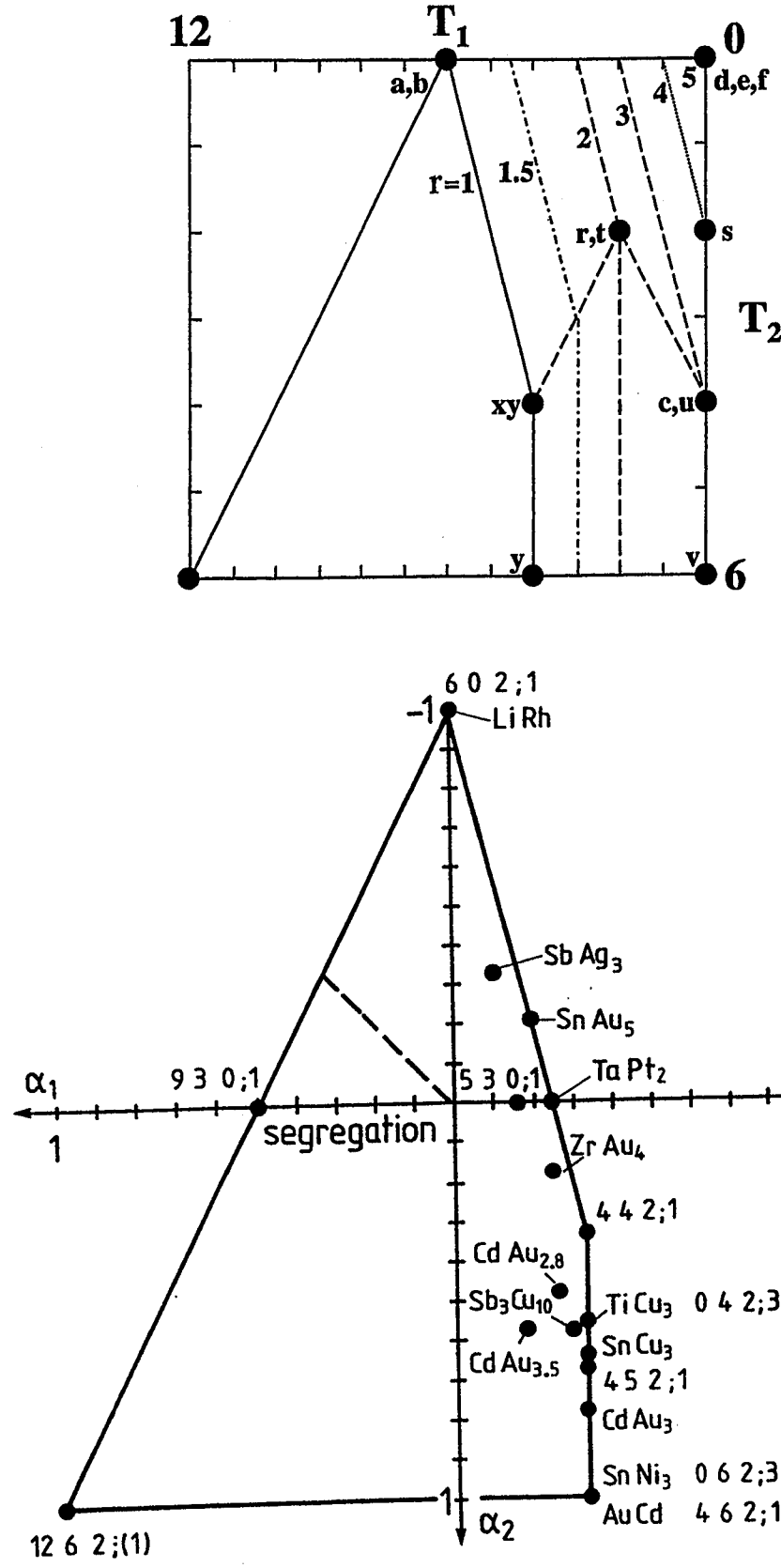

Figure 9: T_1, T_2 (a) and α_1, α_2 (b) structure map of ordered hcp structures with structural units a – y.

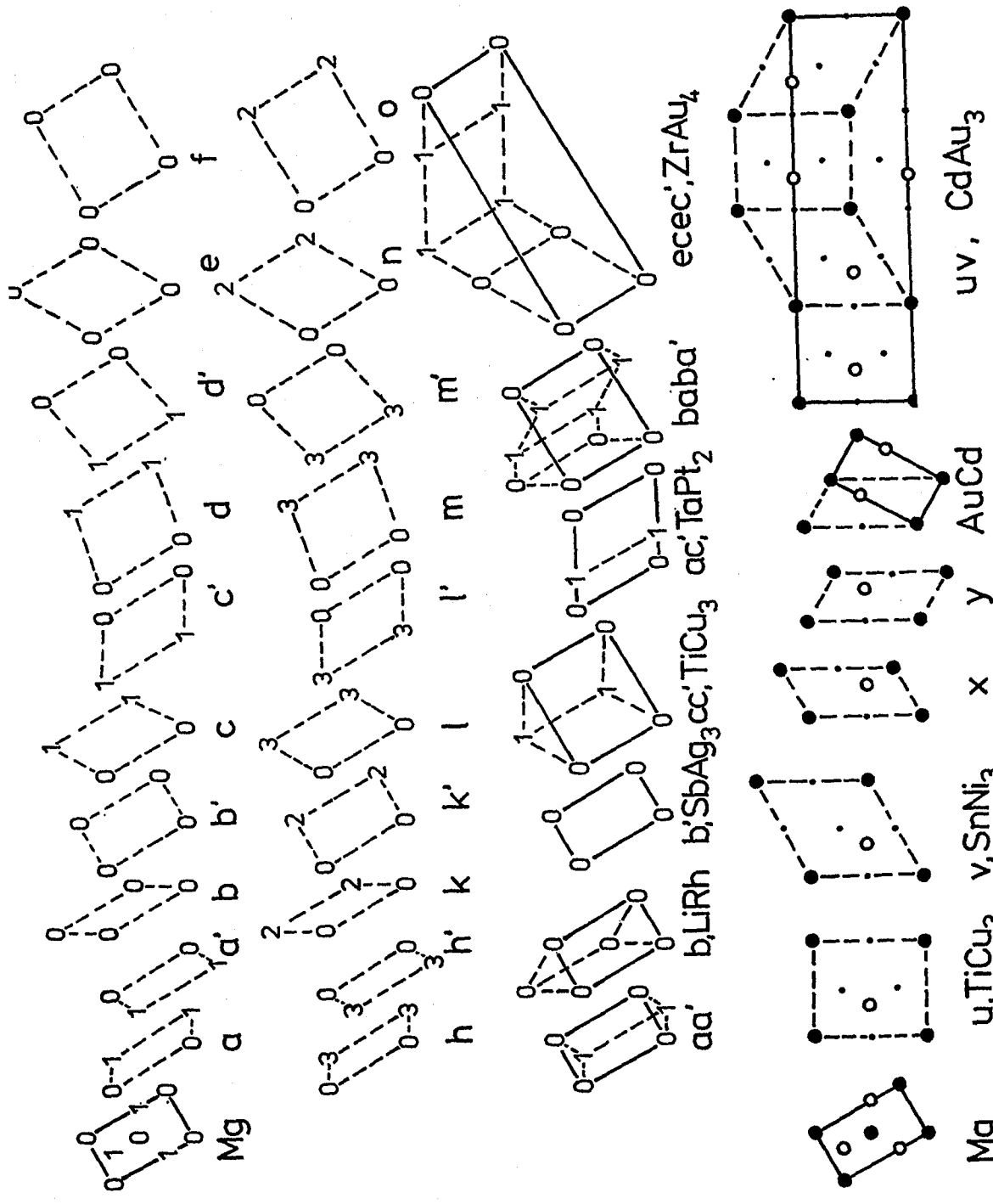

Figure 10: Architecture of hcp structures at the right-hand border of the structure map from structural units a – y. The projection height is given as the layer number for a – o. M atoms (•) and N atoms (·) of first, only M atoms (○) of second layer are shown for u, v, x, y structural units with two layers.

lar as the Ruddlesden-Popper or Aurivillius phases. The VAu_2 or $TaPt_2$ and $ZrAu_4$ structures (Stolz and Schubert, 1962) and the $SnCu_3$, $CdAu_3$ and $(Cd,In)Au_3$ structures (Schubert, 1964) are the first examples for a combination of structural units. The Stolz, Schubert family with structural units a – o and the Schubert family of structures with structural units u – y exhibit different T_2 values (0 – 4 and 4 – 6, respectively) (Table 3).

Only few of the possible MN_y alloy structures are realized as alloys like LiRh, $SbAg_3$, $SnAu_5$ (Table 3). Many other theoretical structures have a higher symmetry than the experimental structures (Section 33) (Hauck and Mika, 1999). All alloy structures (except $Cd_{26}Au_{72}$ and $Cd_{12}Au_{42}$ with T_i values in brackets (Table 3)) are at the border of the structure map with maximum interactions between M atoms. The theoretical structures 6 0 2 ; 1b and 4 4 2 ; 1 (Table 3) at corners of the structure map are candidates in a search for new alloy structures. The structures, which are not at the border of the structure map, are supposed to be metastable at low temperatures.

The 6 0 2 ; 1a (LiRh) and 6 0 2 ; 1b structures are not homometric (identical T_i for all atoms for all i), but differ in the fourth and higher coordination shells (Section 8). These structures at the same location on the structure map with very little differences of the lattice energy are distinguished by T_4, T_5 etc. values or the letters a, b, c. The T_i values ($i = 1 - 3$) are usually sufficient to characterize a crystal structure with $y/x \leq 5$. The T_1 and T_2 values are used for structure maps as a first approximation. Usually the T_1 and T_2 values of the structure families vary with the ratio of structural units.

6 Cubic close-packed structures

The positions of Cu atoms in cubic close-packed (ccp) Cu (Table 1) can be substituted by different atoms M and N in M_xN_y alloys. The reduced rhombohedral cell containing one Cu atom (instead of four in the face-

centered unit cell) is increased systematically (Section 33) (Hauck and Mika, 1999), and the metal positions are occupied to an upper limit of 50% by M atoms. The structures with a higher percentage of M atoms are identical at an exchange of M and N atoms. The s-CN or averaged s-CN values of the minority component M are determined to characterize the structures by T_1 T_2 T_3; y/x (Table 4). The T_1 and T_2 values were plotted in the structure map (Fig.11a) with the same T_1 and T_2 values as the hcp structure map (Fig.9a).

Each metal atom of the ccp structure has $T_1^{\max} = 12$, $T_2^{\max} = 6$ and $T_3^{\max} = 24$ first-, second- and third-nearest neighbors at distances d, $\sqrt{2}d$ and $\sqrt{3}d$ (Fig.1, Table 2). The maximum T_1, T_2, T_3 values are reduced in M_xN_y alloys where $y/x \geq 1$. There are 28 different structures with a single environment of M atoms (Section 33) (Hauck et al., 1988a). The 12 6 24; (1), 6 0 12; 1a,b, 4 4 16; 1 and 4 6 8; 1 (and 0 6 0; 3) structures are the limiting structures (Figs. 11,12). The 6 0 12; 1a and 6 0 12; 1b structures are homometric structures – structures with identical T_i values, but different symmetry (Section 8). The 0 6 0; 3 $AuCu_3$ structure and the 4 6 8; 1 CuAu structure are homologous with identical α_i values (Section 9). These structures can be compared with the hcp 0 6 2; 3 $SnNi_3$ and 4 6 2; 1 AuCd structures for the same T_1 and T_2 values (Fig.9). The 4 4 16; 1 UPb and the 0 4 8; 3 $TiAl_3$ structures correspond to the hcp 4 4 2; 1 and 0 4 2; 3 $TiCu_3$ structures. PtV crystallizes in the CuAu or AuCd structure (Villars and Hulliger, 1987). The 4 4 16; 1 UPb structure is identical to the NbP structure (Villars and Calvert, 1986). The architecture of structures along the 12 6 24; (1) – 6 0 12; 1a boundary is analogous to that for the hcp structures. The M and N atoms are completely segregated in 12 6 24; (1) with decreasing thickness of hexagonal layers progressing along the boundary (Table 4). Close-packed planes of M and N atoms alternate in 6 0 12; 1a CuPt as in the hcp 6 0 2; 1a LiRh structure. The ccp structures at low T_1, including most experimental structures, can be assembled from square layers rather than from hexagonal layers alone as is the case for hcp structures (Fig.12). The structures at the upper right-hand border ($4\alpha_1 + \alpha_2 + 1 = 0$) can be assembled by two sets of structural units a – i. The NaCl related structure of $Al\square_2Cl_3$ (ac′) with two vacancies $\square$ in the ccp metal lattice (Ketelaar, 1935) and Mo_3Al_8 (hgh) (Forsyth and Gran,

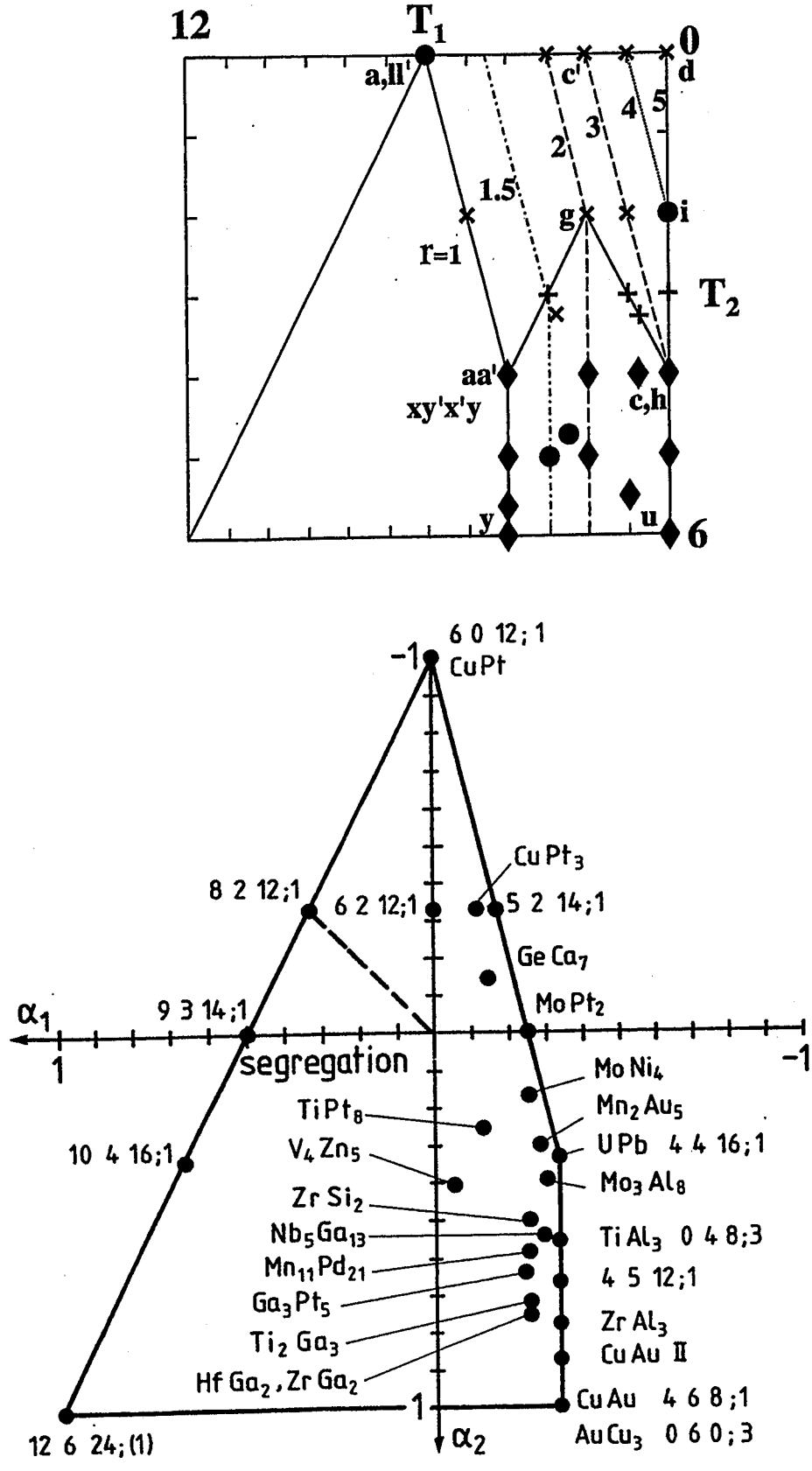

Figure 11: T_1, T_2 (a) and α_1, α_2 (b) structure map of ordered ccp structures of the Brauer (◆), Ketelaar (×), Forsyth, Gran families (+) and others (•).

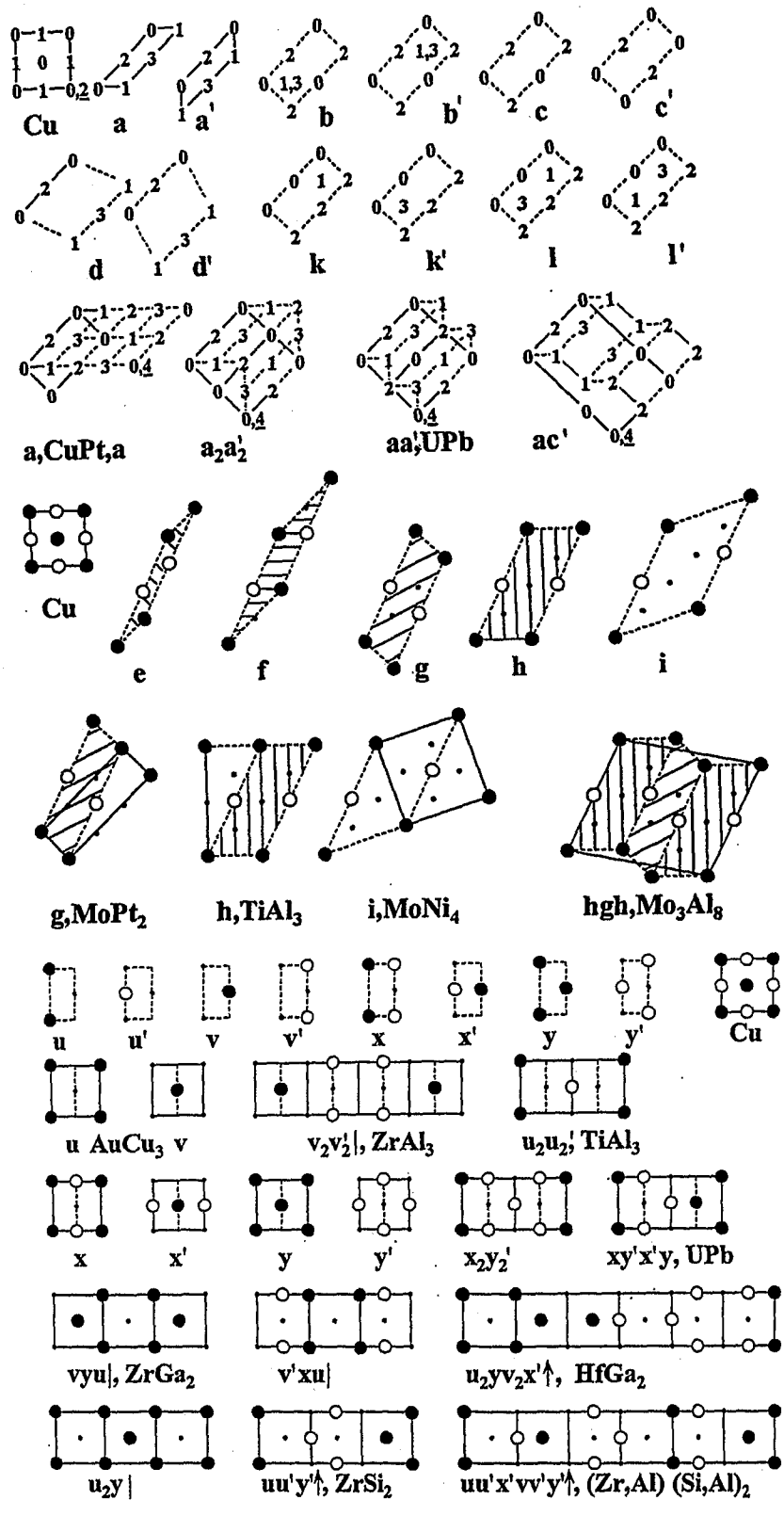

Figure 12: Architecture of ccp structures from a – y structural units and structures with two square layers with M atoms at z = 0 (•) and z = 1/2 (○). Positions of N atoms at z = 0 (·) for pattern recognition. The projection height of M atoms is shown for a – l units with more than two layers. The asymmetrical part of the string of structural units is given for sequences with mirror plane (|) or glide plane (↑).

1962) are the first experimental examples, which can be obtained from combination of a and c′ or h and g structural units, respectively. The ccp Na positions of the NaCl structure are substituted by M = Al and N = □ in $Al□_2Cl_3$. Therefore the NaCl related structures with M and N atoms at Na positions can be characterized by the s-CN values of M atoms (Section 18). The same applies for ZnS related structures as e.g. $CuFeS_2$ with the s-CN values 4 4 16 ; 1 of Cu and Fe atoms (Hauck and Mika, 1998b). The compositions of the structural units are M_xN_y with y/x = 1 (a, b, e, f, l), 5/3 (k), 2 (g), 3 (c, h), 4 (i) and 5 (d).

The 0 6 0 ; 3, 0 4 8 ; 3, 4 6 8 ; 1 and 4 4 16 ; 1 structures can be split into structural units u, v, x and y, which can be combined like the parts of a puzzle to obtain the crystal structures found at the right-hand border (Figs. 11,12). The u′, v′, x′ and y′ units are obtained from the u, v, x and y units by a variation of the origin. The $ZrAl_3$ structure (Brauer, 1939) is obtained from v and v′ units and the CuAu II structure (Johansson and Linde, 1936) from a combination of the x and y structural subunits. The MN_2 structures $ZrGa_2$, $HfGa_2$, $ZrSi_2$, and the Nb_5Ga_{13} structure are obtained by combination of u, v, x and y units (Table 4). The sequences of structural units are also observed in NaCl related structures like $□Nb_3□O_3$ (u_2), MoO_3 (uxv′x′u′), Nb_3O_7F ($u_2xv'_4xu_2$) and R-Nb_2O_5 (xv'_2xu_2) (Hyde and Andersson, 1989). Some of these structures are usually described by antiphase boundaries or shearing. The uu′y′ structural units e.g. of $ZrSi_2$ with uu′y′v′vy sequence can be shifted to the v′vy units as is indicated by an arrow in Fig.12. Other sequences like vyu| in $ZrGa_2$ (vyuuyv) are symmetrical. The symbols | for a mirrorplane or ↑ for the translation by $a/2$ $a/2$ (shear) are useful in particular for long sequences of structural units.

Most of the experimental structures are at boundary lines for the given composition. The only exception in Table 4 is V_4Zn_5, which lies at the boundary line of the structure map belonging to the hexagonal layer with the values 2.5 1.5 2.5 ; 1.25 (Fig.5). Structures, which are not at the boundary line of the structure map, are supposed to be unstable at low temperatures with respect to other structures at the boundary with maximum interactions between M atoms. Sometimes M atoms on one position are disordered, in other cases several positions are disordered

(Hauck and Mika, 1999) and give rise to decreased α_i values.

The structures with a single environment of M atoms can be characterized by square or hexagonal layers (Section 4) with small unit cells:

	square layers	hex. layers
CuAu	0 4 4;1 4 4 4;(1)	2 2 6;1
UPb	0 4 4;1 2 2 0;1	2 4 2;1
$AuCu_3$	0 4 4;1 4 4 4;(1)	0 0 6;3
$TiAl_3$	0 4 4;1 4 4 4;(1) 0 2 0;3	0 2 2;3

The structures with $M^i > 2$ (Table 4) of the Johansson, Linde and Brauer family as e.g. the CuAu II or $ZrAl_3$ structure at the right-hand boundary of the structure map (Fig.11b) consist of u, v, x, y structural units, which are connected by 0 4 4;1 square planes. The other layers of the CuAu–UPb and $AuCu_3$–$TiAl_3$ parent structures do not fit together. The structural units of many structures on the right-hand side of the structure map (Fig.11b) are connected by 2 0 4;1 or 0 4 4;1 square planes (Table 4). Most (theoretical) structures on the left-hand side of the structure map are connected by 6 6 6;(1) hexagonal planes.

The α_1, α_2 values of the different layers of a structure are sometimes similar to the α_1, α_2 values of the structure itself (Figs. 5b,7b,11b) and are located in the same area of the structure map. An example is the 2 0 4;1 square and 2 2 6;1 hexagonal layer of the 6 0 12;1a CuPt structure. In other structures as e.g. 2 2 12;2a $MoPt_2$, the 0 2 0;2 and 2 0 2;2 square layers or the 2 0 2;2 and 0 6 0;2 hexagonal layers are at different locations of the structure map, probably because of the directional bonding of Mo atoms (Hauck and Mika, 1994).

Some metals like bcc Mo, which do not form close-packed structures because of directional bonding of the outer electrons, form close-packed structures in alloys as e.g. cubic close-packed $MoNi_4$ or $MoPt_2$. In other

examples the directional interactions between metal atoms are increased by the formation of an alloy. The CuPd or FeTi alloys e.g. crystallize in an ordered body-centered cubic structure in spite of the close-packed structures of the components. Other pairs of metals like Cu and Rh with the ccp structure for each metal do not form compounds at all but segregate as two limited solid solutions. The s-CN values approach 12 6 24 ; 0 for complete segregation at y/x = 0.

7 Ordered structures of complex close-packed alloys

The structure maps for hcp and ccp ordered alloys M_xN_y are identical with the same numbers of T_1 and T_2 values (Figs. 9,11). The comparison of Table 3 and 4 shows many experimental structures with identical T_1 and T_2 values. Therefore also the T_1, T_2 structure maps of structures with a complex stacking of h and c layers (Table 1) are identical. The structures with identical T_1 and T_2 values exhibit the same kind of hexagonal layers (Table 5). They can be described by the stacking symbol and the ordering of M and N atoms in the hexagonal planes. The T_3 and T_4 values can be obtained from the fraction f of h layers as was outlined in Section 2.

The complex close-packed metals (Table 1) are similar to hcp stacking with only one direction of packing of the hexagonal layers at occupation with M atoms only. All structures of Table 1 contain a 3-fold axis in c direction of the stacked layers at occupation with M atoms only. The metal atoms of the complex structures of Table 1 have already two or more different environments. The architecture of many hcp, ccp and complex close-packed M_xN_y alloys can be characterized by hexagonal layers with composition M_xN_y (instead of M atoms) and the stacking of these layers similar as in Table 1. These structures can be divided in five major groups corresponding to different α_1, α_2 values and different hexagonal layers (Table 5) (Beck, 1969; Zhao et al., 1991; Parthé et al., 1993). The hcp $CdAu_3$ structure e.g. with $\alpha_1 = -0.33$, $\alpha_2 = 0.78$

is gradually altered to the ccp $ZrAl_3$ structure with different stacking of 0 1 4 ; 3 hexagonal layers by variation of the Au content or partial substitution of Au by In in the series: $CdAu_3$, $Cd(Au,In)_{2.8} = Cd_{26}(Au,In)_{72}$ ($Cd_{14}In_8Au_{78}$), $Cd(Au,In)_3 = Cd_{144}(Au,In)_{432}$ ($Cd_{15}In_{10}Au_{75}$) (Wegst and Schubert, 1958; Schubert, 1964) (Table 5). The ccp 0 0 8 ; 5 structure corresponding to hcp $SnAu_5$ and $(ch)_2$ WAl_5 is only observed in the NaCl related $V_6\square C_5$ (V_6C_5) structure with M = $\square$ and N = C (Section 18). The MN_5 composition is obtained by alternating MN_2 und N_3 layers.

8 Structures with identical powder patterns

Some ccp and hcp structures are homometric with identical coordination T_i of all atoms for all i (Fig.13) and some other structures differ in higher coordination spheres (Hauck et al., 1988a). The homometric structures cannot be distinguished by powder diffraction methods, if the lattice is undistorted (Patterson, 1944). Other structures are enantiomorphous, i.e. the crystal structures contain right- or left-hand screw axes which cannot be distinguished by powder diffraction. The homometric, but non-enantiomorphous, structures are characterized by a, b, c, ... The hcp 5 3 0 ; 1a,b structures (Fig.13) are homometric, but differ from the homometric 5 3 0 ; 1d,e structures in the 4-th and higher coordination shells. The hcp 6 0 2 ; 1a,b structures with structural units aa′ or b (LiRh) (Fig.10) differ from the 4-th coordination onward. The ccp 2 2 12 ; 2c structure (Section 18) is different from the homometric 2 2 12 ; 2a,b structures (Fig.13) in the 6-th and higher coordination shells. The crystal structures a, b, c, ... with identical positions on the structure maps (Figs. 9,11) are stabilized by about the same amount of lattice energy and are sometimes coexisting as e.g. the 0 0 8 ; 5b,e,f V_6C_5 stacking variants (Section 18). The homometric structures (Fig.13) can also be considered as stacking variants, where square or hexagonal layers are stacked perpendicularly to the projection plane with different translations x, y, z (Section 16).

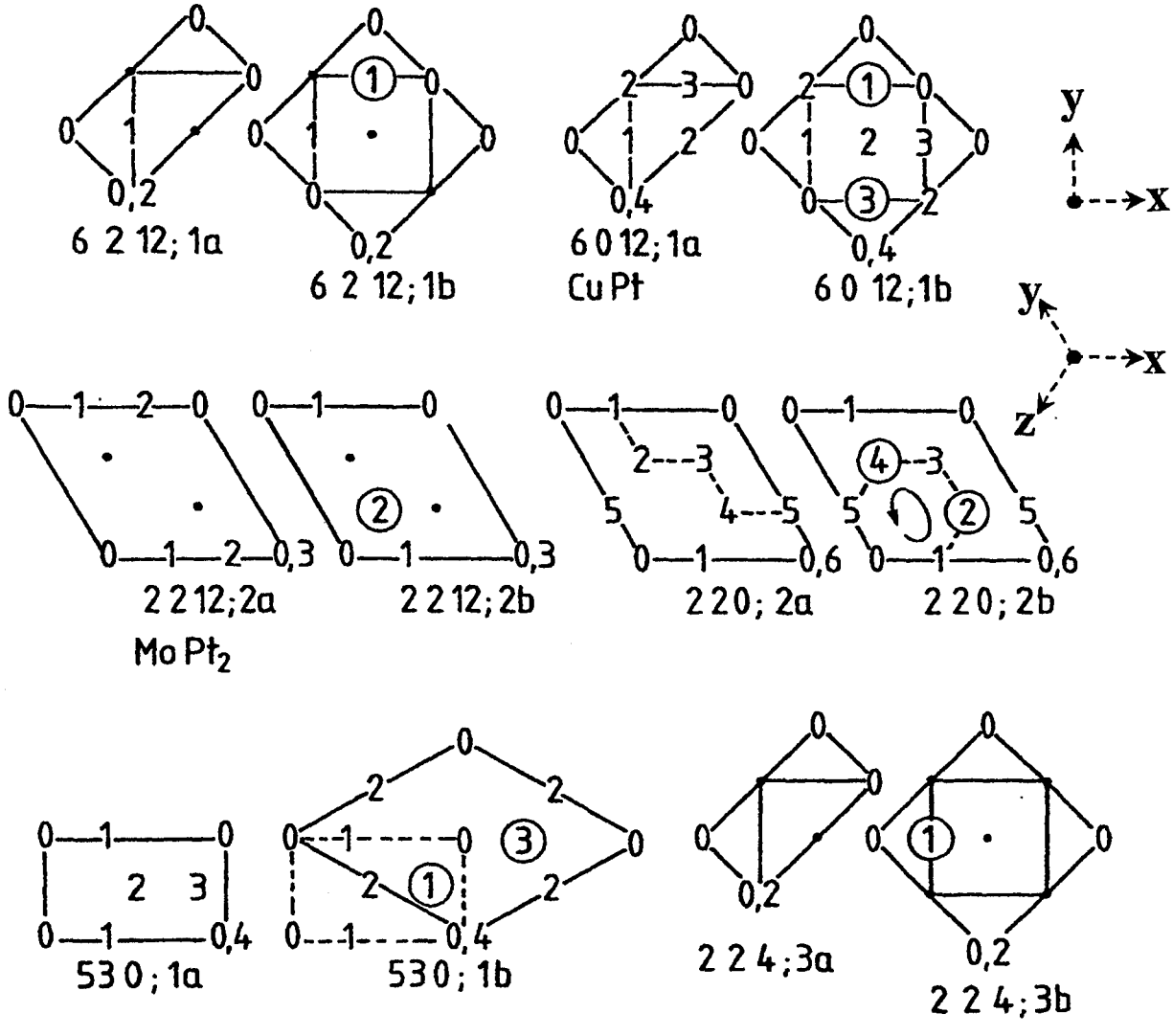

Figure 13: Examples of homometric pairs of stuctures with identical self-coordination numbers T_i. 6 2 12; 1a,b, 6 0 12; 1a,b, 2 2 12; 2a,b and 2 2 4; 3a,b are ccp, 2 2 0; 2a,b, 5 3 0; 1a,b are hcp. The positions of M atoms are given by the projection height. The different M positions of homometric pairs are encircled, N atoms at z = 0 (·), x, y, z coordinates for the translation of identical layers.

There are also homometric structures of close-packed metal atoms with a different stacking sequence but identical T_i values (Mardix, 1990), e.g.

hcchchcchhchchh,

hcchchchhcchhhc,

which are two different structures containing the same unit cell with 15 layers, the same percentage 53.3% of h layers in the same space group *P3m1*. Other structures of Table 1, e.g. 9a and 9c or 9d and 9e have identical T_i for $i = 1 - 8$ but differ in T_9 and higher coordination shells. They are *quasi-homometric* with very little difference of the lattice energy as e.g. the Madelung factors of the NaCl related structures (Hauck et al., 1988b).

9 Homologous series of structures

A second type of special structures exhibits identical α_i values but at different composition y/x. These structures have identical or closely related unit cells and form homologous series of structures which are filled up successively by M atoms until T_i^{max} is reached (Table 6). Each M and each N atom of these structures must have the same set of numbers T_i, respectively. The structure with the lowest M content $y/x = r^*$, $T_1^*\ T_2^*\ T_3^*\ ; r^*$ is filled up with M atoms in steps of $k = r^*, r^* - 1, \ldots, 0$ (Hauck et al., 1988a):

$$\begin{aligned} T_i^k &= T_i^{max} - (T_i^{max} - T_i^*)\, k/r, \\ y/x &= k/(r^* + 1 - k). \end{aligned}$$

The homologous series of structures contain also structures with M and N atoms interchanged as e.g. $AuCu_3$ and Cu_3Au with Cu at Au positions in $CuAu_3$ (Table 6). There are three homologous series for ccp ($r^* = 2$, 3, 4) and two series for hcp ($r^* = 2$, 3) (Table 6). The $r^* = 3$ series for the ccp 0 6 0 ; 3 $AuCu_3$ and 4 6 8 ; 1 CuAu structures corresponds to the hcp 0 6 2 ; 3 $SnNi_3$ and 4 6 2 ; 1 AuCd series at identical α_1, α_2 values (Figs. 9b,11b). The ccp 2 2 12 ; 2a,b structures (Fig.14) can be compared with the hcp 2 2 0 ; 2a,b (Fig.13) or 2 2 2 ; 2 $TaPt_2$ (Fig.10) structures (Hauck et al., 1988a). The pairs of closely related ccp structures 0 4 8 ; 3

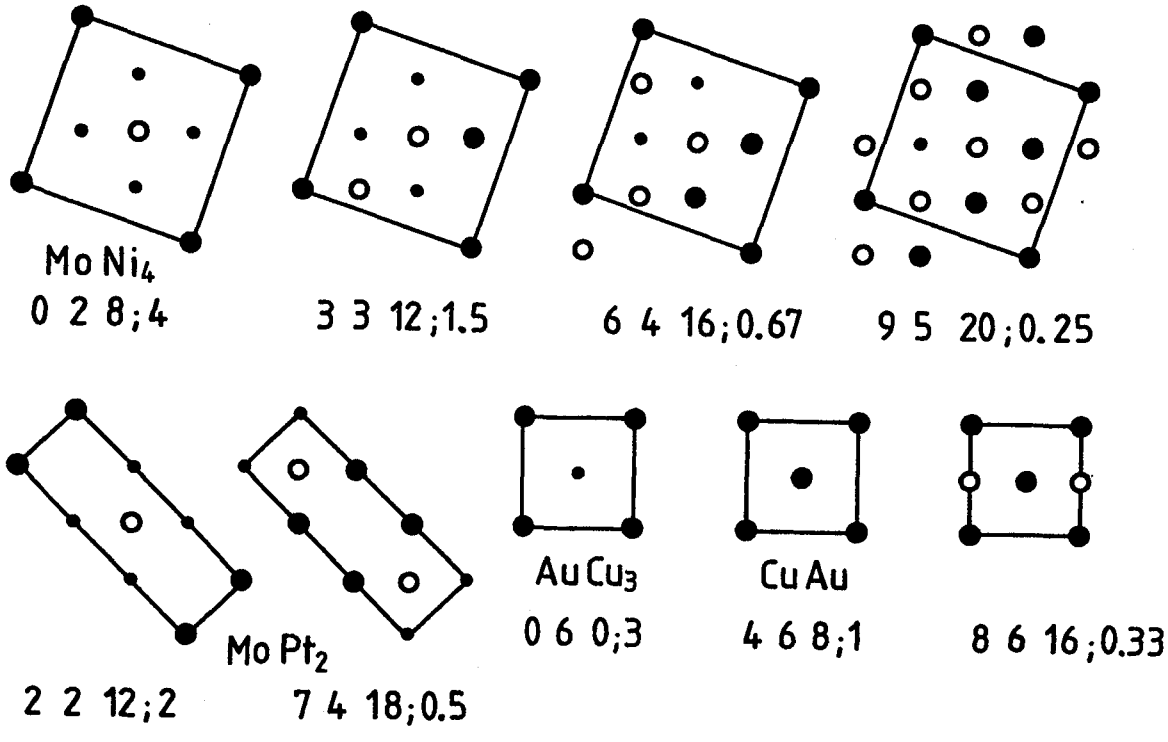

Figure 14: Examples of ccp homologous crystal structures with identical α_i values at different concentration y/x. M atoms at z = 0 (•) and z = 0.5 (○). Positions of N atoms (·) at z = 0 for pattern recognition.

$TiAl_3$ and 4 4 16;1 UPb (Fig.12) and the corresponding hcp 0 4 2;3 $TiCu_3$ and 4 4 2;1 MN structures with structural units baba′ or xy (Fig.10) are *quasi-homologous* because of different α_2 values. The T_i values of quasi-homologous structures are at the border of the T_1, T_2 structure map at the corresponding y/x values. A third group of related structures (homologous II series) exhibits identical α_i values like the 0 0 2;6, (1 2 3;5/2), (2 4 4;4/3), (3 6 5;3/4), (4 8 6;2/5), (5 10 7;1/6), 6 12 8;0 series of the primitive cubic lattice (Section 22). Only the structure with the maximum $r^* = y/x$ value 0 0 2;6 is at the border of the T_1, T_2 structure map. The other values in brackets are inside of the structure map. The same applies to the large number of other structure series. The $TiPt_8$ and V_4Zn_5 structures with different α_i values crystallize even in the same space group at different y/x and can be considered as one structure type (Villars and Calvert, 1986), if the V_4Zn_5 structure is written as $Zn(V_4Zn_4)$. The V_4Zn_5 structure however is not at the border of the T_1, T_2 structure map.

10 Symmetry of ordered phases

The metal atoms of the hcp and ccp lattice have a single environment with a high point symmetry for the metal atoms (*International Tables for Crystallography*, Hahn, 1987; Villars and Calvert, 1986):

$4/m\ \bar{3}\ 2/m$ for the Cu atoms with ccp structure,
$\bar{6}m2$ for the Mg atoms with hcp structure.

The site symmetry is reduced by distortion (d), e.g. of the Cu lattice in In or Hg (Table 1), or by different stacking (s), as e.g. the $(ch)_2$ La or Nd structure, or by formation of ordered structures (o) (Fig.15). Structures with a single environment of all M and N atoms at the corners of the structure maps like $AuCu_3$ or CuAu are usually highly symmetric. Structures containing M atoms with different environments are built from different structural units as e.g. $ZrAl_3$, CuAu II or $ZrGa_2$ (Fig.12). The symmetry of these structures is usually lower because of the differ-

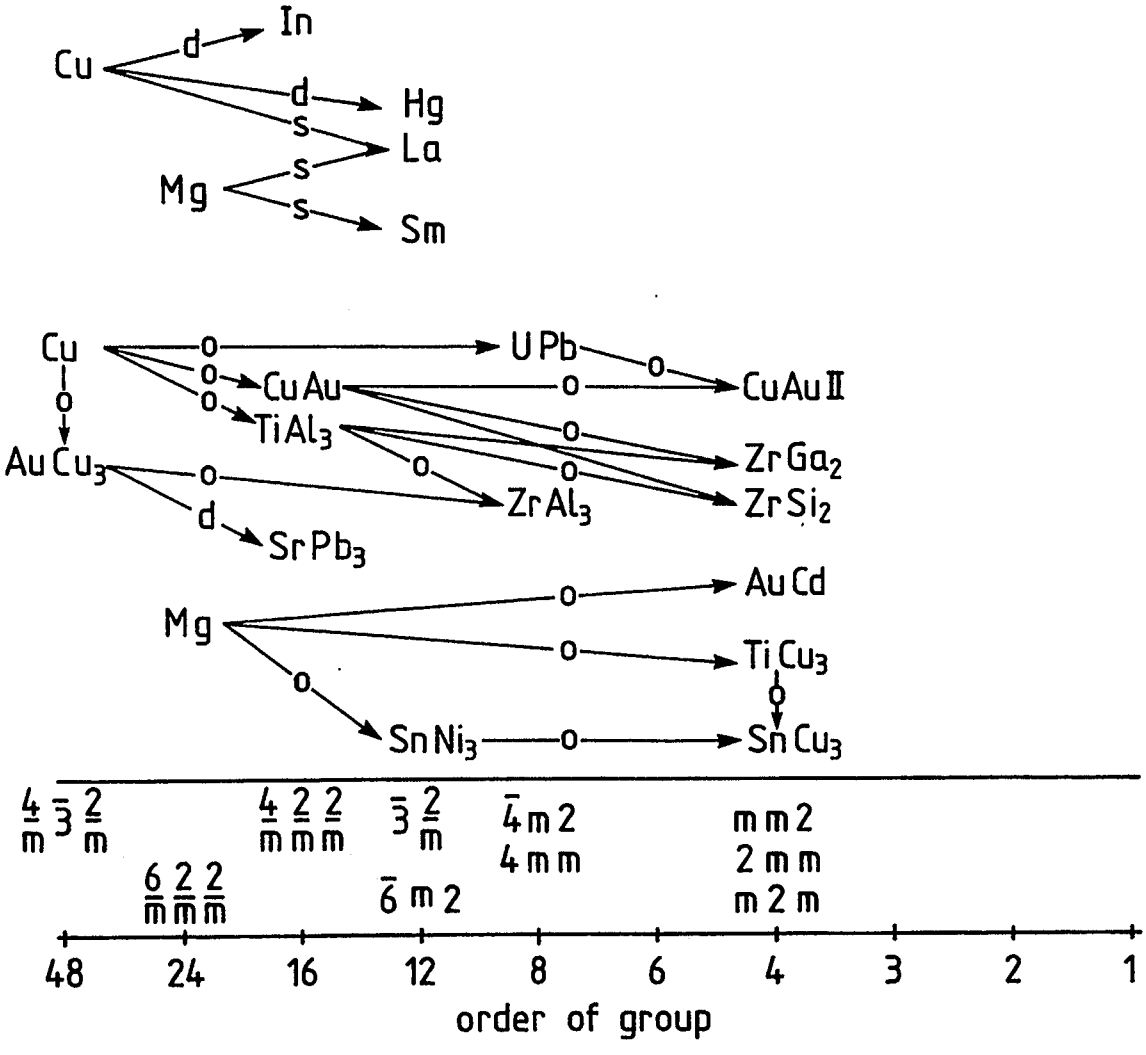

Figure 15: Crystallographic point-group symmetry of M atoms in different ordered alloys M_xN_y. The order of the point symmetry of M atoms is reduced by ordering (o), by stacking (s), e.g. of La atoms in chch layer sequence, or by distortion (d).

ent symmetry elements of the structural units. The populations of the different structure types obey Pauling's rule of parsimony: The number of essentially different kinds of constituents in a crystal tends to be small (Pauling, 1929). Structure types with a single environment of metal atoms M and N ($M^i = 2$) with high symmetry as in the case of hcp alloys with AuCd or $SnNi_3$ structure (Table 3) or the ccp alloys with CuAu, $AuCu_3$, $MoNi_4$ or $MoPt_2$ structure (Table 4) are observed frequently, whereas structures containing metal atoms with different environments as e.g. CuAu II, $ZrGa_2$ or Mo_3Al_8 are rare. The fact, that highly symmetric structures can only be constructed from M and N atoms with a single environment shows that the frequent observation of high symmetry (Laves, 1967) is a consequence of Pauling's rule for small numbers of constituents.

In most cases, the experimentally observed symmetry is identical with the symmetry determined for the undistorted lattice. This can be used to find a structural model of the ordered structure from electron diffraction patterns. Alloys with small single crystal domains of ordered structures can be investigated by electron diffraction to determine the unit cell and the symmetry from the diffraction pattern. These values can be compared with the list of theoretical structures to calculate the powder pattern for x-ray or neutron diffraction.

The symmetry of a few ordered alloys as e.g. NaHg, $CdAu_3$ II, SiU_3 or $SrPb_3$ (Table 4) is further decreased due to distortion by directional bonding similar to that in tetragonal In or rhombohedral Hg compared to cubic Cu (Table 1).

11 Ising model

Crystal structures of ordered alloys M_xN_y have been calculated for central pairwise interactions V_i, $i = 1, 2, 3, \ldots$ with $V_i = V_i^{MM} + V_i^{NN} - 2V_i^{MN}$ between nearest, next-nearest, third, etc. metal atoms within the Ising model (Turchi, 1994). The results obtained for the single square

layer (Kaburagi, 1978), the single hexagonal layer (Kudo and Katsura, 1976; Hiraga and Hirabayashi, 1977), hcp (Kudo and Katsura, 1976) and ccp (Kanamori and Kakehashi, 1977) alloys can be compared with the structures in the structure maps. The present notation $T_1\ T_2\ T_3$; y/x for the self-coordination numbers T_i and concentration y/x is similar to the notation of the structures used by Kanamori and Kakehashi (1977). The interaction parameters V_1 and V_2 between nearest and next-nearest neighbors were varied in the Ising model calculations and the structures obtained by different procedures plotted in a V_1, V_2 coordinate system (de Novion and Landesman, 1985). These plots can be compared with the T_1, T_2 or α_1, α_2 structure maps of Figs. 5, 7, 9 and 11. The parameters α_i seem to be almost proportional to V_i. Only simple structures are obtained by variation of the V_1 and V_2 interaction parameters. The complex structures with different environments of M atoms are only found by the additional variation of V_3, V_4, etc. (Ducastelle, 1991). Structures at different positions on the borderline of the structure map, e.g. CuAu II compared to CuAu, are stabilized by different V_3, V_4, etc., which cause a slightly different V_2 and α_2 (Fig.16).

The interaction parameters $V_i = 0$ for a statistical (random) distribution of M and N atoms correspond with $\alpha_i = 0$. The α_i values are positive for attractive interactions between M atoms and negative for repulsive interactions. The structures can be classified within four fields by consideration of V_1, V_2 only: (I) V_1, $V_2 < 0$, (II) $V_1 < 0$, $V_2 > 0$, (III) $V_1 > 0$, $V_2 < 0$ and (IV) V_1, $V_2 > 0$. These areas are subdivided by the diagonals in Ia, Ib, etc. (Fig.16). Most experimental structures are in (I) or (II), with a repulsive interaction V_1 between nearest-neighbor M atoms. Structures in IIIa and IV, with attractive interactions V_1 between nearest-neighbor M atoms, contain already multiple layers of M and N atoms as a first step towards segregation. Structures with covalent bonding between M atoms are in Ia and IIIb. The structures of IIIb contain clusters, e.g. sheets or rows of M atoms.

The M atoms of structures in IIb are as far apart as possible, which can be correlated with repulsive interactions V_1 between nearest M atoms, e.g. Coulomb repulsion. These structures have the highest Madelung factors (Hauck et al., 1988a). The crystal structures with covalent and

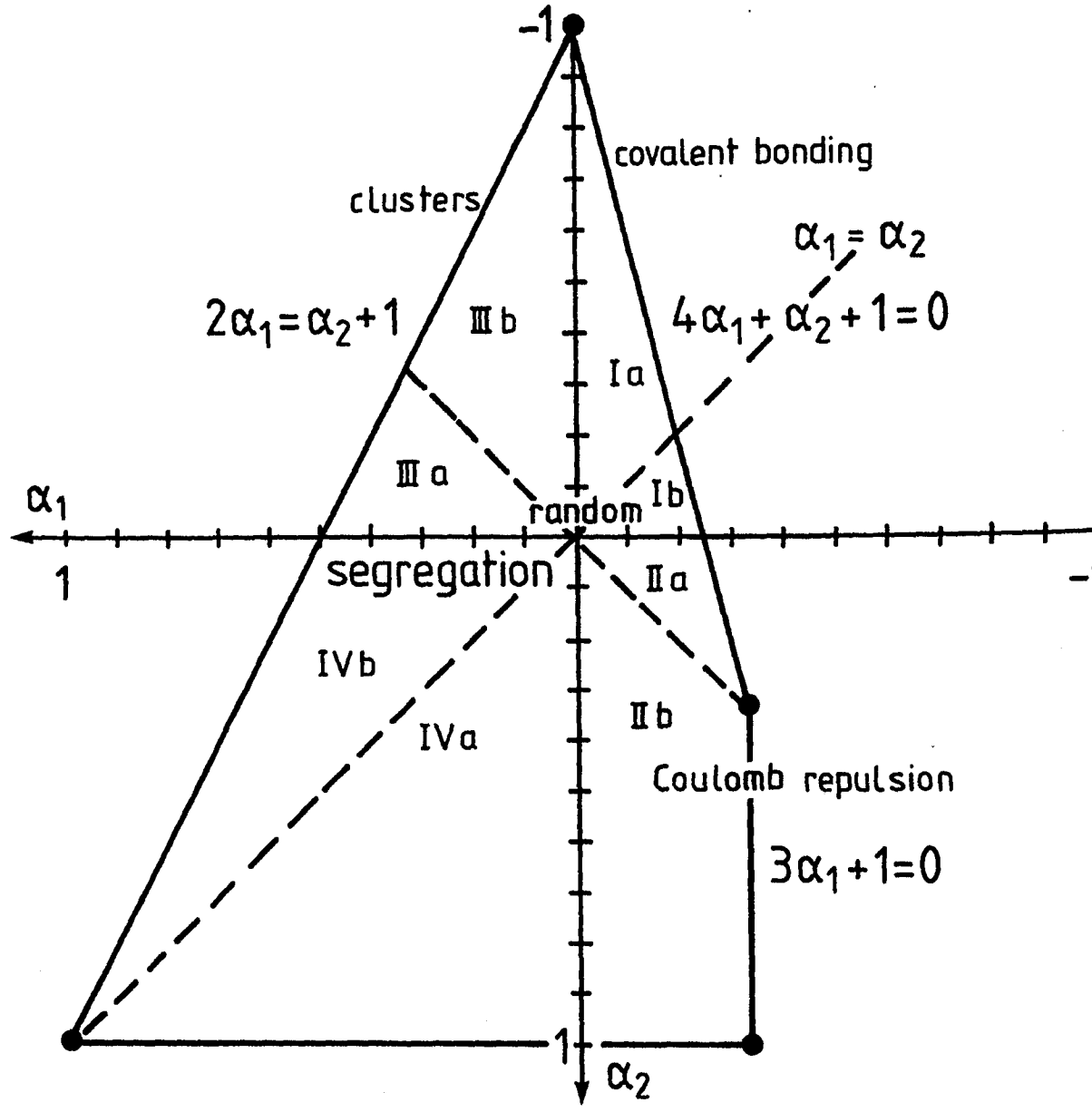

Figure 16: The different areas of the α_1, α_2 structure map of close-packed alloys as derived from the Ising model.

ionic bonding are separated by the line $\alpha_1 = \alpha_2$. The M atoms of ionic compounds with low M content are expected at $T_1 = T_2 = 0$ because of the repulsive interactions. The relation $\alpha_1 = \alpha_2$ however is also valid for covalent compounds with the relation $T_1/T_2 = T_1^{max}/T_2^{max}$ with preferential occupation of the inner coordination shells T_1 and T_2. The line $\alpha_1 = \alpha_2$ of dilute alloys intersects the borderline $4\alpha_1 + \alpha_2 + 1 = 0$ of the hcp and ccp structure maps at concentration y/x = 5. Therefore ionic and covalent compounds with y/x $\geq$ 5 and $T_1 = T_2 = 0$ should be on the line $\alpha_1 = \alpha_2$. Ordered ionic compounds with y/x $<$ 5 are expected with increased T_2, ordered covalent compounds with increased T_1.

The structures with a maximum interaction are at the outer borderlines. Structures with composition y/x = 1, 2 and 5 are on the borderline $4\alpha_1 + \alpha_2 + 1 = 0$ in (I, IIa), structures with y/x = 1 and 3 are on $3\alpha_1 + 1 = 0$ in (IIb) and structures with all compositions on $2\alpha_1 = \alpha_2 + 1$ in (III, IVb). Structures with different composition are in the field, e.g. structures with y/x = 2 are on $4\alpha_1 + 1 = 0$ in (II) (Fig.16) or $T_1 = 2$ (Fig.11) because of geometrical restrictions of the close-packed metal atoms. Structures with y/x = 2 are less frequent than structures with y/x = 1 or 3 (Table 4). They can be considered as a combination of structural units of composition y/x = 1 and 3 as was outlined before. Other structures inside of the α_1, α_2 field like ccp 6 2 12;1a,b have the same composition as structures at the borderline, e.g. 6 0 12;1a,b, 5 2 14;1 or 8 2 12;1 (Fig.11). These structures are supposed to be less favorable than structures at the borderline with maximum interactions between M atoms.

12 Characterization of structures by sequences of structural units

Structures at the left-hand border of the structure map (Figs. 9,11) can be characterized by the sequences of 6 6 6;(1) hexagonal layers with different metal atoms as e.g. LiRhLiRh for hcp LiRh (6 0 2;1a) or CuPtCuPt for ccp CuPt (6 0 12;1a) (Tables 3,4).

Structures at the right-hand border can be characterized by sequences of structural units, which are linked by common interfaces as e.g. uvuv ($CdAu_3$), vu_4vu_4 ($SnCu_3$) (Fig.10, Table 3) or $v_4v'_4$ ($ZrAl_3$), gh_2 (Mo_3Al_8) and vyu_2yv ($ZrGa_2$) (Fig.12, Table 4).

The different series of structures allow a characterization of crystal structures by a sequence of structural units as e.g. aa′ for the UPb structure, or gh for Mn_2Au_5 and hgh for Mo_3Al_8, or $v_2v'_4v_2$ for $ZrAl_3$ and vyu_2yv for $ZrGa_2$ (Fig.12). The three-dimensional structures are described by one-dimensional sequences of structural units. These sequences of units can be analyzed by the one-dimensional Ising model (Fig.2) with T_1 T_2 T_3; y/x = 2 2 2; (1), 1 0 1; 1 and 0 2 0; 1 at segregation of a and b structural units, and the sequences aabb or ab for attractive or repulsive interactions, respectively. Chains of more than two structural units like vyu_2yv for $ZrGa_2$, or $u_2yv_4yu_2$ for Ce_3Sn_7 (Table 4) can be analyzed for clusters (C), single (S), double (D), triple (T) and multi (M) rows of structural elements similar as in Fig.2. The one-dimensional Ising model can explain the reason for small numbers of different structural units (Pauling's rule of parsimony) like the examples given before. The longer sequences of structural units like $v_2v'_4v_2$ ($ZrAl_3$) might segregate in uu'_2u ($TiAl_3$) and u_2 or v_2 structure ($AuCu_3$). Most of the longer sequences are symmetrical like $v_2v'_4v_2$ ($ZrAl_3$) or vyu_2yv ($ZrGa_2$) and can be characterized by the asymmetric sequence and a vertical bar (|) for the mirror plane like $v_2v'_2$ | ($ZrAl_3$) or vyu | ($ZrGa_2$).

13 Disordered alloys

Many alloys form extensive substitutional solid solutions, in particular alloys of metals with similar radii and electronegativity. Some alloys as e.g. AuCu and $AuCu_3$ are disordered at high temperatures and become ordered at lower temperatures (Cenedese and Gaspard, 1984). The same applies to interstitial alloys as e.g. V_6C_5 or Ti_2C (Section 18) which have a disordered distribution of C atoms at high temperatures but an ordering of the C atoms (and vacancies) at lower temperatures (de Novion,

1994). The x-ray or neutron diffraction patterns exhibit diffuse intensity which is concentrated on lines or surfaces in reciprocal space. The diffuse intensity can be analyzed for the short-range order parameters α_i. The experimental values (Schweika, 1985; de Novion and Landesman, 1985) are usually between $\alpha_i = 0$ for a random distribution of metal or C atoms with no diffuse intensity and the values of the ordered alloys (Fig.17) and should shift to the values of the ordered alloys as the order-disorder transition temperature is approached. The relations $4\alpha_1 + \alpha_2 + 1 = 0$ and $\alpha_1 + \alpha_3 = 0$ were obtained for the α_1, α_2, α_3 short-range order parameters of oxides like $LiFeO_2$ and carbides like V_6C_5 from the shape of the diffuse intensity patterns in reciprocal space (Sauvage et al., 1974; Ducastelle, 1991). These relations can be explained by a disordered arrangement of carbon atoms in configurations of structural units a – l allowed by Pauling's electrovalence rule (Section 19) or by the disordered T_i configurations 6 0 12 ; 1, 3 0 10 ; 2, 2 2 12 ; 2, 0 0 8 ; 5 or 4 4 16 ; 1 (Fig.17) (Hauck, 1985). There are many stacking variants of these configurations (Hauck et al., 1988b). The structures of the Ketelaar and Forsyth, Gran families can be obtained by combinations of structural units a – l (Table 4). Nonperiodic sequences of these structural units give rise to diffuse intensity at $4\alpha_1 + \alpha_2 + 1 = 0$. Some ZnS (sphalerite) related structures like Ga_2Te_3 or $AsCu_3Se_4$ give rise to diffuse intensities at $3\alpha_1 + 1 = 0$ (Fig.16) (Sauvage et al., 1974; Hauck and Mika, 1998b). This corresponds to the Johansson, Linde and Brauer family of structures with a disordered sequence of structural units u – y (Table 4). Other disordered alloys and compounds of Fig.17 can probably be described as a disordered mixture of several structural families, including clustered structures at the left-hand border of the map.

A special "disorder" is obtained if structural units a and b alternate aperiodically with the sequence of Fibonacci numbers $n = 1, 2, 3, 5, 8, 13, \ldots$. The iteration of the Fibonacci substitution a $\rightarrow$ ab, b $\rightarrow$ a creates the nonperiodic sequence a $\rightarrow$ ab $\rightarrow$ aba $\rightarrow$ abaab $\rightarrow$ ... at an infinite number of steps. The structural units g (= b) ($MoPt_2$) and h (= a) ($TiAl_3$) of the Forsyth, Gran series e.g. vary in the sequence gh ($n = 2$) or gh_2 ($n = 3$) in Mn_2Au_5 or Mo_3Al_8 (Table 4). An aperiodic sequence of g and h units in the ratio $\tau = (1 + \sqrt{5})/2 \approx 1.62$ (e.g. hghhg at $n = 5$) would be possible at the compositions $Mn_{1.91}Au_5$ or

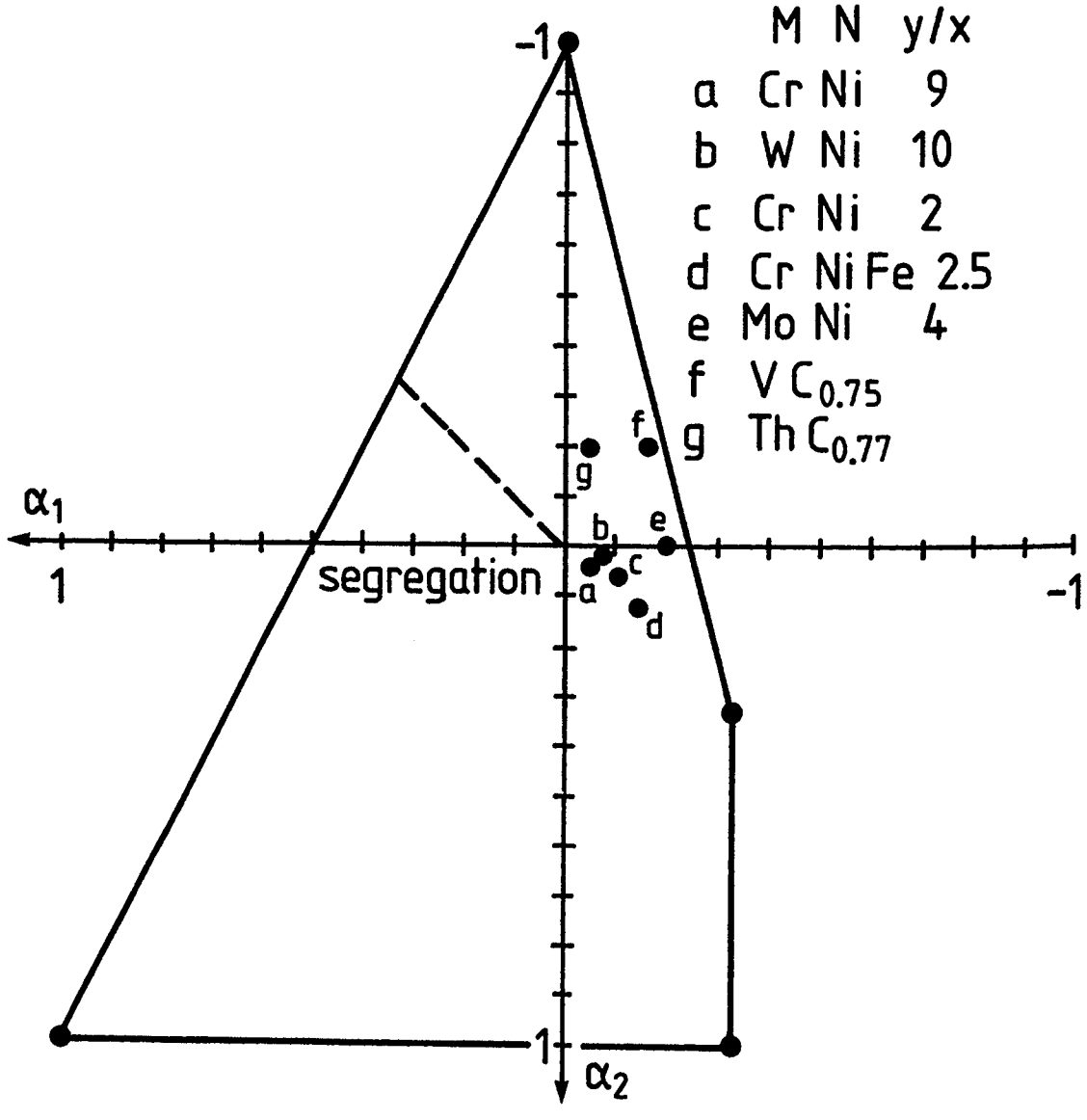

Figure 17: Experimental short-range order parameters α_1, α_2 of disordered alloys M_xN_y or $M_z\square_xC_y$ carbides within the ccp α_1, α_2 structure map.

$Mo_{3.06}Al_8$. The chain of g and h structural units has an infinite number of T_i values with an average of 0 0.76 1.24 ; τ, which is at the border of the structure map at $\alpha_2 = 0$ (Fig.2). The x-ray diagram would show the reflections of the g and h layers similar e.g. to the hexagonal layers of h and c stacking in a Fibonacci sequence with $hc_2/hc \approx 1.62$ (Table 1). The aperiodic sequence in c direction can be analyzed as in other one-dimensional Fibonacci sequences (Steurer, 1990). The two-dimensional Robinson tiling with a substitution

$$a \rightarrow \begin{matrix} a\ b \\ b\ b \end{matrix} \qquad \text{and} \qquad b \rightarrow \begin{matrix} b\ a \\ a\ a \end{matrix}$$

(Allouche and Salon, 1990) or an analogous three-dimensional tiling requires two different structural units, which can be combined two-dimensionally or three-dimensionally at common interfaces like the quasi-homologous square net structures 0 0 4 ; 3 and 0 4 4 ; 1 for a two-dimensional tiling (Section 28) or the quasi-homologous bcc structures 8 6 12 ; (1) (W) and 0 6 12 ; 1 (CsCl) for a two- or three-dimensional aperiodic tiling. The T_i values of the two-dimensional tiling of 0 0 4 ; 3 and 0 4 4 ; 1 approach the corner structure 0 8/3 10/3 ; 5/3 at the right-hand border of the structure map ($T_2 = -2T_1 + 2(3 - r)$) at $T_1 = 0$ (Fig.7a). The three-dimensional Robinson tiling $a \rightarrow [a\ b_7]$ and $b \rightarrow [b\ a_7]$ with $a =$ 8 6 12 ; (1) and $b =$ 0 6 12 ; 1 was solved up to $n = 7$. The density $r_\infty = 3$ follows exactly for each starting value m in the limit $n \rightarrow \infty$. For the square net the same recursion relation also holds for $T_2^{(n)}$ and $T_3^{(n)}$ with $m \geq 2$. Assuming the same behaviour for the bcc series, where the limiting values $T_i^{(\infty)}$ follow only approximately from the starting value m, we obtained with $m = 7$ the values $T_2^{(\infty)} = 4.0005$, $T_3^{(\infty)} = 7.5015$. From this result we conclude, that with $m \rightarrow \infty$ the exact $T_i^{(\infty)}$ values are given by 0 4 7.5 ; 3.

Some structures are known, where structural units of different lattices like bcc and fcc lattices with the proper interface are combined. Structural units can probably also be combined in such a way that fivefold or eightfold symmetry is achieved. The T_i values of these combinations can not be analyzed in T_1, T_2 structure maps as the theoretical examples outlined before.

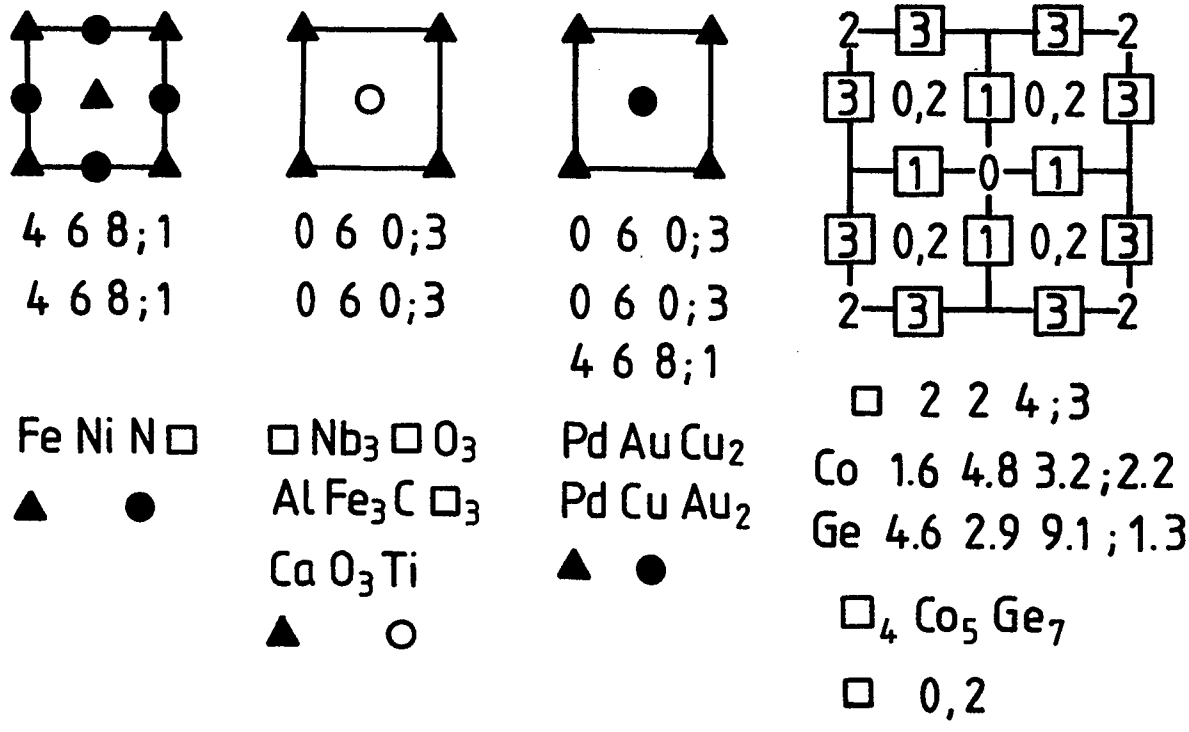

Figure 18: Ternary and quaternary compounds with T_1 T_2 T_3;y/x of different components with composition y/x. Only positions of minority elements are plotted, full and open symbols for elements at projection height z = 0 and 0.5, respectively, or as multiples of $a_0/4$ in cubic Co_5Ge_7.

14 Ordered ternary and quaternary compounds

Most of the observed binary hcp and ccp M_xN_y compounds have two sets of T_i values, which are identical at concentration y/x = 1. Other compounds with three or four sets of T_i values ($M^i = 3$ or 4) (Tables 3,4) are potential candidates for ternary or quaternary alloys. Few ternary and quaternary ordered alloys with close-packed metal structures are known (Fig.18). Alloys with the composition $M_{x_1}M_{x_2}N_y$, $M_{x_1}M_{x_2}M_{x_3}N_y$, $x_j \leq y$ can be described by the self-coordination numbers T_i of the minority components M_{x_j}. There are three sets of T_i values for ternary and four sets for quaternary alloys. The α_1, α_2 values are identical for the 4 6 8;1 or 0 6 0;3 derivative structures (homologous structures) or on the border of the structure map as e.g. for ReAl(Re,Al)$_2$ (Table 8) (quasi-homologous structures). The T_i values of all M_{x_j} can be averaged according to the frequency of their occurrence. The combination of two

values indicates the interactions between both atoms. The combination of the 0 6 0 ; 3 positions of Pd and Au atoms in $PdAuCu_2$ for example yields the same value 4 6 8 ; 1 as the Cu atoms.

The T_i values of the vacancies □ and the Ge atoms of $□_4Co_5Ge_7$ are not on the border of the structure map because of partial disorder. Other alloys forming solid solutions like the binary $CrNi_2$ or the ternary $CrNiFe_{2.5}$ are listed in the Cu structure type (Villars and Calvert, 1986) with a single environment of metal atoms, though the short-range order parameters are different from $\alpha_i = 0$ (Fig.17). Metals with similar radii and electronegativity can also substitute for one component of an ordered binary alloy. Such ternary alloys have been investigated frequently to vary the structure of metals of binary alloys in small steps:

(i) The stacking sequences 7c or 14 instead of 4 ($TiNi_3$) or 9a ($BaPb_3$) were obtained by variation of the Ti–Pt–Ni and Ba–Pb–Tl compositions (Table 5).

(ii) Structures with a different sequence of structural units were obtained e.g. in $(Zr,Al)(Si,Al)_2$ (Schubert, 1964) with uu'x'vv'y' ↑ compared to $ZrSi_2$ (Fig.12) with uu'y' ↑.

(iii) Homologous structures with identical environment of all atoms at different compositions (Table 6) can be filled up with different atoms. The Pd and Au atoms e.g. of $PdAuCu_2$ (Fig.18) have the 0 6 0 ; 3 coordination of the $AuCu_3$ structure. Both Pd and Au atoms together and the two Cu atoms together exhibit the 4 6 8 ; 1 configuration of the CuAu structure. The $MoNi_4$ structure is a potential candidate for a quaternary compound $MoMNNi_2$ at the proper substitution of two Ni atoms by M and N atoms (Table 6).

(iv) Some alloys as e.g. $RhZr_3$ ($AuCu_3$ structure) become unstable on hydrogen loading and segregate or become amorphous (Bowman, 1988).

(v) Other structures, which are unstable as pure alloys, can be stabilized by interstitial atoms, e.g. $AlFe_3$ with the $AuCu_3$ structure in $AlFe_3C$ (Fig.18). Among the 139 known compounds with this structure

(Villars and Calvert, 1986) there are many alloys which are not stable without the presence of interstitial atoms. The atoms of the $AlFe_3C$ structure have the same positions as the atoms of the CaO_3Ti perovskite structure with oxygen atoms at the Fe positions. The sublattice of the metal atoms Ca and Ti in $CaTiO_3$, however, is body-centered with oxygen atoms at the octahedral interstices.

(vi) The crystal structures of some alloys can be varied by insertion of interstitial atoms. The ccp $ZrAl_3$ structure e.g. of $MnPd_3$ (Flanagan et al., 1992) changes to the $AuCu_3$ structure in $MnPd_3H\square_3$, which is isotypic with $AlFe_3C\square_3$ (Fig.18).

If, however, the properties of the three or more components are too different or the concentration of the substituting component is too high, then the alloys become unstable and favor structures without close-packing. As we pointed out in Section 2, close-packing can be expected for identical atoms or at least similar atoms with weak directional bonding and is not likely to be found in a child's drawer containing a collection of differently sized balls.

15 Enhanced covalent bonding in layered compounds and ordered body-centered alloys

A well-defined collection of balls with increasing diameter like golf, table tennis and tennis balls M, N and R can be assembled to layered structures, which are similar to close-packed alloys (Fig.19). Many compounds $M_xN_yR_z$ can be described by sequences of M, N and R layers, which are similar to the close-packed metals (Section 2), but with reduced distances between neighboring layers (Parthé et al., 1993). The hexagonal unit cell with lattice constant $a = b = d$ (diameter of R atoms) has the height $c = n\sqrt{2/3}d$ for n close-packed layers. The distance between two neighboring layers, which is $\sqrt{2/3} \approx 0.8$ for close-packing with $c/a = n\sqrt{2/3}$, decreases to 0.2 – 0.8 for atoms M and N with smaller size and different bond strength M–R or N–R between the atoms of neighbor-

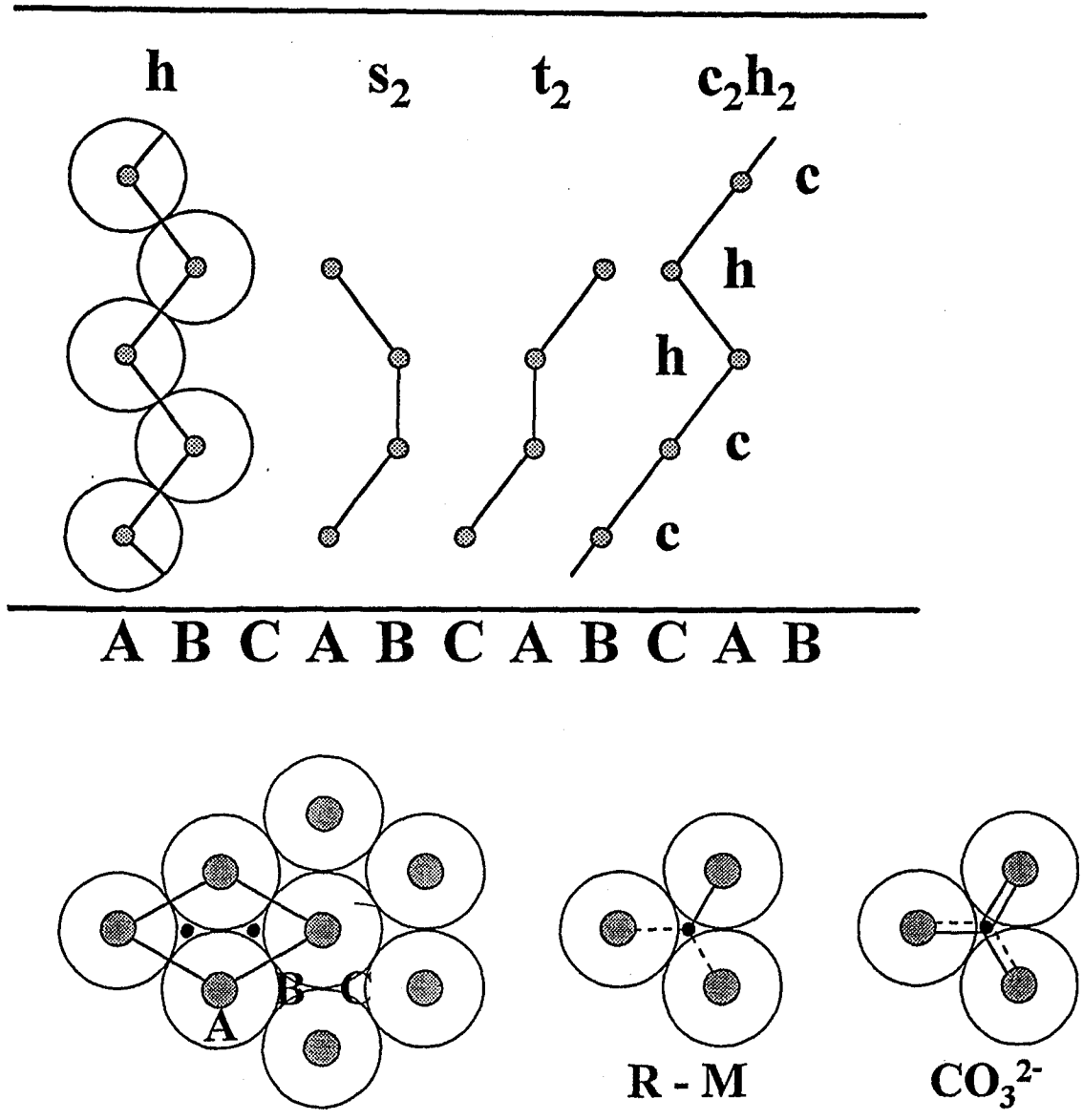

Figure 19: Close-packed hexagonal layer of spheres in A position, unit cell ([001] projection, below) and B or C position of consecutive layers as e.g. ABAB (hh) or BCAC (c_2h_2), (A)BB(A) (s_2) and (C)AA(B) (t_2) as explained in the text ([110] projection, above). The single R–M bond is delocalized to three neighbors similar to CO_3^{2-} (below).

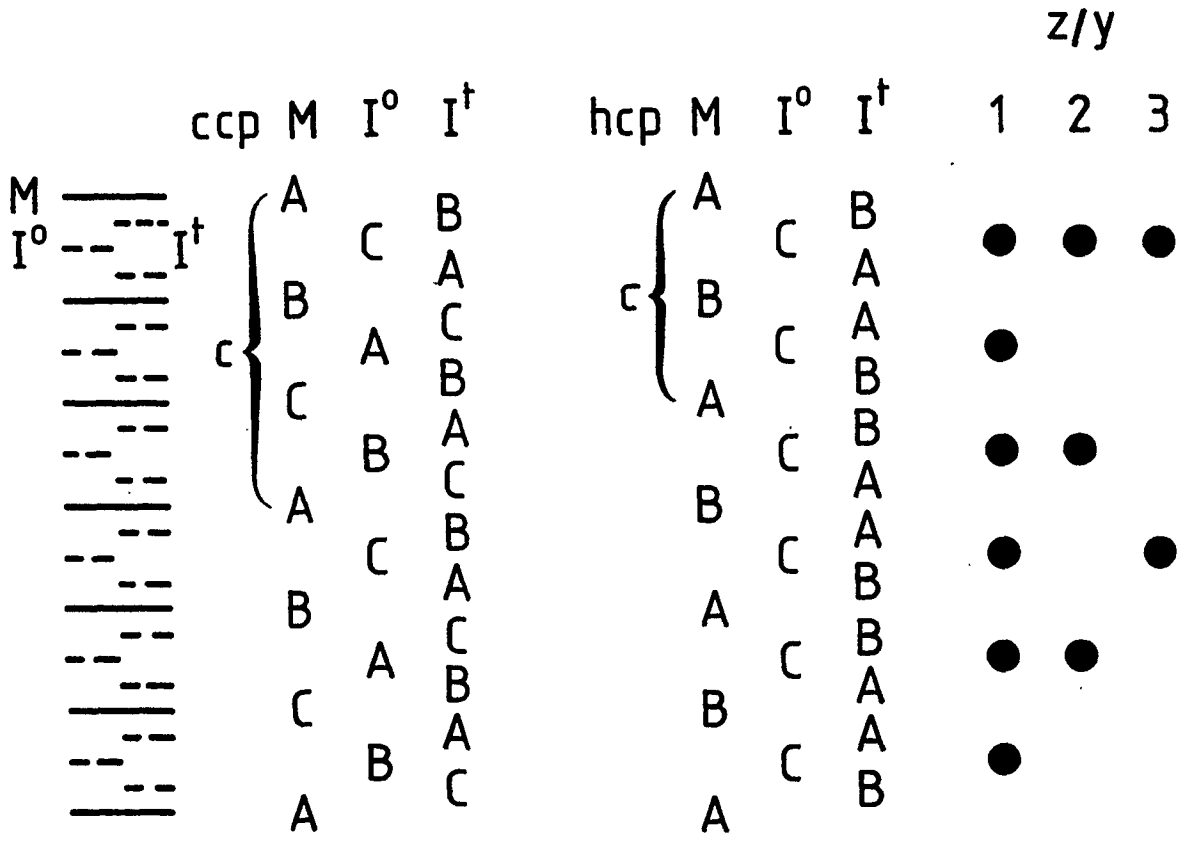

Figure 20: Position of interstitial atoms I^o and I^t in octahedral and tetrahedral sites of the ABC ccp or AB hcp M lattice. Only 1/2 or 1/3 (for ε-Ni_3C) of the octahedral sites I^o at identical positions in c direction of the hcp M lattice are occupied at z/y = 2 or 3, respectively.

ing layers (Table 7). Some compounds like $SnSb_2Te_4$ can be described by a sequence TeSbTeSnTeSbTe of large atoms R = Te, which are approximately close-packed, and smaller atoms M = Sn and N = Sb at octahedral interstices. The hexagonal unit cell with $n = m{\cdot}p$ ($7 \cdot 3 = 21$) layers contains $p = 3$ formula units ($SnSb_2Te_4$) with $m = 7$ atoms. The distance between Sb and Te or Sn and Te layers $\Delta z\, c/a$ is reduced to $\approx$ 0.4. These compounds are usually described by the stacking of R atoms and by sequences of Greek or lower case letters for M and N atoms at tetrahedral or octahedral positions (Hulliger, 1976; Parthé et al., 1993) (Fig.20). The approximate structure can be characterized by two strings in Table 7, if the locations of all M, N and R atoms are characterized by h, c, s or t symbols. The s_2 and t_2 groups with two atoms at the same positions (at different projection height) are defined similar to the h and c symbols (Section 2): The *trans* (or t_2) configuration for different

positions of the neighbors next to t_2 and the *cis* (or s_2) configuration at identical positions (Fig.19). In that case the different coordinations of M in a sequence of RMR atoms can be obtained by the symbol (c = octahedral, h = trigonal prismatic, t or s = tetrahedral) and structures with the same sequence of R and M atoms can be compared by the different coordinations of M atoms or – with other words – the different configurations of the chain (Table 7). The alternative description by sequences of A, B and C positions is not specific and in many cases longer by a factor $p = 2$ or 3 than the present notation as was shown before for the $(ch)_2$ α-Nd, $(hc_2)_2$ Tb HP and $(ch_2)_3$ α-Sm structures (Table 1). These stackings with $M^i = 2$ sets of T_i values (Section 3) are observed in NiAs (ch), NbS_2 (hc_2) and $CdCl_2$ (ch_2) structures at decreased $\Delta z\, c/a$ (I form). Other more complex stackings like $hchc_4$, c_3h_4 or $ch_2c_2h_2$ for MN_2R_4 composition, $chch_3$ (MN_2R_3), hc_3, h_2c_6 or ch_2chc_2h (MNR_2) are not observed for these compositions. Most stackings and layer sequences like TeSbTeSnTeSbTe are symmetric. Some structures like TaS_2 6s with ch_2c_3 stacking can be considered as a combination of ch_2 (MoS_2 3R) and c_3 (CdI_2 C6). Few compounds like ZnS or SiC can occur in many different structures (polytypes), which can be described in series of stackings like $(hc_2)_{2n+1}hc$ or $(hc_2)_{2n+1}hc_3$ at consideration of R = S, C atom packing (Parthé et al., 1993) or $(s_2t_4)_{2n+1}s_2t_2$ and $(s_2t_4)_{2n+1}s_2t_6$ in the present notation (h = s_2, c = t_2). The combinations of ab_2 and ab or ab_3 (h = a, b = c) structural units are approaching point a_2b_4 for s_2t_4 or ab_2 for the hc_2 composition (S) of the structure map (Fig.2b) at large n.

Some structures of ordered ccp alloys like CuAu can be described by sequences of Cu and Au square layers, which are packed in [001] direction (Figs. 3,21). The distance between neighboring layers of spheres with diameter d, $\Delta z\, c/d = \sqrt{2}/2 \approx 0.71$ is reduced to $1/\sqrt{3} \approx 0.58$ in some ordered bcc alloys, or increased to $\Delta z\, c/d = 1$ in the primitive cubic lattice of Po, disordered alloys like $AuBi_4$ or $AuTe_3$ (Villars and Calvert, 1986) and CaF_2 related structures (Section 18, Table 8). The sequences of layers are characterized by the letters V, v or I according to the configurations with the shape of the letter V or v in fcc or bcc and I in the primitive cubic lattice of Po (Galasso, 1970) and the related structures of As, Sb, Bi, Se and Te (Hyde and Andersson, 1989; Burdett, 1995). The I′, i′ or v′ configurations are important for the occupation of octahedral

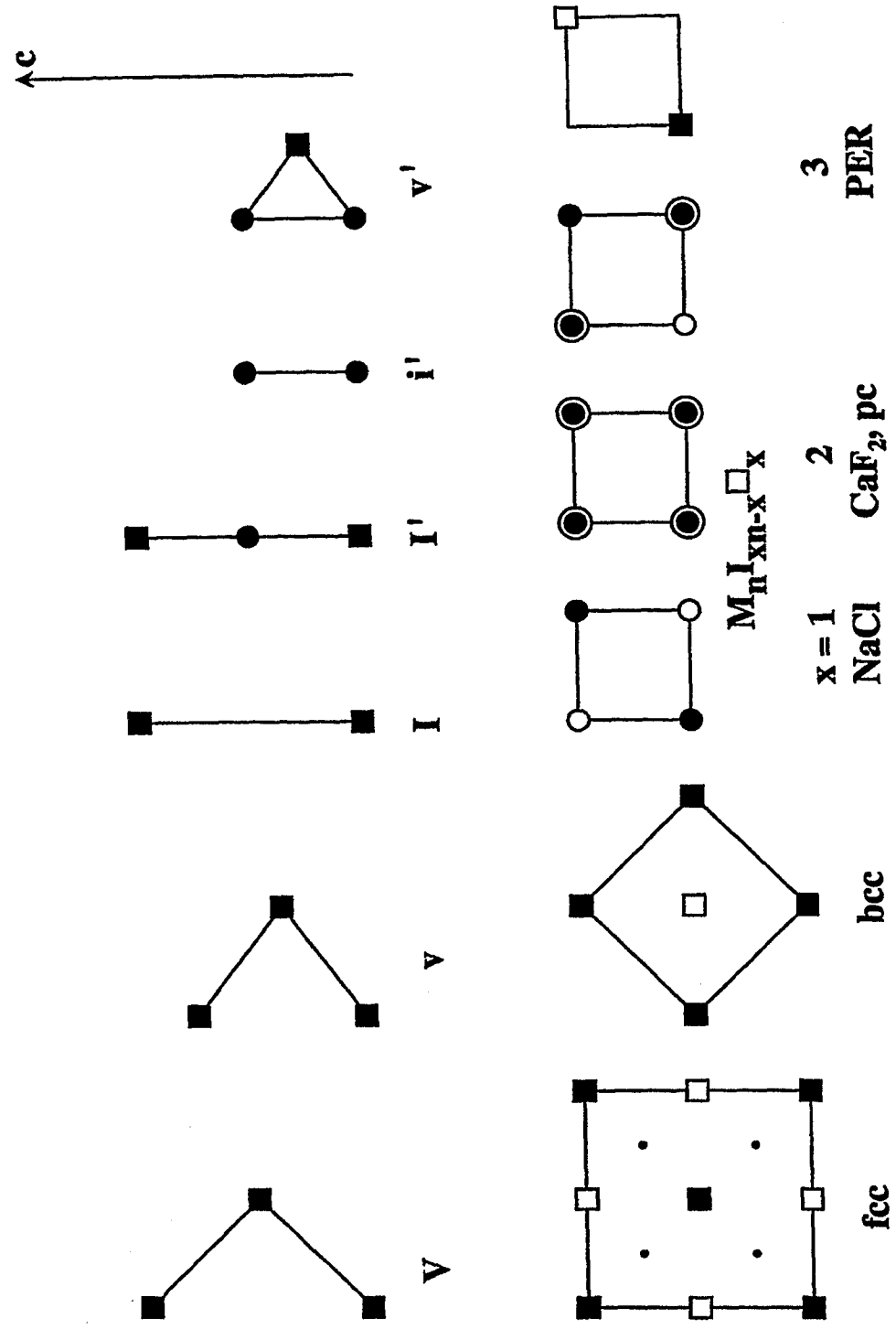

Figure 21: [001] projection of fcc, bcc metal lattices and interstitial alloys $M_nI_{xn-x}\square_x$ with metal atoms at 0 (■) or 0.5 (□) and I atoms at 0 (•) or 0.5 (○). The F atoms of CaF_2 form a primitive cubic (pc) lattice, which are at projection height 0.25 and 0.75 (⊙) of the fcc Ca lattice at the positions (·). The square layers are stacked in c direction in V (fcc), v (bcc), I (pc), I′ (NaCl), i′ and v′ (pc and PER) configurations.

or tetrahedral sites with interstitial I atoms in compounds $M_nI_{xn-x}\square_x$ (Section 18).

Most ordered bcc alloys can be characterized by sequences of layers in [001] or [111] direction (Tables 7,8), which are named by the pioneers, who investigated the structures of the first examples: Au_2Nb_3, Ti_2Cu_3 and Ti_3Cu_4 of the Schubert series (Schubert et al., 1960), and Pb_2Li_7 and Pb_3Li_8 of the Zalkin, Ramsey (1956) series. The structures of the Schubert series can be described by the sequences of metal atoms in [001] direction like MoSiSi (= b) for $MoSi_2$, Ti_2Cu_2 (= d) for the TiCu and $TiCu_2Ti_2Cu_2$ (= bd) for Ti_3Cu_4. The structures of the Zalkin, Ramsey series can be described by sequences of metal atoms in [111] direction like CeCdCd (= k) for $CeCd_2$, AlFeFeFe (= l) for $AlFe_3$ and $PbLi_3PbLi_2PbLi_3$ (= lkl) for Pb_3Li_8. Structures with long sequences of structural units like Pb_3Li_8 (lkl) or clustering like TiCu (Ti_2Cu_2) can segregate to 2 $PbLi_3$ (l) + $PbLi_2$ (k) or Ti + Cu (Section 19).

16 Enhanced repulsive interactions

The following structures with minimum T_1 and maximum T_2 values are obtained at repulsive interactions: 4 6 8 ; 1 of ccp CuAu and 0 6 12 ; 1 of bcc CsCl. The compounds contain alternating square layers of Cu and Au or Cs and Cl atoms, respectively. Vacancies or atoms of neighboring layers are inserted at repulsive interactions between M and N atoms. Part of the M atoms of CsCl (MN) for example are substituted by N atoms in [001] layers with composition MN and N_2 of neighboring layers of the $(Mo,U)U_3$ structure or M_2N_2 and N_4 layers of the $Au(Zn,Au)_3$ structure (Table 9a). Other CsCl related structures like Pu_3Pd_4 or $Zn_3Ga_4Pd_7$ can be described by different [111] layers with composition Pu_6Pd and Pd_7 or Zn_3Ga_4 and Pd_7 (Table 9b). Examples of ordered ccp alloys are $GeCa_7$ with $GeCa_3$ and Ca_4 layers or Ga_3Pt_5 with $PtGa_3$ and Pt_4 layers (Table 9a). The hcp structures $SbAg_3$ or $SnAu_5$ contain layers of SbAg and Ag_2 or $SnAu_2$ and Au_3. These structures indicate little repulsive interactions for Pd, Pt, Ag, Au or Ca atoms.

All other structures of Table 9 are characterized by identical composition y/x of the layers and the three-dimensional alloy structure. The stacking of the layers can be described by the translation x, y and z of the minority component like the translation in x direction in the 2 2 12;2a ($MoPt_2$) structure or the three different translations x, y and z in the homometric 2 2 12;2b structure (Fig.13). The homometric hcp 2 2 0;2a,b structures can be described by the stacking of the 0 6 0;2 MN_2 layers with translations $x\bar{y}$ (2 2 0;2a) or $x\bar{z}y\bar{x}z\bar{y}$ (2 2 0;2b). The stacking of the 2 0 4;1 square layers of homometric ccp CuPt,a and b can be described in a similar way by the translations yyxx in 6 0 12;1a and yyyy in 6 0 12;1b. The number of nearest and next-nearest neighbors in the layers can be visualized by the density of lines in different patterns (Section 28).

17 Valence compounds

In non-metallic valence compounds $M_xN_yR_z$ the number of electrons at the atoms can be completed to octets, if the sum of electrons of M, N and R atoms is eight or a multiple of eight (Parthé et al., 1993; Parthé, 1994; Ellner and Predel, 1994; Villars, 1994):

$$x\,e_M + y\,e_N + z\,e_R = 8z.$$

This equation satisfies the requirement of electroneutrality and can be applied for different distributions of valence electrons e.g. in ZnS (Table 10):

(a) Formation of Zn^{2+} and S^{2-} ions (ionic chain).

(b) The eight electrons (four pairs) form four bonds to Zn atoms in tetrahedral coordination (Parthé et al., 1993; Hauck and Mika, 1998b).

(c) The electrons are shared between neutral S and Zn atoms with two covalent bonds (covalent chain).

Each atom in a close-packed layered compound has three neighbors in the next layer (1 + 3 for tetrahedral t_2 or s_2 configuration) (Fig.19). One bond of –S–Zn– with S in t or s position is delocalized to three Zn atoms. Therefore these bonds are weaker than the remaining bond. The delocalization of the double bond of the S=Zn group enhances the bond strength to three neighbors (= 2/3) compared to the fourth neighbor without bond. The same bond strength 1/3 + 2/3 or 1 + 0 for all Zn atoms is achieved at a consideration of both formulas –S–Zn–S– and S=Zn. The structural data show positive or negative deviations. Equal bonding to all neighboring atoms as in (b) is also achieved for the three M atoms in octahedral or trigonal prismatic coordination, if the chain is symmetric like in –S–Mg– or at consideration of resonance hybrids e.g. of Cu I–Cu and Cu–I Cu or Mg S=Mg and Mg=S Mg. The covalent chain (c) allows close-packed layers of neutral atoms in the [001] plane and different sequences of M, N and R atoms in [110], that can explain the ordering of these atoms in most structures.

Table 10 shows the different combinations for binary and ternary compounds. The R and M atoms usually alternate until an M atom is missing, which is indicated by $e_M = 0$ (Hauck and Mika, 1998b). Therefore chains of RMR occur in 0 2 7_2, (0 6 1_2), 0 4 6_2 and (0 4 2_2) compounds and chains with three or four R atoms in the remaining structures containing 0. The (0 6 1_2) or (0 4 2_2) structures are antistructures to 0 2 7_2 or 0 4 6_2 with $e_N + e_{N'} = 8n$ or $e_R + e_{R'} = 8n$ (Parthé et al., 1993). In normal valence compounds M_xR_z without M–M or R–R bonding the number of bonds pointing to each M or R atom is proportional to the number of R or M atoms (z or x). The R=M–R–M=R chain of M_2R_3 compositions is obtained for divalent R and trivalent M (tetravalent R and hexavalent M must not be considered). The M_3R_4 composition yields the largest chain with three tetravalent M atoms. In ternary compounds the length of the chains is extended, if 2 6 groups are introduced in the 0 3_2 6_3 chain or 3 5 groups in the 0 4_3 5_4 chain at the single bond position. Table 7 shows many experimental examples of $RN(RM)_nRNR$ and $RN(RM)_n$ $RNR(MR)_mNR$ chains. The last example with two different possibilities for the introduction of –N=Al– groups was only observed for the antistructures with composition $N_xC_3Al_{4+x}$ (x = 0 – 4). The chains are symmetrical for x = 2 and 4.

Another theoretical approach is the combination of different chains like S=Zn S=In–S–In=S in $ZnIn_2S_4$ modifications or Te=Bi–Te–Ge–Te–Bi= Te Te=Bi–Te–Bi=Te in $GeBi_4Te_7$ with divalent Ge (Parthé et al., 1993) (Table 7). Layered compounds containing monovalent elements in the composition $1\,4_2\,5_3$, $1_2\,4\,6_3$ or $1\,3\,6_2$ like α-$NaFeO_2$ with a shared single bond Na–O–Fe=O$\cdots$Na–O–Fe=O similar to a =O$\cdots$H–O– hydrogen bond are rare.

Some compounds with trivalent Ga and In contain $\approx$ 30% vacancies at the M′ or N′ positions (Table 7). In that case about one of the three M or N atoms in the neighboring layers is missing and the average of charge of M′ or N′ atoms is reduced to $\approx$ 2. This can explain the occurrence of vacancies in some cases as e.g. the first Ga′ and the Ga″ position in $(Ga,In)_{3-x}InS_5$ with S=Ga′ S=In–S–Ga″–S–Ga′=S ($Ga' = Ga_{0.50}In_{0.17}$, $Ga'' = Ga_{0.67}$). A second formulation S=Ga′ S=In–S–Ga″=S Ga′=S with equivalent Ga′ positions requires no vacancies in Ga″ position. The $(In,Ga)_{4.67}S_7$ and $(In,Ga)_{7.33}S_{11}$ compounds contain R–M–R–M–R units of the In_2S_3 structure with hc_3h stacking, but $\approx$ 0.2 additional M atoms next to the R atoms at the end of the chain (Parthé et al., 1993) (the Pearson symbols are *hP*14 and *hR*72 instead of *hP*12 and *hR*57). The vacancies are probably disordered within the layers. Additional reflections would be observed for ordered layers similar as for structures discussed in Section 16.

The last group of Table 7 considers general valence compounds. These are valence compounds where either the cations do not transfer all their valence electrons – they are used for bonds between them or for non-bonding orbitals – or where the anions due to bonds between themselves do not need as many electrons to complete their octet shell (Parthé et al., 1993). For a compound M_xR_z with

$$x\,(e_M - e_{MM}) + z\,(e_R + e_{RR}) = 8z$$

the average number of remaining valence electrons e_{MM} and e_{RR} at M or R atoms can be used to M–M or R–R bonds, respectively as for Cl–Zr≡Zr–Cl, Te=Pt=Pt=Te or S=Ga–Ga=S in ZrCl, PtTe or GaS and GaSe structures. Bi_2Te_3 II (–Bi=Bi–Te–Te–Te–) and the hexagonal structures of Se and Te mentioned before are examples for –Se–Se– or

–Te–Te– bonding. The Pt_3Te_4 and Pt_2Te_3 structures can be considered as combinations of Te=Pt=Pt=Te and Te=Pt=Te chains. Pt and Zr are supposed to be tetravalent, though they do not belong to the elements considered for valence compounds (Parthé et al., 1993). These atoms with lone electron pairs or low electronegativity (Mg, Zr) given in brackets (Table 10b) are ordered for increasing size (Schubert, 1967). The Zn, Al, Ga and N atoms underlined in Table 10b prefer tetrahedral sites. Divalent Mn, trivalent Fe or In and tetravalent C (bold face) are observed in tetrahedral or octahedral coordination. Besides this some ordered alloys like LiRh, CuPt, Pt_2Sn_3 and some metallic carbides or nitrides like Ta_2C or Th_3N_4 (which are not valence compounds) are also listed in Table 7 because of related structures. The distance between layers $\Delta z\, c/a \approx 0.8$ is normal (N form) in the close-packed metals, decreased to 0.2 – 0.8 at occupation of interstitial sites (I form) or to $\approx$ 0.2 in ordered body-centered alloys (B form). B_4Rh_5 with the sequence RMRMRMRMRMR (Parthé et al., 1993) not allowed in the present scheme is omitted in Table 7. The distance $\Delta z\, c/a$ (at $p = 1$, $z = 1$) between neighboring layers usually corresponds with the bond strength. The distances between Th and N layers e.g. of Th_3N_4 (N≡Th–N=Th=N–Th≡N sequence) are 0.51 (Th–N), 0.31 (Th=N), 0.12 (Th≡N) and 0.49 (N to N of next chain).

18 Occupation of interstitial sites

Compounds with the composition $M_nI_{xn-x}\square_x$, x = 1, 2, 3, can be considered as interstitial alloys, where I = H, C, N, Cl, O, ... atoms occupy interstitial sites like the octahedral or tetrahedral interstices of the ccp lattice of M atoms (Fig.20). All octahedral interstices are filled in NaCl, all tetrahedral interstices in the CaF_2 structure. The NaCl structure is also obtained from the primitive cubic structure (pc), if four corners of the cube are occupied by Na atoms and the remaining four by Cl atoms (Fig.21). The occupation of two positions of the pc lattice by M atoms and the remaining six positions by I atoms yields M_2I_6 or $M_nI_{3n-3}\square_3$ like the perovskite structure $CaTiO_3\square_3$ with vacancies at I positions (PER group). Most superconducting oxides are in this group (Hauck and Mika,

1997).

The undistorted $M_nI_{xn-x}\square_x$ structures can be characterized by the coordination numbers CN of M atoms with I atoms (Fig.22). The CN = 6 (octahedral) coordination of 6 Cl atoms next to each Na atom is reduced, if some I positions are vacant like CN = 3 for Pd in $Pd_2H\square$ (Fig.23a) (Table 11a). The CN = 8 (cubic) coordination of Ca in CaF_2 (pc lattice of F atoms) and the CN = 18 coordination of the M atoms in the PER group are reduced in a similar way. Most compounds can be described by sequences of CN values for sequences of M atoms in [001] (PER group) or [110] direction (NaCl or CaF_2 group). Most sequences of the PER group are symmetrical like CN = 4 10 5 8 5 10, 4 for the sequence Cu'BaCuY'CuBa,Cu' in $YBa_2Cu_3O_7$. The formula $Cu'Ba_2Cu_2Y'O_7$ or CN = 4 10_2 5_2 8 used in the present investigation indicates the sequence of metal atoms with single Cu' and Y' atoms at mirror planes and two Ba and Cu atoms between the mirror planes. The ordering of metal atoms in superconducting oxides corresponds to the [001] series of bcc alloys like $CuLa_2O_4$ or $Cu_2La_3O_7$ with $MoSi_2$ or Os_2Al_3 structure (Table 8) of Cu and La atoms (Fig.23b). The sum of all CN values corresponds to 6y of the total oxygen content like $6 \cdot 7 = 42$ in $Cu'Ba_2Cu_2Y'O_7$ (y = 7) because of the six M–O bonds of each oxygen atom. The same applies for Σ CN = 6y in the NaCl group and Σ CN = 4y for the CaF_2 group.

The three series $M_nI_{xn-x}\square_x$, x = 1, 2, 3, can be compared for example for I = oxygen atoms. The composition of the compounds can be obtained by the proper mixture of MO, $MO_{1.5}$ and $MO_{0.5}$ (NaCl group) or MO_2 (pc and PER group) (Fig.24). There are closely related compounds with composition $M_nO_x\square_{xn-x}$ of the PER' and pc' group with the oxygen atoms as minority component like $CuSr_2O_3\square_6$ (PER') and the Aurivillius phase $WBi_2O_6\square_3$ (3 MO_2) of the PER group or $Cu_2O\square_3$ (pc') and $(Fe, Mn)_2O_3\square$ of the pc group with vacancies as minority component. Less than half of the M atoms of the PER group should have CN $\leq$ 6 like the Cu and Cu' atoms in $Cu'Ba_2Cu_2Y'O_7$ (CN 4 10_2 5_2 8) or the W atom in WBi_2O_6 (CN 6 $12'_2$). The valency of the atoms with CN $\leq$ 6 is q = 4 – 6 in the Aurivillius phases and q = 2 – 3 (formal valency) in compounds of the PER' group because of the formation of stable compounds with perovskite structure like $CaTiO_3$ (CN 12 6) instead of

Figure 22: Coordination numbers of Ca in CaF_2 or $CaTiO_3$, Na in NaCl and in related compounds containing vacancies.

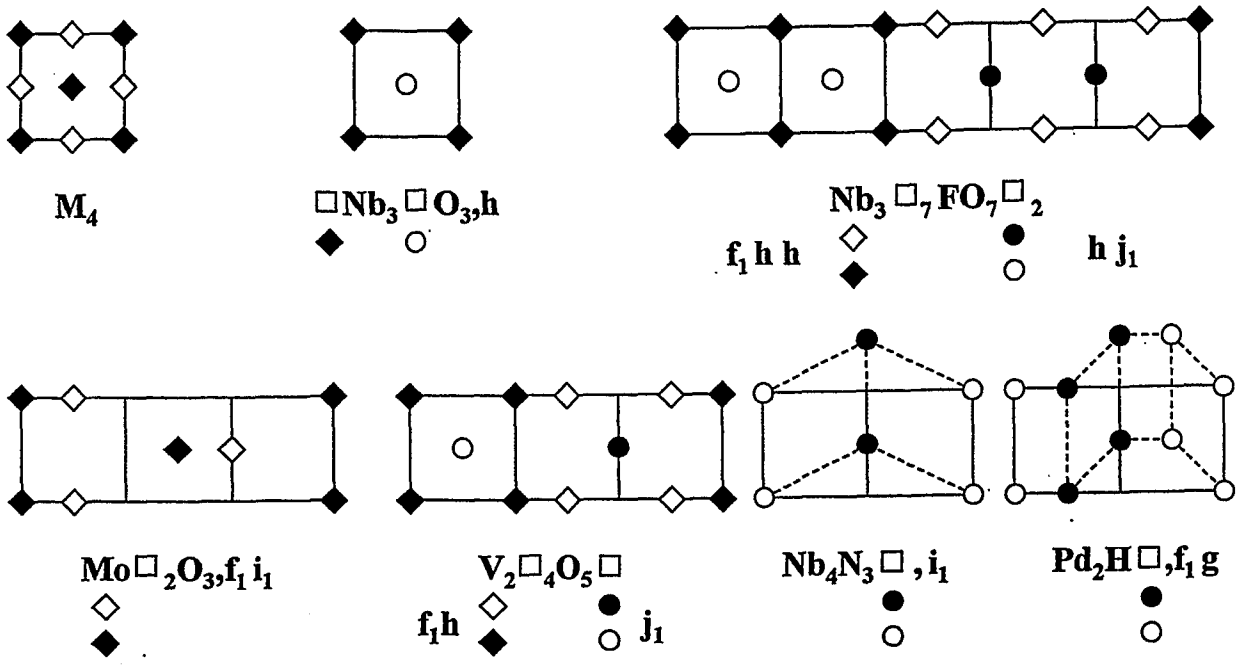

Figure 23: Projection of NaCl (MI) related structures with M atoms at 0 (◆), 0.5 (◇) and I atoms or vacancies □ at 0 (•) or 0.5 (o) (a) and $CaTiO_3$ related structures (b) (next page) with different structural units and different metal atoms (ordered bcc lattice).

layered compounds. Structures with more than 8 M atoms/formula unit usually contain sequences of M atoms with CN = 12 6, 6′ or 8 4 (underlined in Table 12), which can form compounds with $CaTiO_3$, SrO or (Ca,Sr)CuO_2 structure. Many compounds with more than 8 M atoms are difficult to synthesize because of the stability of the $CaTiO_3$, SrO and (Ca,Sr)CuO_2 structure. The other compounds are obtained from 8 different mixtures of M^{3+} = Y, La, Tl, Bi, ..., N^{2+} = Ca, Sr, Ba and Cu: $M_{n'}O_x$, $n' + 1 \leq x \leq 4/3n'$, $3 \leq n' \leq 8$ with 50% or less Cu atoms. The number n' of M atoms/formula unit $M_{n'}O_{n'+1}$ or $M_{n'}O_{n'+2}$ can be obtained from $n' = n/(3-n)$.

The I atoms and vacancy positions of the NaCl group of structures exhibit a ccp lattice. Therefore the undistorted structures can be compared with the alloy structures (Tables 4,11a). The ordering of C atoms in $Gd_2C\square$ or $Ti_2C\square$ corresponds to the ordering of Cu atoms in CuPt,a or b, respectively. The metal atoms of α-$NaFeO_2$ and $LiTbS_2$ occupy the same positions as the Cu and Pt atoms (Table 12). The same applies for $SrCrF_4$ (CuAu), $CuSr_2F_6$ ($CuZr_2$), $TiTe_3O_8$ ($AuCu_3$) and UNa_3F_8

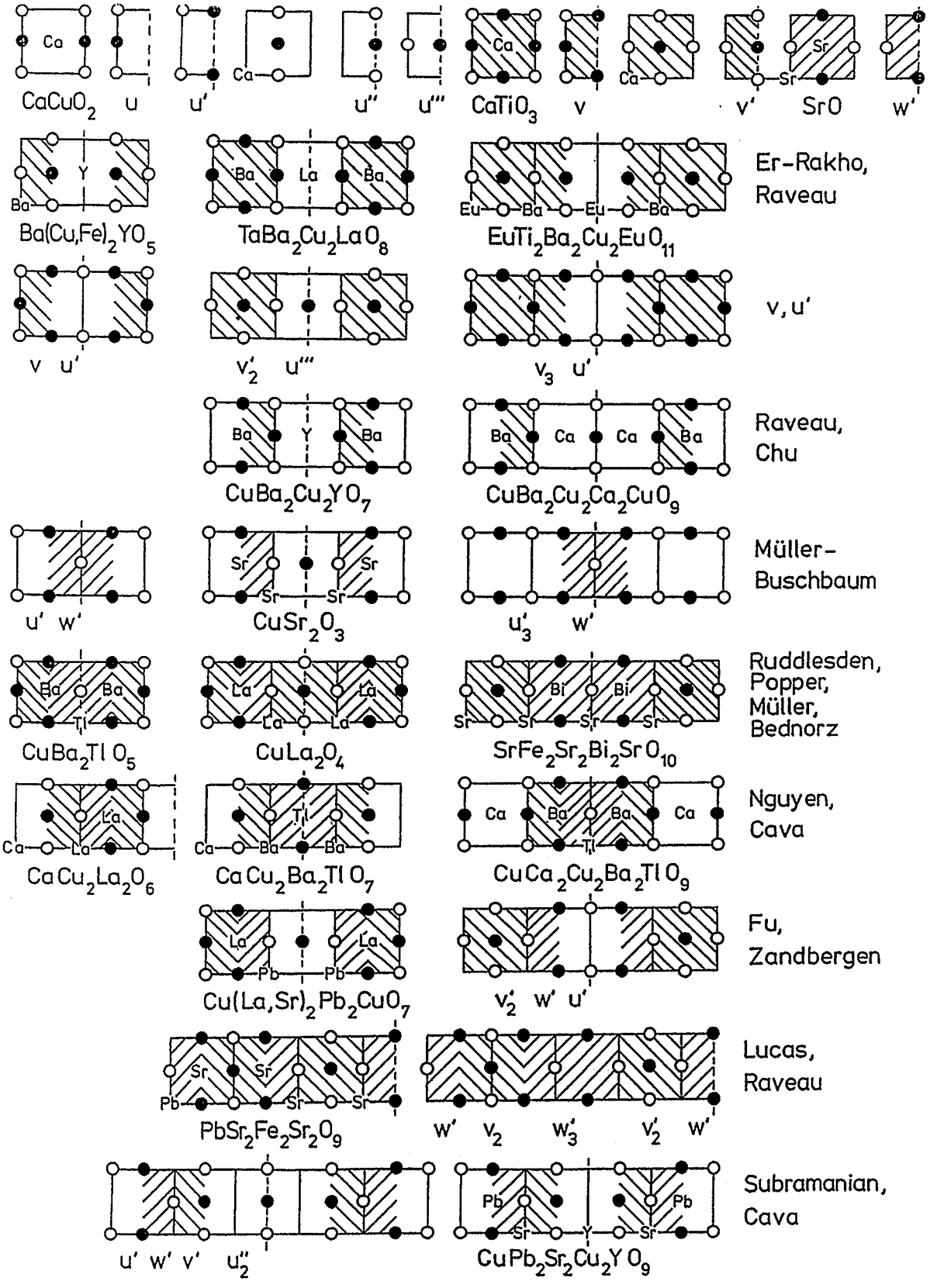
CaCuO2 u u' u'' u''' CaTiO3 v v' SrO w'
Ba(Cu,Fe)2YO5
TaBa2Cu2LaO8
EuTi2Ba2Cu2EuO11
Er-Rakho, Raveau
v u'
v'2 u'''
v3 u'
v, u'
CuBa2Cu2YO7
CuBa2Cu2Ca2CuO9
Raveau, Chu
u' w'
CuSr2O3
u'3 w'
Müller- Buschbaum
CuBa2TlO5
CuLa2O4
SrFe2Sr2Bi2SrO10
Ruddlesden, Popper, Müller, Bednorz
CaCu2La2O6
CaCu2Ba2TlO7
CuCa2Cu2Ba2TlO9
Nguyen, Cava
Cu(La,Sr)2Pb2CuO7
v'2 w' u'
Fu, Zandbergen
PbSr2Fe2Sr2O9
w' v2 w'3 v'2 w''
Lucas, Raveau
u' w' v' u''2
CuPb2Sr2Cu2YO9
Subramanian, Cava

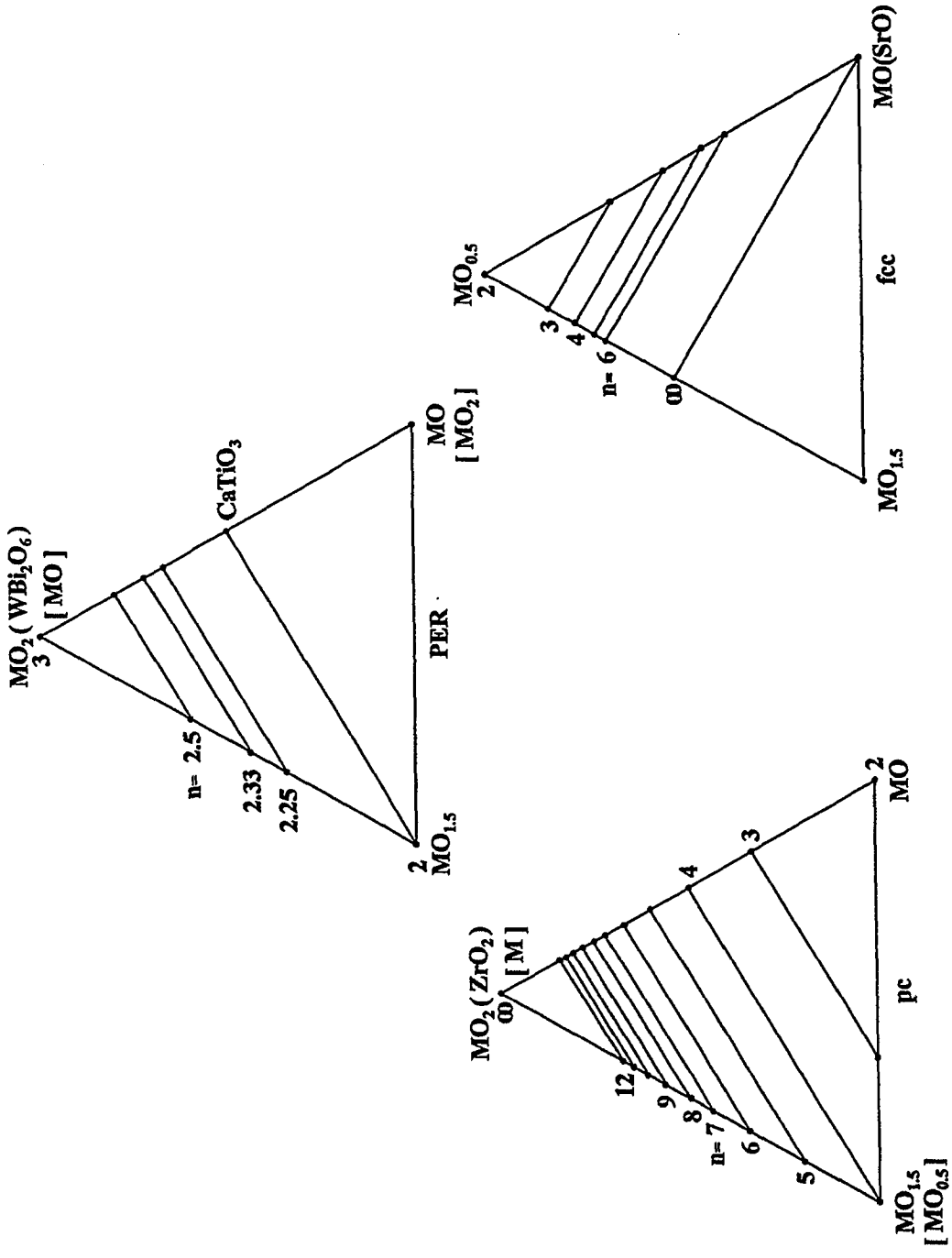

Figure 24: Pseudoternary phase diagrams of $M_nI_{xn-x}\square_x$ structures of the NaCl (x = 1), CaF_2 (x = 2) and PER group (x = 3) and different n values and related $M_nI_x\square_{xn-x}$ structures in brackets. The $n' = n/(3-n)$ values of superconducting oxides $M_{n'}O_{n'+1}$ and $M_{n'}O_{n'+2}$ can be obtained from the n values.

($TiAl_3$) (Wells, 1984). The F or O atoms at tetrahedral interstices have the pc lattice of the CaF_2 structure.

The three-dimensional structure maps for the PER group (Hauck and Mika, 1993) and the pc group contain different polyhedra at different r = y/x values. The four structures 6 12 8;(1), 4 4 0;1, 2 4 8;1 and 0 12 0;1 of the pc group are at the corners of a tetrahedron containing 4 planes and 6 edges. The points 6 12 8;(1), 4 4 0;1 and 0 12 0;1 remain in the T_1 T_2 T_3;r structure map at increased r = y/x values, while new corners occur forming different polyhedra:

range	C	P	C_4	C_5	C_6	C_7	C_8	C_9	C_{10}
$1 < r \leq 5/3$	9	8	7/2 3 0	3 3 0	3/2 3 6	3/2 3 8	0 9 0	0 9 2	
$5/3 < r < 3$	10	8	3 2 0	5/2 2 0	1 2 6	1 2 8	0 6 2	0 6 4	0 7 0
$r = 3$	6	6	2 0 0	0 4 0	0 0 8				
$3 < r < 7$	8	7	2 0 0	1 0 0	0 0 4	0 0 8	0 2 0		
$r \geq 7$	6	6	2 0 0	0 0 0	0 0 8				

The corners C_i at intermediate r values are chosen for r = 1.5, 2 and 5. The variations of the corners at intermediate r values can be expressed by the series

$$
\begin{array}{rcrcrcl}
4\,4\,0;1 & \rightarrow & 3.3\;2.7\;0;1.7 & \rightarrow & 2\,0\,0;r\ (r \geq 3), & & \\
4\,4\,0;1 & \rightarrow & 2.7\;2.7\;0;1.7 & \rightarrow & 2\,0\,0;r\ (r \geq 3) & \rightarrow & 0\,0\,0;r\ (r \geq 7), \\
2\,4\,8;1 & \rightarrow & 1.3\;2.7\;5.3;1.7 & \rightarrow & 0\,0\,8;r\ (r \geq 3), & & \\
2\,4\,8;1 & \rightarrow & 1.3\;2.7\;8;1.7 & \rightarrow & 0\,0\,8;r\ (r \geq 3) & \rightarrow & 0\,0\,0;r\ (r \geq 7), \\
0\;12\;0;1 & \rightarrow & 0\;8\;0;1.7 & \rightarrow & 0\,4\,0;3 & \rightarrow & 0\,0\,0;r\ (r \geq 7), \\
0\;12\;0;1 & \rightarrow & 0\;8\;2.7;1.7 & \rightarrow & 0\,0\,8;r\ (r \geq 3) & \rightarrow & 0\,0\,0;r\ (r \geq 7).
\end{array}
$$

The intermediate points depend linearly on r. The 0 0 8;3 structure forms a homologous series with the 2 4 8;1 and 4 8 8;0.33 structures at constant $\alpha_1 = \alpha_2 = -0.33$ and $\alpha_3 = 1$. The structure maps and structural units of the pc and PER group of structures are very similar (Figs. 25,26). Some structural units like α and β are not possible in the PER group because of the metal atoms at I positions. Other structural

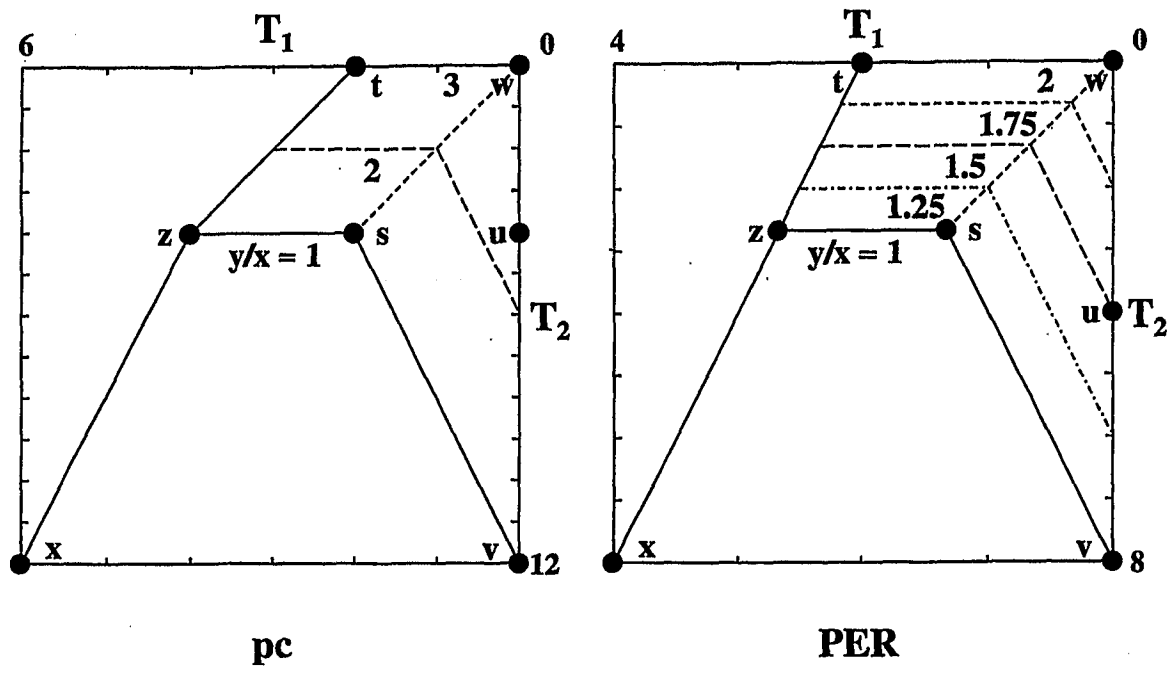

Figure 25: T_1, T_2 structure maps of CaF_2 (pc) and $CaTiO_3$ (PER) related structures with structural units u – z.

units of Fig.26 are identical to structural units u – y of the ccp group (Fig.12). The occupation of 50% of the tetrahedral interstices of the ccp or hcp lattice yields ZnS 3C (sphalerite) or ZnS 2H (wurtzite) (Table 11). The Zn atoms of sphalerite or wurtzite at the second, fourth, sixth I^t layer (Fig.20) form a ccp (ABC) or hcp (AB) lattice. The divalent Zn atoms can be substituted by two or three atoms with different valencies like $SbCu_3S_4$ or $AsCu_3S_4$. The ordering of metal atoms can be compared with ordered alloy structures $TiAl_3$ or $TiCu_3$, respectively (Table 11). The ZnS related adamantane structures however are non-metallic valence compounds (Section 17). Table 11 shows also some structures of the Ni_2In (Lidin and Larsson, 1995) and BiF_3/LaH_3 (Parthé et al., 1993) families of structures, where part of the Ni or F atoms, A = Ni′ or F′, occupy a hcp or ccp lattice. The structures with vacancies □ at the Ni′ or F′ positions can be formulated as $Ni_nIn_n\square_xNi'_{n-x}$ and $(BiF_2)_nF'_{n-x}\square_x$ (Table 11).

The occupation of tetrahedral interstices in ccp metals like CaF_2 with M = Ca at A, B and C positions (Fig.20) yields the sequence ABABCB-CAC,A $\widehat{=}$ $c\,h_2$ of Ca and F atoms with the sequence CaFF,Ca of Ca

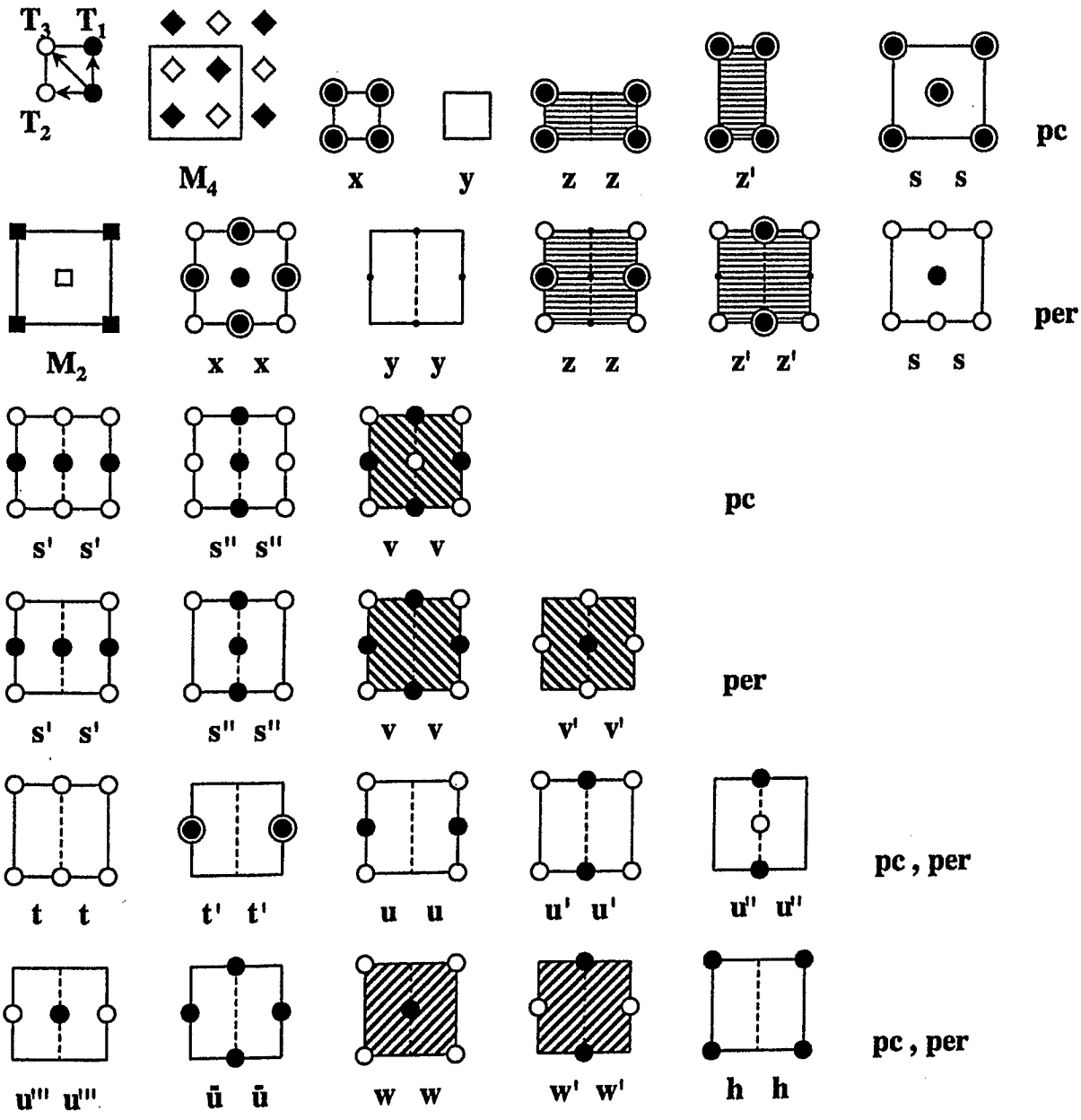

Figure 26: Structural units of pc and PER group with M atoms at projection height 0 (■), 0.5 (◆), 1 (□), 1.5 (◇) and I atoms at 0 (•), 1 (○) or 0 and 1 (⊙) (to be continued on next page).

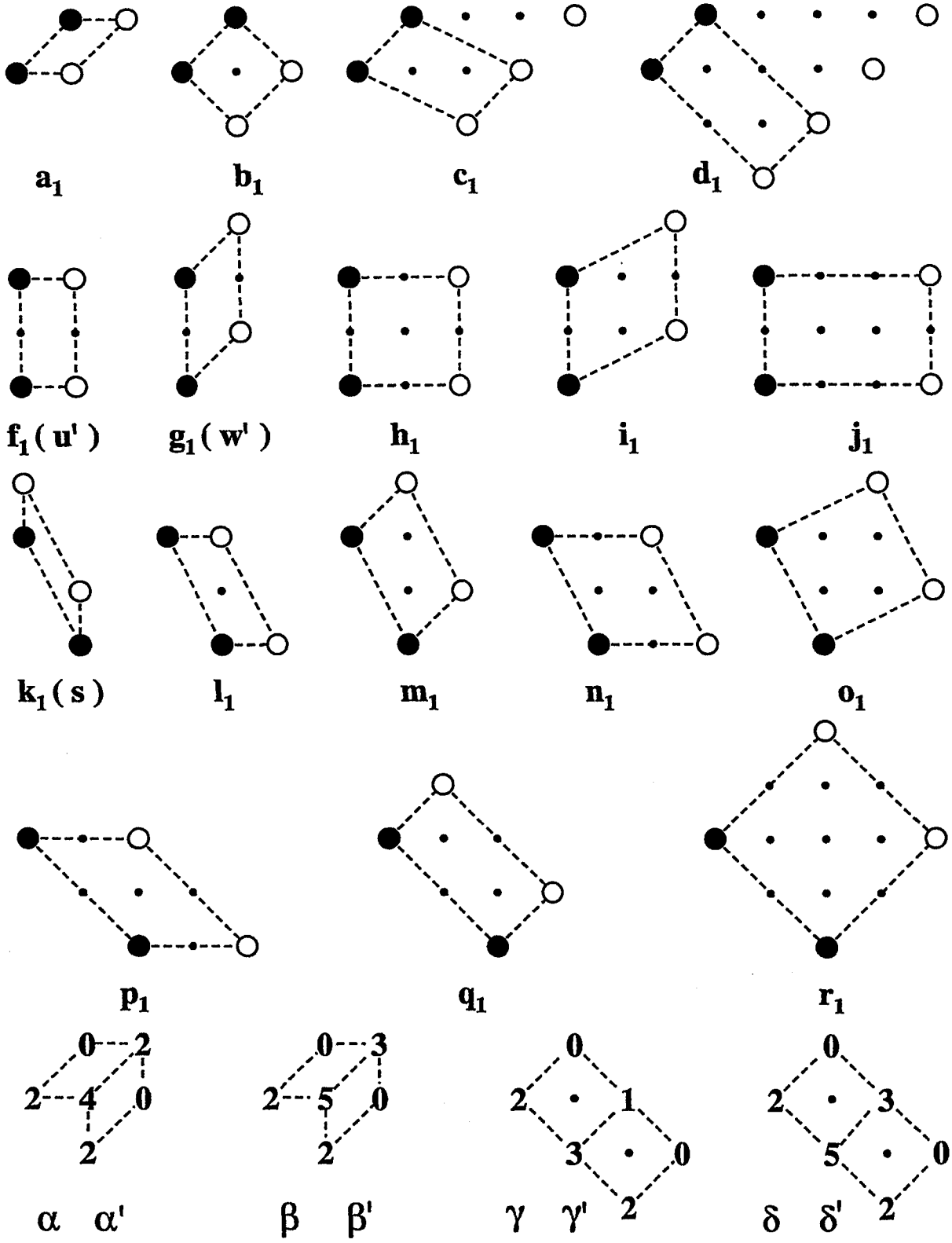
a1
b1
c1
d1
f1 (u')
g1 (w')
h1
i1
j1
k1 (s)
l1
m1
n1
o1
p1
q1
r1
0 2
2 4 0
2
0 3
2 5 0
2
0
2 1
3 0
2
0
2 3
5 0
2
α α'
β β'
γ γ'
δ δ'

and F atoms at a distance $\Delta z\, c/a \approx 0.2$ between Ca and F atoms and ≈ 0.4 between F atoms. Many compounds with different properties like $SnMg_2$ (intermetallic), CeH_2 (interstitial metallic hydride), CeO_2 (ionic conducting oxide) and Li_2O (Li conducting compound with antifluorite structure) are isotypic to CaF_2 (Wyckoff, 1982). The $CdCl_2$ C19 structure with the same sequences RMR and hch (Table 7) contains Cd atoms at octahedral interstices of ccp Cl atoms with $\Delta z\, c/a \approx 0.4$ or 0.8 between Cd and Cl or Cl and Cl atoms, respectively. The $Ni_2\square Al_3$ structure, which is usually considered as a bcc alloy with c_6 stacking and $\Delta z\, c/a \approx 0.2$ (Table 7), changes to the hc_3h stacking of γ-In_2S_3 with the same space group but $\Delta z\, c/a \approx 0.4$ between In and S atoms. The distances of all layers are $\Delta z\, c/a \approx 0.2$ in the BiF_3 or LaH_3 structure at the occupation of all tetrahedral and octahedral interstices with the sequences ABC,A $\widehat{=}$ c of BiFFF,Bi (Fig.20).

The coordination of the Bi atoms corresponds to CN = 14 of the ccp dodecahedron (Fig.27), if the eight F atoms at tetrahedral sites a – h are added to the six F atoms at 1 – 6. The structure of the interstitial (non-metallic) compound BiF_3 is identical to the structure of the ordered bcc alloy $AlFe_3$ (Table 7, B form).

The 74.1% density of cubic close-packed M atoms is increased by 1.7% and 5.3% at complete occupation of all tetrahedral and octahedral interstices by I atoms with $0.225d$ and $0.414d$ of the M atom radii. Therefore the density of ordered bcc alloys like $AlFe_3 \widehat{=} BiF_3$ is not 68.0% as for bcc W with equally sized M, but increased to a maximum of 81% for fcc Bi with an occupation of all interstitial sites. Another example is the 52.4% density of a pc lattice which is increased to 72.9% in the CsCl structure, if the interstitial atom radius is $0.732d$.

The occupation of all tetrahedral interstices I^t in hcp metals (Fig.20) yields the sequence AB,A $\widehat{=}$ hh of atoms MII,M and ABCABACB,A $\widehat{=}$ hc_3 of atoms MIII,M at occupation of tetrahedral and octahedral interstices of the non-existing compounds MI_2 and MI_3, respectively. The distances between the layers are identical to the CaF_2 and BiF_3 structures. The MI_2 and MI_3 compounds are supposed to be unfavorable compared to the CaF_2 and BiF_3 structures because of the short distance

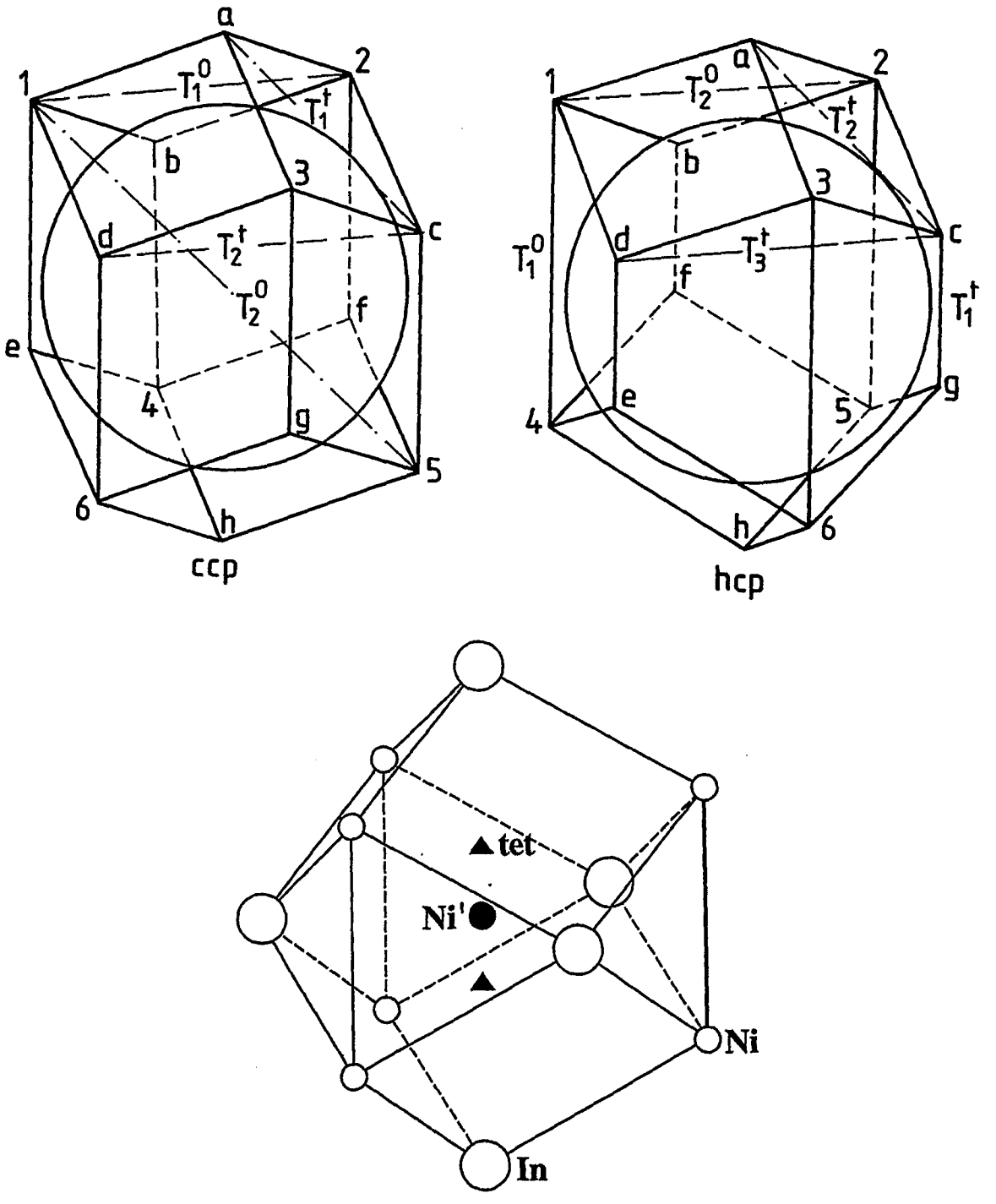

Figure 27: Positions 1 – 6 of octahedral and a – h of tetrahedral sites in the neighborhood of a ccp or hcp M atom with some self-coordination numbers T_i^o and T_i^t of octahedral and tetrahedral interstices and the Edshammar polyhedron of Ni′ of Ni_2In with five In and six Ni neighbors. The Ni′ atoms are between two tetrahedral sites c and g in the hcp In lattice.

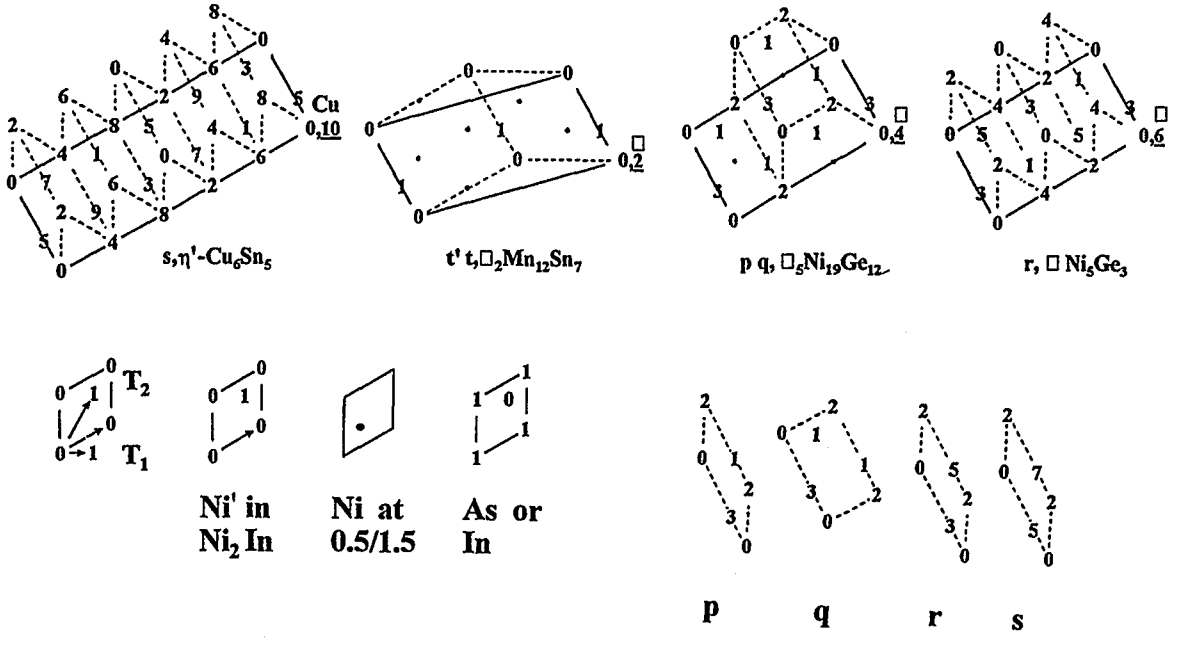

Figure 28: Projection of Ni_2In structure with hcp ordering of Ni′ atoms or vacant Ni′ positions □ in different compounds with structural units p – t.

of $d/\sqrt{6}$ between nearest I atoms compared to $d/\sqrt{2}$ in ccp metals with diameter d of M atoms (like c and g sites in the hcp and ccp M lattice, Fig.27).

The Ni′ atoms of the Ni_2In related series occupy a single position between c and g of the hcp lattice. The Ni′ atom has three M = In atoms at the same projection height and two other M neighbors in the same position A (or B) as Ni′ in the two neighboring layers. The CN = 5 coordination of the trigonal bipyramidal site is also known as Edshammar polyhedron (Larsson et al., 1994), if the six nearest Ni atoms at C positions (octahedral site) are included (Fig.27) (Lidin and Larsson, 1995). Therefore the Ni_2In structure can also be described as a hexagonal close-packed array of Ni′ centered Edshammar, CN = 11 polyhedra, which are empty in the NiAs structure. The Ni_2In related structures contain many ordered phases, which are not known for ordered hcp alloys including a different family of structural units p – t in $Ni_{12}Ge_{12}□_5Ni_7$ (pq) and $Ni_3Ge_3□Ni_2$ (r) (Ellner et al., 1971) (Fig.28).

Octahedral interstices of hcp Nb are occupied by I = N atoms in the δ-NbN structure (or the antistructure NiAs with As at Nb positions, Table 7, I form). The interstitial N atoms of NbN are all on C positions (Fig.20) with a primitive hexagonal (ph) lattice with the same distance $\Delta z\, c/a \approx 0.4$ between neighboring layers as in NaCl. The ph lattice of N atoms has the lattice constants a_{hex} of the hexagonal layer and $c = \sqrt{2/3}\, a_{\text{hex}}$. The distance between two layers is only 82% of the shortest M–M distance in undistorted structures. This can explain why interstitial atom positions at identical projection sites are not occupied in adjacent layers because of the size of interstitial atoms or the Coulomb repulsion between these atoms. Therefore, the ordered distribution of I atoms in hcp metals can be treated as single hexagonal layers (Hiraga and Hirabayashi, 1977) (Table 13). The coordinates of the structure map (Fig.29a,b) are identical with the α_2, α_5, α_7 coordinates of the three-dimensional case with $T_i^{\max} = 2, 6, 12, 2, 6, 24, 6$ for $i = 1 - 7$. The T_1, T_2, T_3 values of the ph lattice contribute less information because of the $T_1 = 0$ values of the right-hand border of the structure map (Fig.29b). The formula $M_nI\square_{n-1}$ is identical to the NaCl group. The Nb atoms of NbN however have a prismatic coordination. The CN = 6 value of N in NbN is reduced to CN = 1 – 5 in the other compounds containing vacancies. The configurations can be obtained from the type and stacking of hexagonal layers.

Structures with a primitive hexagonal lattice and occupation of most positions like the ionic conductor $Li_3N\square_2$ with s-CN values 0 2 8 2 6 4 2 ; 1 of Li atoms and 0 0 0 2 6 0 0 ; 5 of N atoms are very rare. Hexagonal and rhombohedral graphite or the corresponding BN modifications can be described by distorted ph lattices containing vacant positions $\square$ in the center of the honeycomb net with composition $\square C_2$ or $\square$BN and $T_i(\square)$ values 0 0 6 2 6 0 0 ; 2 or 0 0 6 0 6 6 0 ; 2, respectively. The sequences of vacancies in the hexagonal unit cells correspond to the Mg and Cu structures. The N or C atoms in ε-Fe_3N or ε-Ni_3C are ordered in the same way (Table 13). Different ratios c/a_{hex} in these compounds give rise to different sequences of T_i values. At $c/a_{\text{hex}} = 1$ for example the spheres with diameter d of a primitive hexagonal packing (ph′ system) have 2 + 6 = 8 nearest neighbors at distance d, 12 next-nearest neighbors at $\sqrt{2}d$ and 6 third neighbors at $\sqrt{3}d$ (corresponding to T_3 and T_5 values of the ph

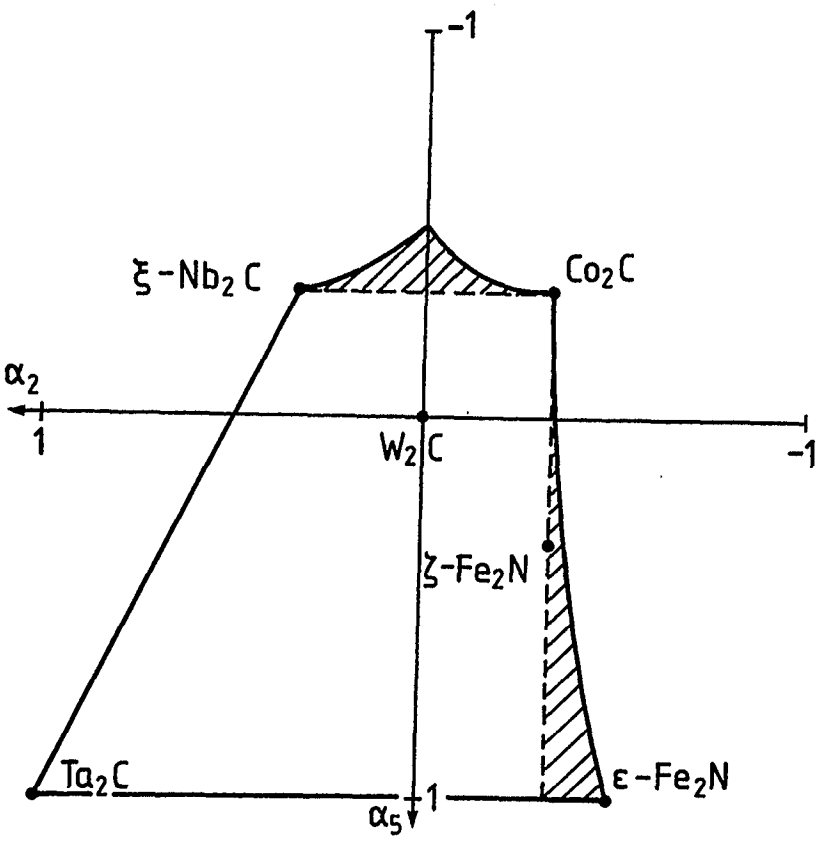
-1
ξ-Nb2C
Co2C
α2
1
W2C
-1
ζ-Fe2N
Ta2C
ε-Fe2N
α5
1

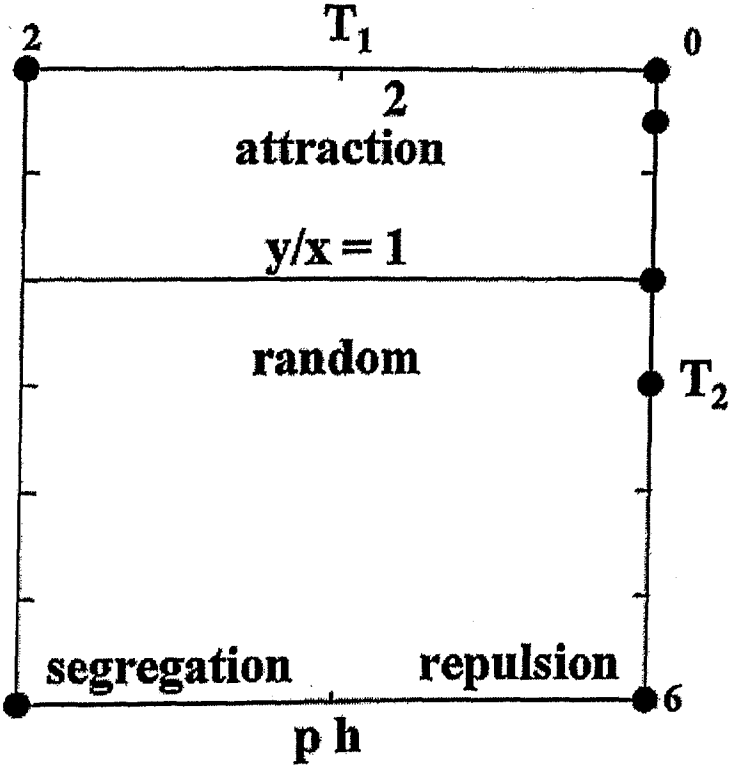
T1
2
0
2
attraction
y/x = 1
random
T2
segregation
repulsion
6
p h

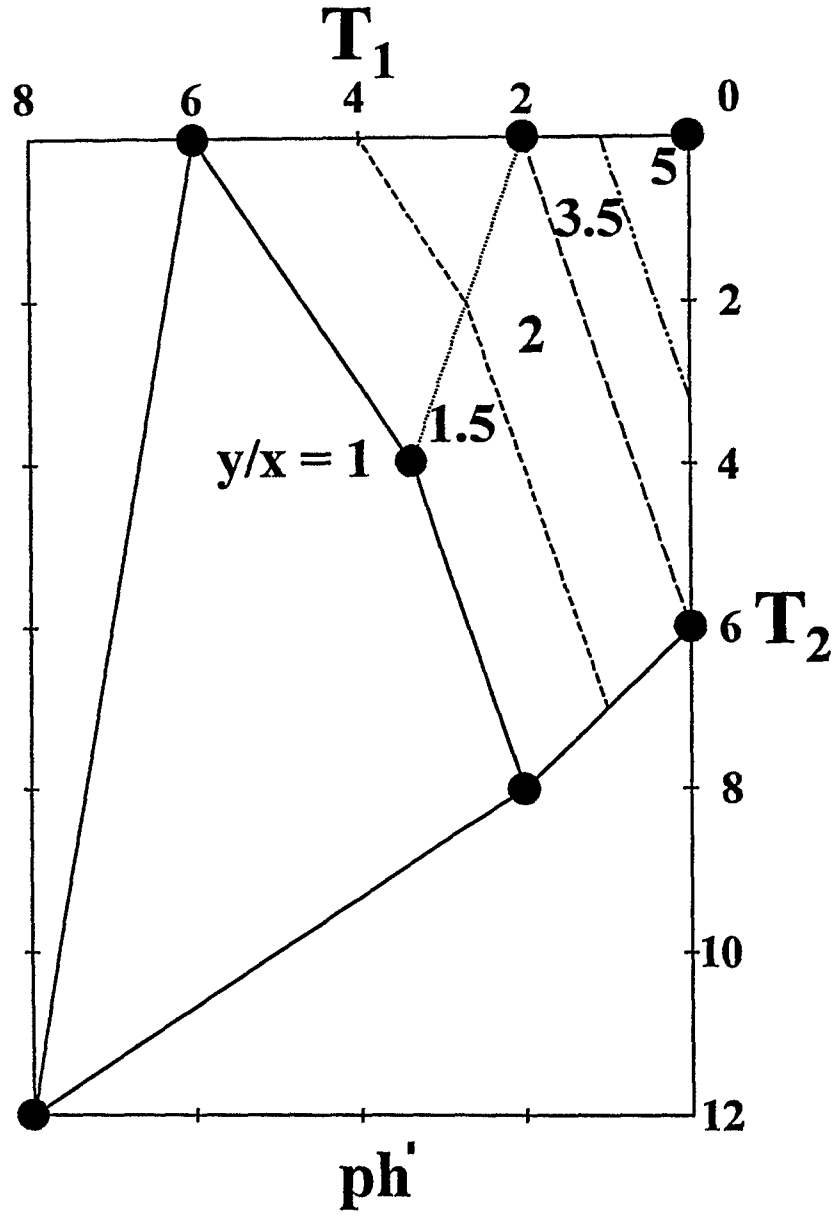

Figure 29: α_2, α_5 structure map of hcp $M_z\square_xI_y$ interstitial alloys, corresponding to α_1, α_2 of hexagonal plane (Fig.6) (a) and T_1, T_2 structure map of primitive hexagonal lattices ph (b) and ph′ (c).

system). The distorted structures with increased distances between the layers $c/a_{hex} > 1$ can be derived from the T_i values of the undistorted ph and ph′ systems (Table 13). The neighboring hexagonal layers of most compounds with $T_1 = 0$ are shifted by translations x, y, z to avoid T_1 neighbors of the ph lattice. Structures with identical projections in [0001] direction are characterized by the same set of T_i values. The T_i values of hexagonal or trigonal structures with fixed x, y, z parameters and structure types containing M atoms in these positions are listed in Section 33 (Table 25). The Kiessling and Ganglberger structure families containing Ta_3B_4 (Kiessling, 1949) and $Zr_2Fe_{12}P_7$ (Ganglberger, 1968) (Table 13) can be identified by different patterns of the hexagonal layers (Section 28).

19 Bonding in interstitial alloys

The interstitial atoms I = H, C, N, ... can occupy the tetrahedral or octahedral sites of the ccp M structure at the composition M_zI_y with $0.5 \leq y/z \leq 1$. The remaining (z − y) octahedral sites are empty. The larger number of metal atoms and interstitial atoms can be neglected in a description of the ordered structures, if the positions of the smaller number of vacant sites □ are considered in the formula $M_z\square_xI_y$, x + y = z. The positions of the M and I atoms must only be considered for the effect of lattice distortion caused by vacancy ordering and for the determination of the space group. The sublattice of vacancies plus interstitial atoms $\square_xI_y$ can be compared with the lattice of ordered M_xN_y alloys (Hauck et al., 1988b). The vacancies and I atoms exhibit the same ABC layer sequence as the metal atoms of ccp M (Fig.20). Therefore the distribution of vacancies of the $\square_xI_y$ sublattice can be described by the same coordination numbers T_1, T_2, T_3 and concentration y/x as for ordered ccp alloys M_xN_y (Table 11a). The carbides Ti_2C, Gd_2C, Ti_8C_5, V_6C_5 and V_8C_7 are located in area Ia of the structure map indicating covalent-type bonding, while the nitrides Ti_2N, Nb_4N_3 and the hydrides Pd_2H and $PdD_{0.8}$ are located at low α_1 indicating Coulomb-type interactions (Fig.30).

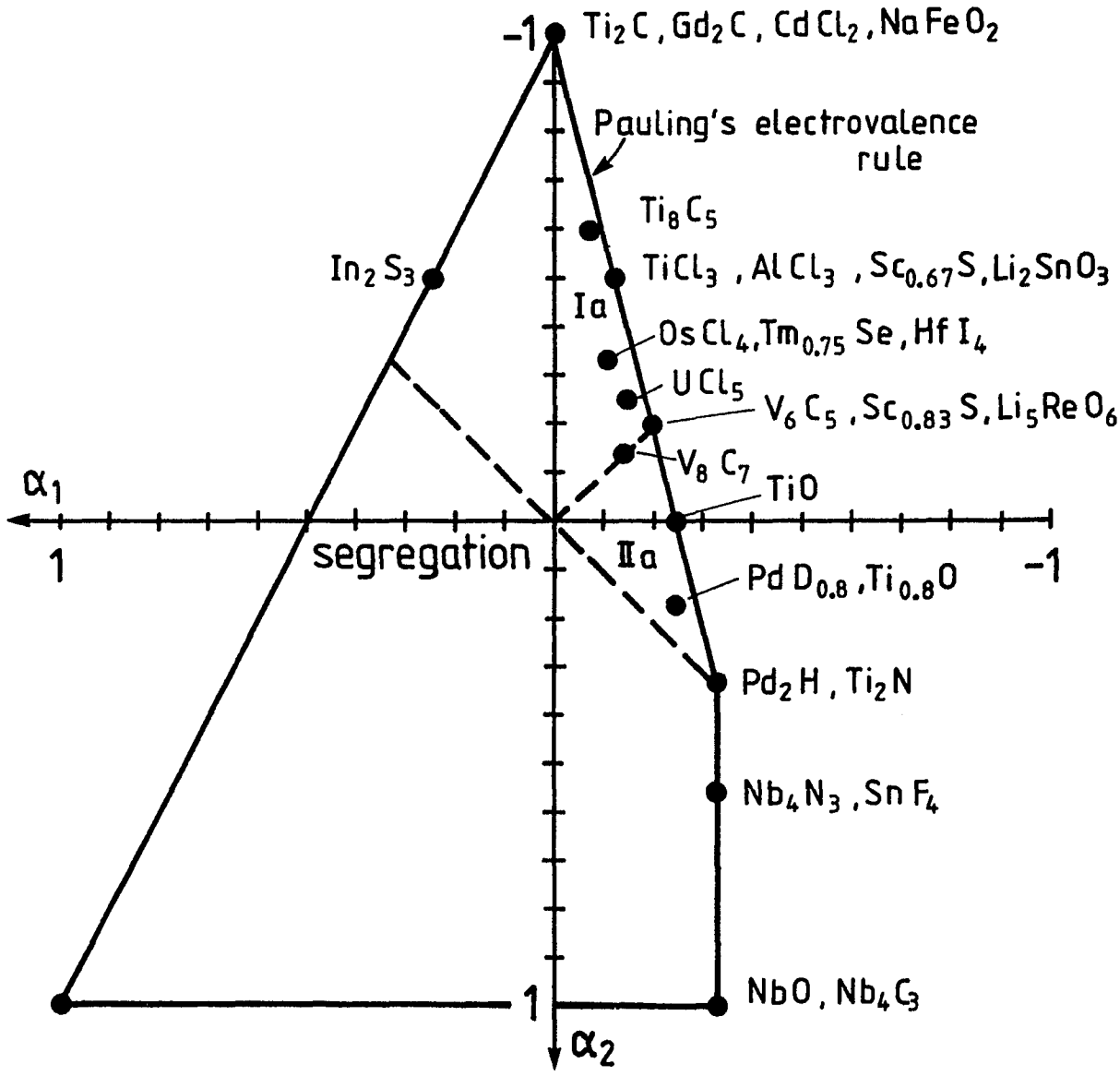

Figure 30: α_1, α_2 structure map of ccp interstitial alloys $M_z\square_xI_y$. Some halides $\square_xM_yI_z$ with metal atoms at octahedral interstices of the ccp I lattice (antitype structure) are also included.

Two other types of interstitial alloys can be compared if the composition is formulated in a similar way to that used for the $M_z\square_xI_y$ compounds with the convention that $z \geq y \geq x$: $\square_xM_yI_z$ with I = O, S, Se, F, Cl, I as in $Ti_{0.8}O$, $Lu_{0.83}S$, $Tm_{0.75}Se$, SnF_4, $AlCl_3$ or HfI_4 (Table 11a) and $\square_xM_y\square'_xO'_y$ as in $\square Ti_2\square O_2$ or $\square Nb_3\square O_3$ (Table 11a) with vacancies in both sublattices (Hauck and Mika, 1988b).

The I = O, S, Se, F, Cl or I atoms are bigger than the M atoms. Therefore the M atoms fill part of the octahedral interstices of the close-packed I lattice. The structures are the antitype of $M_z\square_xI_y$ (Lima-de-Faria et al., 1990). The sublattices of M and I = O atoms of NbO and TiO are only partly filled. The vacancies of the M and the I sublattice form the same structure: 2 2 12 ; 2a for TiO and 0 6 0 ; 3 for NbO (Fig.18).

Most interstitial alloys are metallic, some are superconducting like PdD, TiC, NbN, TiO, NbO or $Sc_{0.83}S$ (Toth, 1971; Moodenbaugh et al., 1978). The halides are non-metallic. Other non-metallic compounds which can be compared with the antitype structure $\square_xM_yI_z$ are the ternary oxides $M_xN_yI_z$, e.g. Li_5ReO_6, Li_2SnO_3 or α-$NaFeO_2$ (Tables 11a,12, Fig.30), with Re, Sn or Fe atoms at the vacancy positions.

The compositional parameters x, y and z = x + y of the non-metallic compounds can not vary independently. The electroneutrality rule requires compensation of the negative charge of the oxygen or halide atoms. The charge q(I) = –2 or –1, respectively, of these anions should be compensated by the electrovalence $q_i/(CN)_i$ of the p_i neighboring metal atoms with coordination number $(CN)_i$ and charge q_i as defined by Pauling (1929 and 1945/1960; Burdett, 1995):

$$\sum \frac{p_i\, q_i}{(CN)_i} = -q(I).$$

The I = O atoms of the $N_yM_xI_z$ compounds, e.g. Li_5ReO_6, Li_2SnO_3 and α-$NaFeO_2$, are coordinated by $p_M = 6x/z = 1$, 2 or 3 M atoms, respectively, M = Re^{7+}, Sn^{4+} and Fe^{3+}, and $p_N = 6y/z = 5$, 4 or 3 N atoms, respectively (N = Li^+ or Na^+ atoms), which compensate the charge –2 of the oxygen atoms according to Pauling's electrovalence rule. The structures of these compounds correspond with the V_6C_5, $TiCl_3$ and

Gd_2C structures (Table 11a) and are at the borderline of the (I, IIa) field of the structure map (Fig.30) with the correlations $4\alpha_1 + \alpha_2 + 1 = 0$ and $\alpha_1 + \alpha_3 = 0$ between α_1, α_2 and α_3 values (Hauck et al., 1989).

The metal atoms of the interstitial alloys M_zI_y, I = H, C, N are surrounded by CN = 6y/z I atoms: CN = 3 at y/z = 0.5, e.g. in $TiC_{0.5}$ or $TiN_{0.5}$; CN = 4 at y/z = 0.67 and CN = 5 at y/z = 0.83, e.g. in V_6C_5. The three I atoms of $MI_{0.5}$ are in the neighboring positions 1, 2, 3 (Fig.27) of facial configuration as in $TiC_{0.5}$ or $GdC_{0.5}$ or further apart at 1, 2, 5 in meridional configuration as in $PdH_{0.5}$, $TiN_{0.5}$ (Table 14) (Hauck, 1981). The self-coordination number T_1 of the 6 0 12; 1b $TiC_{0.5}$ structure is increased compared with the 4 4 16; 1 $TiN_{0.5}$ structure, because of the close distance between I atoms in facial configuration. The M atoms of the facial configuration can be shifted to the C atoms to decrease the M–C bonds by covalent bonding (Fig.27). A reduction of all Ti–N bonds with nitrogen atoms in meridional configuration 1, 2, 5 is not possible. The N atoms of the 4 4 16; 1 $TiN_{0.5}$ structure, however, are further apart and are stabilized by a 1.9% increased Madelung factor for the Coulomb interactions.

The other compounds with $y/z \neq 0.5$, 0.67 or 0.83 as e.g. Ti_8C_5, V_8C_7 or $PdD_{0.8}$ contain two different configurations of M atoms (Hauck et al., 1988b). In Ti_8C_5 e.g. with 6y/z = 3.75, two Ti atoms have three C atoms, and six Ti atoms four C atoms in the same configuration as the compounds Ti_2C and $AlCl_3$ (Table 11a). Ti_8C_5 is located in the vicinity of Ti_2C and $AlCl_3$ of the structure map (Fig.30). The structures close to the borderline with only two different configurations obey Pauling's rule of parsimony (Pauling, 1929). The structures at or close to the borderline $3\alpha_1 + 1 = 0$, e.g. 0 6 0; 3 and 4 6 8; 1, which are observed as ordered alloys, are unfavorable for interstitial compounds because of two or more configurations. The Nb atoms e.g. of 0 6 0; 3 Nb_4C_3 are surrounded either by four or six C atoms. The number of configurations, however, is reduced to a single configuration in NbO (= $\square Nb_3 \square O_3$) and in ternary interstitial alloys $AlFe_3C$ and FeNiN (Fig.18).

The T_1 and T_2 values in the T_1 T_2 T_3; y/x notation of interstitial compounds describe the connection of octahedra by edges and corners, re-

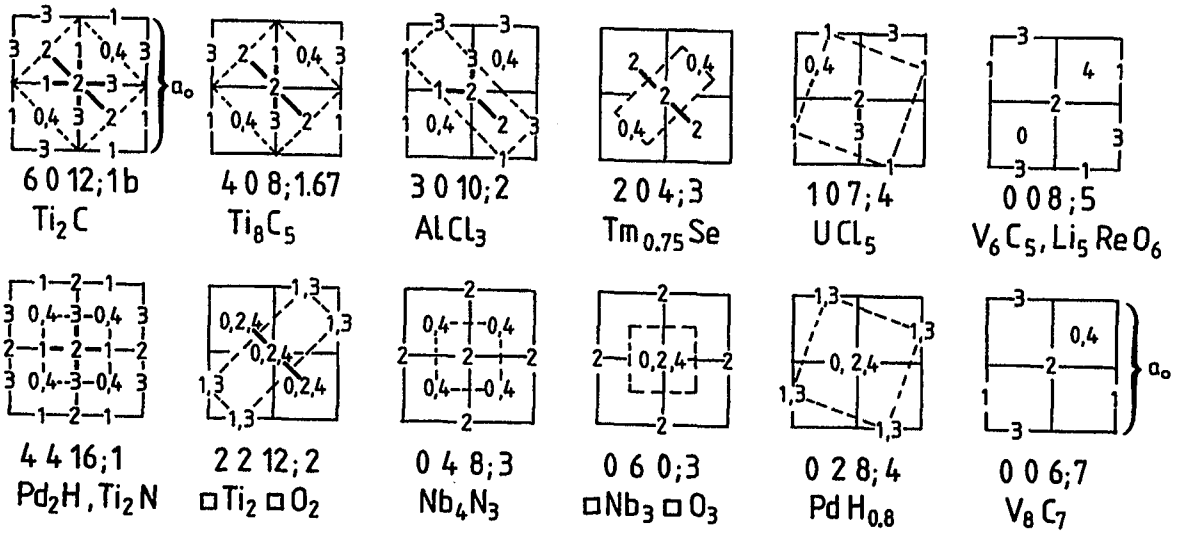

Figure 31: Self-coordination numbers T_1, T_2, T_3 of interstitial atoms in covalent (upper row) or ionic (lower row) compounds. An interstitial atom is placed in the middle of eight face-centered cubic cells with lattice constant a_c. The numbers z give the position of neighboring interstitial atoms at height $z\,a_c/2$. Nearest neighbors are connected by bold lines. The broken lines indicate the unit cells. Ti_2C and V_8C_7 are cubic with lattice constant $a_0 = 2\,a_c$.

spectively. The 1 0 7;4 UCl_5 structure contains UCl_6 octahedra connected by an edge to $(UCl_5)_2$, while the UF_6 octahedra of the 0 2 8;4 UF_5 structure are connected by two corners in a one-dimensional row. The CTi_6 octahedra of the 6 0 12;1b Ti_2C structure are linked by six edges, the NTi_6 octahedra of the 4 4 16;1 $TiN_{0.5}$ structure by 4 corners and 4 edges. The vacancies of 0 0 8;5 $V_6C_5\square$ or the Re atoms of 0 0 8;5 Li_5ReO_6 form isolated octahedra. Similar relations between T_1, T_2, T_3 values and the number of shared faces, edges or corners of the polyhedra of other interstitial alloys are listed in Table 15.

The covalent and ionic compounds can be compared by two series of interstitial compounds $M_z\square_xI_y$, the Ti_2C series with covalent bonding and the Ti_2N series with ionic bonding (Fig.31).

The vacancies of the 4 4 16;1 $Ti_2\square N$ structure are filled up with interstitial atoms in such a way that they are as far apart as possible. These structures with 50, 33, 25, 20 and 12.5% vacancies, shown in the lower row of Fig.31, have a minimum of T_1 coordination. The vacan-

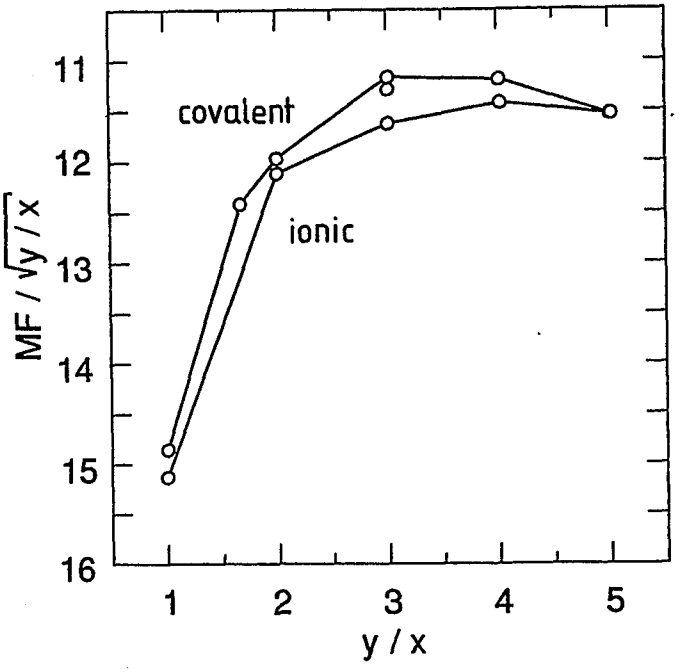

Figure 32: Madelung factors $MF/\sqrt{y/x}$ versus concentration y/x for the undistorted covalent and ionic compounds of Fig.31.

cies of the 6 0 12 ; 1b $Ti_2\square C$ structure in the upper structural series are successively occupied at increased T_1 and $T_2 = 0$. The increased T_1 coordination numbers of this series allow covalent bonding to interstitial atoms in neighboring facial or *cis* configuration. The Madelung factors of these structures are decreased by 1% – 3% (Fig.32). This difference of the lattice energy must be compensated by covalent bonding to stabilize the structure. The $\square V_6$ octahedra of $V_6C_5\square$ or ReO_6 octahedra of Li_5ReO_6 are isolated at the composition $y/x \geq 5$. The vacancies or Re^{7+} atoms are as far apart as possible for a maximum Coulomb energy. Covalent bonding is also favorable at this composition, because of the possibility of decreasing all Re–O bonds of ReO_6 or increasing all $\square$–V distances of the $\square V_6$ octahedra for covalent V–C bonding. Therefore the 0 0 8 ; 5 structure is favorable for both systems. This structure lies at the intersection of the $4\alpha_1 + \alpha_2 + 1 = 0$ boundary line of the structure map (Fig.16) and the $\alpha_1 = \alpha_2$ line for diluted alloys as e.g. V_8C_7 with $T_1 = T_2 = 0$. The 0 0 8 ; 5a–i structures are different stacking variants, which can occur in the same sample like V_6C_5 I, II and III or as disordered structures. Some structures like 0 0 8 ; 5e,f are homometric analogous to

6 0 12 ; 1a,b Ti_2C and Gd_2C (Section 8, Fig.13) (Parthé and Yvon, 1970; Hauck et al., 1988b).

The Zn atoms of ZnS are at tetrahedral sites of the ccp lattice in the sphalerite modification or the hcp lattice in the wurtzite modification. The Zn atoms forming a ccp or hcp lattice as the S atoms can be substituted by other atoms like Cu, Sb or As in $SbCu_3S_4$ (Table 11a) or $AsCu_3S_4$ (Table 11b). The structure of the metal atoms corresponds to the $TiAl_3$ and $TiCu_3$ structures. The T_1 values indicate the number of corner shared tetrahedra (Table 15). Most structures are in the Johansson, Linde and Brauer family of structures with $3\alpha_1 + 1 = 0$ (Fig.16) and satisfy Pauling's electrovalence rule (Hauck and Mika, 1998b).

The coordination numbers CN and the bonding geometries of the metal atoms depend on the size and the hybridization of s, p and d orbitals (Sutton, 1993). The CN = 4 planar coordination is favored for dsp^2 hybridization compared to tetrahedral coordination for sp^3 or d^3s hybridization. The CN = 6 trigonal prismatic coordination occurs for d^4sp instead of d^2sp^3 of octahedral coordination. The CN values vary with the size and number of valence electrons of the elements (Section 29).

20 Magnetic interactions

Transition, rare earth or actinide metal atoms with d or f electrons exhibit a magnetic moment, which gives rise to ferromagnetic or antiferromagnetic ordering below the Curie or Néel temperature, respectively and a small lattice distortion. The spins of different atoms are oriented parallel in ferromagnetic and antiparallel in antiferromagnetic compounds (Oleś et al., 1976). The relation between interaction energies V_i and ordering was investigated by Ising (1925), and a similar treatment applied to the ordering of alloys by different investigators (Section 11). These investigations had shown that the magnetic interactions are less than 1% of the lattice energies of ordered alloys. The arrangement of the spins depends on the distances between atoms, geometry of neighboring

atoms and bonding to other atoms like in the superexchange coupling (Goodenough, 1982). The situation seems to be very similar to interstitial compounds $M_nI_x\square_y$ like the hydrides, where the occupation of tetrahedral or octahedral interstices is supposed to be influenced by the *d* electrons of M atoms, the distances and interactions between H atoms (Section 24). The magnetic metal atoms however are fixed on lattice sites, which are given by the large lattice energy, and the spins must find an optimum arrangement for this situation.

The ordering of the spins can be analyzed for attractive or repulsive interactions in different families of structures with composition $R_nM_xM'_y$, if the metal atoms M with a magnetic moment $\oplus$ and other M atoms M' with $\ominus$ spin direction or vacancies $\square$ are forming one of the lattices of the present investigation. The other atoms, the rest R, can be a single atom like P in PHo with fcc Ho lattice or several atoms like O_3Al in the O_3AlDy structure (Table 16). Ferromagnetic compounds with a single orientation of the spins can be treated as pseudobinary interstitial compounds with $T_i(\square)$ of vacancies or non-magnetic R atoms and T_i(M) of the M atoms. The interactions in antiferromagnetic compounds with a $\oplus$ and $\ominus$ orientation of antiparallel spins are treated as pseudoternary compounds with equal self-coordination numbers for atoms with positive and negative spin direction ($T_i(\oplus) = T_i(\ominus)$) with few exceptions like S_2Cr_2 (0 0 6 ; 2 and 0 3 0 ; 2 for $\oplus$ and $\ominus$ spin directions). The self-coordination numbers T_i(M) of all magnetic atoms with antiparallel spin directions usually show a different point in the structure map because of the different y/x values ($2y/x(M) = y/x(\oplus) - 1$). Compounds with different spin directions like $FePd_{1.6}Pt_{1.4}$ are treated as multinary compounds with different sets of $T_i(\oplus)$ and T_i(M) values for each M atom (Table 16). This alloy is listed also as $Pd_{1.6}Pt_{1.4}Fe$ for the magnetic moments of Fe atoms. The four or five different directions of magnetic moments of Dy atoms in $DyAlO_3$ or Mn atoms in $Mn(OH)_2$ can be combined in different ways. The combinations can be homologous structures (identical α_i values) or quasi-homologous structures at the same border indicating the same kind of interactions for combinations or at different areas of the structure maps. The T_i(M) values correspond to all values of Dy or Mn atoms, respectively. The concentration of magnetic Mn or Cr atoms in $Ga_{1.15}Mn_{2.85}$, $PtMn_3$, $GePd_2Mn$, $(OH)_2Mn$ and S_3Cr_2

is increased to y/x < 1. The underlined T_i(N) or T_i(□) values of the non-magnetic minority component or vacancy for the structure map are different (Sections 2,4). Most T_i values are at the boundaries of the structure maps and can be analyzed for repulsive or attractive interactions. Usually the lattice with the highest density (lowest r values) of magnetic M atoms is preferred like the pc lattice of Dy atoms in $DyAlO_3$ instead of the bcc lattice of Dy and Al atoms. The ordering of different structures like Cu_2AlMn (Heusler alloy) and OEu (NaCl) or O_4ZnCr_2 (O_4MgAl_2 spinel structure) and $TbCo_2$ ($MgCu_2$ Laves phase) can be compared for example in the fcc lattice of M atoms. The magnetic atoms of many cubic, hexagonal, trigonal or tetragonal structure types like the Mn and Eu atoms of Cu_2AlMn/OEu or the Cr and Co atoms of O_4ZnCr_2/$TbCo_2$ occupy positions with fixed x, y, z parameters (Section 33, Table 25). The T_i(M) values of cubic compounds projected in [001] or [111] direction are analyzed for the T_i(M) values of the square or hexagonal layers. The characterization by square layers and translational vectors of these layers is preferred in most cases because of the higher densities (lower r values) of M atoms r(hex) = 3r(square) + 2. Some structure types like fcc 3, 5 and 8 containing different square layers at different projection heights or an overlap of M positions in [001] projection should be projected in [111] direction. Many hexagonal, trigonal or tetragonal structures with fixed x, y, z parameters can be considered as distorted cubic structures with identical projections in [111] or [001] direction. The tetragonally distorted bcc and fcc structures with identical projection patterns are characterized by a slightly distorted bcc′ lattice with T_i values 8 4 2 4 8 16 8. The T_i values of the cubic bcc (8 6 12 $\widehat{=}$ T_1, T_2+T_3, T_4+T_5) or fcc (12 6 24 $\widehat{=}$ T_1+T_2, T_3+T_4, T_5+T_6) structure or of the square plane (4 4 4 $\widehat{=}$ T_2, T_4) can be derived from the bcc′ values in a similar way as was discussed for distorted ph lattices (Section 18). The T_i values of the cubic pc lattice (6 12 8 $\widehat{=}$ T_1+T_2, T_3+T_4, T_5) can be derived from tetragonally distorted pc′ (T_i = 4 2 4 8 8). Other invariant lattice complexes including orthorhombic distortions were derived by Hellner and Schwarz (1994). Different symbols like D (= bcc 1) or W (= fcc 5) are used for the diamond and β-W structures. The fcc 7a and b structures with the Hellner and Schwarz symbols V* and S* are homometric for the M and in the average homometric for the N atoms.

21 Ordering of I atoms on metal surfaces

The compilation of different structures of the primitive cubic (pc) lattice had shown, that the ccp or bcc lattices can be considered as ordered pc lattice, where 50% (ccp) or 75% (bcc) of the metal atom positions are vacant and can be occupied by I = O, Cl, etc. atoms in the NaCl or perovskite group. A similar situation occurs for the two-dimensional ordering of adatoms A on metal surfaces like the square or hexagonal net of structures, if A = H, Xe, Cl atoms or CO, C_6H_6 molecules are adsorbed on the top positions of [001] or [111] ccp metal surfaces (Table 12) (Watson et al., 1994). The composition of the metal surface $M_nA\square_{n-1}$ with a maximum of one A atom/M atom is similar to the NaCl or NiAs group of interstitial alloys. The ratio A/M can be varied at the occupation of hollow or bridge positions. A honeycomb net of A atoms is obtained at occupation of all hollow positions, a kagomé net at occupation of all bridge positions (Fig.33). The compositions can be formulated as $M_nA_{xn-x}\square_x$, with x = 2 (honeycomb net) or x = 3 (kagomé net) similar to the pc and PER groups of structures. The x = 1 or 2 series is obtained for the occupation of hollow or bridge positions on [001] surfaces of ccp or bcc metals (Table 12). Each M atom of the honeycomb net exhibits a maximum coordination number CN = 6, if all hollow positions are occupied. The coordination in the kagomé net includes two additional adatoms with larger M–A bond distances, which are not included for the CN values. The M atoms of [001] surfaces of ccp or bcc metals can have a maximum of CN = 4 A atoms at hollow or bridge positions, if the size of A atoms is smaller than the size d of M atoms (hollow positions) or smaller than $0.7d$ (bridge positions). The occupation of l = CN A atom positions in the hexagon next to each M atom in [111] ccp or [0001] hcp is given by letters a (CN = 6), b (CN = 0), c (CN = 1), o, m or p (CN = 2), v, s or y (CN = 3), o′, m′ or p′ (CN = 4) and c′ (CN = 5) (Fig.34). The different configurations o (ortho), m (meta), p (para), v (vicinal), s (symmetrical) and y (asymmetrical with the shape of the letter y) are similar to those used for benzene derivatives in organic chemistry (Latscha and Klein, 1982). The same applies for the occupation of neighboring sites (*cis* positions) or diagonal sites (*trans* positions) in the square net (Fig.8). The t (*trans*) configuration

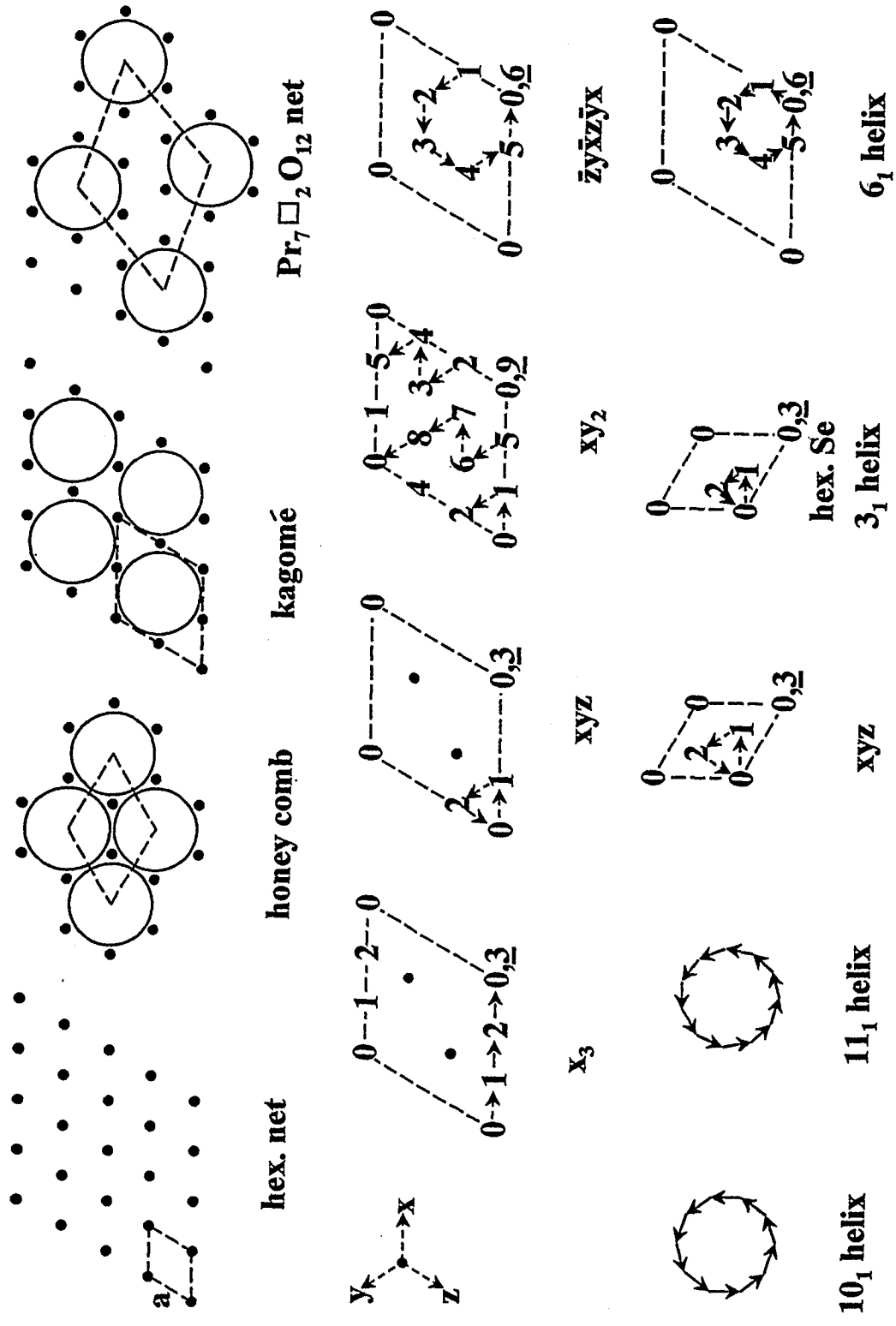

Figure 33: Projection of the hexagonal, honeycomb, kagomé and $Pr_7\square_2O_{12}$ net with composition AB_2, AB_3 and AB_6 of vacancies A = □ at the positions of M atoms (○) and occupied sites B (•). Honeycomb and kagomé net in surface structures at the occupation of hollow or bridge positions, respectively. Layered ccp compounds with translation of A atoms in x, y or z direction, 3_1 or 6_1 helical structures at distortion of close-packed compounds and 10_1 or 11_1 helical structure of DNA.

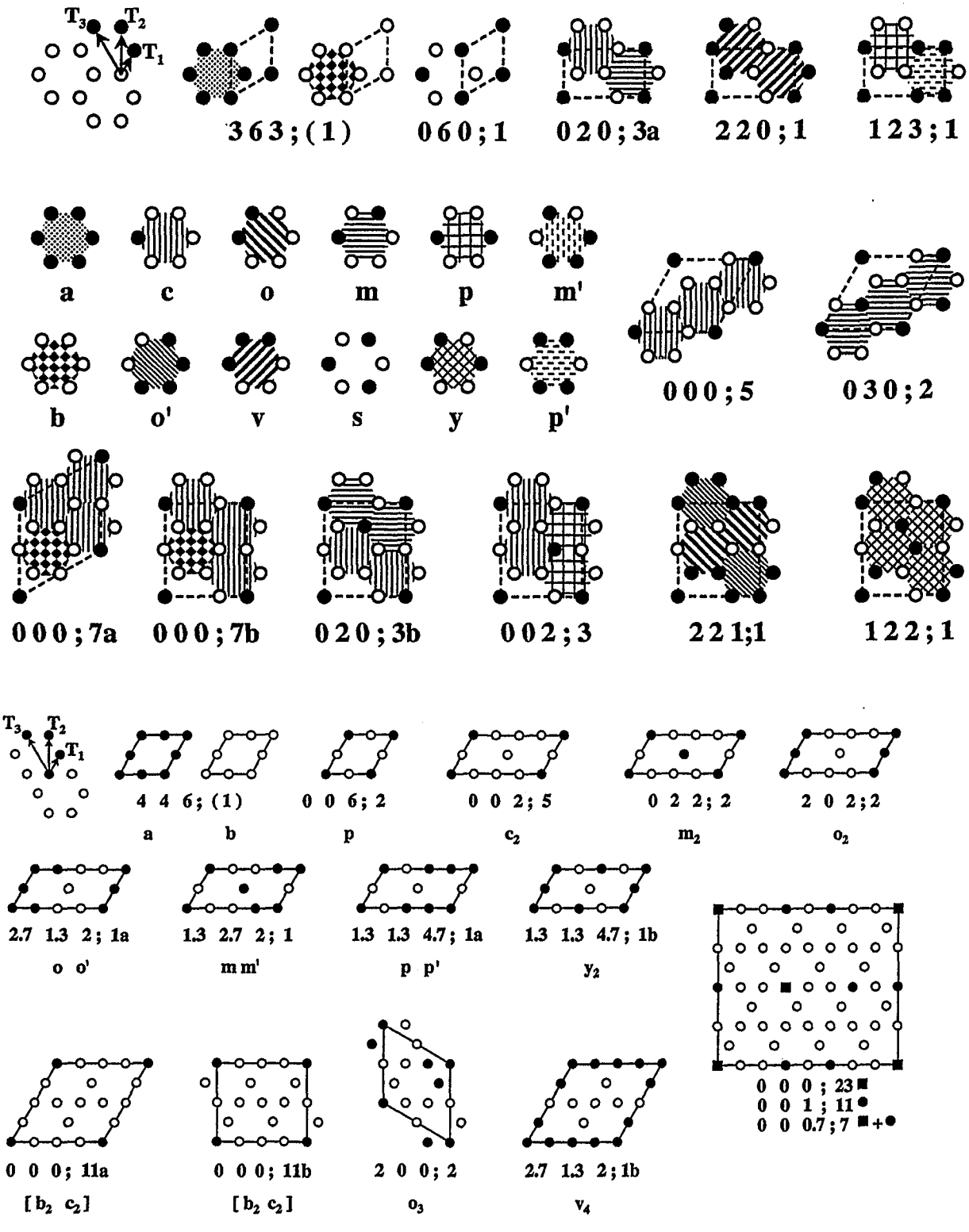

Figure 34: Structures of the honeycomb net (a) and kagomé net (b) with structural units a, c, ... (different shading in honeycomb net).

in the square lattice and s (symmetrical A atom) configuration in the honeycomb or kagomé net are obtained at repulsive interactions between A atoms. The c (*cis*) configuration in the square lattice, v (vicinal) and o (ortho) configuration in the honeycomb or kagomé net are obtained for attractive interactions (Figs. 7,35). Structures with o or p configuration are not possible in the honeycomb system, while a structure with s configuration is not possible in the kagomé net.

22 Related groups of structures

The maximum possible range of T_1, T_2 values of possible structures is reduced in all systems of the present investigation. The different borders can be described by the relations given in the upper part of Table 17. The different constants a_i, b_i, c_i, which depend on T_1^{max}, T_2^{max} and geometrical constraints, are listed in Table 17. The geometrical constraints are given by the minimum range of T_1 and T_2 values at r = 1 and the maximum range for structures with $T_1 = T_2 = 0$ at increased r. Each border can be correlated to a structure series with different structural units. Several series of structures containing similar structural units are listed as structure family. Structures at the left-hand border of the structure maps (B1, B2) can be described by sequences of atoms or layers of atoms. Structures at the right-hand borders of the structure maps (B5 – B7) usually contain double rows of structural units with different atoms like a combination of two squares or rhombs with *cis* occupation in c* (Fig.8) or c′ (Fig.6).

The different groups of structures can be classified in a similar way as the homologous and homometric structures (Sections 8,9).

(1) Quasi-homologous structure groups

The bcc, ccp, perovskite (PER) and square net structures can be obtained from the primitive cubic (pc) lattice, if some sites are excluded or occupied with other atoms. Part of the M atoms of a pc M lattice can be substituted by vacancies or I atoms in the

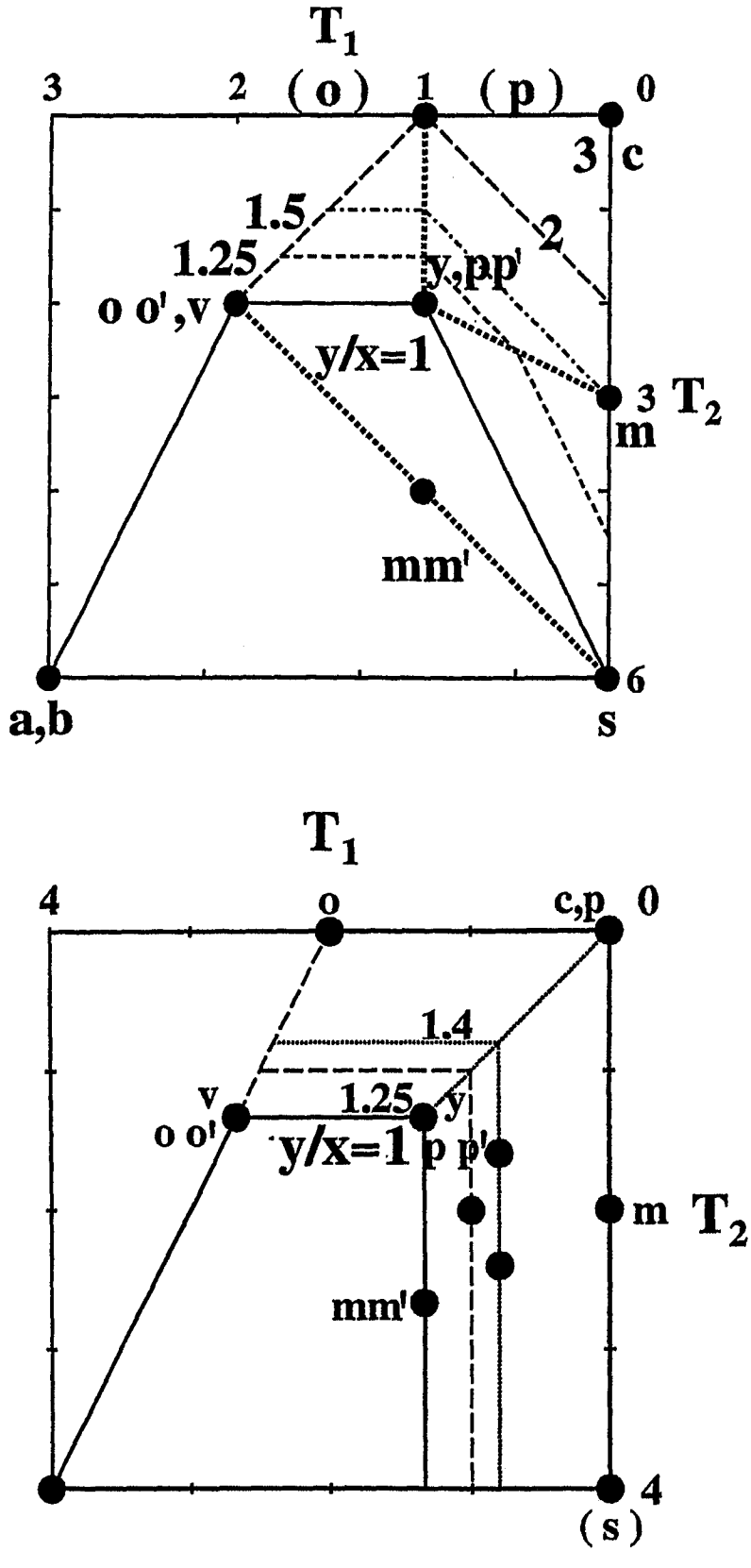

Figure 35: Structure maps of the honeycomb net (a) and kagomé net (b) with T_i values of structural units. Structures with structural units in brackets are impossible.

sequence M_8 (pc), M_6I_2 (anti-perovskite), M_4I_4 (NaCl), M_2I_6 (perovskite, PER group) and I_8 (CaF_2 group). The $M_4\square_4$ and $M_2\square_6$ structures correspond to ccp and bcc metal structure groups. These structures are at the border of the pc structure map with a single set of T_i(M) and T_i(I) values ($M^i = 1$) (Section 33). The bcc system with two M atoms and the PER group with six I atom positions are conjugated systems similar as the combination of two ccp lattices to the NaCl group with the T_i(Na) and T_i(Cl) values 0 12 0;1. Other structures at the border of the pc structure map with $M^i = 1$ are 2 4 8;1 (rectangle), 4 4 0;1 or 4 4 0;2 (square net), 1 8 4;1 (honeycomb related net) and 0 0 2;6 ($Pr_7\square_2O_{12}$ structure net, Fig.33). The vacancies and oxygen atoms of $Pr_7\square_2O_{12}$ form a conjugated system. The ccp lattice of Pr atoms is obtained from the positions of $\square$ or O by the translation $a_c/4$ $a_c/4$ $a_c/4$ (a_c = cubic ccp lattice constant of Pr atoms).

The honeycomb and kagomé nets are quasi-homologous groups of the hexagonal layer with self-coordination numbers 0 6 0;2, 0 0 6;3 and MI_2 or MI_3 composition. Usually the structures of quasi-homologous subgroups are inside of the structure map of the original group (Fig.36). The maximum interactions between I atoms are impossible because of the hindrance of M atoms at I positions (Fig.33).

(2) Quasi-homologous structure groups with similar structure maps

Some groups of structures exhibit similar structure maps with a relation between the T_i(M) values of both maps like the maps of ordered bcc alloys, the square net and the one-dimensional chain (Figs. 37a,7a,2a). The three corners of the bcc structure map (Hauck and Mika, 1997) at repulsion (CsCl structure), attraction (NaTl structure) and segregation can be characterized by the layer sequences MN (CsCl), M_2N_2 (NaTl) and $M_\infty N_\infty$ in the same way as for the chain of M and N atoms (Table 7, B form) or the sequences of M and N atoms in the square net (Fig.8). The structure with sequences M_2N_2 of M and N atoms (2 2 0;1) (Section 28) however is not at the corner of the structure map of the square net. Another example are the structure maps of the pc and PER groups (Fig.25). Many structures can be described by the same or similar structural

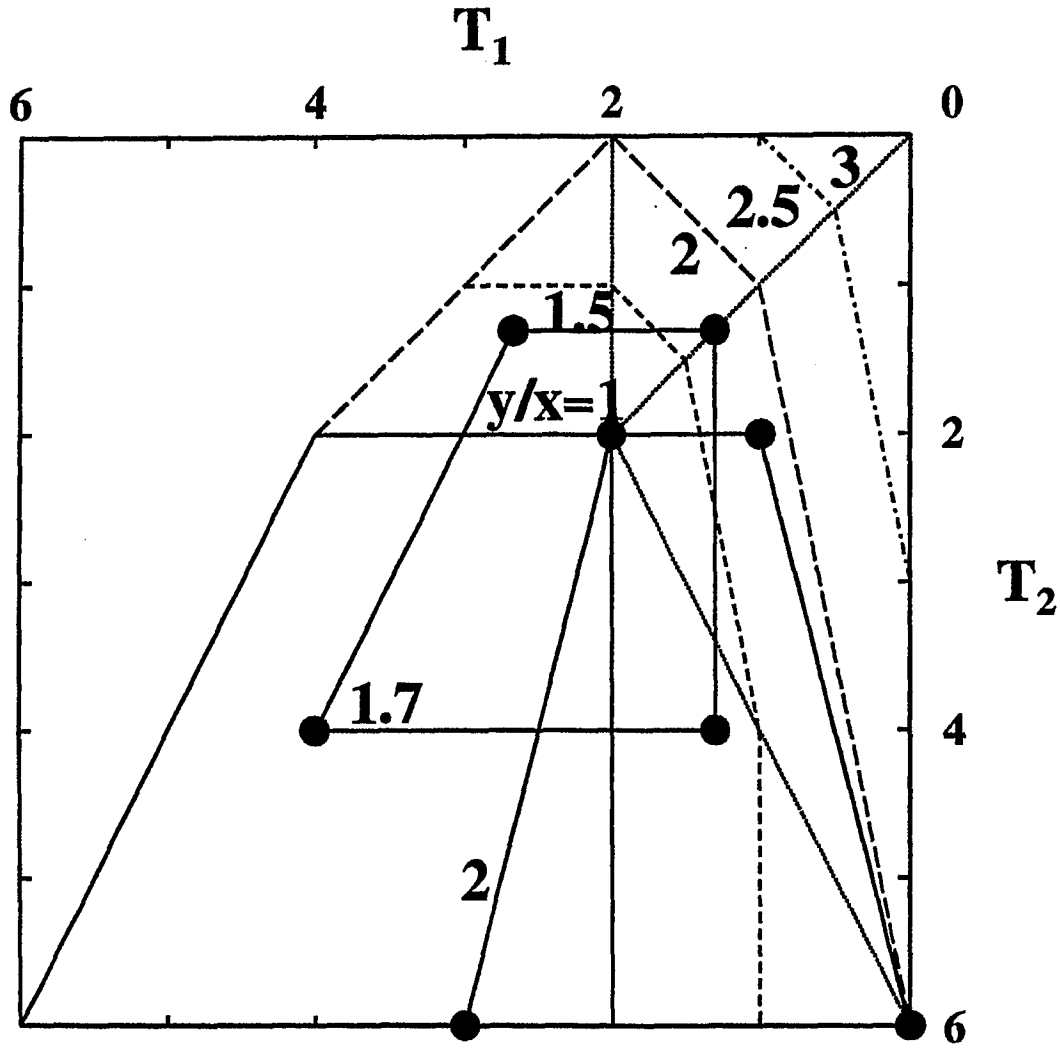

Figure 36: The structures of the honeycomb and kagomé net in the structure map of the hexagonal net. The structures at y/x = 1 correspond to the y/x = 1.7 (honeycomb) or y/x = 2 (kagomé) structures in the hexagonal net and are inside of the hexagonal structure map.

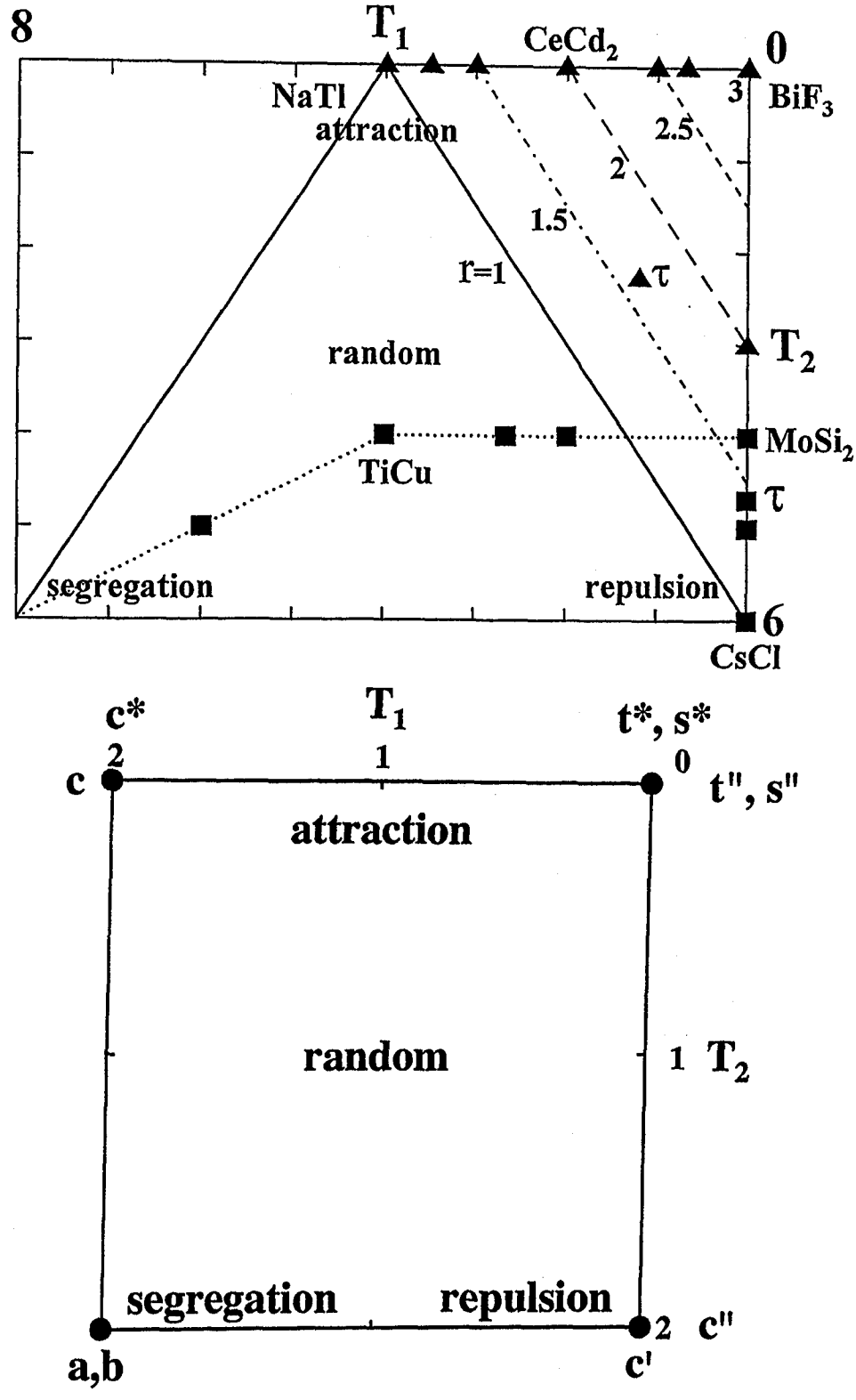

Figure 37: T_1, T_2 structure map for the bcc (a) and rectangle net (b). The bcc structures with layers in [111] (▲) or [001] (■) direction (Tables 7,8) are in different areas. The structures of Fig.38 are combinations of different structural units a, b, s and t.

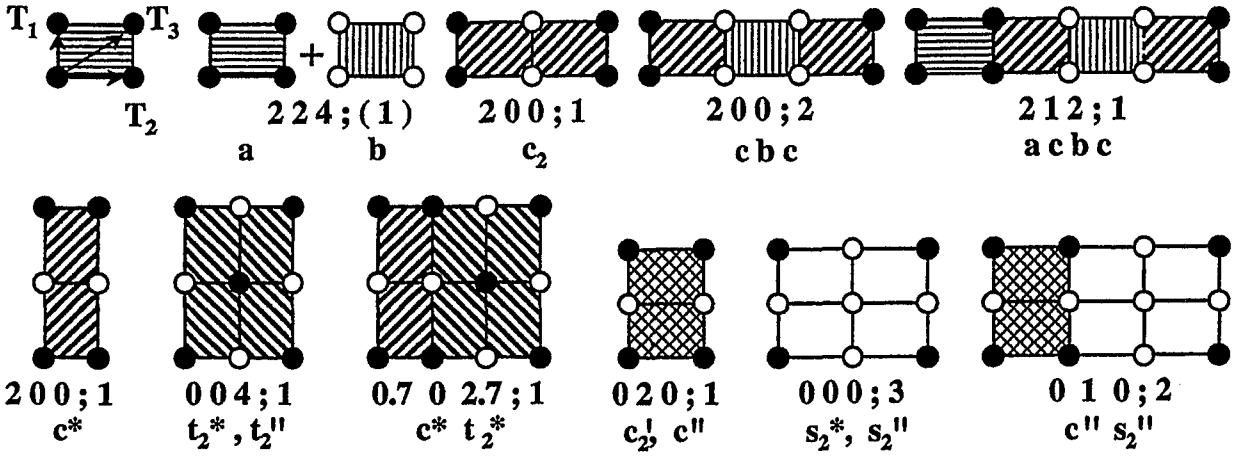

Figure 38: Self-coordination numbers T_1 T_2 T_3;y/x of A atoms in A_xB_y compounds (A = •, B = ○) for the rectangle net. A atoms with concentration y/x $\geq$ 1 are the minority component. The different structural units a, b, c, etc. are shown by different shading.

units (Fig.26).

(3) Quasi-homometric groups

Groups of structures with identical T_1, T_2 structure maps like hcp, ccp and complex close-packed ordered alloys are closely related with slightly different lattice energies because of different T_3 and higher T_i values. Structures of M_xN_y compounds are formed by sequences of M and N layers or sequences of M_xN_y layers (Tables 3–5,9b) with different stacking. The stacking of M and N layers can be described by the letters c and h (Section 2). The stacking of M_xN_y layers is obtained by the translations of M atoms in x, y or z direction in the next layer (Figs. 13,33).

23 Distorted structures

The hexagonal net with s-CN values 6 6 6 (Fig.39) can be distorted in such a way that the angle $\alpha = 120^0$ decreases to $\alpha = 90^0$ of the square net with s-CN values 4 4 4. The intermediate net with $\alpha \approx 103^0$ and s-CN values 4 (2+2) 4 shows the relation to the square net, if the 2 + 2′ atoms are added to 4 4 4. Adding the 1 + 2 atoms to 6 T_1 and 2′ +

3 atoms to $6T_2$ yields the s-CN values of the hexagonal net. A three-dimensional T_1, T_2, T_3 structure map of the rhomb net gives the same information as the T_1, T_2 structure maps of the square or hexagonal net. The structural units of the different structure families are distorted a, b, c, s, t units of the square net (with different s, s′ and t, t′ for the occupation of different single sites s and *trans* positions t in a rhomb).

The rectangle net with s-CN values (2+2) 4 (2+2) (Figs. 37b,38) is another distortion of the 4 4 4 square net, if the $1 + 1'$ and $3 + 3'$ atoms are added to 4 4 4 of the square net at small distortions ($b/a \leq \sqrt{3}$). The different families of structures are the same as for the square net with the same structural units. The T_1, T_2 structure map of the rectangle net however has only the information of the 1 and 1′ atoms. The three-dimensional T_1, T_2, T_3 atlas yields the same information as the T_1, T_2 structure map of the square net.

The different structural units of rectangles or rhombs can be added only in one orientation for a two-dimensional tiling. The situation is similar as for chains of A and B atoms in the direction of nearest neighbors. The 2 1 2 ; 1 structure (Fig.38) for example can be characterized by sequences of A and B atoms AABB or structural units acbc. Both sequences can be analyzed by the structure map of a chain of A and B atoms or a, b and c structural units (Fig.2b), where the s-CN values of AABB (1 0 1 ; 1) or of the units a (0 0 0 ; 3), b (0 0 0 ; 3) and c (0 2 0 ; 1) of the acbc chain correspond to different points of the structure map (Fig.2b). An alternation of abab of a units with other units like b yields M. The single unit ab_n, $n \geq 2$, where a units are separated by two or more other units, yields S. The double row (D) in a sequence $abab_n$ or triple row (T) of three alternating a in $ababab_n$ can be considered as a combination of ab and ab_n.

Molecules with low symmetry are frequently packed with two different orientations a and b. Rows of molecules staggered by a glide lattice operation can produce a very efficient close packing by repeating a molecule of arbitrary form in the space groups 1, 4, 14, 19, 29 or 33 (2, 14, 15 or 16 for centrosymmetric molecules). These space groups are actually the most frequently observed for molecular crystals (Kitaigorodski, 1973).

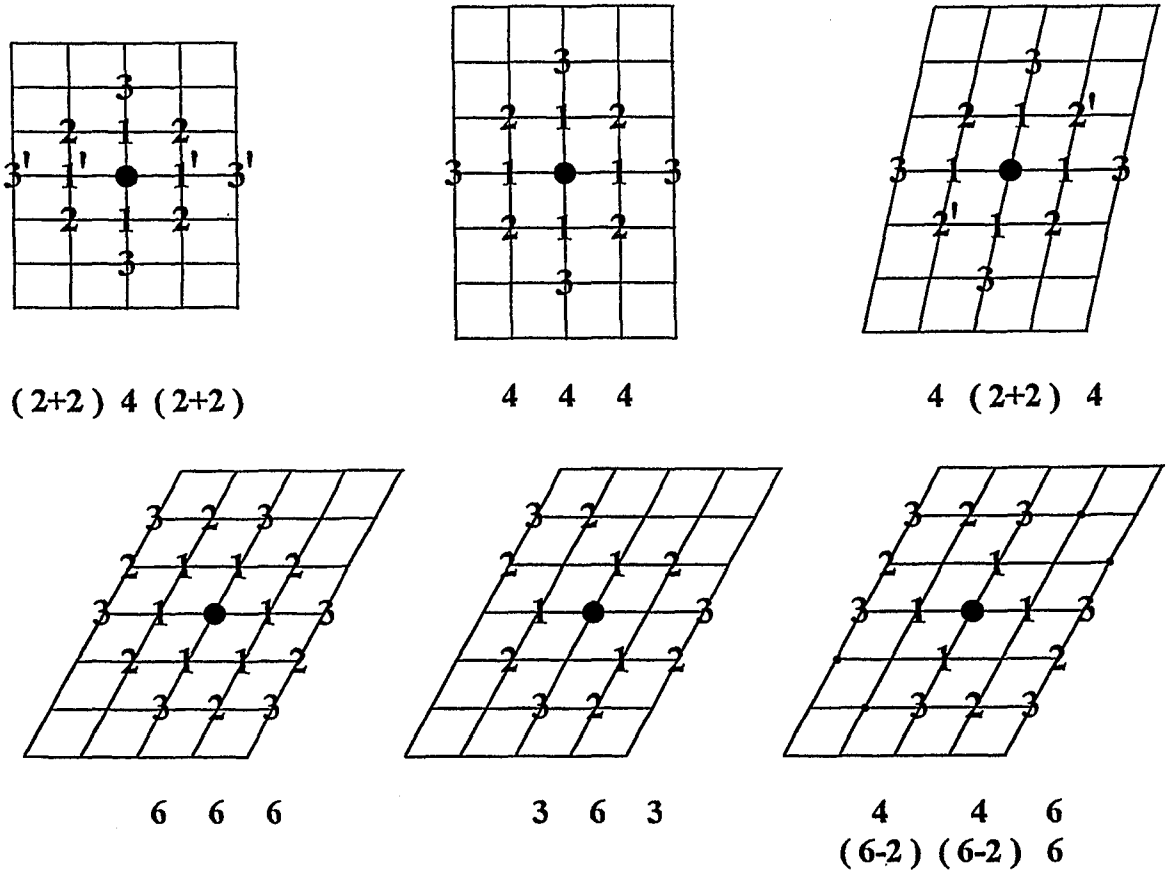

Figure 39: All nearest (1), second (2) and third (3) neighbors T_1, T_2, T_3 of a central atom (•) in the rectangle ((2+2) 4 (2+2)), square (4 4 4), distorted square (4 (2+2) 4), hexagonal (6 6 6), honeycomb (3 6 3) or kagomé (4 4 6) net. The distances from the central atom to 1′, 2′ or 3′ positions are larger than for 1, 2 or 3.

The numbers of molecules with the same orientation like aabb and a two-dimensional tiling in some cases like the β-sheet structure of amino acids depend on the shape and the interactions of the molecules.

Chains of identical atoms Se_3, Se_7 or Se_∞ in $RbDy_3Se_8$ or dimers Se_2 in $La_{10}Se_{19}$ or $LaSe_2$ with Se atoms on a square net (Lee and Foran, 1994) can be characterized by the orientation of neighboring atoms like $\ominus$ for horizontal and $\oplus$ for vertical orientation of two neighboring atoms. Other chains with an increased number of orientations can be characterized by an increased number of symbols similar to magnetic structures (Section 20).

Three-dimensional layered structures can be distorted by variation of the distance $\Delta z\, c/a$ between layers like for ccp and bcc ordered structures (Section 15). The symmetry of most structures is not reduced by this procedure. The variation of x, y, z parameters within the plane is another possibility for distortion. The structures of As, Sb and Bi with $z \approx 0.23$ (Wyckoff, 1982) and $\Delta z\, c/a \approx 0.47$ can be considered as a distortion of the pc lattice ($z = 0.25$, $\Delta z\, c/a \approx 0.41$) or a distortion of trigonal graphite ($z = 1/6$, $\Delta z\, c/a = 1.35$). The symmetry of the crystal remains unchanged for the helix structure of Se or Te with 3_1 symmetry (Fig.33). The bonding between Te atoms in a chiral chain is enhanced. The distance to neighboring Te atoms is increased, if the x parameter of a close-packed layer ($x = 0.33$) is decreased to $x = 0.269$ in Te or 0.217 in Se (Wyckoff, 1982). The distance to neighboring atoms a $\approx$ 0.45 nm and the height of the helix $c = 0.59$ nm in Te or 0.49 nm in Se is similar as the distance $c/3a \approx 0.4$ between the three layers in the pc lattice (Burdett, 1995). The helices with 3_1 or 6_1 symmetry contain 3 or 6 atoms/turn like the 2 2 12;2b and 2 2 0;2b structures (Fig.13). The helices of DNA contain 10 – 11 base pairs/turn (Fig.33) with different distances 0.29 – 0.34 nm in the direction of the helix similar to the different $\Delta z\, c/a$ in layered compounds (Table 7) (Section 26). The α-helix of proteins containing 3.6 amino acids/turn with a distance of 0.15 nm between amino acids is intermediate to the 3_1 or 4_1 helices of inorganic compounds. A two- or three-dimensional periodic combination is avoided in protein and DNA helices.

The loss of the 3-fold axis in [111] layered compounds implies, that the bonding to the three atoms of the neighboring layer is different. The same applies if the 4-fold axis is lost in [001] layered compounds.

24 Physical and chemical properties of structural units

The relation between structural units and properties is known to a large extent in the nucleic acids DNA and RNA with the four bases adenine (**A**), thymine (**T**), cytosine (**C**) or guanine (**G**) which are forming chains in the helix or double helix structure (Glusker et al., 1994). The sequences of three bases (triplets or codons) convey the information for one of the 20 amino acids or in some cases a stop signal to indicate the end of the protein, which is a sequence of different amino acids (Section 26).

Some physical properties can also be related to the structural units u, u′, v and w′ of superconducting oxides (Hauck and Mika, 1997 and 1998a). All superconducting oxides contain v units with the CuO_2 planes and neighboring u′ or w′ units like Cu′O in $Cu'Ba_2Cu_2YO_7$ (u′vu|) or TlO in $CaCu_2Ba_2TlO_7$ (uvw′|), to transfer e^+ charges to the superconducting CuO_2 planes. In high T_c compounds with $T_c > 40K$ the CuO_2 planes are next to insulating u_2 units like in u′vu| = u′v$u_2$vu′ or uvw′| = uvw'_2vu_2vw'_2 . . . .

The sequences of coordination numbers of the metal atoms Cu′BaCuYCu Ba,Cu′ CN = 4 10 5 8 5 10, 4 in $Cu'Ba_2Cu_2YO_7$ or CN = 8 5 9 6′ 9 5, 8 for CaCuBaTlBaCu,Ca in $CaCu_2Ba_2TlO_7$ (Table 12) shows an asymmetric arrangement of the atoms next to the Cu atoms with CN = 5. The CuO_2 layers are bent towards the Ca, Sr or Y atoms, because of the stronger bonding of these atoms to the oxygen atoms compared to the BaO bonding of Ba atoms with CN = 10 or 9. The bond strength is increased by the inductive effect of M atoms in the sequence Ba, Na < Sr < Ca, Li < Mg < M^{3+} < M^{4+} (Hauck and Mika, 1997) similar to the

inductive effect in organic compounds (Glusker et al., 1994; Latscha and Klein, 1982). The Cu'O layers of $Cu'Ba_2Cu_2YO_7$ can not be influenced by the symmetrical neighborhood of Ba atoms.

The principle of a central structural unit with a physical property that can be modified by one or two (different) neighboring units is quite frequent in organic systems like drugs, pigments or pesticides. In diphenylazo compounds for example the yellow color can be modified to orange or red by the inductive effect of OH, NH_2, etc. groups on one phenyl group. One or two H atoms of the other phenyl group are substituted by COOH or SO_3H groups which can react with the amino groups of wool for example for a stable coloring of wool. The same applies for organic acids like

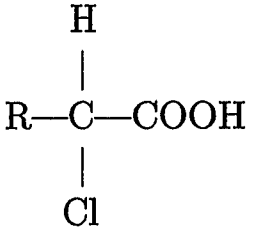

which can be varied by the inductive effect of F > Cl > Br > I, etc. atoms and the different hydrophobic character of short or long chains of R $\widehat{=}$ $(CH_2)_n$–CH_3 groups.

The layered compounds are non-metallic, if the valence rule (Section 17) or Pauling's electrovalence rule (Section 19) are satisfied. Pauling's electrovalence rule is obeyed for the Ketelaar and Forsyth, Gran families of NaCl related compounds and for the Johansson, Linde and Brauer or Schubert families of ZnS (sphalerite and wurtzite) related structures (adamantane structures) (Tables 11,12). The band gap of the semiconducting compounds varies with the lattice constant and the ordering of metal atoms in adamantane structures (Waag et al., 1998). A physical property of a compound is varied by homologous substitution. The physical properties of semiconducting Si for example are varied in GaP or $In(Ga,Al)P_2$ (Table 11a).

The comparison of NaCl related compounds shows attractive interactions in carbides Ti_2C, Gd_2C (6 0 12; 1a,b) with facial configuration of C atoms and repulsive interactions in hydrides or nitrides like Pd_2H,

Ti_2N (4 4 16; 1) with meridional configurations of H or N atoms. Carbides like TaC or HfC exhibit very high melting points (Toth, 1971). The elastic constants are supposed to be related with bonding properties. Compounds with directional covalent bonding like diamond, α-Al_2O_3 (Tables 13,14) or TiC are very hard. These materials are used as abrasives or for coating of tools and other purposes (Toth, 1971).

The compounds of the Thornber, Bevan (1970) family (Table 12) like $Zr_7Ca_2\square_2O_{16}$ ($\alpha\gamma$) or $Zr_3Sc_4\square_2O_{12}$ ($Pr_7\square_2O_{12}$ structure, β(mod7)) are interesting for the SOFC (solid oxide fuel cell) because of the high oxygen mobility in the disordered phase. The perovskites (La,Sr)MnO_3 and (La,Sr)CrO_3 are used as cathode and interconnector materials in the SOFC (Hammou and Guindet, 1997). The compounds of the Raveau, Chu family like $CuBa_2Cu_2YO_7$ and (Ca,Sr)CuO_2 exhibit also a high oxygen mobility and some catalytic properties (Schoonman, 1997; Hauck et al., 1995).

Hydrides like VH_x, Li_2PdH_x or $FeTiH_x$ with structural units g_1, h, q_1 are used for storage of hydrogen (Parthé et al., 1993; Schlapbach et al., 1994). Hydrides like Pd_2H, Pd_5H_4 are interesting because of the high mobility of hydrogen atoms. The preference of H atoms for tetrahedral or octahedral interstices has been explained by the different size of the interstitial sites (Westlake, 1983) or the different mechanisms of MH bonding (Hauck, 1983). The first type of model considers a minimum hole size of 40 pm (or a critical metal atom radius of 139 pm) and a minimum distance of 210 pm between H atoms to be necessary. The larger octahedral site should be occupied in metals with small atomic radii, the smaller tetrahedral site in metals with large atomic radii.

The second type of model is based on a charge transfer between H and metal atoms with different electronegativities ϕ^*:

$M^{\delta-}\,H^{\delta+}$ for metals with high ϕ^*, e.g. M = Cr, Mn, Fe, Co, Ni, Pd,
$M^{\delta+}\,H^{\delta-}$ for metals with low ϕ^*, e.g. M = Li, Na, Ca, Sc, Y, Ti.

The $H^{\delta+}$ atoms prefer the octahedral site with a bonding to the transition metal *d* electrons. The $H^{\delta-}$ occupies octahedral interstices of metals with no *d* electrons, otherwise tetrahedral interstices. Both sites can be

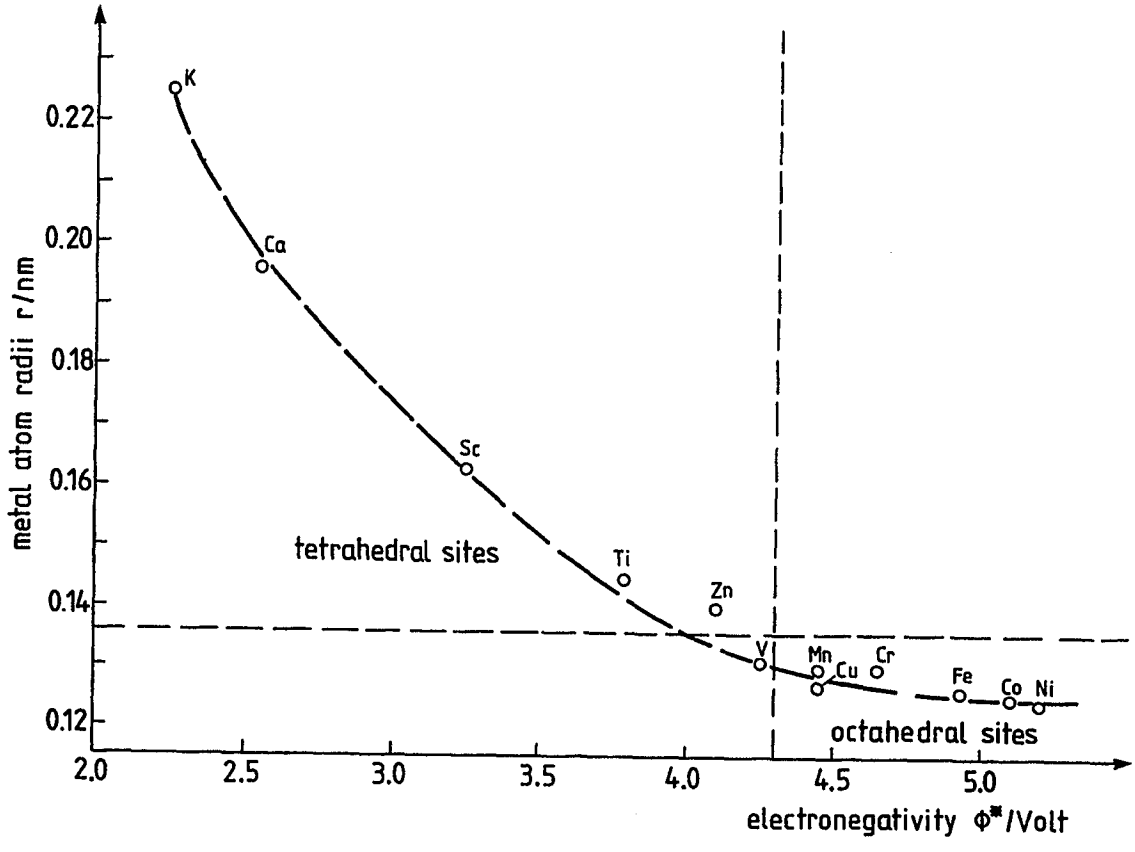

Figure 40: Hydrogen occupancy of octahedral sites in metals with small radii and high electronegativity, otherwise tetrahedral sites.

occupied in vanadium depending on temperature, hydrogen concentration and isotope (Hauck, 1983).

The two models give the same prediction for most metals because of the correlation between small metal atom radii and high electronegativity (Fig.40). The critical radius of metal atoms, 139 pm, corresponds with the cubic lattice constant of 393 pm and can explain the variation from octahedral coordination in $PdD_{0.7}$ and LiH to the tetrahedral coordination in VH_2, etc. (Fig.41). Octahedral sites, however, are also occupied in NaH, KH, RbH or CsH which have larger lattice constants. In rare earth hydrides the smaller tetrahedral sites are occupied first, while octahedral sites are occupied at $H/M \geq 1.95$. This behaviour can be explained by the second type of model with H atoms as a sensitive probe for *d* electrons. The *d* electrons of the rare earth metals are depleted at increasing H content because of the charge transfer to $H^{\delta-}$. The loss

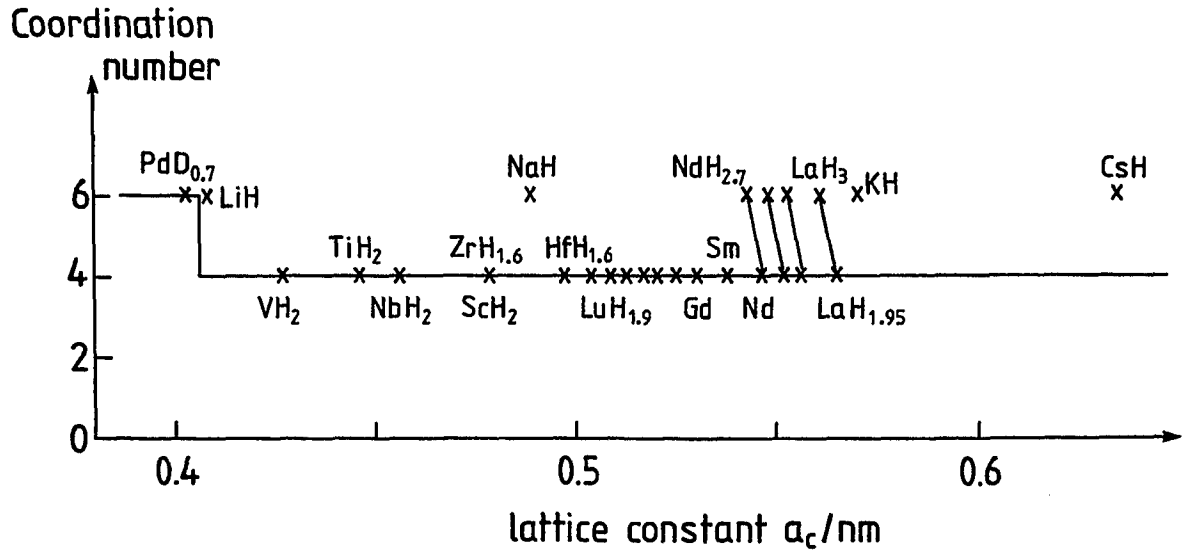

Figure 41: Coordination of hydrogen atoms in ccp M structures with cubic lattice constant a_c.

of d electrons gives rise to a metal-semiconductor transition, different magnetic properties and smaller lattice constants (Hauck, 1983).

The other interstitial atoms I = C, N, O, ... are too big for the occupation of tetrahedral sites. The bonding geometries of the metal atoms however can be related to the hybridization of s, p and d orbitals like the CN = 4 planar (dsp^2) and tetrahedral coordination (sp^3 or d^3s) or the CN = 6 trigonal prismatic (d^4sp) or octahedral coordination (d^2sp^3) (Sutton, 1993). P, S and Se atoms usually prefer tetrahedral coordination, O atoms octahedral coordination as can be seen from the pairs of structures with identical ordering of metal atoms α-$NaFeO_2$–$In(Ga,Al)P_2$, γ-$LiFeO_2$–$CuFeS_2$, Li_2ZrO_3–$GeCu_2Se_3$. The O atoms however can also be in tetrahedral coordination in β-$NaFeO_2$ or $SiLi_2O_3$ (Tables 11,12).

25 Homogeneous sphere packings

A sphere packing is called homogeneous, if all spheres are symmetry-equivalent, otherwise it is called heterogeneous (Koch and Fischer, 1992).

The same applies to the two-dimensional packing of circles. The different packings are characterized by the number of contacts k between the spheres (circles), which is $3 \leq k \leq 12$ ($3 \leq k \leq 6$ for circles). A sphere (circle) packing is called stable, if no sphere (circle) can be moved without moving neighboring spheres (circles) at the same time. A minimum of four (three) contacts per sphere (circle) is required. Not all contacts must fall in one hemisphere (semicircle) (Koch and Fischer, 1992). Stable homogeneous sphere packings are interesting in searching for materials with low density. They are classified in types with constant k at different distortions. Two sphere packings belong to the same type, if there exists a biunique mapping that brings the spheres of one packing onto the spheres of the other packing. The number of types of homogeneous sphere packing is finite. The types of homogeneous circle and sphere packings with cubic or tetragonal symmetry are known (Koch and Fischer, 1992). They can be compared with the two- or three-dimensional structures of Section 4 or Table 21a–d with a single set of T_i values (environment-equivalent) for A and B atoms in A_xB_y. The number of contacts k corresponds to the T_1 values for spheres (circles) with diameter d. The density of the hexagonal lattice ($\rho = 0.907$), square lattice ($\rho = 0.785$), hcp or ccp ($\rho = 0.741$), bcc ($\rho = 0.680$) and pc ($\rho = 0.524$) of A_xB_y compounds is reduced by the factor x/(x + y) (or y/(x + y)), if the A (or B) atom positions are vacant. The $k = T_2$ (or T_3) values, increased diameters (Table 2) and different densities are derived for structures with $T_1 = 0$ (or $T_1 = T_2 = 0$). The two-dimensional 6 6 6; (1), 0 6 0; 2, 0 0 6; 3 (Fig.6), 4 4 4; (1), 0 4 4; 1, 0 0 4; 3 (Fig.8) and 0 0 0; 6 structures ($Pr_7\square_2O_{12}$ net, Fig.33) are homogeneous circle packings (Koch and Fischer, 1992). The number of contacts $k = 5$ ($Pr_7\square_2O_{12}$ net), 4 (0 0 6; 3, kagomé net) or 3 (0 6 0; 2, honeycomb net) between B atoms is obtained for vacant A positions (Section 28). The three-dimensional structures of the pc lattice (Table 21d) 6 8 12; (1), 0 0 8; 3 (bcc) and 0 12 0; 1 (fcc) are stable homogeneous sphere packings, if the B atoms are removed. They correspond to the same type of sphere packing with $k = 6$, 8 and 12 contacts in 0 6 12; 1, 8 6 12; (1) and 0 0 12; 3 in the bcc lattice (Table 21c) or 0 6 0; 3 and 12 6 24; (1) in the ccp lattice (Table 21b). The hcp, ccp or bcc systems contain other stable sphere packings, which are underlined in Table 22 (or underlined with square brackets for stable packings of B atoms at y/x > 1). The structures at

the left-hand borders of the structure maps containing alternating layers of A and B atoms are not stable, if the A or B atoms are removed. Many homogeneous sphere packings of the bcc, fcc and pc lattice belong to the same type with the same space group like 0 6 12 ; 1 (bcc), 0 6 0 ; 3 (fcc) and 6 12 8 ; (1) (pc) with $k = 6$ (Table 22) or the same space group and Pearson symbol like 4 2 4 ; 1.33a,b (bcc) and 4 2 12 ; 1.33a,b (fcc) with $k = 4$ contacts.

The CsCl, NaCl or CaF_2 structures are examples of heterogeneous sphere packings with the ideal ratios of diameters of A and B atoms $d_B/d_A = 0.732$, 0.414 or 0.225, respectively.

26 Colloids, clusters and DNA

An ordering of hard-sphere colloidal crystals was first observed for AB_2 and AB_{13} compositions in native gem opals. They consist of dried arrays of colloidal silica spheres with diameters $d_A = 362$ nm and $d_B = 210$ nm (Sanders, 1980). Colloidal particles like amorphous SiO_2, polymers or inorganic clusters with a particle size of 10 – 2000 nm can be obtained by chemical synthesis and are stabilized sterically by thin ($\approx$ 10 nm) coatings. They are suspended in polar or apolar mixtures of liquids with the same refractive index for transparent suspensions which are suitable for quantitative light scattering. For the proper composition like 50% solvent a process similar to crystallization is observed after several days of sedimentation (Pusey and van Megen, 1986). The particles interact via short-ranged repulsive forces because of the stabilizing layer which mitigates the attractive van der Waals forces of the polymer cores, for example. The interaction between the particles can be tuned by different charges of the coatings and different solvents. The interactions between A atoms as predicted by the structure maps can probably be tested by mixtures A_xB_y of spherical particles A and B with the proper ratio of diameters and suitable coatings. The properties of suspended particles however can differ from those for purely atomic systems due to the presence of the solvent (Pusey and van Megen, 1986). A ccp structure with

disordered stacking in [111] direction with a fraction f = 0.42 – 0.5 of h layers depending on time, temperature and composition was observed for a one-component system (Pusey et al., 1989). The analysis of T_i values in close-packed structures had shown a single set ($M^i = 1$) for hcp or ccp structures (Table 1, Section 2). The repulsive interactions are increased slightly in ccp, because of the ordering of the second-nearest neighbors on a straight line in [110] direction (Fig.1).

Spherical clusters of non-metallic compounds might be obtained only for few diameters because of the requirement for electroneutrality. This is demonstrated for the $i = 1 - 3$ shell of clusters with NaCl structure. Na and Cl atoms form a pc lattice with T_i values 0 12 0 ; 1 compared to the maximum values 6 12 8 of closed shells (Table 23d). A Na atom in the center is coordinated by 0 Na and 6 Cl atoms at T_1, 12 Na and 0 Cl atoms at T_2 and 0 Na and 8 Cl atoms at T_3. The compositions $NaCl_6$, $Na_{13}Cl_6$ and $Na_{13}Cl_{14}$ for spheres with complete occupation of the first, second or third shell have an excess of positive or negative charges. The T_i values for larger clusters containing up to $\approx$ 200 atoms are given in Table 23 for hcp, ccp, bcc and pc compounds with single sets of T_i values for A and B atoms. The rare gases Ar and Xe, which crystallize in the ccp lattice at low temperatures, form clusters with x = 13, 19, 23, 25, 55, 71, 87, 135 and 147 (Sugano and Koizumi, 1998). The magic numbers x = 7, 10, 14, 23 and 30 (^{4}He) and x = 7, 10, 14, 21 and 30 (^{3}He) were found for the different He isotopes, which crystallize in the hcp or ccp structure at low temperatures (Wyckoff, 1982). The T_i values 12 6 2 of a central atom of the hcp packing yields x = 13, 19, 21, 39, 51, 57, 69, 81, 87, 93, 105, 129, 135, 147, ... compared to x = 13, 19, 43, 55, 79, 87, 135, 141, 147, 201 for a ccp cluster. The x = 23, 25, 71 values of Xe and most magic numbers of the He isotopes are not in the list for stable low temperature structures. A similar situation occurs for the magic numbers x = 8, 20, 40, 58, 92 of Na clusters compared with the closed shells of the bcc lattice x = 9, 15, 27, 51, 59, 65, 89, 113 (Table 23c) and for the Si clusters. The diamond structure of crystalline Si is obtained as an ordered bcc structure Si□ with T_i values 4 0 12 ; 1, where half of the positions of the bcc lattice are vacant (□). The cluster sizes x = 5, 17, 29, 35, which are obtained for the occupied shells at $i = 1$, 3, 4, 6, ... (Table 23c), do not coincide with the observed magic numbers

x = 6, 10. Other clusters with reduced density for vacant B positions like the ccp 7 2 10;1 structure exhibit the proper x = 8, 10, 20, 26, 36, 40, 68, 70, 91 values of A = Si or Na atoms. Both positions of A and B atoms are occupied in the CsCl structure (0 6 12;1 of the bcc lattice, Table 23c) and 0 12 0;1 of the pc lattice (Table 23d). Most clusters of the bcc lattice with closed shells at x = 9, 15, 27, etc. and of the pc lattice at x = 7, 19, 27, 33, 51, 75, etc. however are not neutral. All NaCl or CsCl clusters can only be neutral, if one atom like the central atom is missing. Only few magic numbers for clusters coincide with the cluster sizes of closed shells, if the same structure as in the crystalline phase is assumed. Clusters of other metastable phases could be formed by the rapid quenching process. The present compilation shows all spherical clusters with the same surrounding of each atom except the surface atoms, which are different in all kinds of theoretical approaches. Therefore the numbers x of the present investigation might be useful to discuss magic numbers $x \gtrsim 10$ for clusters of A and B atoms.

Microclusters like NaCl are generated by quenching the metal halide vapor of typically 20 Pa at 1000 K within less than 100 microseconds in a helium atmosphere of about 100 Pa at 70 – 300 K (Sattler, 1987). The observation of magic numbers x and y of stable clusters depending on the temperatures of quenching and the methods of analysis are explained by the assumption of neutral spherical clusters, which crystallize from the gas phase. Several atoms of the original clusters evaporate in such a way that charged $Na_xCl^+_{x-1}$ cuboids containing 3 × 3 × 3 (x = 14), 3 × 3 × 5 (x = 23), 3 × 5 × 5 (x = 38) atoms or neutral Na_xCl_x clusters containing 3 × 3 × 4 (x = 18), 2 × 4 × 5 (x = 20), 3 × 4 × 4 (x = 24) atoms are left at increased temperatures. This process is similar to the crystal growth process with a formation of stable external forms and habits of crystals (Wulff, 1901). The present compilation (Table 23) shows all clusters with closed shells. Some special clusters can be obtained by $T_j = a\,j^3 + b\,j^2 + c\,j + 1$. The shells $j = 1, 2, \ldots$ are a selection of the $i = 1, 2, \ldots$ shells, where clusters with the shape of crystals are obtained. This can be demonstrated for the 4 4 4;(1) structure of the square net. The coefficients $a = 0$, $b = c = 2$ yield square clusters with x = <u>5</u>, <u>13</u>, <u>25</u>, 41 atoms for $j = 1, 2, 3, 4$, which coincide with the underlined x values of the 4 4 4;(1) structure (x = <u>5</u>, 9, <u>13</u>, 21, <u>25</u>, 29, 37, 45, ...) for $i =$

1 – 8 (Table 2). The cluster containing 41 atoms does not have a closed shell like the x = 37 and x = 45 clusters. The coefficients are $a = 0$, $b = c = 3$ for hexagonal clusters with x = 7, 19, 37, 61, etc. particles with the 6 6 6 ; (1) structure of the hexagonal net. The situation is similar for the three-dimensional structures. The constants $a = 10/3$, $b = 5$ and $c = 11/3$ were obtained for a packing of cubo-octahedra in the 12 6 24 ; (1) structure of the ccp lattice (Urban, 1998; Wulff, 1901). The underlined magic numbers x = 13, 55, 147 coincide with closed shells for x = 13, 19, 43, 55, 79, 87, 135, 141, 177, 201 (Table 23b). The missing central atom is suggested for the stabilization of clusters (Urban, 1998).

DNA or long chains of proteins can have the size of colloids ($\approx 10^2$ – 10^4 nm). Their structures can be analyzed like a one-dimensional cluster with four to twenty different structural units. The basic components of DNA are alternating units of 2′-deoxyribose (D) and phosphate groups (P) forming a DP chain with phosphodiester bonds between the 5′ position of one deoxyribose and the 3′ position of the next deoxyribose (Dale, 1996; Glusker et al., 1994; Diekerson, 1989). One of the four bases adenine (**A**), thymine (**T**), cytosine (**C**) or guanine (**G**) is attached to the 1′ position of each deoxyribose. Each **A** is linked to a **T** of the neighboring chain by two hydrogen bonds, and each **G** is linked to a **C** by three hydrogen bonds. The **A** and **G** units are larger than the **T** and **C** units. The complementary strands are twisted around each other in the now familiar "double helix", with the bases in the center and the hydrophilic deoxyribose (or ribose in RNA) and phosphate residues on the outside. The exact DNA structure is influenced by several factors such as the sequence of bases and the interaction with the surrounding water. The Watson and Crick structure (B form) is a right-handed helix with 10 base pairs (bp) per turn and a distance $d = 0.34$ nm between the base pairs. A more compact form (A form) with about 11 bp per turn and $d = 0.29$ nm occurs at reduced water content. Certain DNA sequences with alternating **G** and **C** bases tend to form a left-handed helix (Z form), at least over a short distance, with 12 bp per turn and $d = 0.38$ nm. The different rotations give rise to a winding of the helix into coils (Dale, 1996). The *in vitro* structures of the DNA's, however, are not known in detail, and the number of different structures is probably larger than the number of polytypes in layered compounds. The interactions be-

tween the bases of one strand are assumed to be very weak because of the absence of direct bonding (in helices without defects). Dipole-dipole interactions are considered besides the van der Waals interactions because of partial positive or negative charges in the neighborhood of the N–H$\cdots$O or N–H$\cdots$N hydrogen bonds. The sequences of bases deviate from a random distribution ($\alpha_i = 0$) in such a way that attractive or repulsive interactions are preferred in some portions of the DNA.

The ratios r = 1.5 – 7.5 of the nucleic acids **A**, **T**, **C**, **G** like r = (**T** + **C** + **G**)/**A** for the base **A** are similar to those of the layered compounds (r = 1 – 11) (Table 7). The α_1, α_2 values which were obtained from the averaged T_i values are similar to the values of disordered alloys (Fig.17) (Hauck et al., 1999). The α_i values of the bases in different sections of the structure map Ia – IVb (Fig.16) can be correlated with a distinct occurrence of clusters like **AAA** (in IIIb – IVa), isolated bases **A** like **TCG ACT** (in Ia,b) or bases **A** alternating with other bases like **ATA CAG** ..., etc. (in IIa,b). Eighteen different DNA or RNA sections with the same kind of functions (enolase and secA), which occur in bacterias (like secA 15), rats (enolase 15) or human being (enolase 8), were classified in different groups (Table 24). Most DNA's contain clusters, which are avoided in disordered alloys (Section 13).

The mRNA carries the information for the sequence of amino acids in a protein in the form of the genetic code in which each occurrence of one of the 64 groups of three nucleotides (triplets or codons) conveys the information for a specific amino acid (or in some cases a stop signal to indicate the end of the protein) (Dale, 1996). Fifteen amino acids are obtained by symmetrical triplets **AAA** (Lys), **ATA** (Ile), **ACA** (Thr), **AGA** (Arg), **TTT** (Phe), **TCT** (Ser), **TGT** (Cys), **TAT** (Tyr), **CCC** (Pro), **CGC** (Arg), **CAC** (His), **CTC** (Leu), **GGG** (Gly), **GAG** (Glu), **GTG** (Val) and **GCG** (Ala). Arginine (Arg) is obtained by **AGA** or **CGC**.

The remaining five amino acids Asn, Asp, Glu, Met and Trp can be obtained only by non-symmetrical triplets. This is only possible because of a given direction from 5′ to 3′ on each strand (Dale, 1996) and of stop signals (**TAA**, **TAG** or **TGA**).

The increased fraction of **A** and **T** clusters in the first group would be obtained, e.g., at an increased number of **AAA** (Lys) and **TTT** (Phe) clusters, while the increased percentage of double units for **T** in the second group could be possible at an increased number of **TCT** (Ser), **TGT** (Cys) and **TAT** (Tyr).

The different groups can probably be related with a variation of the number of structural units in evolution. The 16 different combinations of two bases (**A**, **C**, **G**, **T**) like **AA**, **AC**, **CA**, **AG**, etc. yield 15 different amino acids. The information of the 16 symmetrical triplets mentioned before is maintained, if the first or last letter is missing. At least one combination like **GA** is required for a stop signal for the production of proteins. 63 instead of 20 amino acids could occur for the combination of three bases (codons) like **AAA** (Lys), **AAC** (Asn), **CAA** (Glu), etc. . The same amino acid is synthesized by several combinations like Gly by the four combinations **GGT**, **GGC**, **GGA** and **GGG**. Usually all combinations are used. The restriction to few combinations in bacterias is probably related with the early stage of evolution and is maintained in few species like the silkworm *B.mori* producing silk with a speed of $\approx$ 100 amino acids/sec (Glusker et al., 1994). The polypeptide of silk contains mainly alternating units of Ser and Gly or Ala and Gly in the sequence Gly–(Ala–Gly)$_2$–[Ser–Gly–(Ala–Gly)$_n$]$_8$– (Ser–Gly)–Ala–Ala–Gly–Tyr. The codons **GGT** and **GGA** for Gly, **TCA** for Ser and **GCT** for Ala are used. Four chains are combined in the β-sheet structure with a connection of the amino acids similar to a zipper. The periodic sequences and the nonperiodic end of the chain Ala–Ala–Gly–Tyr are related with the high strength and the elasticity of silk, respectively. The T_i values of the sequence of amino acids in silk are close to the border of the structure map. How would it look like, if evolution would have selected periodic sequences of bases in DNA and amino acids in proteins, which are on the border of the structure map? The number of different species would have been reduced.

The numbers of different structures N_{H} at the borders of the structure map, which are stabilized by the enthalpy H, and other entropy stabilized structures N_{S} increase by $N_{\mathrm{H}}(n) \approx \mathrm{C_H}\times 10^{0.16n}$ and $N_{\mathrm{S}}(n) \approx \mathrm{C_S}\times 10^{0.26n}$, respectively, where $\mathrm{C_H}$, $\mathrm{C_S}$ depend on r ($\mathrm{C_H} \approx 0.1$ for r = 1) and, for

border structures, on the particular border, for an increased length of the chain n. 1504 structures with different T_i values were selected from 5 200 300 structures at $n = 26$ and r = 1, for example. The natural language of DNA may be compared with the man made language with 26 letters and several thousand words, or with chains of music notes or numbers with 7 or 10 structural units, respectively. The different codons for the same protein can probably be compared with different words with the same meaning like the Roman or Italian VIA, the English WAY and the German WEG. The "evolution" of languages or music within centuries can probably also be analyzed by typical deviations from randomness. Periodic sequences like certain poems (hexameter for example), the ringing of church clocks or the decades 10, 100, 1000, etc. are either nice or useful. The different languages allow a large variety, while identical numbers and music notes are practical for a fast communication with a minimum of errors.

Two types of right-handed helices (A or B form) with 11 or 10 bp per turn and a left-handed helix (Z form) are known (Glusker et al., 1994). Within the cell the DNA helix is wound up into coils (Dale, 1996). For example, bacterial DNA is normally negatively supercoiled to the extent of about one negative turn per 200 bp. The density is increased by the supercoiling. The *Escherichia coli* chromosome, in its expanded state, for example, would be several hundred times longer than the bacterial cell itself (Dale, 1996).

There are six parameters for the exact analysis of the translation and rotation from one base pair to the next, which are correlated and depend to a certain extent upon the choice of the overall helix axis (Diekerson et al., 1989). An approximate description with A, B or Z indices for each base pair in the A, B or Z helix and X values for deviations from the ideal helix by about 10% would show whether there is a correlation between the sequence of bases with, e.g., clustering in certain areas and the approximated configuration of the helix. The sections of the helix containing single bases ($\mathbf{A} + \mathbf{G} \neq \mathbf{C} + \mathbf{T}$) could be indicated by A′, B′, Z′ and X′, respectively.

27 Structure and interactions of atomic nuclei

The atomic nuclei contain x protons M and y neutrons N with slightly different mass and different interactions. They probably can be treated like ordered alloys M_xN_y with large thermal vibrations of the nuclei at temperatures close to the melting point. The ordering of protons and neutrons is compared with small grains of M_xN_y alloys with $x + y \lesssim 208$ in the present investigation. Small grains of M_xN_y alloys usually have the same structure as large single crystals because of the major contribution of nearest and next-nearest neighbors T_1 and T_2 to the lattice energy. The bonding of the surface atoms is different because of the different numbers T_i at the surface. 11 hcp, 19 ccp, 8 bcc and 17 pc structures with identical T_i values were obtained for the borders of the T_1, T_2 structure maps (Tables 21,23). The composition of structures with identical T_1 and T_2 values of the M and N particles (except the particles at the surface) can be obtained from the T_i^M values of the protons, which are the minority component in most cases (Zeldes, 1996). The numbers of all particles including the i-th sphere are obtained from Table 2. The numbers x of protons are the values of Table 23 plus the central position. (The symmetrical configuration is obtained for M_yN_x composition). The ratio $r = y/x$ is ≈ 1 for $x \lesssim 20$ and increases to $r = 126/82 \approx 1.5$ at the upper limit of stable isotopes. The numbers x or y = 2, 8, 20, 28, 50, 82 and 126 are magic numbers with an increased stability of isotopes with x = 2 (He), 8 (O), 20 (Ca), 28 (Ni), 50 (Sn) and 82 (Pb) compared to neighboring elements. Magic numbers of neutrons are obtained for M_xN_y, x = y = 2, 8, 20, $M_{20}N_{28}$, $M_{28}N_{50}$, $M_{50}N_{82}$ and $M_{82}N_{126}$ (Zeldes, 1996).

Two protons and two neutrons are supposed to order in a tetrahedral cluster. The larger values x + y = 16, 40, 48, 56, 78, 100, 132, 164 and 208 can be compared with the $S_i = \sum_{j=1}^{i} T_j^{max}$ values for $i = 1 - I$, where I is defined by $S_I \leq 208$ (Table 2). They are close to the $i = 1 - 11$ sequence of values 13, 19, 43, 55, 79, 87, 135, 141, 177, 201 and 225 of the ccp lattice. The numbers of approximate values 13 ($i = 1$), 19 ($i = 2$), 39 ($i = 4$), 51 ($i = 5$), 57 ($i = 6$), 81 ($i = 8$), 105 ($i = 11$), 135 ($i = 13$), 207 ($i = 18$) in hcp, 15 ($i = 2$), 51 ($i = 4$), 59 ($i = 5$), 137 ($i = 9$),

169 ($i = 10$) in bcc and 19 ($i = 2$), 57 ($i = 5$), 81 ($i = 6$), 203 ($i = 12$) in pc are smaller. The total numbers x + y of M and N atoms at each shell are increased by 1 – 5 compared to the x and y values of isobars with magic numbers x and y. The removal of these extra protons and neutrons at the surface with decreased bonding energy gives rise to non-spherical shape of atomic nuclei. The symmetrical clusters with closed shells of the present investigation however contain an odd number of x + y values, while nuclei with even x and even y values exhibit an increased stability (Zeldes, 1996). Clusters with even x and y values can only be obtained for vacancies in the inner shells or at the central position like the x + y = 4 tetrahedron, the x + y = 8 cube or the x + y = 12 cubo-octahedron or icosahedron. The sequence of T_i^{M} values 1 6 12 0 8 0 22 0 32 0; 1.5 and $T_i^{\max}$ values 3, 12, 24, 8, 8, 22, 22, 32, 32, 44 are required for stable isotopes with magic x (and y) values. The pairwise interactions between protons are obtained for $T_1 = 1$. We suggest vacant positions in the central part. The sequence of $T_i^{\max}$ values 2, 1, 12, 24, 8, 6, 24, 24, 24, 32, 12, 48 is obtained for a bcc lattice with 6 and 5 vacancies in the T_1 and T_2 shell, respectively. The proton in the center and the $T_2 = 2$ and $T_3 = 1$ nucleons are forming a tetrahedron. Structures with $T_1 = 1$ nearest proton for pairwise interactions can not be obtained in close-packed lattices at r = 1 to 2.5. The minimum number $T_1 = 4$ at r = 1 is decreased at increased r values ($T_1 = 6 - 2r$) (Sections 5,6).

28 Classification of symmetrical patterns

The chemist and Nobel prize winner of 1909 W. Ostwald published three collections of symmetrical patterns based on the square, hexagonal and honeycomb nets (Ostwald, 1922). The origin of a unit cell containing $p \times p$ points ($p = 1 - 4$ or 5) is connected to nearest, second, third, etc. neighbors in a systematic way and symmetrical lines obtained by the different mirror planes. The 190 patterns on single sheets of transparent paper can be combined to a large number of new patterns. They can be characterized by the numbers T_i of $i = 1, 2, \ldots$ nearest, next-nearest, ... neighbors and the ratio y/x of x points, which are connected by lines, and y other points of the unit cell.

The structures of the two-dimensional nets were investigated in a systematic way in Sections 4 and 21. Figure 42 shows a selection of these structures in a similar way as given by Ostwald. The unit cell containing x + y positions for A_xB_y compositions is shown by dots. (The unit cell is defined by two non-collinear lines from one dot, the origin, and the two parallel lines, which are not shown in Fig.42. All points at the corners (origin) of the unit cell and all points at the edges of the unit cell, which are shared with neighboring unit cells, are counted as single points.) The structures are characterized by the T_i; r=y/x values of the x A positions. The T_i values of A positions, which are connected by lines, are underlined. The A positions are connected by solid lines to T_1 nearest neighbors and by dashed lines to T_2 next-nearest neighbors in most cases. The T_2 lines are omitted for some structures containing clusters of A positions to show the clustering more clearly. All A and all B positions of the hexagonal net with T_i of A positions 0 6 0;2, 0 0 6;3, 0 0 0 6;6 and 0 4 4;1, 0 0 4;3, 0 0 0 4;4, 2 2 0;1 of the square net have identical sets of T_i values ($M^i = 2$). The patterns of these structures (except 2 2 0;1) at different corners of the structure maps are identical, if the T_3 or T_4 neighbors of 0 0 6;3 and 0 0 4;3 or 0 0 0 6;6 and 0 0 0 4;4 structures are connected by lines. The A positions can not be occupied in many surface structures because of the occupation by metal atoms (Section 21). The forbidden positions are indicated by circles in Figure 42 and the remaining positions of the honeycomb, kagomé, $Pr_7\square_2O_{12}$, etc. nets divided in A and B positions in the usual way. Crystal structures like $Pr_7\square_2O_{12}$ containing hexagonal or square layers of atoms can be visualized by these patterns and a translational vector to neighboring layers. Figure 42 shows also the hexagonal layers of the $Ta_2C \mathrel{\widehat{=}} I_2Cd$, Ta_3B_4 and $Zr_2Fe_{12}P_7$ structures of the Bozorth, Kiessling and Ganglberger families of the ph/ph′ lattice (Section 18) with solid and dashed lines for T_1 and T_2 translations. The Zr atoms of the Ganglberger family are indicated by circles. These examples might demonstrate the different kinds of combinations of hexagonal layers.

The metal atoms of the different modifications of $Ta_2C\square$, $Nb_2C\square$, $Co_2C\square$, $Fe_2N\square$ and $Ni_3C\square_2$ listed in Table 13 (Bozorth family) form a hcp packing on A and B sites at z = 0 and 1, which are not shown in Fig.42. The C or N atoms of these compounds occupy 50% of the C sites (octahedral

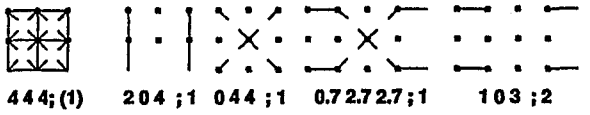
444;(1)
204 ;1
044 ;1
0.72.72.7;1
103 ;2

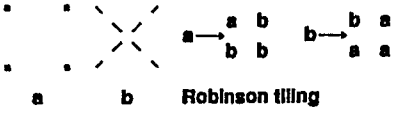
a
b
Robinson tiling

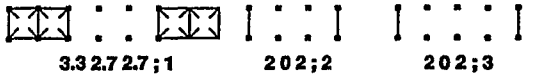
3.32.72.7;1
202;2
202;3

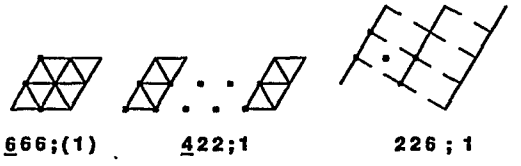
666;(1)
422;1
226 ; 1

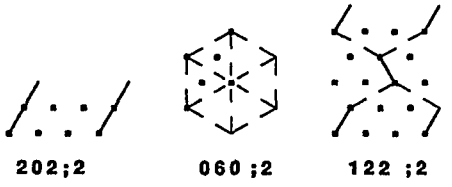
202;2
060 ;2
122 ;2

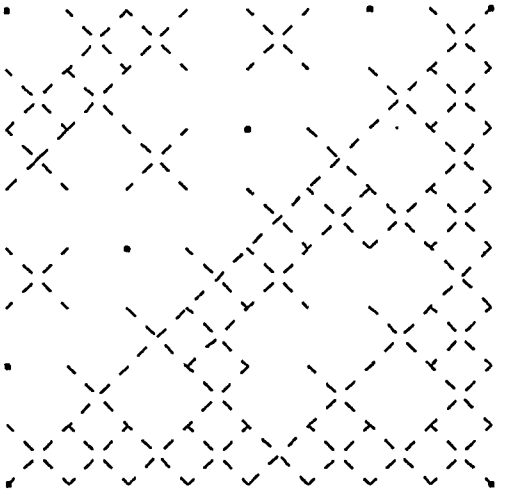
0 2.88 3.36 ; 1.56

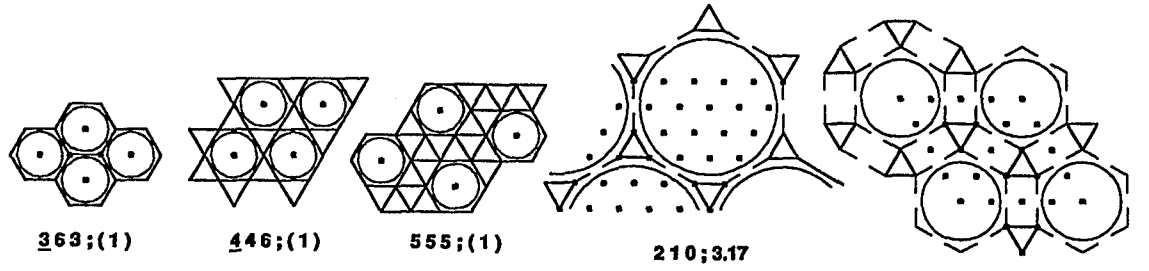
363;(1)
446;(1)
555;(1)
blocked structures
210;3.17
blocked structures
222;1.7

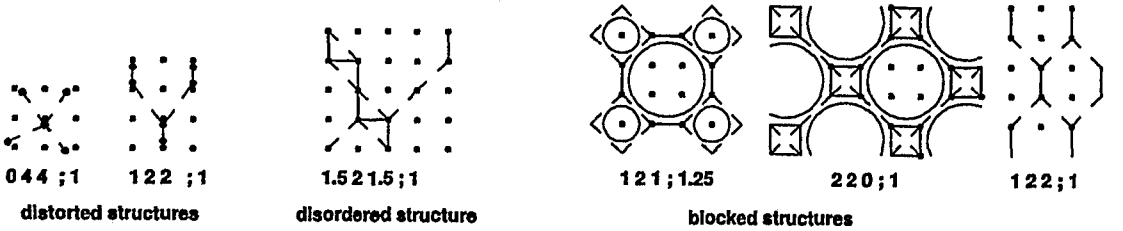
044 ;1
122 ;1
distorted structures
1.521.5;1
disordered structure
121;1.25
220;1
122;1
blocked structures

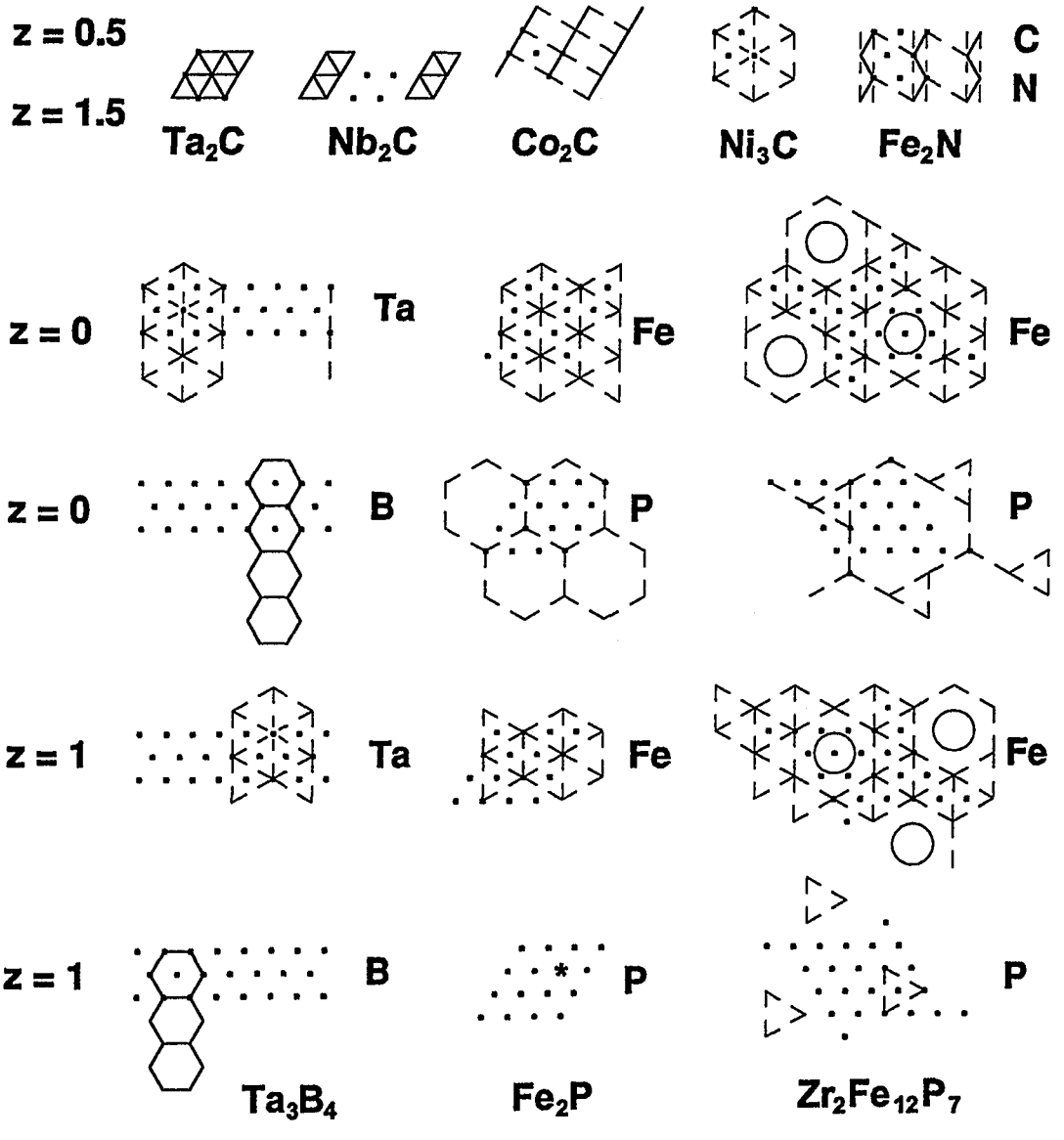
z = 0.5
z = 1.5
Ta2C
Nb2C
Co2C
Ni3C
Fe2N
C
N
z = 0
Ta
Fe
Fe
z = 0
B
P
P
z = 1
Ta
Fe
Fe
z = 1
B
P
P
Ta3B4
Fe2P
Zr2Fe12P7

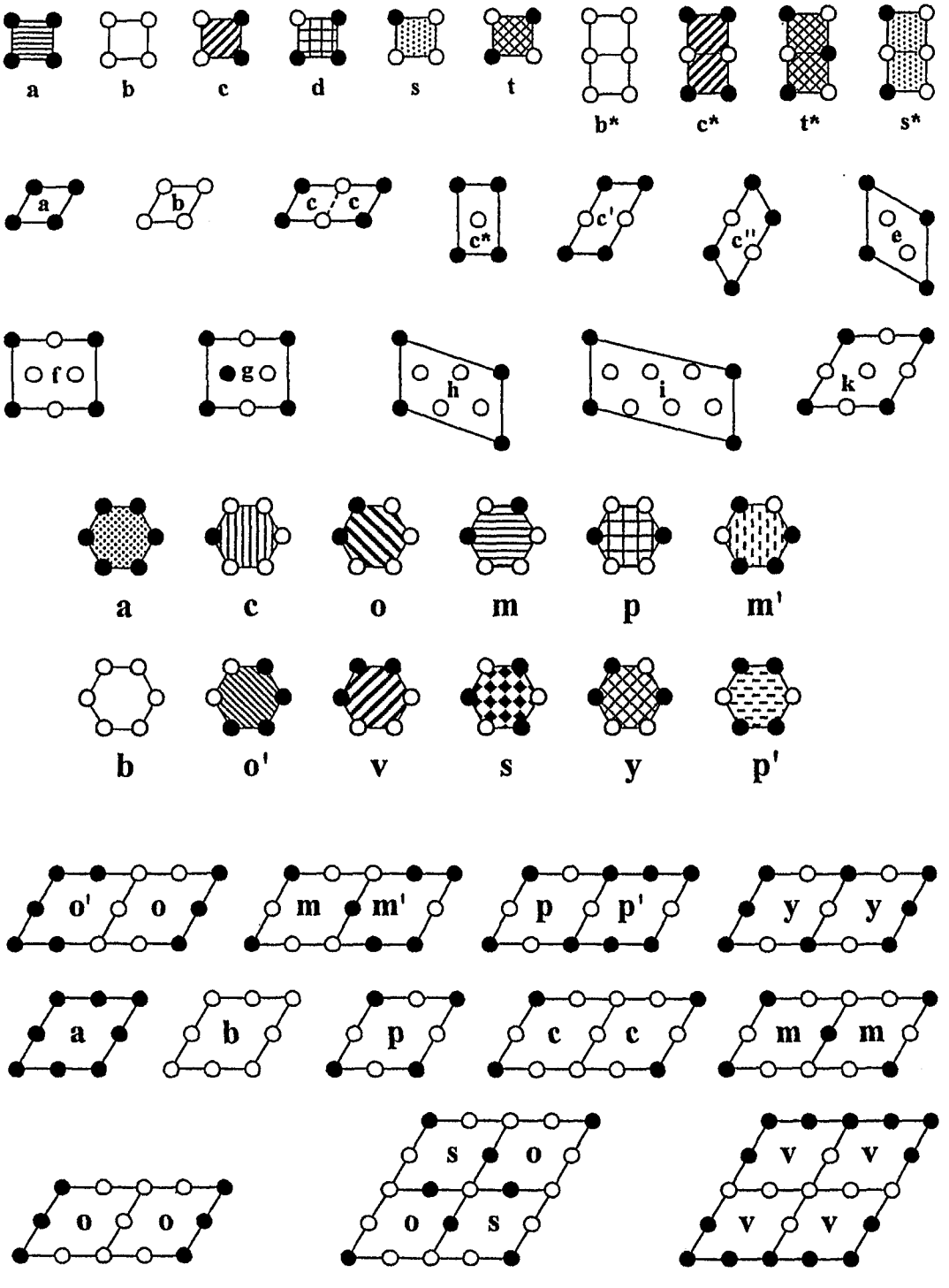

Figure 42: Periodic patterns A_xB_y, which are based on the square or hexagonal net and related nets like honeycomb or kagomé net with T_1 T_2 T_3 ; y/x values. The unit cell with x A and y B atom positions are indicated by points. The T_1 and T_2 neighbors of A positions are linked by solid or dashed lines, respectively (in $\underline{6}$ 6 6 ; (1) etc. only T_1 neighbors). The structural units can be enlarged and photocopied to obtain a two-dimensional jig-saw puzzle.

interstices) by alternation of occupied and vacant (□) hexagonal layers at z = 0.5 and 1.5 in $Ta_2C\square \mathrel{\widehat{=}} I_2Cd\square$ or identical layers C□ or N□ in $Nb_2C\square$, $Co_2C\square$, $Fe_2N\square$ (or $C\square_2$ in Ni_3C). The antistructure CdI_2 (Bozorth, 1922) is the first compound of this family (Table 13).

The Fe atoms of "undistorted" Fe_2P (x(Fe) = 0.33 and 0.67 instead of 0.26 and 0.59) occupy only 1/3 of the A and B positions at z = 0 and 1, respectively (Fig.42). The distance between Fe atoms is increased from a_{hex} = 0.271 nm in Fe_2N to a_{hex} = 0.587 nm in Fe_2P to intercalate two P atoms on C positions at z = 0 and one P atom on C positions at z = 1. The projection of the unit cell of Ni_3C for example containing three points for the $C\square_2$ layers in C positions is increased to nine points in Fe_2P with three A, B and C positions in each case at the same projection height. The composition $Fe_3P_2\square_4$ at z = 0 and $Fe_3P\square_5$ at z = 1 add to a total of $Fe_6P_3\square_9$ or $Fe_2P\square_3$. The composition of the two layers is varied in $Zr_2Fe_{12}P_7\square_{21}$ (Ganglberger, 1968) with 21 positions in each layer of the unit cell by insertion of Zr atoms (○ in Fig.42). The neighboring positions of Zr atoms are not occupied because of the increased size and repulsive interactions. Other compounds of this family contain clusters of three ($Zr_6Ni_{20}P_{13}\square_{39}$) or six atoms ($(La, Ce)_{12}Rh_{30}P_{21}\square_{63}$) or mixtures of single atoms and clusters in different configurations (Madar et al., 1987; Pivan et al., 1987; Parthé et al., 1993). An even number of A, B and C positions in $Co_2P \mathrel{\widehat{=}} Co_8P_4\square_{12}$ and related compounds allows the occupation with two P atoms in each layer.

Different areas of the two layers are occupied in Ta_3B_4 (Kiessling, 1949) and related compounds (Table 13). The 14 positions of the projected structure (Fig.42) are occupied by three Ta atoms on A positions and four Bor atoms on A and C positions at z = 0 or three Ta atoms on C positions and four Bor atoms on B and C positions at z = 1. The occupation of the different A, B and C positions varies also within the layer because of 14 points instead of 12 points. The Ta atoms of the z = 0 layer for example occupy B positions instead of A in the next area on the right-hand side of the unit cell (Fig.42).

Symmetrical structures at the corners of the structure maps with a single set of T_i values for A (or A and B atoms) are usually more pleasant com-

pared to structures at the borders with reduced symmetry. Ostwald cites J.W. Goethe: Beauty is a matter of regularity. The blocked structures of the Ganglberger family and some complex structures which are related to the patterns of homogeneous sphere packing (Section 25) (Koch and Fischer, 1992) are attractive. (The identical length of solid and dashed lines for homogeneous sphere packing is impossible in the hexagonal or square net. The B positions of these structures with different sets of T_i values are encircled.)

The patterns of the hexagonal and square net are related, if the rhombs, which are obtained from two neighboring triangles of the hexagonal net, are compared with the squares. The rhombs with $\alpha = 120^0$ can be distorted to the squares with $\alpha = 90^0$ in a continuous way with similar stuctural units. An increased number of structural units is obtained for orthorhombic (rectangular) or monoclinic (oblique) distortions (general parallelogram). In that case the structural units can be assembled only in one direction. The patterns at the border of the structure maps can be characterized by sequences of structural units (Section 21).

All kinds of patterns with reduced number of symmetry elements are usually less attractive. This can be demonstrated in an educational program for teaching symmetry in arts and nature. A typical example would be the creation of a unit cell containing eight positions x + y on a squared paper or a graphic computer program. The choice of four A positions for r = 1 structures, the extension to neighboring unit cells and the connection of nearest (and next-nearest) A positions by solid (and dashed) lines yield many different patterns. The individual result might indicate the creativity of the artist. Some will put all A positions in one half of the unit cell like 3 2 2;1 or patterns with low symmetry like 1.5 2 2;1 or 1 2 2.5;1. Others will occupy alternating lines (2 0 4;1) or create symmetrical patterns with a single set of T_i values for all positions like 0 4 4;1 and 2 2 0;1. They have to think about the proper distribution, but avoid the averaging of different T_i values in other structures. Those who have analyzed some solutions might be able to search for a specific pattern like 0 3 2;1.5 of the square net or 0 3 0;2 of the honeycomb net, if they are supported by the structure maps with the structural units. (The solutions are shown in Figs. 8,34.) The next

more sophisticated step could be the analysis of patterns containing figures like stars or leaves instead of points (mandalas) or the analysis of the three-dimensional case in architecture. Also the discussion of practical aspects like shorter walking distances or smaller densities for the arrangement of houses in cities or trees in forests like the $Pr_7\square_2O_{12}$ net instead of 0 4 4;1 (square net) for houses or 0 6 0;2 instead of 2 2 6;1 (hexagonal net) for trees might be useful. Solutions with T_1 or $T_2 =$ 1 or 2 are interesting for folklore dances with a variation of T_1 nearest and T_2 next-nearest partners. The direction of the dancing people (or of adatoms moving on surfaces, etc.) can be shown by arrows instead of lines. Those who prefer jig-saw puzzles might enlarge and photocopy the structural units of Fig.42. Some informations will also be available on the internet (http://www.fz-juelich.de/iff/personen/J.Hauck) for an analysis of a pattern by computer graphics.

29 Conclusions

Close-packed alloys are obtained for weak interactions between metal atoms like Mg or Cu. The bonding between metal atoms is enhanced in α-Nd, α-Sm or Tb HP structures with different stackings (ch), (ch_2) or (hc_2) (Table 1), which are also observed in NiAs, $CdCl_2$ and NbS_2 structures with decreased $\Delta z\, c/a$ values (Table 7). The distances between hexagonal or tetragonal layers are varied in Hg or In (Table 1) and to a larger extent in ordered body-centered alloys of the Zalkin, Ramsey family with hexagonal layers or the Schubert family with square layers (Tables 7,8). Interstitial atoms I = O, Cl, H can be inserted in different octahedral, tetrahedral, prismatic and other sites like Ni′ in Ni_2In related structures (Table 11b). These structures can be characterized by the self-coordination numbers T_i(I) of I atoms with I atoms similar to T_i(M) of ordered alloys (Table 11a,b). The I atoms can also be adsorbed on metal surfaces like [001] or [111] surfaces of ccp alloys. The composition of the interstitial alloys and surface structures $M_n\square_xI_{nx-x}$ varies with the ratio $I/M = x(n-1)/n$ with x = 1 for the NaCl group, x = 2 for the CaF_2 related structures and x = 3 for the superconducting oxides, which are related to the $CaTiO_3$ structure (PER group). The occupation of hollow

or bridge positions on [001] ccp metal surfaces corresponds to x = 1 or x = 2, respectively, the occupation of hollow or bridge positions on [111] surfaces of ccp alloys to x = 2 or x = 3, respectively. The interstitial compounds and surface structures can be characterized by sequences of coordination numbers CN (Table 12) with different configurations like 4^t (tetrahedral), 4^p (planar) or o, m, p (CN = 2 with ortho-, meta- or para-configurations) (Figs. 34a,b,42). The interactions between I atoms are reduced because of the M atoms at I atom positions. The structures are inside of the corresponding structure maps for $M_n\square_xI_{nx-x}$ with M = I atoms (Fig.36).

The ordering of interstitial atoms or magnetic moments in the same structure families as close-packed metal atoms shows the coexistence of different views of sphere packing, which were discussed for many centuries (Brunner, 1971) like the statement of Boscovich (1758): "Atoms are centres of interaction whose diameter are negligible or of minor interest as compared to their separations", or the Wiener-Sohncke principle: "points are disposed around each point in the same way as around every other" (Wiener, 1863; Sohncke, 1879). The last statement is correlated with the problem of homogeneous sphere packing (Koch and Fischer, 1992). Most structures at the corners of the structure maps and some additional structures listed in Section 33 have a single set of T_i values ($M_i = 1$).

The present compilation of structures is a general crystallographic approach similar to W. Ostwald's two-dimensional patterns and his last chemical textbook "Principles of Chemistry" with the subtitle "A Chemistry without Substances" covering general concepts and relationships (laws of nature) which can be applied on all substances without dependence on their nature (Ostwald, 1907).

The numbers of shells i and the self-coordination numbers T_i of M atoms in these shells were extended to $i = 11 - 18$ (Table 23), to compare the magic numbers x and y of stable isotopes M_xN_y with x protons and y neutrons or small clusters of atoms with $x + y \lesssim 208$ with the x and y values of closed shells. The enhanced stability of these isotopes and deviations from spherical shape for other isotopes (Zeldes, 1996) are in-

dications for an ordering process. The relation between ordering and interactions however can be difficult for very small particles which can convert to energy. Heisenberg points out that a qualitative distinction between elementary particles and larger compound particles is impossible, while other scientists suggest a different treatise (Heisenberg, 1971). A proton for example can convert to a neutron and pion, a Λ-hyperon and kaon or three quarks. Particles with very strong attractive or repulsive interactions can not order in different areas of the structure maps. A strong deviation from balanced interactions will give rise to clusters, which can not be separated for attractive interactions, and to a continuous separation of the particles for repulsive interactions. Different energies give rise to a variation of the distances between elementary particles or compound particles.

The lattice constants of different elements like C, Si, Ge and Sn are increased because of the increased distances between 2, 3, 4 and 5 s and p electrons. The $(2s)$ and $(2p)^3$ electrons of carbon atoms for example are forming a tetrahedral "cluster", where electrons with identical spin are as far apart as possible (Kettle, 1992). The atoms are "blocked structures" (Section 28) like the bcc 4 0 12;1 structure with an occupation of the T_1 shell by electrons. Different "clusters" are formed in graphite with an occupation of the $T_1 = 2$ and $T_2 = 3$ shells of the ph lattice by electrons or in lead with $T_1 = 12$ of the fcc lattice. The $T_1 = 4$ configuration of the square net or the $T_1 = 2$ configuration of the chain are preferred by atoms with increased numbers of electrons like Se, Te or I, which are forming polyanions (Parthé et al., 1993).

Large particles are either not ordered because of the lack of mobility (like balls in a drawer) or they form inhomogeneous clusters without other particles of the same kind (like planets with $T_i = 0$). Identical forces on the same kind of particles with a minimum of deviations are required for ordering as is demonstrated by ocean waves or lattice defects.

The structures of ordered alloys and interstitial compounds can be characterized by sequences of structural units or by sequences of layers and the x, y, z translations of neighboring layers. The T_i(M) or T_i(I) values of M or I atoms are usually in the same area of the structure maps of

three-dimensional and two-dimensional structures. Different locations like the 2 0 2 ; 2, 0 6 0 ; 2 hexagonal layers or 0 2 0 ; 2, 2 0 2 ; 2 square layers of the ccp 2 2 12 ; 2a $MoPt_2$ structure indicate a directional bonding of Mo atoms with a distortion of the structure. A stronger distortion is obtained in the $MoSi_2$ structure, which is usually considered as ordered bcc structure. Many ordered bcc alloys $M_xN_yR_z$ can be described by sequences of x M, y N and z R layers similar to some ordered hcp or ccp alloys (Tables 7,8). The reduced distances between layers are related to an increased directional bonding in c direction (or decreased bonding in the a, b plane). The consideration of bcc and pc metals (Po) as a chain similar to hcp and ccp suggests an increased directional bonding at an increased percentage of h layers (c_3 (Cu), hc_2 (Tb HP), ch (α-Nd), ch_2 (α-Sm), h_2 (Mg)) and reduced distances between layers (c_3 (Cu, Hg, In, Po, W), hc_2 (Tb HP, CdI_2), ch (α-Nd, NiAs), ch_2 (α-Sm, MoS_2)) (Table 7). Next-nearest neighbors of the c_3 chain are further apart than in the h_2 chain (Fig.19). The periodic system with the low-temperature modifications of the elements (Fig.43) suggests a periodic sequence of bcc, hcp, ccp crystal structures with some deviations like the diamond (ZnS) structure of C, Ge and Sn, or the helical structure of Se and Te with increased directional bonding instead of the bcc structure (Sutton, 1993). The C atoms of diamond exhibit the same structure as the Tl atoms in the ordered bcc alloy NaTl. The Na positions are vacant in the diamond structure. The structures of As, Se and Po can be obtained in a similar way from distorted CsCl with vacant Cs positions. The number of vacancies is increased in an idealized α-Mn (0 0 1.24 ; 6.45) with the x, y, z parameters of the 58 Mn atoms 1/3 ($w = 0.317$, $u = 0.356$), 1/4 ($v' = 0.278$), 1/12 ($u' = 0.089$) and 0 ($v = 0.042$) instead of the observed values in brackets (Wyckoff, 1982). Usually the directional bonding decreases at increased atomic radii (Buchanan and Park, 1997) like in ccp Ca and Sr, hcp Tc and Re or ccp Pb (bcc Ba seems to be an exception).

A periodic variation of the crystal structures with a periodic variation of directional bonding in the sequence ccp hcp bcc hcp, ccp ... (Fig.43) is obtained for the elements Ne He Li Mg, Ca Y Ta Re, Pt Cd Sn M and Pb N Po R. The sequence of these and neighboring elements is similar to the relative ordering number $\mathcal{M}$ (Table 18). The bcc crystal structure with directional bonding is replaced by other structures like α-Mn, Ga,

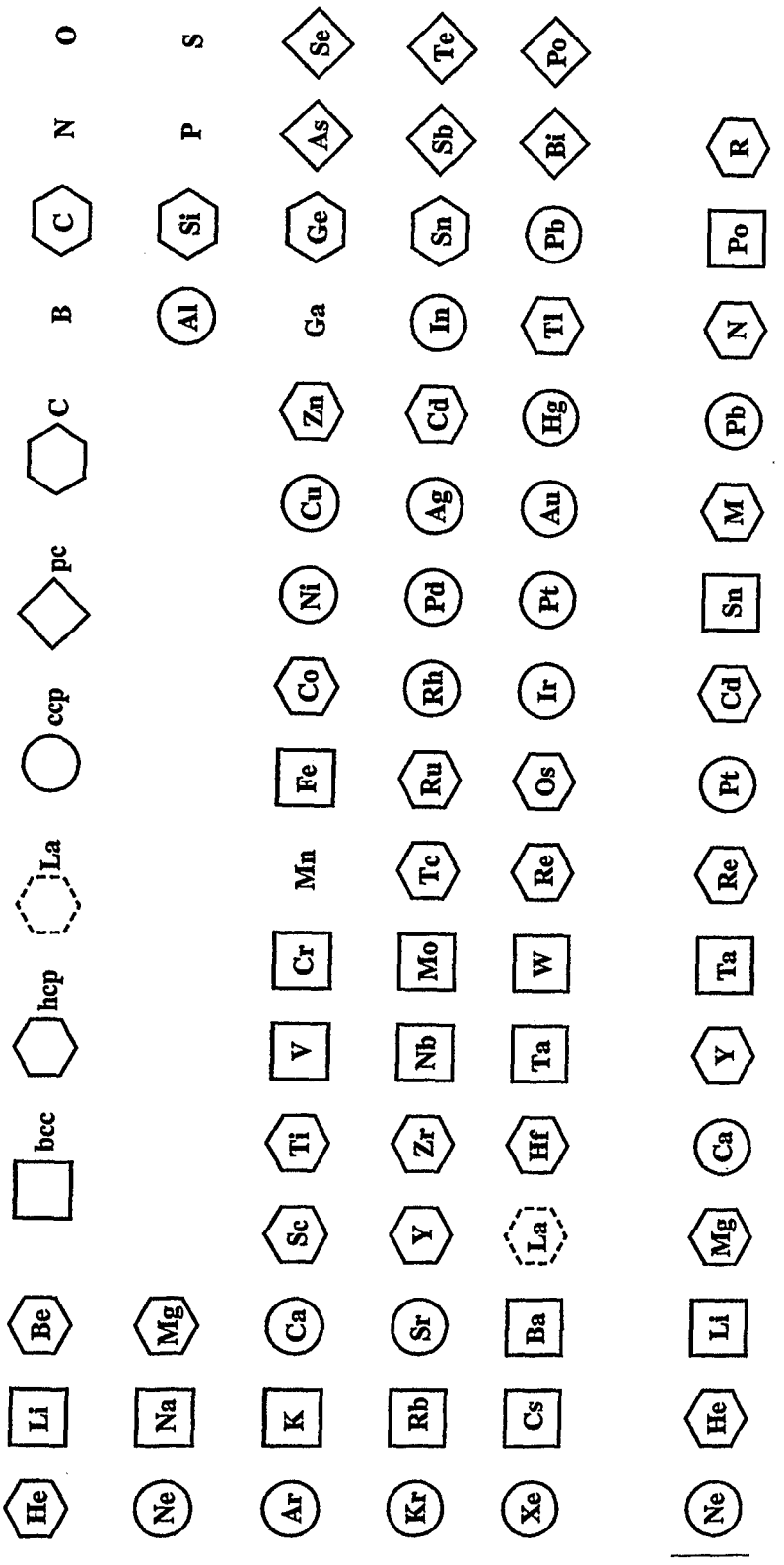

Figure 43: Crystal structures of metal atoms at room temperature and of noble gases at decreased temperatures. Comparison with a periodic variation of ccp hcp bcc hcp sequence of structures in the last row.

C, As, Se and Po. The hcp elements M, N and R with weak directional bonding are not observed in the right hand area of the periodic system.

Some exceptions of crystal structures, which are not at the border of the structure maps, are also found in ordered alloys. Most of the ordered bcc alloys are at the surface of the three-dimensional T_1, T_2, T_3 structure map (Hauck and Mika, 1997). The layered [111] structure like MNM_2N_2, which can be obtained by a combination of the sequences MN (CsCl structure) and M_2N_2 (NaTl structure) (Table 7), yields the s-CN values 2.9 2 10.7 ; 1 instead of 2.9 1.7 T_3 ; (1), which can be obtained by adding other structural units in very large unit cells (suprema) (Fig.37a). Other combinations of both structures are impossible because of geometrical constraints. Some structures of the bcc system are at the border of the three-dimensional T_1 T_2 T_3 ; y/x structure map, but inside of the T_1, T_2 projection (Fig.37a). The same applies to the hcp ZnS related structure of α-LiSiNO with s-CN values 6 2 2 ; 1 (Hauck and Mika, 1998b).

Few structures like $Cd_{26}Au_{72}$ (Table 3) or $ZnAu_3$ (Teuho et al., 1987) (Fig.44) can be considered as a combination of structural units u, v and the 2 2 2 ; 3 structure for $Cd_{26}Au_{72}$ or u – y (Fig.12) for $ZnAu_3$ with some other (dashed) additional units. The T_1, T_2 values of these structures are close to the border of the structure maps. Other structures can be considered as a combination of structural units from different systems like CaF_2 and W (Parthé et al., 1993). Quasicrystals are probably nonperiodic combinations of such units. If the size and bonding of the components is too different, then the close-packed alloys become unstable and favor structures without close-packing.

Binary compounds AB, AB_2 and AB_3 from the different groups of the present investigation are plotted in structure maps with the relative ordering numbers $\mathcal{M}_A$ and $\mathcal{M}_B$ as parameters (Pettifor, 1994) (Table 18, Fig.45). Most of the structures are in different areas of the field with $\mathcal{M}_A + \mathcal{M}_B > 103$ (right of the dashed line in Fig.45). The proper composition of new compounds can be selected from this structure map, the relative ordering numbers, electronegativities, pseudopotential radii sum (Table 18) or coordination numbers for interstitial compounds (Table 19).

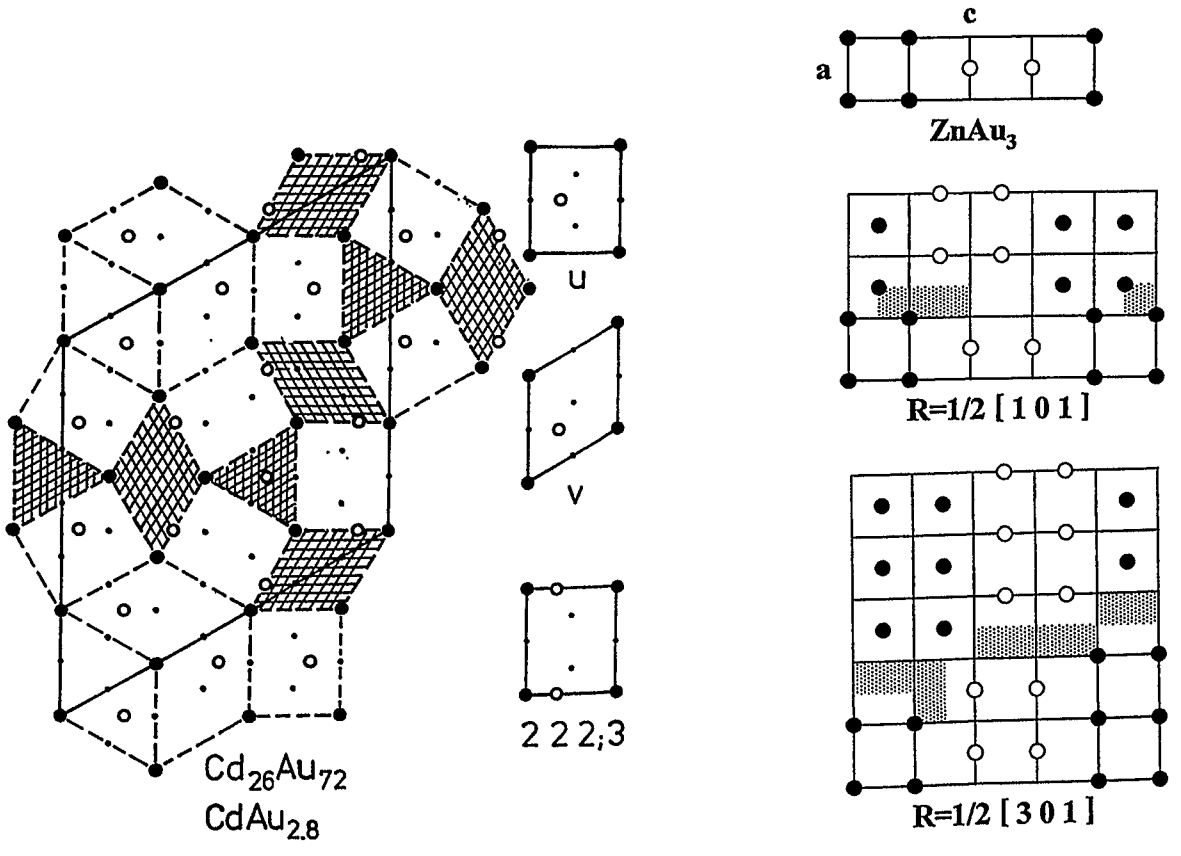

Figure 44: Projection of the $Cd_{26}Au_{72}$ structure (Table 3) and different non-stoichiometric $ZnAu_{3-x}$ structure variants (Table 4) with non-periodic shear planes (Hyde and Andersson, 1989). Cd or Zn atoms at 0 (•) or 0.5 (○). The dashed areas are structural units, which are not at the boundary of the structure maps.

New structures of ordered alloys or interstitial compounds can be analyzed, if the unit cell or reduced unit cell (Table 20) is determined by electron diffraction. The structural units and T_1, T_2 structure maps of the present investigation can help to find the proper structure model for the refinement of weak superstructure reflections of samples, which are twinned by the ordering process. The large number of theoretical structures is reduced to a small number, if the size of the jig-saw puzzle is known.

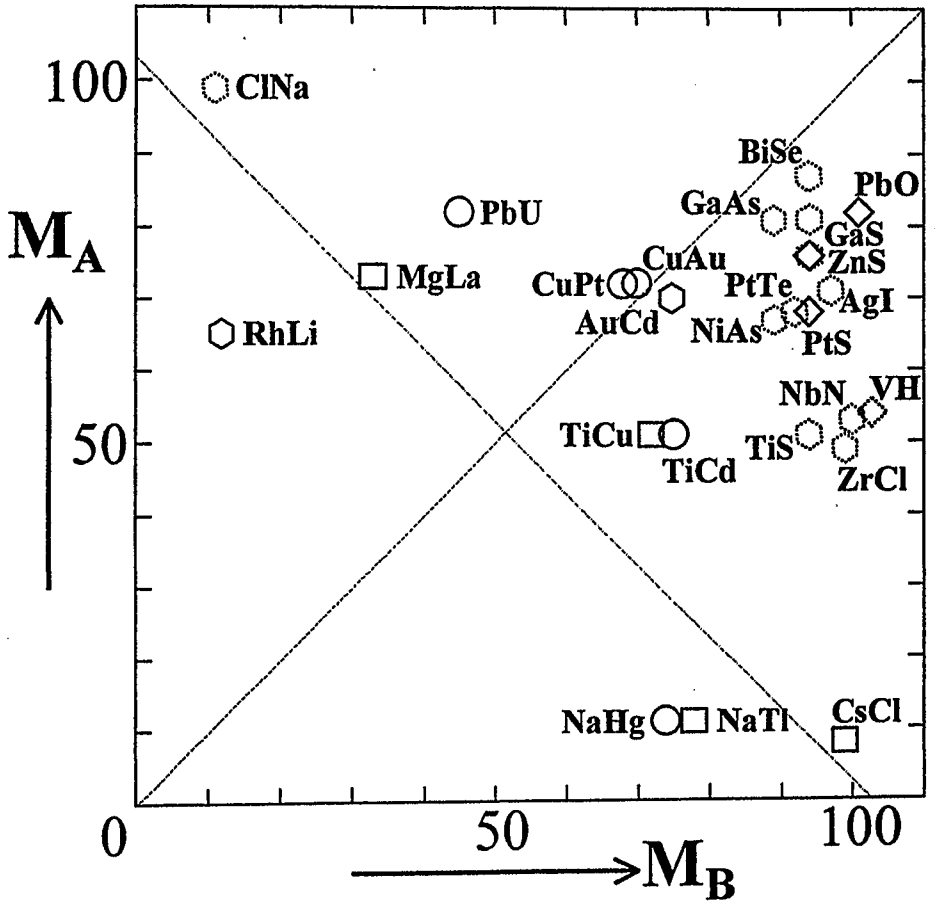

Pettifor structure map for AB compounds

RhLi
AuCd

CuPt
PbU
CuAu
NaHg
TiCd

CsCl
MgLa
NaTl
TiCu

PbO
PtS
ZnS

VH

ZnS
AgI
GaAs
ClNa
NiAs
NbN
TiS
ZrCl
PtTe
GaS
BiSe

Figure 45: Structure maps for AB (a), AB_2 (b) and AB_3 (c) compounds of Table 3 (hexagon), 4 (○), 5 (dashed hexagon), 7, 8, 13 (dashed hexagon, □ or ◇) with the relative ordering numbers $\mathcal{M}_A$ and $\mathcal{M}_B$ of A and B atoms (Table 18) (to be continued on next pages).

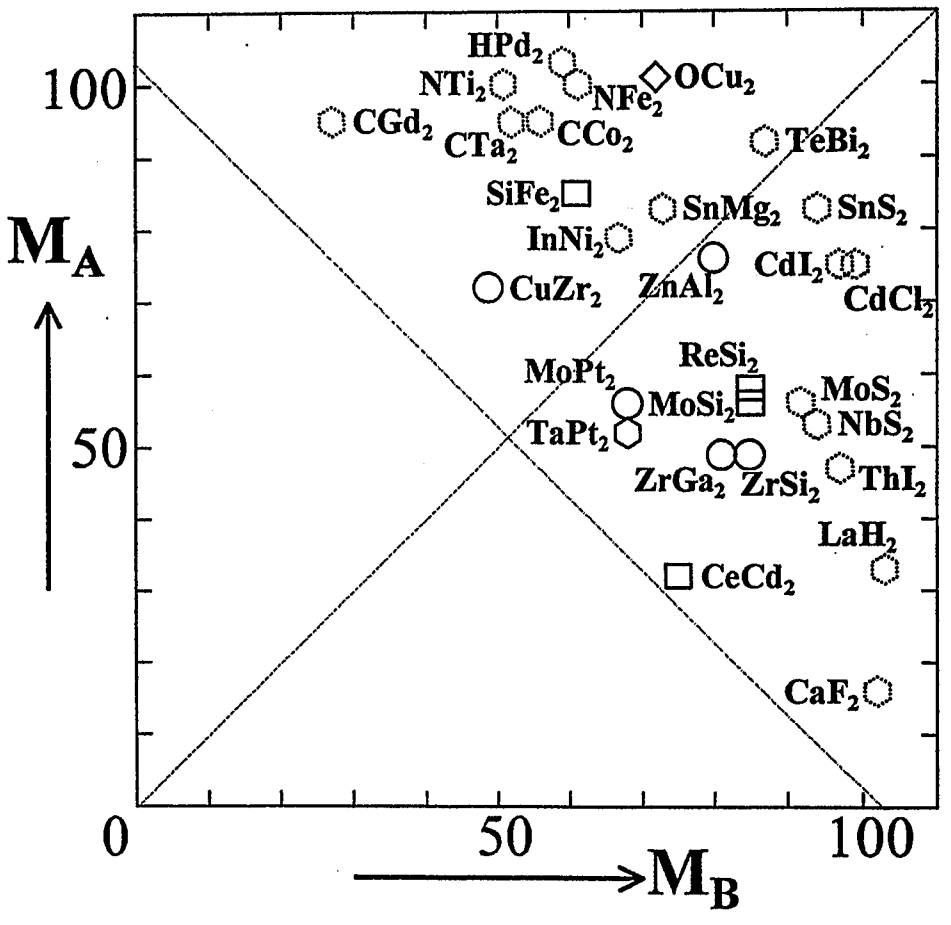

Pettifor structure map for AB_2 compounds

⬡ $TaPt_2$	○ $ZnAl_2$	□ $CeCd_2$	◇ OCu_2	⬡ MoS_2	⬡ $InNi_2$
	○ $MoPt_2$	□ $SiFe_2$		⬡ CdI_2	⬡ CGd_2
	○ $ZrSi_2$	□ $ReSi_2$		⬡ CTa_2	⬡ NTi_2
	○ $ZrGa_2$	□ $MoSi_2$		⬡ NbS_2	⬡ HPd_2
	○ $CuZr_2$			⬡ $CdCl_2$	⬡ LaH_2
				⬡ CaF_2	⬡ CCo_2
				⬡ $SnMg_2$	⬡ NFe_2
				⬡ SnS_2	⬡ ThI_2
				⬡ $TeBi_2$	

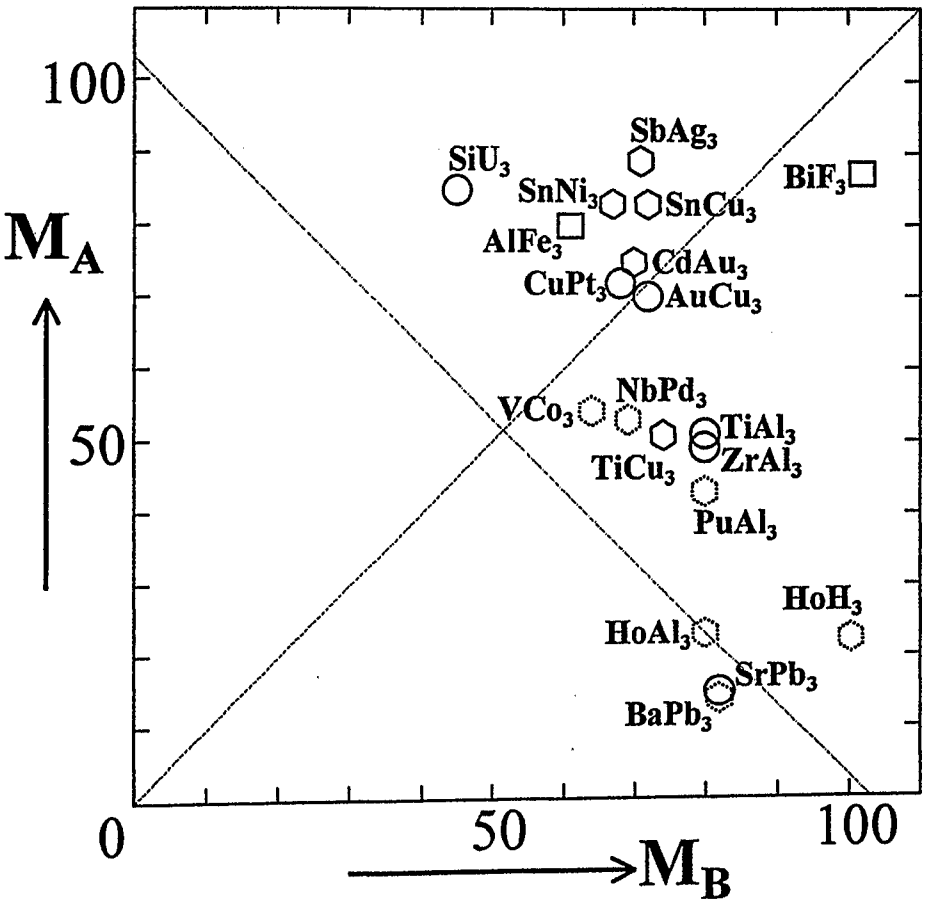

Pettifor structure map for AB_3 compounds

$SbAg_3$	$CuPt_3$	BiF_3	$PuAl_3$
$TiCu_3$	$TiAl_3$	$AlFe_3$	VCo_3
$SnCu_3$	$ZrAl_3$		$BaPb_3$
$CdAu_3$	$AuCu_3$		$HoAl_3$
$SnNi_3$	SiU_3		$NbPd_3$
	$SrPb_3$		HoH_3

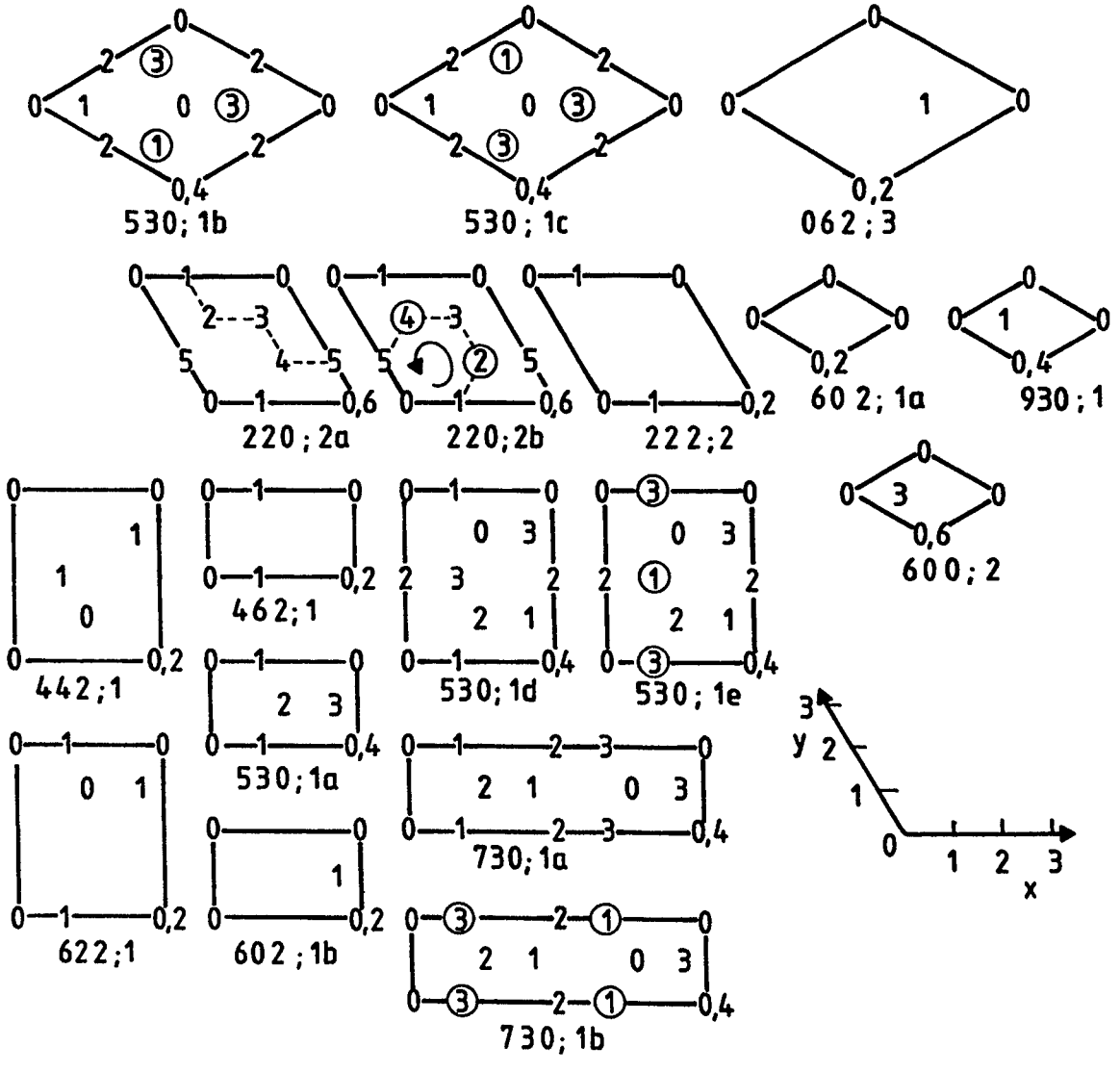

Figure 46: Projections of hcp (a), ccp (b), bcc (c) and pc structures (d) of Table 21a–d (to be continued).

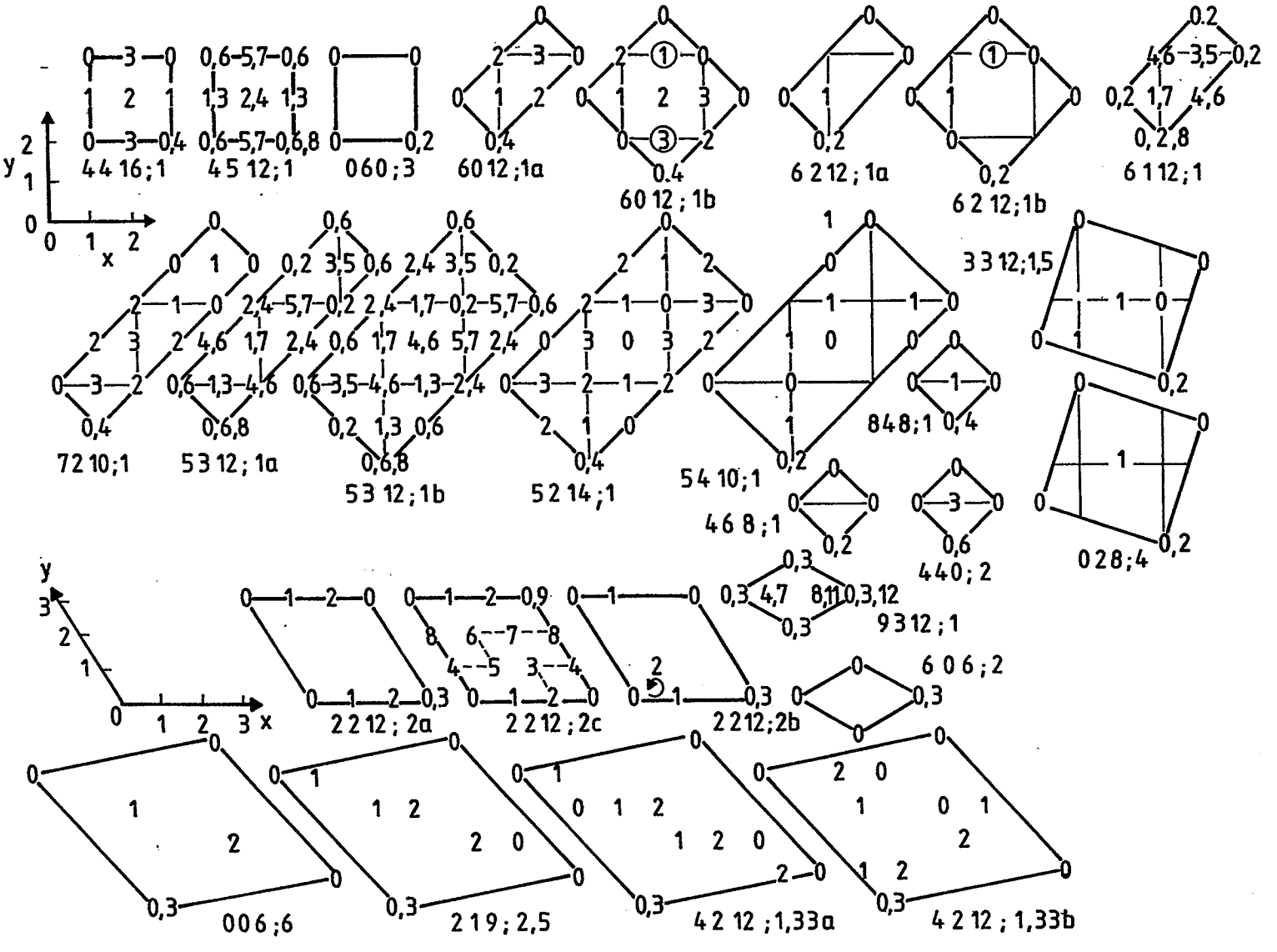
44 16;1
45 12;1
060;3
6012;1a
6012;1b
6212;1a
6212;1b
6112;1
3312;1,5
7210;1
5312;1a
5312;1b
5214;1
5410;1
848;1
468;1
440;2
028;4
9312;1
606;2
2212;2a
2212;2c
2212;2b
006;6
219;2,5
4212;1,33a
4212;1,33b

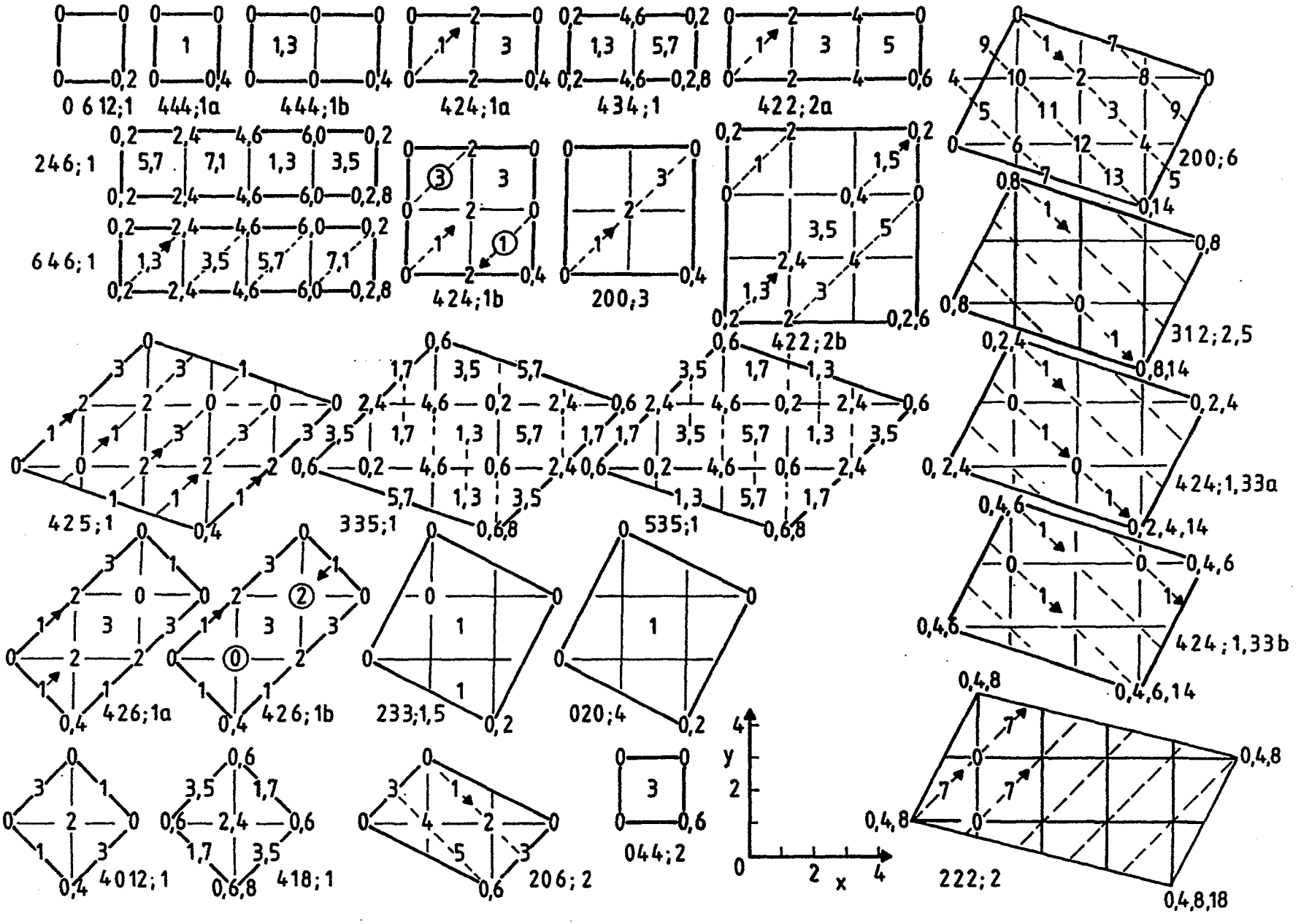
0 6 12;1
444;1a
444;1b
424;1a
434;1
422;2a
246;1
646;1
424;1b
200;3
422;2b
200;6
312;2,5
424;1,33a
424;1,33b
425;1
335;1
535;1
426;1a
426;1b
233;1,5
020;4
4012;1
418;1
206;2
044;2
222;2

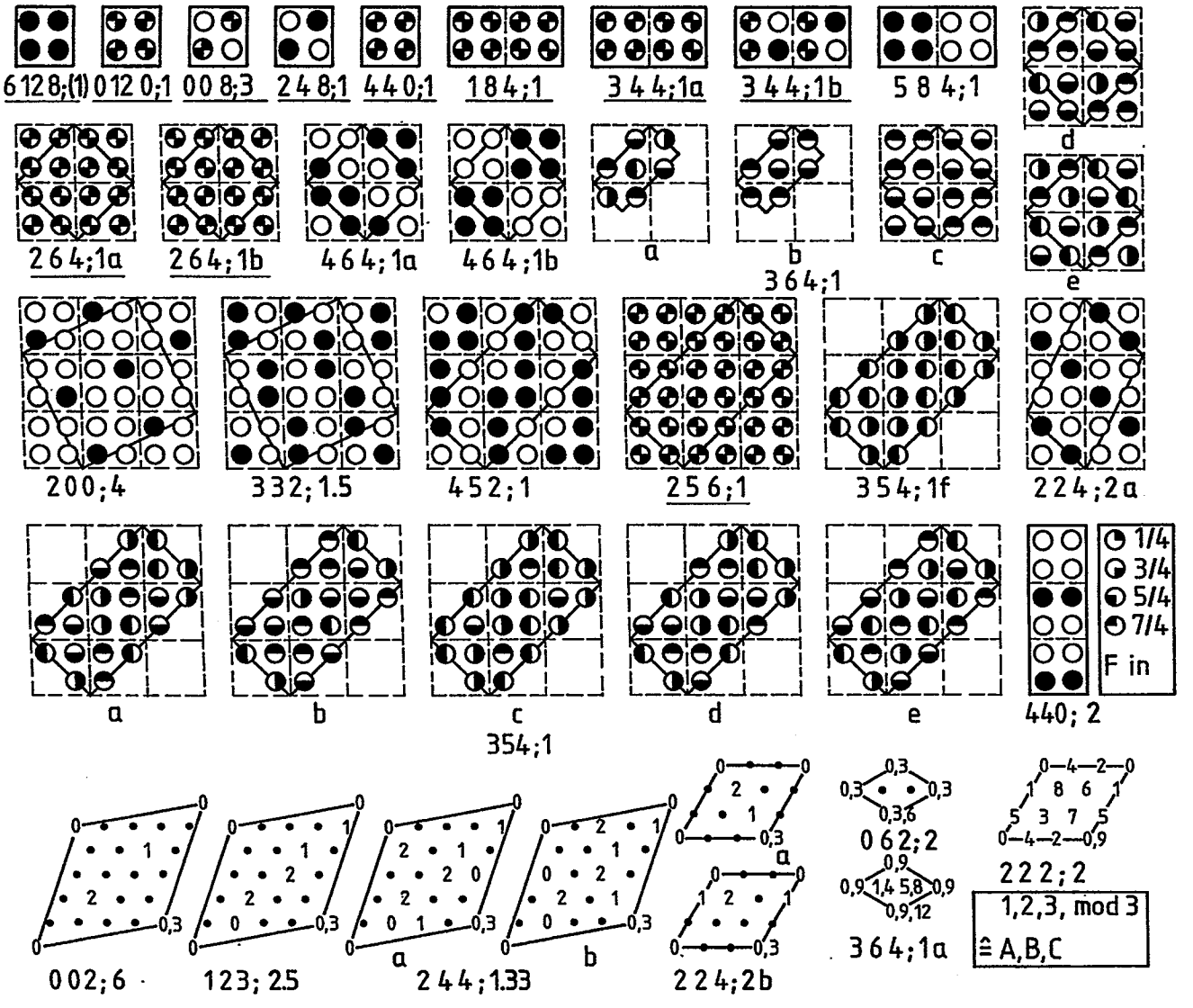
6128;(1) 0120;1
008;3
248;1
440;1
184;1
344;1a
344;1b
584;1
264;1a
264;1b
464;1a
464;1b
a
b
364;1
c
d
e
200;4
332;1.5
452;1
256;1
354;1f
224;2a
a
b
c
354;1
d
e
440; 2
1/4
3/4
5/4
7/4
F in
002;6
123; 25
244;1.33
a
b
224;2b
062;2
364;1a
222;2
1,2,3, mod 3
≙ A,B,C

30 Notation

A, B, C	positions of metal atoms in hexagonal layers
K, L	positions of metal atoms in square layers
m	number of atoms/formula unit
n	number of hexagonal layers
$n = 2$	layers in A, B positions of hcp or h hexagonal close-packed structures
$n = 3$	layers in A, B, C positions of ccp or c cubic close-packed structures
p	number of sequences/unit cell
d	diameter of atoms = distance between the nearest M atoms
a=d, c=$n\sqrt{2/3}d$	hexagonal lattice constants of structures with n layers
a_c=$\sqrt{2}d$	lattice constant of cubic fcc unit cell (Fig.3)
f=h/(h+c)	fraction of h layers in complex close-packed structures
M_xN_y, r=y/x$\geq$1	alloy composition with minority component M
T_i=T_i(M) or T_i(I)	self-coordination numbers of M atoms with M atoms or I atoms with I atoms for i=1, 2, ... coordination shell
k=T_i^A or T_1^B	number of contacts between the spheres of A or B atoms
T_i(M,N)	coordination numbers of M atoms with N atoms
CN	coordination number of M atoms with other atoms
p_i	i = M or N, number of metal atoms M or N next to each interstitial atom I = O, Cl, etc. in antistructures
q_i	charge of M or N atoms
T_i^{max}	maximum self-coordination number in pure metals
T_1 T_2 T_3 ; y/x	characterization of crystal structures by the M atom environment, where T_i is the number of ith nearest neighbors and y/x the ratio of the components

$(T_1\ T_2\ T_3\,;\mathrm{y/x})$	s-CN values, which are not on the boundary of the structure map
α_i, $-1 \leq \alpha_i \leq 1$	Cowley's short-range order parameter, $\alpha_i T_i^{\max} = T_i - (T_i^{\max} - T_i)/\mathrm{r}$, the α_1, α_2 parameters are used for structure maps
$\pm V_i$	repulsive (−) or attractive (+) interactions between M atoms, e.g. Coulomb repulsion or covalent bonding
M^i	number of M and N atoms with different environment (= different T_i values)
c, h, t, s	notation for the stacking of hexagonal layers (Fig.19)
$\Delta\mathrm{z}\ c/a$	distance between hexagonal layers
$\Delta\mathrm{z}\ c/d$	distance between square layers
abc ...	sequence of structural units
|	mirror plane, the asymmetric sequence (Fig.12) of structural units abc| should be completed to the periodic sequence abccba
↑	translation $a_\mathrm{c}/2\ a_\mathrm{c}/2$ at the interface of structural units to continue a sequence of structural units abc↑ in the periodic sequence abca′b′c′ of shear structures with antiphase boundaries
[abc]	two- or three-dimensional tiling of structural units.

31 References

Allouche, J.-P., and Salon, O. (1990). In *Quasicrystals, Networks, and Molecules of Fivefold Symmetry* (ed. J. Hargittai). VCH Publishers, New York, p.97.

Beattie, H.J. Jr. (1967). In *Intermetallic Compounds* (ed. J.H. Westbrook). Wiley, New York, p.144.

Beck, P.A. (1969). In *Advances in X-ray Analysis*, **12** (eds. C.S. Barrett, J.B. Newkirk and G.R. Mallett). Plenum Press, New York, p.1.

de Boer, F.R., Boom, R., Mattens, W.C.M., Miedema, A.R., and Niessen, A.K. (1988). *Cohesion in Metals: Transition Metal Alloys (Cohesion and Structure*, Vol. 1) (eds. F.R. de Boer and D.G. Pettifor). North-Holland, Amsterdam.

Boscovich, R.J. (1758). *Theoria Philosophiae Naturalis Redacta ad Unicam Legem Virium in Natura Existentium.* For a review, see *Roger Joseph Boscovich, Studies of his Life and Work* (1961) (ed. L.L. White). George Allen & Unwin Ltd., London, pp.106, 120, 121.

Bowman, R.C. Jr. (1988). In *Hydrogen Storage Materials* (ed. R.G. Barnes). *Mater. Sci. Forum*, **31**, 197.

Bozorth, R.M. (1922). *J. Amer. Chem. Soc.*, **44**, 2232.

Brauer, G. (1939). *Z. anorg. allg. Chem.*, **242**, 1.

Brunner, G.O. (1971). *Acta Crystallogr.*, **A27**, 388.

Buchanan, R.C., and Park, T. (1997). *Materials Crystal Chemistry*, Marcel Dekker, New York.

Burdett, J.K. (1995). *Chemical Bonding in Solids.* Oxford University Press, Oxford.

Carlsson, A.E., and Meschter, P.J. (1994). In *Intermetallic Compounds*, **1** (eds. J.H. Westbrook and R.L. Fleischer). Wiley, Chichester, p.55.

Cenedese, P., and Gaspard, J.P. (1984). *Mat. Res. Soc. Symp. Proc.*, **21**, 51.

Dale, J.W. (1996). *Molecular Genetics of Bacteria.* Wiley, Chichester.

Diekerson, R.E. et al. (1989). *J. Mol. Biol.*, **205**, 787.

Ducastelle, F. (1991). In *Cohesion and Structure*, **3** (eds. F.R. de Boer and D.G. Pettifor). North-Holland, Amsterdam.

Ellner, M., Gödecke, T., and Schubert, K. (1971). *J. Less-Common Metals*, **24**, 23.

Ellner, M., and Predel, B. (1994). In *Intermetallic Compounds*, **1** (eds. J.H. Westbrook and R.L. Fleischer). Wiley, Chichester, p.91.

Flanagan, T.B., Craft, A.P., Niki, Y., Baba, K., and Sakamoto, Y. (1992). *J. Alloys and Compounds*, **184**, 69.

Forsyth, J.B., and Gran, G. (1962). *Acta Crystallogr.*, **15**, 100.

Galasso, F.S. (1970). *Structure and Properties of Inorganic Solids.* Pergamon Press, Oxford.

Ganglberger, E. (1968). *Monatshefte für Chemie*, **99**, 557.

Glusker, J.P., Mitchell, L., and Rossi, M. (1994). *Crystal Structure Analysis for Chemists and Biologists.* VCH, Weinheim.

Goodenough, J.B. (1982). In *Handbook on the Physics and Chemistry of the Rare Earths*, **5** (eds. K.A. Gschneidner, Jr. and L. Eyring). North-Holland, Amsterdam, p.215.

Hahn, Th. (ed.) (1987). *International Tables for Crystallography*, Vol.A. D. Reidel, Dordrecht.

Hammou, A., and Guindet, J. (1997). In *The CRC Handbook of Solid State Electrochemistry* (eds. P.J. Gellings and H.J.M. Bouwmeester). CRC Press, Boca Raton, p.407.

Hauck, J. (1981). *J. Less-Common Met.*, **77**, 99.

Hauck, J. (1983). *J. Less-Common Met.*, **94**, 123.

Hauck, J. (1985). *J. Less-Common Met.*, **105**, 283.

Hauck, J., Henkel, D., and Mika, K. (1988a). *Z. Phys. B – Cond. Matt.*, **71**, 187.

Hauck, J., Henkel, D., and Mika, K. (1988b). *Z. Kristallogr.*, **182**, 297.

Hauck, J., Henkel, D., and Mika, K. (1989). *Int. J. Mod. Phys.*, B**3**, 1425.

Hauck, J., and Mika, K. (1993). *Int. J. Mod. Phys.*, B**7**, 3423.

Hauck, J., and Mika, K. (1994). In *Intermetallic Compounds*, **1** (eds. J.H. Westbrook and R.L. Fleischer). Wiley, Chichester, p.277.

Hauck, J., Bickmann, K., Bischof, B., Janning, E., and Mika, K. (1995). *Materials Letters*, **22**, 221.

Hauck, J., and Mika, K. (1997). In *Studies of High Temperature Superconductors*, **25** (ed. A. Narlikar). Nova Science Publishers, Commack NY, p. 1.

Hauck, J., and Mika, K. (1998a). *Supercond. Sci. Technol.*, **11**, 614.

Hauck, J., and Mika, K. (1998b). *J. Solid State Chem.*, **138**, 334.

Hauck, J., and Mika, K. (1999). *Z. Kristallogr.*, **214**, 443.

Hauck, J., Henkel, D., Klein, M., and Mika, K. (1999). *J. Solid State Chem.*, **145**, 150.

Heisenberg, W. (1971). *Schritte über Grenzen – Gesammelte Reden und Aufsätze.* Piper, München.

Hellner, E., and Schwarz, R. (1994). In *Intermetallic Compounds*, **1** (eds. J.H. Westbrook and R.L. Fleischer). Wiley, Chichester, p.309.

Hiraga, K., and Hirabayashi, M. (1977). *J. Physique*, **38**, C7: 224.

Ho, S.-M., and Douglas, B.E. (1968). *J. Chem. Educ.*, **45**, 474.

Hulliger, F. (1976). In *Physics and Chemistry of Materials with Layered Structures* (ed. F. Lévy), Vol.5. D. Reidel, Dordrecht.

Hyde, B.G., and Andersson, S. (1989). *Inorganic Crystal Structures.* Wiley & sons, New York.

Ising, E. (1925). *Z. Phys.*, **31**, 253.

Johansson, C.H., and Linde, J.O. (1936). *Ann. d. Physik*, **25**, 1.

Kaburagi, M. (1978). *J. Phys. Soc. Japan*, **44**, 54.

Kanamori, J., and Kakehashi, Y. (1977). *J. Physique*, **38**, C7: 274.

Ketelaar, J.A.A. (1935). *Z. Kristallogr.* (A), **90**, 237.

Kettle, S.F.A. (1992). *Symmetry and Structure.* Wiley, Chichester.

Kiessling, R. (1949). *Acta Chem. Scand.*, **3**, 603.

Kitaigorodski, A.I. (1973). *Molecular Crystals and Molecules.* Academic Press, New York.

Koch, E., and Fischer, W. (1992). In *International Tables for Crystallography* (ed. A.J.C. Wilson), Vol.C. Kluwer Academic Publishers, Dordrecht, p.654.

Kudo, T., and Katsura, S. (1976). *Progr. Theor. Phys.*, **56**, 435.

Larsson, A.-K., Stenberg, L., and Lidin, S. (1994). *Acta Crystallogr.*, B**50**, 636.

Latscha, H.P., and Klein, H.A. (1982). *Organische Chemie.* Springer, Berlin, p.88.

Laves, F. (1967). In *Intermetallic Compounds* (ed. J.H. Westbrook). Wiley, New York, p.129.

Lee, S., and Foran, B. (1994). *J. Am. Chem. Soc.*, **116**, 154.

Lidin, S., and Larsson, A.-K. (1995). *J. Solid State Chem.*, **118**, 313.

Lima-de-Faria, J., and Figueiredo, M.O. (1969). *Z. Kristallogr.*, **130**, 41 and 54.

Lima-de-Faria, J., Hellner, E., Liebau, F., Makovicky, E., and Parthé, E. (1990). *Acta Crystallogr.*, A**46**, 1.

Madar, R., Ghetta, V., Dhahri, E., Chaudouet, P., and Senateur, J.P. (1987). *J. Solid State Chem.*, **66**, 73.

Mardix, S. (1990). *Acta Crystallogr.*, A**46**, 133.

Mika, K., and Hauck, J. (1990). *Acta Crystallogr.*, **46**, Suppl. C-269.

Mika, K., Hauck, J., and Funk-Kath, U. (1994). *J. Appl. Crystallogr.*, **27**, 1052.

Moodenbaugh, A.R., Johnston, D.C., Viswanathan, R., Shelton, R.N., Delong, L.E., and Fertig, W.A. (1978). *J. Low Temp. Phys.*, **33**, 175.

de Novion, Ch. (1994). In *Intermetallic Compounds*, **1** (eds. J.H. Westbrook and R.L. Fleischer). Wiley & sons, Chichester, p.559.

de Novion, Ch., and Landesman, J.P. (1985). *Pure & Appl. Chem.*, **57**, 1391.

Ogawa, S. (1974). In *Order-Disorder Transformations in Alloys* (ed. H. Warlimont). Springer, Berlin, p.240.

Oleś, A., Kajzar, F., Kucab, M., and Sikora, W. (1976). *Magnetic Structures by Neutron Diffraction.* Państwowe Wydawnictwo Nakowe, Warszawa.

Ostwald, W. (1922). *Die Welt der Formen – Entwicklung und Ordnung der gesetzlich=schönen Gebilde (The World of Patterns – Development and Order of the Legal=beautiful Figures).* Unesma, Leipzig.

Ostwald, W. (1907). *Principles of Chemistry – A chemistry without Substances.* Steinkopff, Leipzig.

Parthé, E., and Yvon, K. (1970). *Acta Crystallogr.*, B**26**, 153.

Parthé, E., Gelato, L., Chabot, B., Penzo, M., Cenzual, K., and Gladyshevskii, R. (1993). *TYPIX: Standardized Data and Crystal Chemical Characterization of Inorganic Structure Types.* In *Gmelin Handbook of Inorganic and Organometallic Chemistry*, **1**. Springer, Berlin.

Parthé, E., (1994). In *Intermetallic Compounds*, **1**, (eds. J.H. Westbrook and R.L. Fleischer). Wiley & sons Ltd. Chichester, p.343.

Patterson, A.L. (1944). *Phys. Rev.*, **65**, 195.

Patterson, A.L., and Kasper, J.S. (1959/1967). In *International Tables for X-ray Crystallography*, **II** (eds. J.S. Kasper, and K. Lonsdale). The Kynoch Press, Birmingham, p.342.

Pauling, L. (1929). *J. Am. Chem. Soc.*, **51**, 1010.

Pauling, L. (1945/1960). *The Nature of the Chemical Bond.* Cornell University Press, Ithaca NY.

Pearson, W.B. (1967). In *Metal Physics and Physical Metallurgy*, **8** (ed. G.V. Raynor). Pergamon Press, Oxford.

Pearson, W.B. (1972). *The Crystal Chemistry and Physics of Metals and Alloys.* Wiley–Interscience, New York.

Pettifor, D.G. (1994). In *Intermetallic Compounds*, **1**, (eds. J.H. Westbrook and R.L. Fleischer). Wiley & sons Ltd. Chichester, p.419.

Pivan, J.-Y., Guérin, R., and Sergent, M. (1987). *J. Solid State Chem.*, **68**, 11.

Pusey, P.N., and van Megen, W. (1986). *Nature*, **320**, 340.

Pusey, P.N., van Megen, W., Bartlett, P., Ackerson, B.J., Rarity, J.G., and Underwood, S.M. (1989). *Phys. Rev. Lett.*, **63**, 2753.

Sanders, J.V. (1980). *Phil. Mag.*, **42**, 705.

Sato, H., and Toth, R.S. (1965). In *Alloying Behavior and Effects in Concentrated Solid Solutions*, (ed. T.B. Massalski), *Metallur. Soc. Conf.*, **29**, 295.

Sattler, K. (1987). In *Microclusters* (eds. S. Sugano, Y. Nishina and S. Ohnishi). Springer, Berlin, p.107.

Sauvage, M., Parthé, E., and Yelon, W.B. (1974). *Acta Crystallogr.* **A30** 597.

Schlapbach, L., Meli, F., and Züttel, A. (1994). In *Intermetallic Compounds*, **2**, (eds. J.H. Westbrook and R.L. Fleischer). Wiley & sons Ltd. Chichester, p.475.

Schoonman, (1997). In *The CRC Handbook of Solid State Electrochemistry* (eds. P.J. Gellings and H.J.M. Bouwmeester). CRC Press, Boca Raton, p.161.

Schubert, K. (1964). *Kristallstrukturen zweikomponentiger Phasen (Crystal Structures of Binary Phases).* Springer, Berlin.

Schubert, K. (1967). In *Intermetallic Compounds* (ed. J.H. Westbrook). Wiley, New York, p.100.

Schubert, K., Anantharaman, T.R., Ata, H.O.K., Meissner, H.G., Pötzschke, M., Rossteutscher, W., and Stolz, E. (1960). *Die Naturw.*, **47**, 512.

Schweika, W. (1985). Jül. Report 2004, Forschungszentrum Jülich.

Shannon, R.D. (1976). *Acta Crystallogr.*, **A32**, 751.

Sohncke, L. (1879). *Entwickelung einer Theorie der Kristallstruktur.* B.G. Teubner, Leipzig, p23.

Steurer, W. (1990). *Z. Kristallogr.*, **190**, 179.

Stolz, E., and Schubert, K. (1962). *Z. Metallkunde*, **53**, 433.

Sugano, S., and Koizumi, H. (1998). *Microcluster Physics.* Springer, Berlin.

Sutton, A.P. (1993). *Electronic Structure of Materials.* Clarendon Pr., Oxford.

Teuho, J., Mäki, J., and Hiraga, K. (1987). *Acta Metall.*, **35**, 721.

Thornber, M.R., and Bevan, D.J.M. (1970). *J. Solid State Chem.*, **1**, 536.

Toth, L.E. (1971). *Transition Metal Carbides and Nitrides.* Academic Press, New York.

Turchi, P.E.A. (1994). In *Intermetallic Compounds*, **1** , (eds. J.H. Westbrook and R.L. Fleischer). Wiley & sons Ltd., Chichester, p.21.

Urban, J. (1998). *Cryst. Res. Technol.*, **33**, 1009.

Villars, P. (1994). In *Intermetallic Compounds*, **1**, (eds. J.H. Westbrook and R.L. Fleischer). Wiley & sons Ltd., Chichester, p.227.

Villars, P., and Calvert, L.D. (1986). *Pearson's Handbook of Crystallographic Data for Intermetallic Phases*, Volumes 1–3. Am. Soc. for Metals, Metals Park OH.

Villars, P., and Hulliger, F. (1987). *J. Less-Common Met.*, **132**, 289.

Villars, P., Mathis K., and Hulliger, F. (1989). In *Cohesion and Structure. The Structures of Binary Compounds*, **2** (eds. F.R. de Boer and D.G. Pettifor). North-Holland, Amsterdam, p.1.

Waag, A., Litz, Th., Fischer, F., Lugauer, H.-J., Baron, T., Schüll, K., Zehnder, U., Gerhard, T., Lunz, U., Keim, M., Reuscher, G., and Landwehr, G. (1998). *J. Crystal Growth*, **184/185**, 1.

Watson, P.R., Van Hove, M.A., and Hermann, K. (1994). *Atlas of Surface Structures*: Volume 1. *J. Phys. and Chem. Reference Data.* Monograph No **5**

Wegst, J., and Schubert, K. (1958). *Z. Metallkunde*, **49**, 533.

Wells, A.F. (1984). *Structural Inorganic Chemistry.* Clarendon Press, Oxford.

Westlake, D.G. (1983). *J. Less-Common Met.*, **91**, 1.

Wiener, C. (1863). *Die Grundzüge der Weltordnung.* I. *Atomlehre.* Winter, Leipzig, p.82.

Wulff, G. (1901). *Z. Krystallogr.*, **34**, 449.

Wyckoff, R.W.G. (1982). *Crystal structures* Volumes 1–3. Krieger, Malabar FL.

Zalkin, A., and Ramsey, W.J. (1956). *J. Phys. Chem.*, **60**, 234.

Zalkin, A., Ramsey, W.J., and Templeton, D.H. (1956). *J. Phys. Chem.*, **60**, 1275.

Zeldes, N. (1996). In *Handbook of Nuclear Properties*, (eds. D. Poenaru and W. Greiner). Clarendon Press, Oxford, p.13.

Zhao, J.-T., Gelato L., and Parthé, E. (1991). *Acta Crystallogr.*, C**47**, 479.

Table 1: Stacking sequences of all $n \leq 9$ hexagonal layers and some experimental structures with $n > 9$ with stacking symbols and number M^i of metal atoms with different coordination (Fig.1), T_i(h) or T_i(c) values of the chain of hc_x, ch_x, etc. stacking sequences, prototype, space group (here and in the following determined by a program (Mika et al., 1994)) and Pearson symbol (PS).

layers n	T_i(h) or T_i(c) ; r chain	stacking symbols	M^i	proto-type	PS	space group	popul-ation
segregation or clustering of h and c at left border of the map							
2	2 2 2 ; (1)	h	1	Mg	$hP2$	$P6_3/mmc$	271
3	2 2 2 ; (1)	c	1	Cu	$cF4$	$Fm\bar{3}m$	369
				Hg	$hR1$	$R\bar{3}m$	5
				In	$tI2$	$I4/mmm$	28
5	1 0 0 ; 1.5	h_2c_3	2			$P\bar{3}m1$	
7a	1.3 0.7 0 ; 1.3	c_3h_4	3			$P\bar{3}m1$	
8e	1 0 0 ; 3	h_2c_6	3			$P\bar{3}m1$	
9b	1.3 0.7 0 ; 2	c_3h_6	3			$P\bar{3}m1$	
combination of c_2h_2, ch and ch_x or hc_x							
4	0 2 0 ; 1	ch	2	α-Nd	$hP4$	$P6_3/mmc$	33
6b	0 0 2 ; 2	hc_2	2	Tb HP	$hP6$	$P6_3/mmc$	1
8a	0 0 0 2 ; 3	ch_3	2	M_xN_y		$P6_3/mmc$	
9a	0 0 2 ; 2	ch_2	2	α-Sm	$hR3$	$R\bar{3}m$	32
12	1 0 1 ; 1	h_2c_2	2	M_xN_y		$R\bar{3}m$	
14	0 0 1 ; 2.5	ch_2ch_3	2	M_xN_y		$P6_3/mmc$	
21	0 0 0 ; 6	ch_6	2	M_xN_y		$R\bar{3}m$	
6a	0 1 0 ; 2	$chch_3$	3	M_xN_y		$P\bar{6}m2$	
7b	0.7 0 1.3 ; 1.3	$ch_2c_2h_2$	3			$P\bar{3}m1$	
7c	0 1 0 ; 2.5	$hchc_4$	3	M_xN_y		$P\bar{3}m1$	
8b	0 1 0 ; 3	$chch_5$	3			$P\bar{6}m2$	
8c	0.5 1 1.5 ; 1	ch_2chc_2h	3			$P\bar{3}m1$	
8f	0 0 0 2 ; 3	hc_3	3			$P6_3/mmc$	
9c	0.7 0 0.7 ; 2	$ch_4c_2h_2$	3			$P3m1$	
10	0 1 1 ; 1.5	$chch_2$	3	M_xN_y		$P6_3/mmc$	
15	0 1 1 ; 1.5	$hchc_2$	3	M_xN_y		$R\bar{3}m$	
9f	0.5 0.5 1 ; 1.25	$hchc_2h_2c_2$	4			$P\bar{3}m1$	
9g	0 0 1 ; 3.5	hc_2hc_5	4			$P\bar{3}m1$	
∞	0 0.76 1.24 ; τ	Fibonacci	∞				
combinations inside of the map							
8d	1 0.5 1 ; 1	$c_2hc_2h_3$	4			$P\bar{6}m2$	
9d	1 1 0.5 ; 1.25	c_4hch_3	4			$P3m1$	
9e	0.5 1 0.5 ; 1.25	h_2c_3hchc	5			$P3m1$	

Table 2: Self-coordination numbers $T_i = T_i^{\max}$ of pure metals in hexagonal and square plane, hcp, ccp, bcc, pc and R_i^2/d^2 values, R_i = radius of i-th shell, d = diameter of spheres.

i	$T_i^{\max}$	R_i^2/d^2	$T_i^{\max}$	R_i^2/d^2	$T_i^{\max}$	R_i^2/d^2	$T_i^{\max}$	R_i^2/d^2	$T_i^{\max}$	R_i^2/d^2	$T_i^{\max}$	R_i^2/d^2
	hex. plane		square		hcp		ccp		bcc		pc	
1	6	1	4	1	12	1	12	1	8	1	6	1
2	6	3	4	2	6	2	6	2	6	4/3	12	2
3	6	4	4	4	2	8/3	24	3	12	8/3	8	3
4	12	7	8	5	18	3	12	4	24	11/3	6	4
5	6	9	4	8	12	11/3	24	5	8	4	24	5
6	6	12	4	9	6	4	8	6	6	16/3	24	6
7	12	13	8	10	12	5	48	7	24	19/3	12	8
8	6	16	8	13	12	17/3	6	8	24	20/3	30	9
9	12	19	4	16	6	6	36	9	24	8	24	10
10	12	21	8	17	6	19/3	24	10	32	9	24	11
11	6	25	4	18	12	20/3	24	11	12	32/3	8	12
12	6	27	8	20	24	7	24	12	48	35/3	24	13
13	12	28	12	25	6	22/3	72	13	30	12	48	14
14	12	31	8	26	12	25/3	48	15	24	40/3	6	16
15	6	36	8	29	12	9	12	16	24	43/3	48	17
16	12	37	4	32	24	29/3	48	17	24	44/3	36	18
17	12	39	8	34	12	10	30	18	8	16	24	19
18	12	43	4	36	12	31/3	72	19	48	51/3	24	20
19	6	48	8	37	2	32/3	24	20	24	52/3	48	21
20	18	49	8	40	12	11	48	21	48	56/3	24	22

Table 3: Hexagonal close-packed alloys M_xN_y characterized by the self-coordination numbers T_i of M atoms in the hcp structure and in each hexagonal plane, number M^i of metal atoms with different sets of hcp T_i values, sequences of structural units (Fig.10), space group and Pearson symbol (PS).

T_i(M) ; r hcp	T_i(M) ; r hex. plan.	M^i	proto-type	PS	space group	struct. units
layers of M and N atoms in [001] direction						
12 6 2 ; (1)	6 6 6 ; (1)	1	Mg	*hP*2	$P6_3/mmc$	$M_\infty N_\infty$
9 3 0 ; 1	6 6 6 ; (1)	2			$P\bar{3}m1$	M_2N_2
6 0 2 ; 1a	6 6 6 ; (1)	2	LiRh	*hP*2	$P\bar{6}m2$	MN
[120] structural units a – o (Stolz, Schubert, 1962)						
6 0 2 ; 1a	6 6 6 ; (1)	2	LiRh	*hP*2	$P\bar{6}m2$	b
6 0 2 ; 1b	2 2 6 ; 1	2	MN		*Pmmn*	aa′
4 4 2 ; 1	2 4 2 ; 1	2	MN	*oP*20	*Pnma*	aba′b
2 2 2 ; 2	0 6 0 ; 2	2	$TaPt_2$	*oC*12	*Cmcm*	ac′
2 0 2 ; 3	2 2 6 ; 1	4	$SbAg_3$	*oP*4	*Pmm*2	b′
0 4 2 ; 3	0 2 2 ; 3	3	$TiCu_3$	*oP*8	*Pmmn*	cc′
0 2 2 ; 4	0 4 0 ; 4	5	$ZrAu_4$	*oP*20	*Pnma*	ecec′
0 0 0 ; 5	0 6 0 ; 2	3	$SnAu_5$	*hR*6	*R*32	e
[220] structural units u – y (Schubert, 1964)						
4 4 2 ; 1	2 4 2 ; 1	2	MN	*oP*20	*Pnma*	xy
4 6 2 ; 1	2 2 6 ; 1	2	AuCd	*oP*4	*Pmma*	y
0 4 2 ; 3	0 2 2 ; 3	3	$TiCu_3$	*oP*8	*Pmmn*	u
0 4.4 2 ; 3	0 1.6 2.8 ; 3	7	$SnCu_3$	*oC*80	*Cmcm*	vu_4
0 4.7 2 ; 3	0 1.3 3.3 ; 3	7	$(Cd,In)Au_3$	*oC*48	*Cmcm*	vu_2
0 5 2 ; 3	0 1 4 ; 3	5	$CdAu_3$	*oC*32	*Cmcm*	vu
0 6 2 ; 3	0 0 6 ; 3	2	$SnNi_3$	*hP*8	$P6_3/mmc$	v
other structures						
(0.9 3.7 2 ; 2.8)	0 2.3 2.8 ; 2.8	12	$Cd_{26}Au_{72}$	*hP*98	$P6_3/mmc$	
0 4 2 ; 3.3	0 2 2 ; 3.3	5	Sb_3Cu_{10}	*hP*26	$P6_3/m$	
(1 4 2 ; 3.5)	0 1 3 ; 3.5	6	$Cd_{12}Au_{42}$	*hP*54	$P6_3/mcm$	

Table 4: Cubic close-packed alloys M_xN_y characterized by the self-coordination numbers T_i of M atoms in ccp structures and in square planes (only occupied planes perpendicular to the direction with highest symmetry are included), number M^i of metal atoms with different sets of T_i values, sequences of structural units (Fig.12), space group and Pearson symbol (PS).

T_i(M) ; r ccp	T_i(M) ; r square	M^i	proto-type	PS	space group	struct. units
layers of M and N atoms in [111] direction						
12 6 24 ; (1)	4 4 4 ; (1)	1	Cu	$cF4$	$Fm\bar{3}m$	$M_\infty N_\infty$
9 3 12 ; 1		2	MN	$hR4$	$R\bar{3}m$	M_2N_2
6 0 6 ; 2		2	$ZnAl_2$	$hP3$	$P\bar{3}m1$	MN_2
6 0 12 ; 1a	2 0 4 ; 1	2	CuPt,a	$hR2$	$R\bar{3}m$	MN
[110] structural units a – d, k, l (Ketelaar, 1935)						
6 0 12 ; 1a	2 0 4 ; 1	2	CuPt,a	$hR2$	$R\bar{3}m$	a
6 0 12 ; 1b	2 0 4 ; 1	2	CuPt,b	$cF32$	$Fd\bar{3}m$	ll′
4 4 16 ; 1	0 4 4 ; 1	2	UPb	$tI8$	$I4_1/amd$	aa′
2.7 3.3 10.7 ; 1.7	2 0 4 ; 1	5	$(Zn,Ga)_3Au_5$	$oI32$	$Ibam$	bcb′c
3 0 10 ; 2b	2 0 4 ; 1	3	$Al\square_2Cl_3$	$mC12$	$C2/m$	ac′
2 0 4 ; 3	2 0 4 ; 1	3	$CuPt_3$	$oC8$	$Cmmm$	c′
0 4 8 ; 3	0 4 4 ; 1	3	$TiAl_3$	$tI8$	$I4/mmm$	c
[210] structural units e – i (Forsyth, Gran, 1962)						
4 4 16 ; 1	0 4 4 ; 1	2	UPb	$tI8$	$I4_1/amd$	eg
4 6 8 ; 1	4 4 4 ; (1)	2	CuAu	$tP4$	$P4/mmm$	f
			NaHg	$oC16$	$Cmcm$	
2 2 12 ; 2a	2 0 2 ; 2	2	$MoPt_2$	$oI6$	$Immm$	g
1 3 10 ; 2.5	1 1 0 ; 2.5	4	Mn_2Au_5	$mC14$	$C2/m$	gh
0.7 3.3 9.3 ; 2.7	0.7 1.3 0 ; 2.7	6	Mo_3Al_8	$mC22$	$C2/m$	gh_2
0 4 8 ; 3	0 4 4 ; 1	3	$TiAl_3$	$tI8$	$I4/mmm$	h
0 2 8 ; 4a	0 0 0 ; 4	2	$MoNi_4$	$tI10$	$I4/m$	i

Table 4 (continued)

T_i(M) ; r ccp	T_i(M) ; r square	M^i	proto-type	PS	space group	struct. units
[001] structural units u – y (Johansson, Linde, 1936; Brauer, 1939)						
4 4 16 ; 1	0 4 4 ; 1	2	UPb	$tI8$	$I4_1/amd$	xy′x′y
4 5.6 9.6 ; 1	0 4 4 ; 1	6	CuAu II	$oI40$	$Imma$	$yx_9y'x'_9$
4 6 8 ; 1	4 4 4 ; (1)	2	CuAu	$tP4$	$P4/mmm$	x
2 4 8 ; 2a	0 4 4 ; 1	3	$ZrSi_2$	$oC12$	$Cmcm$	uu′y′v′vy
2 4 8 ; 2b	0 4 4 ; 1	4	$(Zr,Al)(Si,Al)_2$	$oC24$	$Cmmm$	uu′x′vv′y′ u′uxv′vy
2 5 4 ; 2a	0 4 4 ; 1	4	$ZrGa_2$	$oC12$	$Cmmm$	vyu_2yv
2 5 4 ; 2b	0 4 4 ; 1	3	$HfGa_2$	$tI24$	$I4_1/amd$	u_2yv_2x' $u'_2y'v'_2x$
1.3 4 8 ; 2.3	0 4 4 ; 1	6	Gd_3Sn_7	$oC20$	$Cmmm$	u′uyv v'_2vyuu'
1.3 5.3 2.7 ; 2.3	0 4 4 ; 1	6	Ce_3Sn_7	$oC20$	$Cmmm$	$u_2yv_4yu_2$
1 5.5 2 ; 2.5	0 4 4 ; 1	7	Ce_2Sn_5	$oC28$	$Cmmm$	$v'_3y'u'_6y'v'_3$
0.8 4 8 ; 2.6	0 4 4 ; 1	10	Nb_5Ga_{13}	$oC36$	$Cmmm$	$uu'_2uyvv'_2v_2$ $v'_2vyuu'_2u$
0 4 8 ; 3	0 4 4 ; 1	3	$TiAl_3$	$tI8$	$I4/mmm$	$u_2u'_2$
0 5 4 ; 3	0 4 4 ; 1	3	$ZrAl_3$	$tI16$	$I4/mmm$	$v_4v'_4$
			$CdAu_3$ II	$tI16$	$I4mm$	
0 6 0 ; 3	0 4 4 ; 1	2	$AuCu_3$	$cP4$	$Pm\bar{3}m$	u
			SiU_3	$tI16$	$I4/mcm$	
			$SrPb_3$	$tP4$	$P4/mmm$	
other structures						
(5 4 6 ; 1.25)	(1 2 1 ; 1.25)	3	V_4Zn_5	$tI18$	$I4/mmm$	
3 5 6 ; 1.5	3 3 3 ; 0.25	4	Ti_2Ga_3	$tP10$	$P4/m$	
2.7 4.7 5.3 ; 1.7	0 0 4 ; 3	4	Ga_3Pt_5	$oC16$	$Cmmm$	
	0 4 4 ; 1					
0 0 0 ; 7	0 0 4 ; 3	3	$GeCa_7$	$cF32$	$Fm\bar{3}m$	
0 2 0 ; 8	0 0 0 ; 8	3	$TiPt_8$	$tI18$	$I4/mmm$	

Table 5: Complex close-packed ordered alloys M_xN_y with the same hexagonal planes as hcp or ccp structures, space group and Pearson symbol (PS).

layers	stacking symbol	T_i(M) ; r hex. plan.	prototype	PS	space group
2	hh	2 2 6 ; 1	AuCd	$oP4$	$Pmma$
3	ccc	2 2 6 ; 1	CuAu	$tP2$	$P4/mmm$
6b	$(hc_2)_2$	2 2 6 ; 1	IrTa	$oP12$	$Pmma$
9a	$(ch_2)_3$	2 2 6 ; 1	$LiSn(Nb_2Rh_3)$	$mP6$	$P2/m$
2	hh	0 6 0 ; 2	$SnAu_5$	$hR6$	$R32$
3	ccc	0 6 0 ; 2	0 0 8 ; 5		$P3_112$
4	$(ch)_2$	0 6 0 ; 2	WAl_5	$hP12$	$P6_322$
2	hh	0 2 2 ; 3	$TiCu_3$	$oP8$	$Pmmn$
3	ccc	0 2 2 ; 3	$TiAl_3$	$tI8$	$I4/mmm$
6b	$(hc_2)_2$	0 2 2 ; 3	β-$NbPd_3$	$oP24$	$Pmmn$
12	$(h_2c_2)_3$	0 2 2 ; 3	β-$NbPt_3$	$mP48$	$P2_1/m$
2	hh	0 1 4 ; 3	$CdAu_3$	$oC32$	$Cmcm$
3	ccc	0 1 4 ; 3	$ZrAl_3$	$tI16$	$I4/mmm$
4	$(ch)_2$	0 1 4 ; 3	$MgAu_3$	$oC64$	$Cmcm$
6a	$chch_3$	0 1 4 ; 3	$Cd(Au,In)_{2.8}$	$oC96$	$Amm2$
9a	$(ch_2)_3$	0 1 4 ; 3	$Cd(Au,In)_3$	$mC576$	$C2/m$
10	$(chch_2)_2$	0 1 4 ; 3	$MgAu_3$	$oC160$	$Cmcm$
2	hh	0 0 6 ; 3	$SnNi_3$	$hP8$	$P6_3/mmc$
3	ccc	0 0 6 ; 3	$AuCu_3$	$cP4$	$Pm\bar{3}m$
4	$(ch)_2$	0 0 6 ; 3	$TiNi_3$	$hP16$	$P6_3/mmc$
6b	$(hc_2)_2$	0 0 6 ; 3	$PuAl_3$, VCo_3	$hP24$	$P6_3/mmc$
7c	$hchc_4$	0 0 6 ; 3	$Ti(Pt_{0.89}Ni_{0.11})_3$	$hP28$	$P\bar{3}m1$
9a	$(ch_2)_3$	0 0 6 ; 3	$BaPb_3$	$hR12$	$R\bar{3}m$
10	$(chch_2)_2$	0 0 6 ; 3	γ-$Ta(Pd_{0.67}Rh_{0.33})_3$	$hP40$	$P6_3/mmc$
12	$(h_2c_2)_3$	0 0 6 ; 3	$PuGa_3$	$hR16$	$R\bar{3}m$
14	$(ch_2ch_3)_2$	0 0 6 ; 3	$Ba(Pb_{0.8}Tl_{0.2})_3$	$hP56$	$P6_3/mmc$
15	$(hchc_2)_3$	0 0 6 ; 3	$HoAl_3$	$hR20$	$R\bar{3}m$

Table 6: Self-coordination numbers of some homologous series with different r* and k values (see text).

r*	k	T_i(M) ; r	type	T_i(M) ; r	type
		ccp		**hcp**	
2	2	2 2 12 ; 2a	$MoPt_2$,b	2 2 0 ; 2a,b	
2	1	7 4 18 ; 1/2a	Pt_2Mo,b	7 4 1 ; 1/2a,b	
2	0	12 6 24 ; 0	Cu	12 6 2 ; 0	Mg
3	3	0 6 0 ; 3	$AuCu_3$	0 6 2 ; 3	$SnNi_3$
3	2	4 6 8 ; 1	CuAu	4 6 2 ; 1	AuCd
3	1	8 6 16 ; 1/3	Cu_3Au	8 6 2 ; 1/3	Ni_3Sn
3	0	12 6 24 ; 0	Cu	12 6 2 ; 0	Mg
4	4	0 2 8 ; 4	$MoNi_4$		
4	3	3 3 12 ; 3/2			
4	2	6 4 16 ; 2/3			
4	1	9 5 20 ; 1/4	Ni_4Mo		

Table 7: Composition, space group (SG), Pearson symbol (PS), layer and stacking sequences of [111] $M_xN_yR_z$ layered compounds with h, c, s_2, t_2 notation (Fig.19). The distance between layers $\Delta z\, c/a$ varies in N (normal), I (interstitial alloys) and B form (body-centered cubic alloys).

$M_xN_yR_z$	SG	PS	layer sequ.	stacking sequ.
RM, RMR, $(RM)_2R$ or $(RM)_3R$ chains (I form with $0.2 \leq \Delta z\, c/a \leq 0.8$)				
ZnS 3C	216	*cF*8	RM	t_2
ZnS 2H	186	*hP*4	RM	s_2
ZnS 4H	186	*hP*8	RM	s_2t_2
ZnS 6H	186	*hP*12	RM	s_2t_4
ZnS 12R	160	*hR*24	RM	s_4t_4
NaCl	225	*cF*8	RM	c_2
TiC	225	*cF*8	RM	c_2
NiAs	194	*hP*4	RM	hc
NNb δ'	194	*hP*4	RM	hc
TiS HT	166	*hR*18	RM	hc hc c_2
C_2Mo_3	194	*hP*12	RM	hc_5
TiP	194	*hP*8	RM	hc_3
N(Ta,Mn)	194	*hP*8	RM	hc_3
MoS_2 2H	194	*hP*6	RMR	h_3
CdI_2 C6	164	*hP*3	RMR	c_3
CTa_2	164	*hP*3	RMR	c_3
NbS_2 2H HT	194	*hP*6	RMR	chc
$CdCl_2$ C19	166	*hR*9	RMR	hch
CaF_2	225	*cF*12	RMR	hch
$SnMg_2$	225	*cF*12	RMR	hch
LaH_2	225	*cF*12	RMR	hch
CdI_2 C27	186	*hP*6	RMR	hc_2
N(ScTa)	186	*hP*6	RMR	hc_2
MoS_2 3R	160	*hR*9	RMR	ch_2
$TaSe_2$ 4H(b)	194	*hP*12	RMR	$c_3$chc
ThI_2 β	194	*hP*12	RMR	$h_3$hch
$NbSe_2$ 4s(d2)	187	*hP*12	RMR	$c_3h_3c_3$chc
$NbSe_2$ 4H LT	187	*hP*12	RMR	$chch_2cchcch_2$
$TaSe_2$ 4s(c)	186	*hP*12	RMR	chc ch_2
$NbSe_2$ 4s(d1)	156	*hP*12	RMR	ch_2c_2hchc c_3
TaS_2 6s	160	*hR*18	RMR	ch_2 c_3
SnS_2 18R	166	*hR*27	RMR	c_3hc_2 chc
Bi_2Te_3 I	166	*hR*15	RMRMR	c_5
Pt_2Sn_3	194	*hP*10	RMRMR	hchch
In_2S_3 γ	164	*hP*5	RMRMR	hc_3h
La_2O_3	164	*hP*5	RMRMR	hc_3h

Table 7 (continued)

$M_xN_yR_z$	SG	PS	layer sequence	stacking sequ.
RM, RMR, $(RM)_2R$ or $(RM)_3R$ chains (I form with $0.2 \leq \Delta z\, c/a \leq 0.8$)				
C_3Al_4	166	*hR*21	RMRMRMR	hs_2cs_2h
Th_3N_4	166	*hR*21	RMRMRMR	hc_5h
As_3Sn_4	166	*hR*21	RMRMRMR	c_7
C_3V_4	166	*hR*21	RMRMRMR	c_7
$RN(RM)_n$ RNR chains				
$SnSb_2Te_4$	166	*hR*21	RNRMRNR	c_7
$InIn_2Te_4$ HP	166	*hR*21	RNRMRNR	c_7
$FeFe_2S_4$	166	*hR*21	RNRMRNR	hchchch
$MgAl_2Se_4$	166	*hR*21	RNRMRNR	hs_2cs_2h
$(Cr, Fe)(Ga, Fe)_2Se_4$	166	*hR*21	RNRMRNR	ct_2ct_2c
$FeGa_2S_4$ α	164	*hP*7	RNRMRNR	ht_2ct_2h
$Pb_2Bi_2Se_5$	164	*hP*9	$RN(RM)_2RNR$	c_9
$Fe_2Ga_2S_5$ 2H	194	*hP*18	$RN(RM)_2RNR$	ht_2chct_2h
$Fe_2Ga_2S_5$ 3R	166	*hR*27	$RN(RM)_2RNR$	$ht_2c_3t_2h$
$(Mn_2In_2)Se_5$	166	*hR*27	$RN(RM)_2RNR$	$ct_2c_3t_2c$
$Mg_2Al_2Se_5$	164	*hP*9	$RN(RM)_2RNR$	$hs_2c_3s_2h$
$Ge_3As_2Te_6$	166	*hR*33	$RN(RM)_3RNR$	c_{11}
$Ge_4As_2Te_7$	166	*hR*39	$RN(RM)_4RNR$	c_{13}
$Ge_5As_2Te_8$	164	*hP*15	$RN(RM)_5RNR$	c_{15}
$RN(RM)_nRNR(MR)_mNR$ chains				
NC_3Al_5	186	*hP*18	RNRNRMRNR	hs_2cs_4h
$N_2C_3Al_6$	166	*hR*33	RNRMRNRMRNR	hs_4cs_4h
$N_3C_3Al_7$	186	*hP*26	$RN(RM)_2RNRMRNR$	hs_6cs_4h
$N_4C_3Al_8$	166	*hR*45	$RN(RM)_2RNR(MR)_2NR$	hs_6cs_6h
combinations of chains				
$TlInS_2$	194	*hP*8	RNRM	c_3h
$NaFeO_2$ α	166	*hR*12	RNRM	c_4
$ZnIn_2S_4$ IIb	186	*hP*14	RM RNRNR	hs_2ct_2h
$ZnIn_2S_4$ IIIa	160	*hR*21	RM RNRNR	hs_2cs_2h

Table 7 (continued)

$M_xN_yR_z$	SG	PS	layer sequence	stacking sequ.
combinations of chains				
$ZnIn_2S_4$ I	156	*hP*7	RM RNRNR	ht_2ct_2h
$ZnIn_2S_4$ VIa	160	*hR*42	RM RNRNR	hs_2ct_2h ht_2cs_2h
$ZnIn_2S_4$ IIa	164	*hP*14	RNRNR MR	ht_2ct_2h
			RM RNRNR	
$Zn_2In_2S_5$ IIa(1)	186	*hP*18	RM RNRMRNR	$ht_2ct_2s_2h$
$(Zn_2In_2)S_5$ IIa(2)	186	*hP*18	RM RNRMRNR	hs_2cs_4h .
$Zn_2In_2S_5$ IIIa	160	*hR*27	RM RNRMRNR	$hs_2ct_2s_2h$
$(Zn_3In_2)S_6$ Ia	164	*hP*11	RM RM RNRMRNR	$hs_2t_2ct_2s_2h$
$Zn_3In_2S_6$ Ib	156	*hP*11	RM RM RNRMRNR	$hs_2t_2ct_2s_2h$
$GeBi_4Te_7$	164	*hP*12	RNRMRNR RNRNR	c_{12}
chains containing vacancies at M′ or N′ positions				
$(Ga,In)_{3-x}InS_5$	186	*hP*18	RM′ RNRM′RM′R	hs_2cs_4h
$(Zn,In)_{4-x}(Se,S)_5$ IIb	164	*hP*18	RN′ RM′ RNRN′R	$hs_2t_2ct_2h$
			RN′RNR M′R N′R	$ht_2ct_2s_2h$
$(In,Ga)_{4.67}S_7$	164	*hP*14	RN′RMRN′R $(RM')_2R$	ht_2ct_2h hc_3h
$(In,Ga)_{7.33}S_{11}$	166	*hR*72	RM′RMRNR $(RM')_2R$	hs_2ct_2h hc_3h
			RN′ RMRM′R	ht_2cs_2h
M–M bonding				
ZrCl	166	*hR*12	RM_2R	c_4
PtTe	12	*mC*8	RM_2R	c_4
GaS 2H (β)	194	*hP*8	RM_2R	hs_2h
GaSe 3R (γ)	160	*hR*12	RM_2R	cs_2h
GaSe 4H (δ)	186	*hP*16	RM_2R	cs_2hhs_2h
GaSe 2H (ε)	187	*hP*8	RM_2R	cs_2chs_2h
Ta_2CS_2	166	*hR*15	RMNMR	c_5
Ta_2CS_2 LT	164	*hP*5	RMNMR	hc_3h
Pt_3Te_4	166	*hR*21	RM_2R RMR	c_7
Pt_2Te_3	166	*hR*30	RMR RM_2R RMR	c_{10}
BiSe	164	*hP*12	RMRMR RMRMR M_2	c_{12}
Bi_4Se_3	166	*hR*21	RMRMR M_2	c_7
Bi_2Te	166	*hR*27	RMRMR M_2 M_2	c_9
As	166	*hR*6	M_2	c_2
Bi_2Te_3 II	160	*hR*5	M_2 R_3	c_5

Table 7 (continued)

$M_xN_yR_z$	SG	PS	layer sequence	stacking sequ.
–M–M– or –M–N– bonding (N form with $\Delta z\, c/a \approx 0.8$)				
LiRh	187	*hP*2	MN	h_2
CuPt	166	*hR*6	MN	c_2
$ZnAl_2$	164	*hP*3	MN_2	c_3
α-Nd	194	*hP*4	M_∞	ch
Tb HP	194	*hP*6	M_∞	hc_2
α-Sm	166	*hR*9	M_∞	ch_2
MN_n, M_2N_n (B form with $\Delta z\, c/a \approx 0.2$ (Zalkin, Ramsey, 1956; Zalkin et al., 1956))				
CsCl	221	*cP*2	MN	c_2
MgLa	221	*cP*2	MN	c_2
$CeCd_2$	164	*hP*3	MN_2	c_3
BiF_3, $AlFe_3$	225	*cF*16	MN_3	c_4
LaH_3	225	*cF*16	MN_3	c_4
NaTl	227	*cF*16	M_2N_2	c_4
$AlMnCu_2$	225	*cF*16	MRNR	c_4
$AgSbLi_2$	216	*cF*16	MNR_2	c_4
Al_2Li_3	166	*hR*15	M_2N_3	c_5
$SiFe_2$ HT	164	*hP*6	$MNMN_3$	c_6
$Ni_2\square Al_3$	164	*hP*5	MRMRNR	c_6
Ni_2Al_3	164	*hP*5	RMRMR	hc_3h
Si_2Li_5	166	*hR*21	MN_2MN_3	c_7
Ga_4Li_5	164	*hP*9	$M_2N_2M_2N_3$	c_9
$Ge_2Cu_2Li_5$	164	*hP*9	MNR_2NMR_3	c_9
Pb_3Li_8	166	*hR*33	$MN_2MN_3MN_3$	c_{11}
Pb_2Li_7	164	*hP*9	MN_3MN_4	c_{11}

Table 8: Composition, layer sequence and T_i(M) values of fcc (V form), bcc (v form) and CaF_2 (I form) and related compounds with stacking of square layers in [001] direction.

$M_xN_yR_z$		SG	PS	T_i(M) bcc/ccp/pc
layered [001] structures (Schubert et al., 1960) (Fig.21) (v form with $\Delta z\, c/d \approx 0.6$, **bcc**)				
CsCl	a (MN)	221	*cP*2	0 6 12; 1
$MoSi_2$	b (MN_2)	139	*tI*6	0 4 4; 2
$ReSi_2$	b	71	*oI*6	0 4 4; 2
VAu_2	b	63/38	*oC*12	0 4 4; 2
$AlAu_2$	b	62	*oP*12	0 4 4; 2
AB_3	c (MN_3)	123	*tP*4	0 4 4; 3
γ-TiCu	d (M_2N_2)	129	*tP*4	4 4 4; 1
Au_2Nb_3	e (M_2N_3)	139	*tI*10	4 4 4; 1.5
AB_2	f (M_2N_4)	129	*tP*6	4 4 4; 2
AB	g (M_4N_4)	129	*tP*8	6 5 8; 1
Ti_3Cu_4	bd	139	*tI*14	2.7 4 4; 1.3
Ti_2Cu_3	bdb	129	*tP*10	2 4 4; 1.5
Os_2Al_3	ab	139	*tI*10	0 5 8; 1.5
Ti_3Pd_5	bab	123	*tP*8	0 4.7 6.7; 1.7
ReAl(Re,Al)$_2$	MRNR	123	*tP*4	0 4 4; 3 (M,N) 0 6 12; 1 (R)
CuAu related structures in [001] projection with composition of Cu/Au layer (V form with $\Delta z\, c/d \approx 0.7$, **ccp**)				
Ti_2Ga_3	M_4N/N_5	83	*tP*10	3 5 6; 1.5
MN_3	MN/N_2	65	*oC*4	2 2 4; 3a
$PdCu_4$	M_2N_3/N_5	84	*tP*20	1 1 4; 4
$\square_4Co_5Ge_7$	N_5R_3/ M_4R_4	107	*tI*24	2 2 4; 3/ 1.6 4.8 3.2; 2.2/ 4.6 2.7 9.1; 1.3
CuAu	a (MN)	123	*tP*4	4 6 8; 1
$CuZr_2$	b (MN_2)	139	*tI*6	4 4 0; 2
TiCd	d (M_2N_2)	129	*tP*4	8 4 8; 1
layered [001] structures (I form with $\Delta z\, c/d \approx 1$, **pc**)				
Po	M	221	*cP*1	6 12 8; (1)
Pb$\square$O	a (MN)	129	*tP*4	4 4 0; 1
$M_3\square_2O_4$	b (MN_2)	139	*tI*14	4 4 0; 2
$M_2\square O_3$	c (MN_3)	129	*tP*10	4 4 0; 3
M$\square$O	d (M_2N_2)	123	*tP*8	5 8 4; 1
$M_3\square_2O_4$	ac	129	*tP*14	4 4 0; 2
M$\square$O	ad	99	*tP*12	4.7 6.7 2.7; 1

Table 9a: Self-coordination numbers T_i(M) of M atoms with M atoms in $i = 1 - 3$ shells and y/x of M_xN_y composition of M and N atoms in ordered alloys and related structures (Section 18). The structures are ordered for different structure families with sequences of structural units or a two-dimensional tiling of units shown in square brackets. Square net, structural units from Fig.8.

T_i(M) ; y/x square	struct. units	ccp alloy [001]	bcc alloy [001]
T_2=2T_1–4	a, b, c		
4 4 4; (1)	a, b	Cu, NaCl	W, CsCl
3 2 2; 1	acbc		
2 0 4; 1	c_2	CuPt a,b	γ-TiCu
2 0 3.3; 1.3	c_3bc_3		Ti_3Cu_4
3 2 2; 1.5	bcacb		Os_2Al_3
2 0 2; 2	cbc	$MoPt_2$	
T_2=–2T_1+2(3–r)	b*, c*, s*, t*		
2 0 4; 1	c*	CuPt a,b	
1 2 3; 1	$c_2^*t_2^*$		
0 4 4; 1	t_2^*	UPb	NaTl
1 1 1; 1.5	[c*s**t]	$PdCu_4$	
0 0 4; 3	s_2^*	$GeCa_7$, Ga_3Pt_5	
0 0 2; 3	s_2^{**}		
T_1=0	b, c, s, t		
0 4 4; 1	t_2	UPb	NaTl, $AlFe_3$, $AuMn_3$, $GaLi_2$, $(Mo,U)U_3$
0 3 2; 1.5	t_3s_2		
0 2 0; 2	s_2t	$CuZr_2$	
0 2 0; 3	tsbs	$TiAl_3$	
0 1.6 0.8; 3	$[b_4s_{12}t_4]$	Mn_9Au_{31}	
0 0 0 4; 4	$[bs_4]$	$MoNi_4$, Ti_2Ga_3	
0 0 0 0 0 4; 8	$[b_5s_4]$	$TiPt_8$	
others			
2 2 0; 1	d_2s_2	TiCd,	$Au(Zn,Au)_3$
(1 2 1; 1.25)	$[bc_4t_4]$	V_4Zn_5	Sb_2Tl_7 (z=0)
1.3 1.3 0; 2.3	$[b_3c_2ds_3t]$		Sn_3Li_7
1 1 0; 2.5	$[b_2c_2ts_2]$	Mn_2Au_5	
0.7 1.3 0; 2.7	$[b_3c_2t_2s_4]$	Mo_3Al_8	

Table 9b: Same as Table 9a, except for hexagonal net, structural units from Fig.6.

T_i(M) ; y/x hex. plan.	struct. units	ccp alloy [111]	hcp alloy [0001]	bcc [111]
	a, b, c			
6 6 6 ; (1)	a, b	Cu	Mg	NaTl
4 2 2 ; 1	acbc	TiCu		
2 2 6 ; 1	c_2	CuAu	AuCd	
2 0 2 ; 2	cbc	$MoSi_2$, $MoPt_2$		
	c*, e – i			
2 2 6 ; 1	c*	CuAu	AuCd, $SbAg_3$	
0 6 0 ; 2	e	$MoPt_2$	$TaPt_2$, $SnAu_5$	
0 4 1 ; 2.5	ef	Mn_2Au_5		
0 3.3 1.3 ; 2.7	ef_2	Mo_3Al_8		
0 2 2 ; 3	f	$TiAl_3$	$TiCu_3$	
2 4 2 ; 1	g, g′			
0 2 0 ; 4	h	$MoNi_4$		
0 4 0 ; 4	ei		$ZrAu_4$	
0 2 0 ; 6	i			
	c′, c″, k			
2 2 6 ; 1	c′, c″	CuAu	AuCd	
2 2.4 5.2 ; 1	c'_9c''	CuAu II		
2 4 2 ; 1	c′c″			
1.5 1.5 4.5 ; 1.5	$[c'_3c''_3k_2]$	Ti_2Ga_3		
1 1 4 ; 2a	c′k	$ZrGa_2$		
1 1 4 ; 2b	c′kc″k	$HfGa_2$		
0 0 6 ; 3	k	$AuCu_3$	$SnNi_3$	
T_1=0	b, f′, k, k′			
0 2 2 ; 3	f′	$TiAl_3$	$TiCu_3$	
0 1.6 2.8 ; 3	f'_4k		$SnCu_3$	
0 1 4 ; 3	f′k	$ZrAl_3$	$CdAu_3$	
0 1.3 1.3 ; 4.3	$[b_4k'_{12}]$			
0 0 0 6 ; 6				Pu_3Pd_4
0 0 7 ; 7	$[b_8k'_8]$			

Table 9b (continued)

T_i(M) ; y/x hex. plan.	struct. units	ccp alloy [111]	hcp alloy [0001]	bcc [111]
others				
2.5 1.5 2.5 ; 1.25		V_4Zn_5		
2 2 2 ; 1.3				$Zn_3Ga_4Pd_7$
(1 2 2 ; 2a)	c′f′	$ZrSi_2$		
(1 2 2 ; 2b)	c′f′c″f′	$(Zr,Al)(Zr,Si)_2$		
(0.4 2 2 ; 2.6)	$c'f'_4$	Nb_5Ga_{13}		
(0 2.3 2.8 ; 2.8)	$[e_3f_6k_4]$		$Cd_{26}Au_{72}$	

Table 10a: Composition $M_xN_yR_z$ and different types of chains RM, $(RM)_nR$, (n = 1 – 3) and RNRM, which can be formed by atoms with one, two or three bonds, number of valence electrons e_i of i = M, N and R atoms and some experimental or theoretical examples (in brackets).

$M_xN_yR_z$	$e_Me_Ne_R$	covalent chain	ionic chain
RM	1 7	I–Cu	$\overline{\lvert I \rvert}$Cu
RM	2 6	S=Zn or –S–Zn–	$\overline{\lvert S \rvert}$Zn
RM	3 5	N≡Al or –N=Al– or =N–Al=	$\overline{\lvert N \rvert}$Al
RM	4 4	–C≡Si– or =C=Si=	$\overline{\lvert C \rvert}$Si
RMR	0 2 7_2	I–Cd–I	$\overline{\lvert I \rvert}Cd\overline{\lvert I \rvert}$
RMR	0 6 1_2	(Cu–S–Cu)	Cu$\overline{\lvert S \rvert}$Cu
RMR	0 4 6_2	S=Sn=S	$\overline{\lvert S \rvert}Sn\overline{\lvert S \rvert}$
RMR	0 4 2_2	(Mg=C=Mg)	Mg$\overline{\lvert C \rvert}$Mg
$(RM)_2R$	0 3_2 6_3	S=In–S–In=S	$\overline{\lvert S \rvert}In\overline{\lvert S \rvert}In\overline{\lvert S \rvert}$
$(RM)_2R$	0 5_2 2_3	(Mg=N–Mg–N=Mg)	Mg$\overline{\lvert N \rvert}Mg\overline{\lvert N \rvert}Mg\overline{\lvert N \rvert}$Mg
$(RM)_3R$	0 4_3 5_4	N≡Th–N=Th=N–Th≡N	$\overline{\lvert N \rvert}Th\overline{\lvert N \rvert}Th\overline{\lvert N \rvert}Th\overline{\lvert N \rvert}$
$(RM)_3R$	0 4_3 3_4	Al≡C–Al=C=Al–C≡Al	Al$\overline{\lvert C \rvert}Al\overline{\lvert C \rvert}Al\overline{\lvert C \rvert}$Al
RNRM	2 4 5_2	N≡Th–N=Mg or –N=Th=N–Mg–	$\overline{\lvert N \rvert}Th\overline{\lvert N \rvert}$Mg
RNRM	6 4 3_2	Al≡C–Al=S or –Al=C=Al–S–	Al$\overline{\lvert C \rvert}Al\overline{\lvert S \rvert}$

Table 10b: Different elements with e_i valence electrons in the order of increasing size (Schubert, 1964). The elements shown in brackets contain also other electrons. Zn, Al, Ga and N atoms (underlined) occupy tetrahedral, Mn, In, C and trivalent Fe (bold face) tetrahedral or octahedral sites.

e_i	
1	Cu Ag Li
2	(Ni Co Fe **Mn**) <u>Zn</u> (Ge) Cd Hg (Sn Mg Pb Th)
3	(Ni **Fe** Cr) <u>Al</u> <u>Ga</u> **In** (Bi)
4	**C** Si (Pt Mo W Ta Nb) Sn (Zr)
5	<u>N</u> P As
6	S Se Te
7	Cl Br I

Table 11a: Self-coordination numbers T_i(A) and y/x of ccp alloys M_xN_y and NaCl, BiF_3 or ZnS (sphalerite) related structures, which can be characterized by the T_i(A) of square planes or structural units a – y (Fig.12).

T_i(A) ; y/x ccp	T_i(A) ; y/x square	$Na_n\square_xCl_{n-x}$ $(BiF_2)_n\square_xF'_{n-x}$	M_xN_y (Cu)	$M_xN_yS_{x+y}$ (ZnS)	struct. units
6 0 12 ; 1a	2 0 4 ; 1	$Gd_2\square C$	CuPt,a	$In(Ga,Al)P_2$	a
6 0 12 ; 1b	2 0 4 ; 1	$Ti_2\square C$	CuPt,b		11′
4 4 16 ; 1	0 4 4 ; 1	$Pd_2\square H$, $Ti_2\square N$/ $(NdH_2)H_{0.5}\square_{0.5}$	UPb	$CuFeS_2$	aa′/eg
4 0 8 ; 1.7		$Ti_8\square_3C_5$	M_3N_5		
6 0 6 ; 2	2 0 2 ; 2	$S_3\square In_2$	$ZnAl_2$		MN_2
3 0 10 ; 2a	1 0 2 ; 2	$Cl_3Ti\square_2$	MN_2		
3 0 10 ; 2b	1 0 3 ; 2	$Cl_3Al\square_2$	MN_2		ac′
3 0 10 ; 2c	1 0 2 ; 2	$S_3\square Sc_2$	MN_2		
2 2 12 ; 2a	2 0 2 ; 2	$\square Ti_2\square O_2$	$MoPt_2$	$GeCu_2Se_3$	g
2 2 12 ; 2c				β-$\square Ga_2Se_3$	
1 3 10 ; 2.5			Mn_2Au_5	$Si_2(NiCu_4)S_7$	gh
2 0 4 ; 3	2 0 4 ; 1	$Se_4\square Tm_3$, $Cl_4Os\square_3$	$CuPt_3$		c′
2 0 8 ; 3	0 0 4 ; 3	$I_4Hf\square_3$	MN_3		
0 4 8 ; 3	0 4 4 ; 1	$Nb_4\square N_3$, $F_4Sn\square_3$ $(CeH_2)H_{0.25}\square_{0.75}$	$TiAl_3$	$SbCu_3S_4$	c/h
0 6 0 ; 3	0 4 4 ; 1	$\square Nb_3\square O_3$, $Nb_4\square C_3$	$AuCu_3$	$Cd(\square In_2)Se_4$	u
1 0 7 ; 4	0 0 0 ; 4	$Cl_5U\square_4$	MN_4		
0 2 8 ; 4	0 0 0 ; 4	$F_5U\square_4$, $Pd_5\square H_4$, $O_5\square Ti_4$	$MoNi_4$		i
0 0 8 ; 5a	0 0 2 ; 5	$S_6\square Lu_5$	MN_5		
0 0 8 ; 5b	0 0 0 ; 5	$V_6\square C_5$ III	MN_5		
0 0 8 ; 5e	0 0 2 ; 5	$V_6\square C_5$ I, $S_6\square Sc_5$	MN_5		
0 0 8 ; 5f		$V_6\square C_5$ II, O_6ReLi_5	MN_5		
0 0 6 ; 7	0 0 0 ; 7	$V_8\square C_7$	MN_7		
0 0 0 ; 7	0 0 4 ; 3	$O_8Mg_6Mn\square$	MN_7		

Table 11b: T_i(A) values and structural units of hcp alloys M_xN_y and Ni_2In or ZnS (wurtzite) related structures with structural units of Fig.10, 28.

T_i(A) ; y/x hcp	T_i(A) ; y/x hex. plan.	$Ni_nIn_n\square_xNi'_{n-x}$ (Ni_2In)	M_xN_y (Mg)	$M_xN_yS_{x+y}$ (ZnS)	struct. units
4 4 2 ; 1	2 4 2 ; 1 $x\bar{x}$	$Ni_2Sn_2\square Ni$		β-$NaFeO_2$	xy/aba'b
3.6 2.4 0 ; 1.4	0 6 0 ; 2 $\bar{x}x\bar{y}y$	$Ni_{12}Ge_{12}\square_5Ni_7$	M_5N_7 (a)		pq
3 3 2 ; 1.5	1 5 1 ; 1.5 $5x5\bar{x}$	$Mn_5Sn_5\square_2Mn_3$		$M_2N_3S_5$	ac'aba'ca'b
2 2 0 ; 2a	0 6 0 ; 2 $z\bar{z}$	$Ni_3Ge_3\square Ni_2$		α'-$\square Ga_2S_3$	r
2 2 0 ; 2b	0 6 0 ; 2 $z\bar{y}x\bar{z}y\bar{x}$	$M_3N_3\square M_2$		α-$\square Al_2S_3$	
2 2 2 ; 2	0 6 0 ; 2 $x\bar{x}$	$M_3N_3\square M_2$	$TaPt_2$	$SiLi_2O_3$	t/ac'/a'c
1 3 1 ; 2.5	0 4 1 ; 2.5 $2x2\bar{z}$	$M_7N_7\square_2M_5$		$Si_2Cu_5S_7$	
(2 2 2 ; 2.5)	0 4 1 ; 2.5 $y\bar{y}$	$Mn_7Sn_7\square_2Mn_5$			tt'
(2 2 2 ; 3)	0 2 2 ; 3 $y\bar{y}$	$M_4N_4\square M_3$			t'
4 0 0 ; 3	2 2 6 ; 1 $x\bar{x}$	$M_4N_4M\square_3$	MN_3 (b)		hh'
1.3 1.3 0 ; 3	0 6 0 ; 2 $2x\bar{z}2\bar{y}$	η^6-$Cu_4Sn_4Cu\square_3$	MN_3 (c)		kh'h'
1 2 0 ; 3	0 4 0 ; 3 $2\bar{z}2x$	η^8-$Cu_4Sn_4Cu\square_3$			khkh
0 4 2 ; 3	0 2 2 ; 3 $2\bar{y}2y$	$M_4N_4M\square_3$	$TiCu_3$	$AsCu_3S_4$	cc'/u
0 6 2 ; 3	0 0 6 ; 3 $2\bar{y}2y$	$Fe_4Ge_4\square Fe_3$	$SnNi_3$	$Zn(P\square Ag)S_4$	v
0 6 2 ; 3	0 0 6 ; 3 $2\bar{y}2y$	$Pd_7Tl_9\square_2Pd_6$	$SnNi_3$		v
(1 3 0 ; 3a)	0 0 6 ; 3 $2\bar{y}\bar{x}$	$M_8N_8\square_2M_6$			v'v''v'''
(1 3 0 ; 3b)	0 0 6 ; 3 $2\bar{y}\bar{y}2\bar{y}\bar{z}$	$Pd_7Pb_9\square_2Pd_6$			v''v'''
(1 3 0 ; 3c)	0 0 6 ; 3 $2\bar{y}\bar{x}$	$Pt_7In_9\square_2Pt_6$			v'
0 2 0 ; 4	0 2 0 ; 4 $2\bar{x}2z$	η'-$Cu_5Sn_5Cu\square_4$			s
0 2 2 ; 4	0 4 0 ; 4 $6x6\bar{x}$	$M_5N_5M\square_4$	$ZrAu_4$		ecec'

(a) layer sequence M_2N, $(MN_2)_3$
(b) layer sequence $(MN)_2$, $(N_2)_2$
(c) layer sequence $(MN_2)_3$, N_3

Table 12: Sequences of CN values of structure families with structural units (Figs. 12,23,26,28,34). The structure families are named by the pioneers who discovered the first compound of the family. The underlined values CN 12 6 for $CaTiO_3$, 8 4 for $(Sr,Ca)CuO_2$ and 6′ for SrO can segregate in long sequences or combinations. The number p_M of M = Fe, Tb, Dy, ... atoms next to each O atom in antistructures like $NaFeO_2$, or Ni′ next to each In atom in Ni_2In related structures, in brackets.

struct. unit	T_i(A) ; y/x	$M_nO_{xn-x}\square_x$ ($M_nO_x\square_{xn-x}$)	CN
PER group u′w series (Müller-Buschbaum)			$\underline{8\,4_2}\,7_2\,\underline{6'_n}$
w_2	0 0 8 ; 2	($VH\square_2$, $SrO\square_2$)	6′
$u'w'u'''$ |	0 2.7 2.7 ; 2	$CuSr_2O_3\square_6$	$4\,7_2$
u'_2	0 4 0 ; 2	$(Sr,Ca)CuO_2$	8 4
uv series (Er-Rakho, Raveau)			$\underline{6\,12_2}\,5_2\,\underline{8_2\,4}$
uv |	0 6.4 0 ; 1.4	$Ba(Cu,Fe)_2YO_5$	$12\,5_2\,8$
v_2	0 8 0 ; 1	$CaTiO_3\square_3$	12 6
vu′ series			$\underline{12\,6_2}\,10_2\,\underline{4_2\,8}$
vu′ |	0 6.4 0 ; 1.4	$M_4O_5\square_7$	$6\,10_2\,4$
uu′v series (Raveau, Chu)			$\underline{8\,4_2}\,10_2\,5_2\,\underline{8_2\,4}$
u′vu |	0 5.7 0 ; 1.6	$CuBa_2Cu_2YO_7$	$4\,10_2\,5_2\,8$
vw series (Ruddlesden-Popper, Müller-Bednorz)			$\underline{12\,6_2}\,9_2\,\underline{6'_n}$
vw′v′ |	0 6 2 ; 1.25	$CuLa_2O_4$	$6\,9_2$
vw′ |	0 4.8 3.2 ; 1.4	$CuBa_2TlO_5$	$6\,9_2\,6'$
vw'_3v' |	0 4 4 ; 1.5	$CuSr_2Bi_2O_6$	$6\,9_2\,6'_2$
$v_2w'v'_2$ |	0 6.9 1.1 ; 1.14	$LaCu_2La_2O_7$	$12\,6_2\,9_2$
uvw′ series (Nguyen, Cava)			$\underline{8\,4_2}\,8_2\,5_2\,9_2\,\underline{6'}$
uvw′v′u″ |	0 5.33 1.33 ; 1.5	$CaCu_2La_2O_6$	$8\,5_2\,9$
uvw′ |	0 4.57 2.29 ; 1.57	$CaCu_2Ba_2TlO_7$	$8\,5_2\,9_2\,6'$
$u''v'w'_3vu$ |	0 4 3 ; 1.625	$CaCu_2Sr_2Bi_2O_8$	$8\,5_2\,9_2\,6'_2$

Table 12 (continued)

struct. unit	T_i(A); y/x	$M_nO_{xn-x}\square_x$ ($M_nO_x\square_{xn-x}$)	CN
hcp/Ni_2In interstitial alloys p – t (Ellner et al., 1971)			
pq	3.6 2.4 0; 1.4	$Ni_{12}Ge_{12}\square_5Ni_7$	$(2\,3_4)$
r	2 2 0; 2a	$Ni_3Ge_3\square Ni_2$	$(3_2\,4)$
s	0 2 0; 4	η'-$Cu_5Sn_5Cu\square_4$	(1)
ccp interstitial alloys a – d, k, l (Ketelaar, 1935)			
a	6 0 12; 1a	α-$NaFeO_2$	(3)
ll′	6 0 12; 1b	$LiTbS_2$	(3)
aaa′a′	5 2 14; 1	$NaDyO_2$	(3)
ac′	3 0 10; 2b	$\square_2AlCl_3$	(2)
ac′a′c′	3 0 10; 2c	β-Na_2PtO_3	(2)
c′dc′d	1 0 6; 4	K_4UO_5	$(1_2\,2)$
e – i (Forsyth, Gran, 1962)			
g	2 2 12; 2a	Li_2ZrO_3	(2)
i	0 2 8; 4a	Na_4UO_5	$(1_2\,2)$
u – y (Johansson, Linde, 1936; Brauer, 1939)			
xy′x′y	4 4 16; 1	γ-$LiFeO_2$	(3)
u_2u_2'	0 4 8; 3	$Nb_4N_3\square$	$[4_2\,5_2]$
u	0 6 0; 3	$Nb_4C_3\square$	$[4_3\,6]$

Table 12 (continued)

struct. unit	T_i(A); y/x	$M_nO_{xn-x}\square_x$ ($M_nO_x\square_{xn-x}$)	CN
pc group (α - δ (Thornber, Bevan, 1970))			
$\alpha\gamma$	0 0 1; 8	$Pr_9O_{16}\square_2$	$[6^d\,7_{14}\,8_3]$
$\alpha\beta\alpha'\delta'$-	0 0 1; 9	$Pr_{10}O_{18}\square_2$	$[6^d\,7_{14}\,8_5]$
$\alpha'\beta\alpha\delta$			
$\beta\delta'\beta\delta$	0 0 0 0 3; 11	$Pr_{12}O_{22}\square_2$	$[7_8\,8_4]$
β (mod7)	0 0 2; 6	$Pr_7O_{12}\square_2$	$[6^d\,7_6]$
β (mod11)	0 0 0 0 4; 10	$Tb_{11}O_{20}\square_2$	$[7_8\,8_3]$
honeycomb net (hollow positions on [111] surfaces)			
a, b	3 6 3; (1)	MI_2	6
v_2	2 2 0; 1	$Si_2\square_2$	3
$[c_2p_2]$	0 0 2; 3	$Rh_4(CO)(C_2H_3)\square_6$	$[3_2\,3_2']$
s	0 6 0; 1	$RuH\square$	1
m_3	0 3 0; 2		2
cm	0 2 0; 3a	$Ru_2O\square_3$	1 2
c_3	0 0 0; 5	$Ti_3C\square_5$	2
$[bc_3]$	0 0 0; 7a	$Ru_4O\square_7$	$[0\,1_3]$
kagomé net (bridge positions on [111] surfaces)			
o_3	2 0 0; 2	$Si_2\square Bi_3\square_6$	2
$[b_4c_{12}]$	0 0 0.7; 7	$Pt_{16}(C_6H_6)_2(CO)_4\square_{42}$	$[0_4\,1_{12}]$
$[b_8c_8]$	0 0 1; 11	$Pt_{16}(CO)_4\square_{44}$	$[0_8\,1_8]$
$[b_2c_2]$	0 0 0; 11a	$Ge_4S\square_{11}$	$[0_2\,1_2]$
$[b_{12}c_4]$	0 0 0; 23	$Pt_{16}(C_6H_6)_2\square_{46}$	$[0_{12}\,1_4]$
hexagonal net (top positions on [111] surfaces)			
a, b	6 6 6; (1)	SiCl	1
e	0 6 0; 2	$Ru_3(CO)\square_2$	$1\,0_2$
k	0 0 6; 3	$As_4Ga_3\square$	$1_3\,0$

Table 12 (continued)

struct. unit	T_i(A) ; y/x	$M_nO_{xn-x}\square_x$ ($M_nO_x\square_{xn-x}$)	CN
square lattice hollow positions on [001] surfaces			
a, b	4 4 4 ; (1)	NiAl	4
c	2 0 4 ; 1	$Si_2Co\square$	2
t	0 4 4 ; 1	$\square Cu_3O_2\square_2$	2
t_3s_2	0 3 2 ; 1.5	$Cu_5Pb_3\square_2$	$2_3\,1_2$
s	0 0 2 ; 3	$Cu_4I\square_3$	1
bridge positions on [001] surfaces			
a, b	4 4 4 ; (1)	$NiSi_2$	4
t	0 4 4 ; 1	$Si_2Sb_2\square_2$	2
tsbs	0 2 0 ; 3	$Ge_2S\square_3$	2101
s	0 0 2 ; 3	$Pd_2(CO)\square_3$	1
tsb_3s	0 2 0 ; 5	$Ta_3O\square_5$	210_31
top positions on [001] surfaces			
cbc	2 0 2 ; 2	$Si_2\square$	101

Table 13a: Hexagonal close-packed interstitial alloys with different occupation at octahedral sites, T_i; y/x values of the primitive hexagonal lattice ph ($i = 1 - 7$) and hexagonal planes with translations x, $\bar{x}$ or 2x to next layer. T_1 T_2 T_3 (hex.plane) $\widehat{=}$ T_2 T_5 T_7 (ph), T_1 T_2 T_3 (ph') $\widehat{=}$ T_1+T_2 T_3 T_5 (ph).

T_i(A); y/x ph'	T_i(A); y/x ph	T_i(A); y/x hex. plan.		Proto-type	SG	PS
Bozorth (1922)						
8 12 6; (1)	2 6 12 2 6 24 6; (1)	6 6 6; (1)		NiAs, δ'-NbN	194	*hP*4
6 0 6; 1	0 6 0 2 6 12 6; 1	6 6 6; (1)		α-$Ta_2C\square$	164	*hP*3
(4 4 2; 1a)*	0 4 4 2 2 16 2; 1	4 2 2; 1	2x	ξ-$Nb_2C\square$	62	*oP*12
2 8 2; 1	0 2 8 2 2 12 6; 1	2 2 6; 1	x	$Co_2C\square$	58	*oP*6
2 8 4; 1	0 2 8 2 4 8 2; 1	2 4 2; 1	x	ζ-$Fe_2N\square$	60	*oP*12
0 6 6; 2a	0 0 6 0 6 6 0; 2	0 6 0; 2	x	ε-$Ni_3C\square_2$	167	*hR*8
Kiessling (1949)						
0 3.2 4.4; 3.4	0 0 3.2 2 4.4 0 0; 3.4	0 4.7 0; 2.7**		$V_5B_6\square_{11}$, V	65	*oC*22
2.3 0 3.3; 2.7	0 2.3 0 2 3.3 7.3 1; 2.7	2.3 3.3 1; 2.7**		B		
2 8 5.3; 1	0 2 8 2 5.3 5.5 2; 1	2 5.3 2; 1**		$\square$		
0 2.7 4.7; 3.7	0 0 2.7 2 4.7 0 0; 3.7	0 4.7 0; 3.7	7y	$Ta_3B_4\square_7$, Ta	71	*oI*14
2.5 0 4; 2.5	0 2.5 0 2 4 7 1.5; 2.5	2.5 4 1.5; 2.5	7y	B		
2 8 5.42; 1	0 2 8 2 5.4 5.1 2; 1	2 5.4 2; 1	7y	$\square$		
0 2 5; 4	0 0 2 2 5 0 0; 4	0 5 0; 4	5x	$V_2B_3\square_5$, V	63	*oC*20
2.3 0.7 4.7; 2.3	0 2.3 0.7 2 4.7 6 2; 2.3	2.3 4.7 2; 2.3	5x	B		
2 8 5.6; 1	0 2 8 2 5.6 4.8 2; 1	2 5.6 2; 1	5x	$\square$		
Ganglberger (1968)						
0 6 6; 2b	0 0 6 2 6 0 0; 2	0 6 0; 2	x$\bar{x}$	$Fe_2P\square_3$, Fe	189	*hP*9
0 0 2; 5a	0 0 0 2 2 8 0; 5	0 3 0; 3.5**		P		
2 8 4.7; 1	0 2 8 2 4.7 6.7 2; 1	2 4.7 2; 1**		$\square$		
0 0 0; 20	0 0 0 2 0 0 0; 20	0 0 0; 20	7x	$\underline{Zr}_2Fe_{12}P_7\square_{21}$	174	*hP*21
0 5 2; 2.5	0 0 5 2 5 0 0; 2.5	0 5 0; 2.5	7x	Fe		
0 0 6; 5a	0 0 0 2 6 0 0; 5	0 6 0; 2**		P		
2 8 6; 1	0 2 8 2 6 4 2; 1	0 6 0; 2**		$\square$		
0 0 2; 12	0 0 0 2 2 0 0; 12	0 2 0; 12	7x	$\underline{Zr}_6Ni_{20}P_{13}\square_{39}$	174	*hP*39
0 4.2 4.8; 2.9	0 0 4.2 2 4.8 0 0; 2.9	0 4.8 0; 2.9	7x	Ni		
0 0 6; 5a	0 0 0 2 6 0 0; 5	0 6 0; 2**		P		
2.2 7.7 5.7; 1	0.1 2.1 7.7 2 5.7 4.8 2.1; 1	2.1 5.7 2.1; 1**		$\square$		
0 0 3; 9.5	0 0 0 0 3 3 0; 9.5	0 3 0; 9.5		$Zn_3\underline{Ga}_4Pd_7\square_{28}$	146	*hR*14
0 0 2; 13	0 0 0 0 2 2 0; 13	0 2 0; 13		Zn		
0 0 6; 5b	0 0 0 0 6 6 0; 5	0 6 0; 5		Pd		
0 6 6; 2a	0 0 6 0 6 6 0; 2	0 6 0; 2	x	Ga+Zn+Pd		

Table 13a (continued)

T_i(A) ; y/x ph′	T_i(A) ; y/x ph	T_i(A) ; y/x hex. plan.	Proto-type	SG	PS
other structures					
2 8 6 ; 1	0 2 8 2 6 4 2 ; 1	0 6 0 ; 2**	ε-Fe_2N	164	*hP*9
(3.3 5.3 2 ; 1)	0 3.3 5.3 2 2 14.7 3.3 ; 1	(6 6 6 ; (1)/ 2 2 6 ; 1)			
(2.7 6.7 2 ; 1)	0.7 2 6.7 0.7 2 13.3 6 ; 1	2 2 6 ; 1 xx0			
(4 4 3.3 ; 1)	2 2 4 2 3.3 10.7 3.3 ; 1	(2 4 2 ; 1/ 2 2 6 ; 1)			
(2.7 6.7 4 ; 1)	0.7 2 6.7 0.7 4 12 2 ; 1	2 4 2 ; 1 xx0			
0 6 6 ; 2b	0 0 6 2 6 0 0 ; 2	0 6 0 ; 2 x$\bar{x}$	ε-Fe_3N	182	*hP*8
3 0 6 ; 2	0 3 0 2 6 6 3 ; 2	0 6 0 ; 2**	$AlB_2\square_3$, $\square$	191	*hP*3
0 6 6 ; 2b	0 0 6 2 6 0 0 ; 2	0 6 0 ; 2 x$\bar{x}$	$Co_2P\square_2$, Co	62	*oP*12
0 0 2 ; 5b	0 0 0 2 2 8 0 ; 5	0 2 0 ; 5	P		
0 4 2 ; 3a	0 0 4 2 2 0 2 ; 3	0 2 2 ; 3 x			
0 4 2 ; 3b	0 0 4 2 2 4 2 ; 3	0 2 2 ; 3 y$\bar{z}$			
0 2 2 ; 4	0 0 2 0 2 8 0 ; 4	0 2 0 ; 4 x			
0 0 6 ; 5a	0 0 0 2 6 0 0 ; 5	0 6 0 ; 2**	AlB_2, Al	191	*hP*3
0 0 4 ; 6	0 0 0 2 4 4 0 ; 6	0 4 0 ; 6 3x	CrB, Cr	63	*oC*8
2 0 2 ; 6	0 2 0 2 2 4 0 ; 6	2 2 0 ; 6 3x	B		

* on the borders of the T_1 T_2 T_3 ; y/x polyhedron
** containing different hexagonal layers

Table 13b: All ph structures with single T_i(A) and single T_i(B) values from the reduced cells of Section 33 (structures in curly brackets are homometric), SG and PS, electroneutral clusters (clusters without central atom in brackets).

T_i(A); y/x ph′	T_i(A); y/x ph	T_i(A); y/x hex. plan.	SG	PS	x + y neutr. clust.
8 12 6 20 24 24 36 8 24 24 18 48; (1)	2 6 12 2 6 24 6; (1)	6 6 6; (1)	191	*hP*1	
(6 8 2 8 12 8 12 6 16 8 6 24; 1)	2 4 8 2 2 12 2; 1	4 2 2; 1	51	*oP*4	
6 0 6 8 12 24 12 6 0 24 6 24; 1	0 6 0 2 6 12 6; 1	6 6 6; (1)	191	*hP*2	
(5 6 2 8 10 12 20 5 12 16 8 24; 1a) }	1 4 6 0 2 10 2; 1	4 2 2; 1 z	12	*mC*8	(26)
(5 6 2 8 10 12 20 5 12 16 8 24; 1b) }	2 3 6 2 2 10 2; 1	3 2 2; 1	12	*mC*16	(26)
(4 6 2 8 12 16 20 4 12 8 10 24; 1)	1 3 6 0 2 12 2; 1	3 2 2; 1 y	2	*aP*8	(20,204,252)
(4 4 4 12 8 16 20 4 8 16 10 16; 1)*	2 2 4 2 4 12 2; 1	2 4 2; 1	51	*oP*4	(8)
(4 4 3 12 12 12 20 4 8 12 8 24; 1)	2 2 4 2 3 10 4; 1	2 3 4; 1	12	*mC*16	(8,46,70,94)
(4 4 2 12 16 8 20 4 8 8 10 32; 1a)* }	0 4 4 2 2 16 2; 1	4 2 2; 1 2z	63	*oC*8	(8)
(4 4 2 12 16 8 20 4 8 8 10 32; 1b)* }	2 2 4 2 2 8 6; 1	2 2 6; 1	47	*oP*2	(8)
(3 6 4 8 14 12 20 3 12 8 8 24; 1a)* }	1 2 6 0 4 14 2; 1a }	2 4 2; 1 $\bar{z}$	12	*mC*8	(26,70,94)
(3 6 4 8 14 12 20 3 12 8 8 24; 1b)* }	1 2 6 0 4 14 2; 1b }	2 4 2; 1 0x	63	*oC*16	(26,70,94)
(3 6 3 10 14 12 16 3 12 12 8 28; 1)	1 2 6 0 3 14 4; 1	2 3 4; 1 2$\bar{z}$	2	*aP*8	
(3 6 2 12 14 12 12 3 12 16 12 24; 1a) }	1 2 6 0 2 14 6; 1a }	2 2 6; 1 0y	71	*oI*8	(46)
(3 6 2 12 14 12 12 3 12 16 12 24; 1b) }	1 2 6 0 2 14 6; 1b }	2 2 6; 1 cycl.	70	*oF*32	(46)
(3 6 2 12 14 12 12 3 12 16 12 24; 1c) }	0 3 6 2 2 14 2; 1	3 2 2; 1 2y	12	*mC*16	(46)
2 8 4 8 12 16 12 2 16 16 6 24; 1	0 2 8 2 4 8 2; 1	2 4 2; 1 x	63	*oC*8	(20,204,252)
2 8 3 12 8 12 20 2 16 12 8 24; 1	0 2 8 2 3 10 4; 1	2 3 4; 1 x	12	*mC*16	(20,26,130)
2 8 2 16 4 8 28 2 16 8 14 8; 1	0 2 8 2 2 12 6; 1	2 2 6; 1 y	71	*oI*4	
(4 4 2 8 8 12 20 4 8 16 6 16; 4/3a) }	2 2 4 2 2 8 2; 4/3a }	2 2 2; 4/3	10	*mP*7	21
(4 4 2 8 8 12 20 4 8 16 6 16; 4/3b) }	2 2 4 2 2 8 2; 4/3b }	2 2 2; 4/3	174	*hP*7	21
6 0 6 6 0 12 0 8 12 0 18 24; 2	0 6 0 0 6 0 6; 2	6 6 6; (1)	191	*hP*3	21
(4 4 0 4 8 4 12 8 16 8 0 20; 2)	2 2 4 2 0 4 2; 2	2 0 2; 2	65	*oC*6	27
(2 4 0 8 8 10 12 8 4 8 0 14; 2)	0 2 4 0 0 10 2; 2	2 0 2; 2 $\bar{y}$	12	*mC*6	9,21
2 0 6 14 0 12 0 8 12 0 18 24; 2	2 0 0 2 6 12 0; 2	0 6 0; 2	191	*hP*3	9,27
0 6 6 0 12 0 18 8 0 12 18 0; 2	0 0 6 0 6 6 0; 2	0 6 0; 2 y	166	*hR*3	21
(3 2 1 5 4 9 16 3 4 14 3 8; 2.5)	2 1 2 2 1 4 1; 2.5	1 1 1; 2.5	10	*mP*7	
2 0 0 8 12 0 12 2 0 0 6 24; 3	2 0 0 2 0 0 6; 3	0 0 6; 3	191	*hP*4	
2 0 0 2 0 6 12 2 0 12 0 0; 6	2 0 0 2 0 0 0; 6	0 0 0; 6	175	*hP*7	21

Table 14: Interstitial alloys $M_z\square_xI_y$ with single configuration of tetrahedral or octahedral sites (Fig.27).

y/z	$M_z\square_xI_y$	Configuration	
	ccp		
0.5	Ti_2C, Gd_2C	1 – 3	facial
0.5	Ti_2N, Pd_2H	1, 2, 5	meridional
0.67	Li_2SnO_3, $AlCl_3$	1 – 4	*cis*
0.67	$\square Ti_2\square O_2$, Li_2ZrO_3, Na_2PtO_3	1, 2, 5, 6	*trans**
0.75	Fe_3O_4	1 – 3	h
0.83	V_6C_5, Li_5ReO_6	1 – 5	
1	TiC	1 – 6	
2	LaH_2		a – h
2.5	$LaH_{2.5}$	1, 2, 5	a – h
3	LaH_3, CeD_3	1 – 6	a – h
	hcp		
0.5	Ta_2C	1 – 3	
0.5	Co_2C, ξ-Nb_2C, ζ-, ε-Fe_2N	2 – 4	
0.67	Cr_2S_3	1 – 4	
0.67	α-Al_2O_3	2 – 5	
0.83	Cr_5S_6	1 – 5	
1	δ'-NbN	1 – 6	
3	HoD_3	1 – 6	a – h

* Some atoms of $\square Ti_2\square O_2$, etc., have a *cis* configuration.

Table 15: The T_i(I) or T_i(M) values of different groups of structures with composition $M_nI_x\square_{xn-x}$ or $I_nM_x\square_{xn-x}$ of the antitype indicating the number of shared polyhedra.

group	□ at	polyhedra	number of shared faces	edges	corners	system
NaCl	Na/Cl	octahedra	–	T_1	T_2	ccp
CaF_2	F	tetrahedra	–	T_1	T_2	pc
CaF_2	Ca	cubes	–	T_1	–	ccp
ZnS	Zn/S	tetrahedra	–	–	T_1	ccp/hcp
NbN	N	octahedra	T_1	T_2	T_3	ph
NiAs	As	prisms	–	T_1	T_2	hcp
$CaTiO_3$	O	distorted octah.	T_2	T_3,T_4	T_5	PER
$CaTiO_3$	M	CN 18	T_2	–	T_3	bcc
NbH	H	distorted tetrah.	–	T_1,T_2	T_3	PER
CsCl	Cs/Cl	cubes	T_2	T_3	T_5	bcc
Ni_2In	Ni′	CN 11 (Edsham.)	T_1	–	T_2	hcp
BiF_3	F′	CN 14 (dodecah.)	T_1	–	T_2	ccp

Table 16: s-CN values $T_i(\oplus)$ and $T_i(\mathrm{M})$ of M atoms with $\oplus$ or $\ominus$ spin in compounds with composition $\mathrm{R}_n\mathrm{M}_x\mathrm{M}'_y$ with $T_i(\mathrm{M}) = T_i(\oplus + \ominus)$. The non-magnetic atoms R are not considered in the different systems. s-CN values, which are not at the borders of structure maps, in brackets. The $T_i(\mathrm{N})$ values of the non-magnetic R atoms or vacancies are underlined, if the magnetic atoms are the majority components with y/x < 1.

$\mathrm{R}_n\mathrm{M}_x\mathrm{M}'_y$	$T_i(\oplus)$; r	$T_i(\mathrm{M})$; r
pc		
$ZrAlCo_2$	6 12 8 ; (1)	–
β_1-ZnMn/O_3LaCr/O_3ErFe	0 12 0 ; 1	6 12 8 ; (1)
Pt_3Fe (a)/O_3CrEr/O_3FeEr	2 4 8 ; 1	6 12 8 ; (1)
HoRh (i)/AuMn/O_3NdMn	4 4 0 ; 1	6 12 8 ; (1)
O_3AlDy (↘)	0 4 0 ; 3	–
O_3AlDy (↘↖)	2 4 8 ; 1	–
O_3AlDy (↘↗)	4 4 0 ; 1	–
O_3AlDy (↘↙)	0 12 0 ; 1	6 12 8 ; (1)
O_3CrDy (↓)	0 0 8 ; 3	–
O_3CrDy (↓↑),(↓←)	2 4 8 ; 1	6 12 8 ; (1)
fcc		
Cu_2AlMn/OEu	12 6 24 ; (1)	–
NDy	11.1 5.1 20.6 ; 1	12 6 24 ; (1)
$As_{0.5}Se_{0.5}U$	(10.7 5.3 18.7 ; 1)	12 6 24 ; (1)
$As_{0.67}Se_{0.33}U$	(10 5 16 ; 1)	12 6 24 ; (1)
AsU	(8 4 8 ; 1)	12 6 24 ; (1)
PHo/O_2Tb/Pd_2InMn	6 0 12 ; 1a	12 6 24 ; (1)
Cl_6K_2Ir/S_2Mn	4 4 16 ; 1	12 6 24 ; (1)
Se_2Mn	4 4.7 13.3 ; 1	12 6 24 ; (1)
Te_2Mn/γ-Mn/PU/O_2U	4 6 8 ; 1	12 6 24 ; (1)
$As_{0.6}Se_{0.4}U$/Cl_6K_2Re	(8 4 8 ; 1.5)	12 6 24 ; (1)
Au_2AlMn	(4 4 0 ; 7)	12 6 24 ; (1)
O_4MgV_2 (1)	2 0 8 ; 3	6 0 12 ; 1b
O_4ZnCr_2 (↗)	1 0 4.5 ; 7	–
O_4ZnCr_2 (↗↙)	4 0 6 ; 3	–
O_4ZnCr_2 (↗↖)	2 0 8 ; 3	–
O_4ZnCr_2 (↙↖)	2 0 7 ; 3	–
O_4ZnCr_2 (↗↙↖)	4.3 0 9.5 ; 1.7	6 0 12 ; 1b
O_4CoCr_2 (↗),(←),(↓)	0 0 4 ; 11	–
O_4CoCr_2 (↖),(↘)	0 0 0 12 ; 7	–
O_4CoCr_2 (↗←)	1 0 4 ; 5	–
O_4CoCr_2 (↗↖)	1.6 0 4.8 ; 3.8	–
O_4CoCr_2 (↖↘)	2 0 4 ; 3	–

Table 16 (continued)

$R_nM_xM'_y$	$T_i(\oplus)$; r	T_i(M); r
fcc		
O_4CoCr_2 (↗←↓)	2 0 4; 3	–
O_4CoCr_2 (↗←↖)	2.9 0 6.9; 2.43	–
O_4CoCr_2 (↗↖↘)	3.5 0 8; 2	–
O_4CoCr_2 (↗←↓↖)	4 0 8; 1.7	–
O_4CoCr_2 (↗←↖↘)	4.8 0 10.4; 1.4	6 0 12; 1b
$S_4Cu_{0.5}In_{0.5}Cr_2$ (1)	3 0 0; 7	–
$S_4Cu_{0.5}In_{0.5}Cr_2$ (1+2)	4 0 4; 3	–
$S_4Cu_{0.5}In_{0.5}Cr_2$ (1+2+3)	5 0 8; 1.7	6 0 12; 1b
O_4GeCo_2 (•)	1 0 2; 7	–
O_4GeCo_2 (• ○)	2 0 4; 3	–
O_4GeCo_2 (○ □)	4 0 6; 3	–
O_4GeCo_2 (• □)	2 0 6; 3	–
O_4GeCo_2 (• ○ □)	4.3 0 8.7; 1.7	6 0 12; 1b
O_4FeFe_2 (high T)	2 0 8; 3	6 0 12; 1b
O_4FeFe_2 (low T)	0 0 4; 7	6 0 12; 1b
$TbCo_2$	6 0 12; 1b	–
$Ga_{1.15}Mn_{2.85}$	0 4 8; 3	0 4 8; 3
Pd_3Mn	0 5 0; 7	0 5 4; 3
$MnPd_3$	(6 4.5 8; 3)	(6 4.5 10; 1)
$PdMn/MnPd/O_4V_2Mn/CCo_2Mn_2$	0 6 0; 3	4 6 8; 1
CMn_2Co_2	4 6 8; 1	–
$Pd_{1.6}Pt_{1.4}Fe$	0 2 0 4; 7	0 6 0; 3
$FePd_{1.6}Pt_{1.4}$	0 6 0; 3	–
$PtMn_3$	2.7 4 10.7; 1.7	0 6 0; 3
Pt_3Fe (c)	(5 4 10; 1)	–
$O_{12}Al_5Dy_3$ (←)	$T_{10} = 4$; 63	–
$O_{12}Al_5Dy_3$ (↑↓)	T_8=2; 31	–
$O_{12}Al_5Dy_3$ (←↑)	0 0 1; 31	–
$O_{12}Al_5Dy_3$ (←↑↓)	0 0 1.3; 20.3	–
$O_{12}Al_5Dy_3$ (←↑ ⊕)	0 0 2; 20.3a	–
$O_{12}Al_5Dy_3$ (←↑ ⊖)	0 0 2; 20.3b	0 0 4; 9.7
bcc		
$O_{12}Ca_3Ge_3Mn_2/Cl_2Cr$	(4 2 4; 1)	8 6 12; (1)
O_4Al_2Co	0 0 12; 3	4 0 12; 1
Al_2Dy/Co_2Tb	4 0 12; 1	–
$GePd_2Mn$ ($Mn_{0.04}$)	0 6 12; 1/	0 0 12; 3
($Mn_{0.96}$)	0 0 12; 3	
F_4K_2Ni	0 0 4; 5a	0 4 4; 2
O_4Ca_2Mn	0 0 4; 5b	0 4 4; 2

Table 16 (continued)

$R_nM_xM'_y$	$T_i(\oplus)$; r	$T_i(M)$; r
ph		
TiO_3Fe (a)/α-Fe_2O_3	0 3 0 1 6 9 3 ; 2	0 0 6 0 6 6 0 ; 2
TiO_3Co (b)	1 0 3 0 6 12 0 ; 2	0 0 6 0 6 6 0 ; 2
TiO_3Mn (c)/O_3Cr_2	0 0 6 0 6 6 0 ; 2	0 0 6 0 6 6 0 ; 2
S_3Cr_2 ($\oplus$)	0 0 6 0 6 6 0 ; 2	–
S_3Cr_2 ($\ominus$)	0 3 0 1 6 9 3 ; 2	0 3 0 1 6 9 3 ; 2
$(OH)_2Mn$ (↑)	0 0 0 2 6 0 0 ; 5	–
$(OH)_2Mn$ (↑↓)	2 0 0 2 6 12 0 ; 2	–
$(OH)_2Mn$ (↑↗),(↑↖),(↗↘)	0 0 6 2 6 0 0 ; 2	–
$(OH)_2Mn$ (↑↙),(↑↘),(↗↖)	0 3 0 2 6 6 3 ; 2	–
$(OH)_2Mn$ (↑↓↗)	1.3 2 4 2 6 12 2 ; 1	–
$(OH)_2Mn$ (↑↗↘)	0 2 8 2 6 4 2 ; 1	–
$(OH)_2Mn$ (↑↙↘)	0 6 0 2 6 12 6 ; 1	2 6 12 2 6 24 6 ; (1)
hcp		
O_2SYb_2	9 3 0 ; 1	12 6 2 ; (1)
O_2SDy_2	(5 3 0 ; 1)	12 6 2 ; (1)
O_2SHo_2	6 0 2 ; 1	12 6 2 ; (1)
β-SMn	4 4 2 ; 1	12 6 2 ; (1)
O_3YMn (↑)	0 0 2 ; 5	–
O_3YMn (↑↓),(↑↖),(↑↗), (↘↗)	2 2 2 ; 2	–
O_3YMn (↑↘),(↑↙),(↘↙)	3 0 2 ; 2	–
O_3YMn (↑↓↘)	4.7 2.7 2 ; 1	–
O_3YMn (↑↘↙)	6 0 2 ; 1	12 6 2 ; (1)

Table 17: Constants a_i, b_i, c_i of different relations between T_1, T_2 values for borders B1, ..., B7 (Section 22).

$$
\begin{aligned}
&\text{B1}: && T_1 = a_1, && \\
&\text{B2}: && T_2 = a_2 T_1 - b_2, && \\
&\text{B3}: && T_2 = a_3 T_1 - b_3, && 1 \le r \le a_4/b_4, \\
&\text{B4}: && T_2 = a_4 - b_4 r, && 1 \le r \le a_4/b_4, \\
&\text{B5}: && T_2 = -a_5 T_1 + b_5(c_5 - r), && 1 \le r \le c_5, \\
&\text{B6}: && T_2 = -a_6 T_1 + b_6(c_6 - r), && 1 \le r \le c_6, \\
&\text{B7}: && T_1 = a_7 - b_7 r, && 1 \le r \le a_7/b_7.
\end{aligned}
$$

	B1	B2		B3		B4		B5			B6			B7	
	a_1	a_2	b_2	a_3	b_3	a_4	b_4	a_5	b_5	c_5	a_6	b_6	c_6	a_7	b_7
chain	–	2	2	–	–	0	0	–	–	–	2	2	2	0	0
net															
rectangle	2	–	–	–	–	2	0	–	–	–	–	–	–	0	0
square	–	2	4	–	–	0	0	–	–	–	2	2	3	0	0
hexagonal	–	2	6	1	2	4	2	1	2	3	5	6	3	4	2
honeycomb	–	4	6	2	2	4	2	2	2	3	4	6	2	0	0
								$3/2 \le r \le 3$			$1 \le r \le 3/2$				
kagomé	–	2	4	–	–	8/3	4/3	–	–	–	–	–	–	8/3	4/3
lattice															
pc	–	4	12	2	4	6	2	–	–	–	4	6	3	0	0
ph	2	–	–	–	–	4	2	–	–	–	–	–	–	0	0
ph′	–	6	36	1	–6	0	0	3/2	6	5/2	3	8	11/4	–	–
				2/3	–20/3			$1 \le r \le 2$			$1 \le r \le 2$				
											3	2	5	0	0
											$2 \le r \le 5$				
bcc	–	3/2	6	–	–	0	0	–	–	–	3/2	3	3	0	0
diamond*	–	6	12	4	6	6	2	2	5	13/5	6	11	23/11	0	0
								$1 \le r \le 5/3$			$1 \le r \le 5/3$				
								2	2	4					
								$5/3 \le r \le 4$							
ccp/hcp	–	1	6	–	–	0	0	2	6	3	2	2	5	6	2
								$1 \le r \le 2$			$2 \le r \le 5$				
perovskite	–	4	8	–	–	16/3	8/3	–	–	–	4	8	2	0	0

* Additional border B3′: $T_2 = 2T_1 + 2 - 2r$, $1 \le r \le 2$, $T_2 = 2T_1 - 2$, $r \ge 2$.

32 Appendix A: Relative ordering numbers, valence electrons, pseudopotential radii and coordination numbers of the elements

Table 18: Relative ordering number $\mathcal{M}$ for structure maps (Pettifor, 1994), number of valence electrons VE, electronegativity X and pseudopotential radii sum $(r_s + r_p)$ of the elements for the ΔVE, ΔX and $\Delta(r_s + r_p)$ coordinates of the three-dimensional structure-stability plots (Villars, 1994). No VE, X and $r_s + r_p$ values are given for $\mathcal{M}$ = 1 – 6 (He – Rn) and $\mathcal{M}$ = 34 – 41 (Lr – Cm).

$\mathcal{M}$	El.	VE	X	$r_s + r_p$	$\mathcal{M}$	El.	VE	X	$r_s + r_p$	$\mathcal{M}$	El.	VE	X	$r_s + r_p$
7	Fr	1	0.70	4.37	45	U	3	1.7	4.72	75	Cd	12	1.40	2.215
8	Cs	1	0.77	4.31	46	Pa	3	1.5	4.96	76	Zn	12	1.44	1.88
9	Rb	1	0.80	4.10	47	Th	4	1.3	4.98	77	Be	2	1.45	1.08
10	K	1	0.80	3.69	48	Ac	3	1.10	3.12	78	Tl	3	1.69	2.235
11	Na	1	0.89	2.65	49	Zr	4	1.70	2.825	79	In	3	1.63	2.05
12	Li	1	0.90	1.61	50	Hf	4	1.73	2.91	80	Al	3	1.64	1.675
13	Ra	2	0.90	3.53	51	Ti	4	1.86	2.58	81	Ga	3	1.70	1.695
14	Ba	2	1.08	3.402	52	Ta	5	1.94	2.79	82	Pb	4	1.92	2.09
15	Sr	2	1.13	3.21	53	Nb	5	2.03	2.76	83	Sn	4	1.88	1.88
16	Ca	2	1.17	3.00	54	V	5	2.22	2.43	84	Ge	4	1.99	1.56
17	Yb	3	1.1	3.59	55	W	6	1.79	2.735	85	Si	4	1.98	1.42
18	Eu	3	1.15	3.94	56	Mo	6	1.94	2.72	86	B	3	1.90	0.795
19	Sc	3	1.50	2.75	57	Cr	6	2.00	2.44	87	Bi	5	2.14	1.997
20	Lu	3	1.2	3.37	58	Re	7	2.06	2.68	88	Sb	5	2.14	1.765
21	Tm	3	1.2	3.60	59	Tc	7	2.18	2.65	89	As	5	2.27	1.415
22	Er	3	1.2	3.63	60	Mn	7	2.04	2.22	90	P	5	2.32	1.24
23	Ho	3	1.2	3.65	61	Fe	8	1.67	2.11	91	Po	6	2.40	1.90
24	Dy	3	1.15	3.67	62	Ru	8	1.97	2.605	92	Te	6	2.38	1.67
25	Y	3	1.41	2.94	63	Os	8	1.85	2.65	93	Se	6	2.54	1.285
26	Tb	3	1.2	3.89	64	Co	9	1.72	2.02	94	S	6	2.65	1.10
27	Gd	3	1.1	3.91	65	Rh	9	1.99	2.52	95	C	4	2.37	0.64
28	Sm	3	1.2	4.14	66	Ir	9	1.87	2.628	96	At	7	2.64	1.83
29	Pm	3	1.15	3.99	67	Ni	10	1.76	2.18	97	I	7	2.76	1.585
30	Nd	3	1.2	3.99	68	Pt	10	1.91	2.70	98	Br	7	2.83	1.20
31	Pr	3	1.1	4.48	69	Pd	10	2.08	2.45	99	Cl	7	2.98	1.01
32	Ce	3	1.1	4.50	70	Au	11	1.19	2.66	100	N	5	2.85	0.54
33	La	3	1.35	3.08	71	Ag	11	1.07	2.375	101	O	6	3.32	0.465
42	Am	3	1.3	4.89	72	Cu	11	1.08	2.04	102	F	7	3.78	0.405
43	Pu	3	1.3	4.91	73	Mg	2	1.31	2.03	103	H	1	2.10	1.25
44	Np	3	1.3	4.93	74	Hg	12	1.49	2.41					

Table 19: Coordination numbers CN of M atoms with valencies +1, ..., +8 (VE) in the order of increasing radii (Shannon, 1976).

VE	Ions
	CN = 2
1	H D Cu Pd Ag
2	Hg
6	U
	CN = 3
1	Hg
2	Be
3	B
4	C Te
5	N
	pyram.
3	Sb
5	Cl Br I
	CN = 4
1	Li Cu Na Ag K
2	Be Ni Mg Cu Co Zn Fe Mn Cd Hg
3	B Al Ga Fe In Tl
4	C Si Mn Ge Co Cr Ti Sn Hf Zr Pb Te
5	P Mn As Cr V Mo Nb
6	S Fe Mn Cr Se Mo W Te U
7	Cl Mn Br Tc Ru Re I
8	Ru Os Xe
	square
1	Ag
2	Ni Cu Pt Pd Fe Ag Pb
3	Br Ag Au Sb

Table 19 (continued)

VE	Ions
	CN = 5
1	Na Ag
2	Ni Cu Mg Co Zn Mn Cd
3	Al Ga Mn Fe Sb Bi
4	Ti V Sn Zr Pb
5	P V
6	Os Mo W
	CN = 6
1	Li Cu Na Ag Hg Au K Tl Rb Cs Fr
2	Be Fe Co Mn Ni Mg Ge Cu Cr Zn V Pt Ti Pd Ag Cd Ca Yb Hg Tm Dy Np No Eu Sr Pb Ba
3	N B P Al Cu Co Fe Ni Mn As Cr Ga V Rh Ti Ru Ir Mo Ta Nb Sc Ag Sb Pd In Au Lu Yb Tm Tl Er Y Ho Dy Tb Gd Eu Cf Sm Bk Pm Cm Am Nd Pr Pu Np Ce U Bi La Pa Ac
4	C S Si Ni Se Mn Ge Co Cr V Fe Rh Ti Pd Ru Pt Ir Re Os Tc Mo W Ta Nb Sn Hf Zr Tb Pb Cf Bk Pr Cm Am Pu Np Ce U Pa Th Po Te
5	N P As Cr V Rh Ru Pt Ir Au Os Re Tc Sb Mo W Ta Nb Pu Np U Bi Pa I
6	S Se Cr Os Re Te Mo W Po Pu Np U
7	F Cl Br Mn Os Re I Tc At Np
8	Xe
	CN = 7
1	Na Ag K Rb
2	Mn Cd Ca Yb Tm Dy Eu Sr Am Sm Pb Ba
3	Yb Er Y Dy Tb Gd Eu Sm Ce La
4	Sn Hf Zr U
5	Ta Nb U
6	Mo U

Table 19 (continued)

VE	Ions
	CN = 8
1	Li Na Ag K Tl Rb Cs
2	Mg Zn Co Fe Mn Cd Ca Yb Hg Dy Eu Sr Am Sm Pb Nd Ba Ra
3	Fe Sc In Lu Tl Yb Tm Er Ho Y Dy Tb Gd Eu Sm Am Pm Nd Pr Ce La Bi
4	V Ti Nb Sn Hf Zr Tb Cf Bk Pb Cm Am Pu Pr Ce Np U Pa Th Po
5	Cr Ta Nb Pa
6	U
	CN = 9
1	Na K Rb Cs
2	Ca Eu Sr Am Sm Pb Nd Ba
3	Lu Yb Tm Er Ho Y Dy Tb Gd Eu Sm Pm Nd Pr Ce La
4	Zr U Th
5	Pa
	CN = 10
1	K Rb Cs
2	Ca Eu Sr Pb Ba
3	Ho Ce La
4	Ce Th
	CN = 11
1	Rb Cs
2	Pb Ba
4	Th
	CN = 12
1	Na K Tl Rb Cs
2	Cd Ca Sr Pb Ba Ra
3	Sm Nd Ce La
4	Ce U Th
	CN = 14
1	Rb

33 Appendix B: Reduced unit cells of the hcp, ccp, bcc and pc lattice, structures with a single set of T_i values, group-subgroup relations and isotopes

Table 20a: Reduced unit cells and space groups (SG) of all possible **hcp** alloys MN_y (y= 1, 3, 5, ..., 15) with self-coordination numbers T_i(M) (i = 1 - 6) of M atoms. The cell parameters a^2, b^2, c^2, **bc**, **ac**, **ab** should be divided by 6 to have the unit cell of the LiRh or Mg structure in units of $a_0 = 1$, $c_0 = \sqrt{8/3}$ (first line). The Cartesian coordinates of **a**, **b** and **c** for a possible representation of the Bravais lattice should be multiplied by 0.5 (x), $\sqrt{3}/2$ (y) and $\sqrt{8/3}$ (z-component).

#	T_i(M) ; y	a^2	b^2	c^2	bc	ac	ab	SG	a	b	c
1	6 0 2 6 12 6 ; 1	6	6	16	0	0	−3	187	2 0 0	$\bar{1}\,\bar{1}$ 0	0 0 1
2	6 0 0 6 0 6 ; 3	6	6	64	0	0	−3	187	2 0 0	$\bar{1}\,\bar{1}$ 0	0 0 2
3	2 0 2 2 4 6 ; 3	6	16	18	0	0	0	25	2 0 0	0 0 1	0 2 0
4	2 0 0 2 8 6 ; 3	6	18	22	−9	−3	0	44	2 0 0	0 $\bar{2}$ 0	$\bar{1}$ 1 1
5	6 0 0 6 0 6 ; 5	6	6	144	0	0	−3	187	2 0 0	$\bar{1}\,\bar{1}$ 0	0 0 3
6	2 0 2 0 4 2 ; 5	6	16	42	0	−3	0	35	2 0 0	0 0 1	$\bar{1}$ 3 0
7	2 0 0 0 4 2 ; 5	6	22	34	−7	0	−3	8	2 0 0	$\bar{1}\,\bar{1}$ 1	0 $\bar{2}$ $\bar{1}$
8	0 0 2 6 0 0 ; 5	16	18	18	−9	0	0	187	0 0 1	$\bar{3}\,\bar{1}$ 0	3 $\bar{1}$ 0
9	0 0 0 6 6 0 ; 5	18	18	22	9	9	9	155	3 1 0	0 2 0	1 1 1
10	2 0 2 0 4 2 ; 7	6	16	72	0	0	0	25	2 0 0	0 0 1	0 4 0
11	2 0 0 2 0 6 ; 7a	6	18	64	0	0	0	25	2 0 0	0 $\bar{2}$ 0	0 0 2
12	2 0 0 2 0 6 ; 7b	6	18	70	−9	−3	0	44	2 0 0	0 $\bar{2}$ 0	$\bar{1}$ 1 2
13	2 0 0 0 4 2 ; 7	6	22	58	4	3	3	8	2 0 0	1 $\bar{1}$ 1	1 3 1
14	2 0 0 0 0 2 ; 7	6	34	34	−2	0	0	35	2 0 0	0 $\bar{2}$ 1	0 2 1
15	0 0 2 2 0 2 ; 7	16	18	24	0	0	0	25	0 0 1	$\bar{3}\,\bar{1}$ 0	2 $\bar{2}$ 0
16	0 0 2 0 0 6 ; 7	16	24	24	−12	0	0	187	0 0 1	$\bar{4}$ 0 0	2 $\bar{2}$ 0
17	0 0 0 2 4 2 ; 7a	18	22	24	−6	0	−9	5	3 1 0	$\bar{1}\,\bar{1}$ 1	$\bar{2}$ 2 0
18	0 0 0 2 4 2 ; 7b	18	22	22	−10	0	0	35	3 1 0	$\bar{1}$ 1 $\bar{1}$	$\bar{1}$ 1 1
19	0 0 0 0 4 6 ; 7	22	22	24	−6	−6	−10	42	1 1 1	1 1 $\bar{1}$	$\bar{4}$ 0 0
20	2 0 2 0 4 2 ; 9	6	16	114	0	−3	0	35	2 0 0	0 0 1	$\bar{1}$ 5 0
21	2 0 0 0 4 2 ; 9	6	22	88	−2	0	−3	8	2 0 0	$\bar{1}\,\bar{1}$ 1	0 4 1
22	2 0 0 0 0 2 ; 9	6	34	58	−11	−3	0	8	2 0 0	0 $\bar{2}$ 1	$\bar{1}$ 3 1
23	0 0 2 2 0 0 ; 9	16	18	42	−9	0	0	35	0 0 1	$\bar{3}\,\bar{1}$ 0	4 $\bar{2}$ 0
24	0 0 0 2 4 0 ; 9	18	22	40	−10	0	−9	5	3 1 0	$\bar{1}\,\bar{1}$ 1	2 $\bar{2}$ $\bar{1}$
25	0 0 0 2 2 0 ; 9	18	22	34	−7	−9	0	5	3 1 0	$\bar{1}$ 1 $\bar{1}$	$\bar{3}$ 1 1
26	2 0 2 0 4 2 ; 11	6	16	162	0	0	0	25	2 0 0	0 0 1	0 6 0
27	2 0 0 2 0 6 ; 11a	6	18	144	0	0	0	25	2 0 0	0 $\bar{2}$ 0	0 0 3
28	2 0 0 2 0 6 ; 11b	6	18	150	−9	−3	0	44	2 0 0	0 $\bar{2}$ 0	$\bar{1}$ 1 3
29	2 0 0 0 4 2 ; 11	6	22	130	8	3	3	8	2 0 0	1 $\bar{1}$ 1	1 $\bar{5}$ $\bar{1}$
30	2 0 0 0 0 2 ; 11a	6	34	82	−14	0	0	6	2 0 0	0 $\bar{2}$ 1	0 $\bar{2}$ $\bar{2}$
31	2 0 0 0 0 2 ; 11b	6	42	64	0	0	−3	35	2 0 0	$\bar{1}$ $\bar{3}$ 0	0 0 2

Table 20a (continued)

#	T_i(M) ; y	a^2	b^2	c^2	bc	ac	ab	SG	a	b	c
32	2 0 0 0 0 2 ; 11c	6	42	70	15	3	3	8	2 0 0	1 $\bar{3}$ 0	1 $\bar{1}$ 2
33	0 0 2 2 0 0 ; 11	16	18	54	0	0	0	25	0 0 1	$\bar{3}$ $\bar{1}$ 0	3 $\bar{3}$ 0
34	0 0 2 0 0 2 ; 11	16	24	42	−6	0	0	6	0 0 1	$\bar{4}$ 0 0	1 $\bar{3}$ 0
35	0 0 0 6 0 0 ; 11a	18	18	64	0	0	−9	187	3 1 0	$\bar{3}$ 1 0	0 0 2
36	0 0 0 6 0 0 ; 11b	18	18	70	9	9	9	155	3 1 0	0 2 0	1 1 2
37	0 0 0 2 4 0 ; 11	18	22	54	−9	0	−9	5	3 1 0	$\bar{1}$ $\bar{1}$ 1	$\bar{3}$ 3 0
38	0 0 0 2 2 0 ; 11	18	22	40	−4	0	0	3	3 1 0	$\bar{1}$ 1 $\bar{1}$	$\bar{2}$ 2 1
39	0 0 0 2 0 0 ; 11	18	34	34	7	9	9	44	3 1 0	0 2 1	3 $\bar{1}$ 1
40	0 0 0 0 4 2 ; 11	22	22	42	−3	−3	−10	8	1 1 1	1 1 $\bar{1}$	$\bar{5}$ 1 0
41	0 0 0 0 2 2 ; 11a	22	24	40	12	10	6	1	1 1 1	4 0 0	2 $\bar{2}$ 1
42	0 0 0 0 2 2 ; 11b	22	24	34	0	−7	−6	1	1 1 1	$\bar{4}$ 0 0	0 2 $\bar{1}$
43	2 0 0 0 4 2 ; 13	6	22	178	11	3	3	8	2 0 0	1 $\bar{1}$ 1	1 5 2
44	2 0 0 0 0 2 ; 13	6	34	106	−5	−3	0	8	2 0 0	0 $\bar{2}$ 1	$\bar{1}$ $\bar{3}$ $\bar{2}$
45	0 0 2 2 0 0 ; 13	16	18	78	−9	0	0	35	0 0 1	$\bar{3}$ $\bar{1}$ 0	5 $\bar{3}$ 0
46	0 0 2 0 0 0 ; 13	16	42	42	−21	0	0	174	0 0 1	$\bar{5}$ $\bar{1}$ 0	4 $\bar{2}$ 0
47	0 0 0 2 4 0 ; 13	18	22	70	−7	0	−9	5	3 1 0	$\bar{1}$ $\bar{1}$ 1	3 $\bar{3}$ $\bar{1}$
48	0 0 0 2 2 0 ; 13	18	22	58	−1	−9	0	5	3 1 0	$\bar{1}$ 1 $\bar{1}$	$\bar{4}$ 2 1
49	0 0 0 2 0 0 ; 13	18	34	40	−2	0	−9	5	3 1 0	$\bar{3}$ 1 1	2 $\bar{2}$ 1
50	0 0 0 0 2 0 ; 13	22	34	40	16	10	7	1	1 1 1	$\bar{3}$ $\bar{1}$ 1	2 $\bar{2}$ 1
51	2 0 0 0 4 2 ; 15	6	22	226	−5	0	−3	8	2 0 0	$\bar{1}$ $\bar{1}$ 1	0 $\bar{6}$ $\bar{2}$
52	2 0 0 0 0 2 ; 15	6	34	136	−4	0	0	6	2 0 0	0 $\bar{2}$ 1	0 4 2
53	0 0 2 2 0 0 ; 15	16	18	96	0	0	0	25	0 0 1	$\bar{3}$ $\bar{1}$ 0	4 $\bar{4}$ 0
54	0 0 2 0 0 2 ; 15a	16	24	72	0	0	0	25	0 0 1	4 0 0	0 4 0
55	0 0 2 0 0 2 ; 15b	16	24	78	−12	0	0	35	0 0 1	$\bar{4}$ 0 0	2 4 0
56	0 0 2 0 0 0 ; 15	16	42	42	−6	0	0	35	0 0 1	$\bar{5}$ 1 0	$\bar{1}$ $\bar{3}$ 0
57	0 0 0 2 4 0 ; 15	18	22	94	10	9	9	5	3 1 0	1 1 1	5 $\bar{3}$ 1
58	0 0 0 2 2 0 ; 15	18	22	70	−2	0	0	3	3 1 0	$\bar{1}$ 1 1	3 $\bar{3}$ 1
59	0 0 0 2 0 2 ; 15a	18	24	64	0	0	0	25	3 1 0	$\bar{2}$ 2 0	0 0 2
60	0 0 0 2 0 2 ; 15b	18	24	70	−6	−9	0	5	3 1 0	$\bar{2}$ 2 0	$\bar{1}$ $\bar{1}$ 2
61	0 0 0 2 0 2 ; 15c	18	24	70	−12	0	0	35	3 1 0	$\bar{2}$ 2 0	1 $\bar{1}$ 2
62	0 0 0 2 0 0 ; 15a	18	34	58	11	9	9	5	3 1 0	0 2 $\bar{1}$	$\bar{1}$ 3 1
63	0 0 0 2 0 0 ; 15b	18	40	40	−8	0	0	35	3 1 0	$\bar{2}$ 2 1	2 $\bar{2}$ 1
64	0 0 0 0 4 2 ; 15a	22	22	78	−6	−6	−10	42	1 1 1	1 1 $\bar{1}$	$\bar{7}$ 1 0
65	0 0 0 0 4 2 ; 15b	22	22	72	0	0	−10	35	1 1 1	1 1 $\bar{1}$	$\bar{6}$ 2 0
66	0 0 0 0 2 2 ; 15a	22	24	58	−6	−1	−6	1	1 1 1	$\bar{4}$ 0 0	1 3 $\bar{1}$
67	0 0 0 0 2 2 ; 15b	22	24	58	6	4	6	1	1 1 1	4 0 0	1 $\bar{3}$ 1
68	0 0 0 0 2 0 ; 15a	22	40	40	4	10	10	5	1 1 1	$\bar{4}$ 0 1	2 $\bar{2}$ 1
69	0 0 0 0 2 0 ; 15b	22	34	42	9	3	7	1	1 1 1	0 $\bar{2}$ 1	5 $\bar{1}$ 0
70	0 0 0 0 0 6 ; 15a	24	24	64	0	0	−12	187	4 0 0	$\bar{2}$ $\bar{2}$ 0	0 0 2
71	0 0 0 0 0 6 ; 15b	24	24	70	6	12	12	42	4 0 0	2 $\bar{2}$ 0	2 0 2
72	0 0 0 0 0 2 ; 15a	24	34	34	−2	0	0	35	4 0 0	0 $\bar{2}$ 1	0 2 1
73	0 0 0 0 0 2 ; 15b	24	34	40	−2	−12	0	8	4 0 0	0 $\bar{2}$ 1	$\bar{2}$ 2 1
74	0 0 0 0 0 2 ; 15c	24	40	40	8	12	12	44	4 0 0	2 2 1	2 2 $\bar{1}$
75	0 0 0 0 0 0 ; 15	34	34	40	−16	−16	−2	42	3 1 1	$\bar{3}$ $\bar{1}$ 1	2 $\bar{2}$ $\bar{1}$
76	0 0 0 6 0 0 ; 17	18	18	144	0	0	−9	187	3 1 0	$\bar{3}$ 1 0	0 0 3

Table 20b: Reduced unit cells and space groups (SG) of all **ccp** alloys MN_y (y = 1 – 8) with self-coordination numbers T_i(M) (i = 1 – 3) of M atoms. The cell parameters a^2, b^2, c^2, **bc**, **ac**, **ab** are in units of $a_0/2$ of fcc Cu structure. The Cartesian coordinates of **a**, **b** and **c** for a possible representation of the Bravais lattice in the same units.

#	T_i(M) ; y	a^2	b^2	c^2	**bc**	**ac**	**ab**	SG	**a**	**b**	**c**
1	12 6 24 ; (1)	2	2	2	1	1	1	225	1 1 0	0 1 1	1 0 1
2	6 0 12 ; 1a	2	2	6	1	1	1	166	1 1 0	0 1 $\bar{1}$	$\bar{1}$ 2 1
3	4 6 8 ; 1	2	2	4	0	0	0	123	1 1 0	$\bar{1}$ 1 0	0 0 2
4	6 0 6 ; 2	2	2	12	0	0	–1	164	1 1 0	$\bar{1}$ 0 $\bar{1}$	$\bar{2}$ 2 2
5	4 4 0 ; 2	2	2	10	–1	–1	0	139	1 1 0	$\bar{1}$ 1 0	0 $\bar{1}$ 3
6	2 2 12 ; 2a	2	4	6	–2	–1	0	71	1 1 0	0 0 $\bar{2}$	$\bar{2}$ 1 1
7	6 0 6 ; 3	2	2	22	1	1	1	166	1 1 0	0 1 1	3 $\bar{2}$ 3
8	4 4 0 ; 3	2	2	16	0	0	0	123	1 1 0	$\bar{1}$ 1 0	0 0 4
9	2 2 4 ; 3	2	4	8	0	0	0	47	1 1 0	0 0 2	$\bar{2}$ 2 0
10	2 0 6 ; 3	2	6	6	–1	0	–1	12	1 1 0	$\bar{2}$ 1 1	1 $\bar{1}$ 2
11	2 0 4 ; 3	2	6	6	–2	0	0	65	1 1 0	$\bar{1}$ 1 $\bar{2}$	$\bar{1}$ 1 2
12	0 6 0 ; 3	4	4	4	0	0	0	221	2 0 0	0 2 0	0 0 2
13	0 4 8 ; 3	4	4	6	–2	–2	0	139	2 0 0	0 $\bar{2}$ 0	$\bar{1}$ 1 2
14	6 0 6 ; 4	2	2	34	1	1	1	166	1 1 0	0 1 $\bar{1}$	$\bar{3}$ 4 3
15	4 4 0 ; 4	2	2	26	–1	–1	0	139	1 1 0	$\bar{1}$ 1 0	0 $\bar{1}$ 5
16	2 2 4 ; 4	2	4	14	–2	–1	0	71	1 1 0	0 0 $\bar{2}$	$\bar{3}$ 2 1
17	2 0 4 ; 4	2	6	10	2	1	1	12	1 1 0	$\bar{1}$ 2 1	1 0 3
18	0 2 8 ; 4	4	6	6	1	2	2	87	2 0 0	1 $\bar{2}$ 1	1 1 2
19	6 0 6 ; 5	2	2	48	0	0	–1	164	1 1 0	$\bar{1}$ 0 $\bar{1}$	$\bar{4}$ 4 4
20	4 4 0 ; 5	2	2	36	0	0	0	123	1 1 0	$\bar{1}$ 1 0	0 0 6
21	2 2 4 ; 5	2	4	18	0	0	0	47	1 1 0	0 0 2	$\bar{3}$ 3 0
22	2 0 4 ; 5	2	6	14	2	1	1	12	1 1 0	$\bar{1}$ 2 $\bar{1}$	$\bar{1}$ 2 3
23	2 0 2 ; 5a	2	6	12	0	0	0	10	1 1 0	$\bar{1}$ 1 $\bar{2}$	$\bar{2}$ 2 2
24	2 0 2 ; 5b	2	6	14	–3	–1	0	12	1 1 0	$\bar{1}$ 1 $\bar{2}$	$\bar{2}$ 1 3
25	2 0 0 ; 5	2	8	10	–2	–1	0	12	1 1 0	$\bar{2}$ 2 0	0 $\bar{1}$ 3
26	0 4 0 ; 5	4	4	10	0	–2	0	65	2 0 0	0 $\bar{2}$ 0	$\bar{1}$ 0 3
27	0 2 4 ; 5	4	6	8	–2	0	–2	12	2 0 0	$\bar{1}$ $\bar{2}$ 1	0 2 2
28	0 0 8 ; 5	6	6	6	1	2	3	12	2 1 1	1 $\bar{1}$ 2	2 $\bar{1}$ $\bar{1}$
29	6 0 6 ; 6	2	2	66	1	1	1	166	1 1 0	0 1 1	5 $\bar{4}$ 5
30	2 2 4 ; 6	2	4	26	–2	–1	0	71	1 1 0	0 0 $\bar{2}$	$\bar{4}$ 3 1
31	2 0 4 ; 6	2	6	18	–1	0	–1	12	1 1 0	$\bar{2}$ 1 $\bar{1}$	$\bar{1}$ 1 4
32	2 0 0 ; 6	2	10	12	–4	0	–1	12	1 1 0	$\bar{1}$ 0 $\bar{3}$	$\bar{2}$ 2 2
33	0 2 4 ; 6	4	6	10	–1	0	–2	12	2 0 0	$\bar{1}$ $\bar{2}$ 1	0 $\bar{1}$ $\bar{3}$
34	0 0 6 ; 6	6	6	6	–1	–1	–1	148	2 1 1	$\bar{1}$ $\bar{1}$ 2	1 $\bar{2}$ $\bar{1}$

Table 20b (continued)

#	T_i(M) ; y	a^2	b^2	c^2	bc	ac	ab	SG	a	b	c
35	6 0 6 ; 7	2	2	86	1	1	1	166	1 1 0	0 1 $\bar{1}$	$\bar{5}$ 6 5
36	2 2 4 ; 7	2	4	32	0	0	0	47	1 1 0	0 0 2	$\bar{4}$ 4 0
37	2 0 4 ; 7	2	6	24	–2	0	–1	12	1 1 0	$\bar{2}$ 1 1	2 $\bar{2}$ 4
38	2 0 2 ; 7a	2	6	22	–2	0	0	10	1 1 0	$\bar{1}$ 1 2	3 $\bar{3}$ 2
39	2 0 2 ; 7b	2	6	22	–1	–1	0	12	1 1 0	$\bar{1}$ 1 $\bar{2}$	$\bar{3}$ 2 3
40	2 0 0 4 ; 7a	2	8	16	0	0	0	47	1 1 0	$\bar{2}$ 2 0	0 0 4
41	2 0 0 4 ; 7b	2	8	18	–4	0	0	65	1 1 0	$\bar{2}$ 2 0	1 $\bar{1}$ 4
42	2 0 0 2 ; 7a	2	10	14	1	1	1	12	1 1 0	0 1 3	3 $\bar{2}$ 1
43	2 0 0 2 ; 7b	2	12	12	–4	0	0	65	1 1 0	$\bar{2}$ 2 2	2 $\bar{2}$ 2
44	0 4 0 ; 7a	4	4	16	0	0	0	123	2 0 0	0 2 0	0 0 4
45	0 4 0 ; 7b	4	4	18	–2	–2	0	139	2 0 0	0 $\bar{2}$ 0	$\bar{1}$ 1 4
46	0 2 4 ; 7	4	6	14	2	2	2	12	2 0 0	1 $\bar{2}$ 1	1 $\bar{2}$ $\bar{3}$
47	0 2 0 4 ; 7	4	8	8	0	0	0	123	2 0 0	0 $\bar{2}$ 2	0 2 2
48	0 2 0 2 ; 7	4	8	10	–4	0	0	65	2 0 0	0 $\bar{2}$ 2	0 3 1
49	0 0 4 4 ; 7	6	6	8	0	0	–2	65	2 1 1	$\bar{2}$ 1 1	0 $\bar{2}$ 2
50	0 0 4 2 ; 7a	6	6	8	0	–2	–1	2	2 1 1	$\bar{1}$ 2 $\bar{1}$	$\bar{2}$ 0 2
51	0 0 4 2 ; 7b	6	6	10	–2	–2	–2	69	2 1 1	$\bar{2}$ 1 1	0 $\bar{3}$ 1
52	0 0 2 ; 7	6	8	8	4	2	2	12	2 1 1	2 $\bar{2}$ 0	2 0 $\bar{2}$
53	0 0 0 12 ; 7	8	8	8	4	4	4	225	2 2 0	0 2 2	2 0 2
54	6 0 6 ; 8	2	2	108	0	0	–1	12	1 1 0	$\bar{1}$ 0 $\bar{1}$	$\bar{6}$ 6 6
55	2 2 4 ; 8	2	4	42	–2	–1	0	71	1 1 0	0 0 $\bar{2}$	$\bar{5}$ 4 1
56	2 0 4 ; 8	2	6	30	1	1	1	164	1 1 0	$\bar{1}$ 2 1	2 $\bar{1}$ 5
57	2 0 0 2 ; 8a	2	10	18	–3	0	–1	65	1 1 0	$\bar{1}$ 0 3	3 $\bar{3}$ 0
58	2 0 0 2 ; 8b	2	12	14	0	–1	0	12	1 1 0	$\bar{2}$ 2 $\bar{2}$	$\bar{2}$ 1 3
59	0 2 4 ; 8	4	6	18	3	2	2	12	2 0 0	1 $\bar{2}$ $\bar{1}$	1 1 $\bar{4}$
60	0 2 0 0 ; 8a	4	10	10	1	2	2	139	2 0 0	1 $\bar{3}$ 0	1 0 $\bar{3}$
61	0 2 0 0 ; 8b	4	10	10	–3	0	–2	12	2 0 0	$\bar{1}$ $\bar{3}$ 0	0 1 $\bar{3}$
62	0 0 6 0 ; 8a	6	6	12	0	0	–3	2	2 1 1	$\bar{1}$ $\bar{2}$ 1	2 $\bar{2}$ $\bar{2}$
63	0 0 6 0 ; 8b	6	6	14	3	3	3	164	2 1 1	1 $\bar{1}$ 2	3 $\bar{2}$ $\bar{1}$
64	0 0 4 ; 8	6	6	10	1	2	1	166	2 1 1	$\bar{1}$ 2 1	0 $\bar{1}$ 3

Table 20c: Reduced unit cells and space groups (SG) of all **bcc** alloys MN_y (y = 1 – 8) with self-coordination numbers T_i(M) (i = 1 – 3) of M atoms. The cell parameters a^2, b^2, c^2, **bc**, **ac**, **ab** are in units of $a_0/2$ of the bcc W structure. The Cartesian coordinates of **a**, **b** and **c** for a possible representation of the Bravais lattice in the same units.

#	T_i(M) ; y	a^2	b^2	c^2	**bc**	**ac**	**ab**	SG	**a**	**b**	**c**
1	8 6 12 ; (1)	3	3	3	–1	–1	–1	229	1 1 1	1 $\bar{1}$ $\bar{1}$	$\bar{1}$ 1 $\bar{1}$
2	4 2 4 ; 1a	3	3	8	0	0	–1	65	1 1 1	$\bar{1}$ $\bar{1}$ 1	2 $\bar{2}$ 0
3	0 6 12 ; 1	4	4	4	0	0	0	221	2 0 0	0 2 0	0 0 2
4	4 2 2 ; 2a	3	3	19	–1	–1	–1	69	1 1 1	$\bar{1}$ $\bar{1}$ 1	3 $\bar{3}$ $\bar{1}$
5	2 0 6 ; 2	3	8	8	–4	0	0	164	1 1 1	$\bar{2}$ 0 2	2 $\bar{2}$ 0
6	0 4 4 ; 2	4	4	11	–2	–2	0	139	2 0 0	0 2 0	$\bar{1}$ $\bar{1}$ 3
7	4 2 2 ; 3	3	3	32	0	0	–1	65	1 1 1	$\bar{1}$ $\bar{1}$ 1	4 $\bar{4}$ 0
8	2 0 2 ; 3	3	8	11	0	–1	0	10	1 1 1	$\bar{2}$ 0 2	1 $\bar{3}$ 1
9	2 0 0 ; 3	3	11	11	–5	–1	–1	166	1 1 1	$\bar{3}$ 1 1	1 $\bar{3}$ 1
10	0 4 4 ; 3	4	4	16	0	0	0	123	2 0 0	0 2 0	0 0 4
11	0 2 4 ; 3	4	8	8	0	0	0	123	2 0 0	0 2 2	0 2 $\bar{2}$
12	0 2 2 ; 3	4	8	11	–4	–2	0	71	2 0 0	0 $\bar{2}$ $\bar{2}$	$\bar{1}$ 3 $\bar{1}$
13	0 0 12 ; 3	8	8	8	4	4	4	225	2 2 0	0 2 2	2 0 2
14	4 2 2 ; 4	3	3	51	–1	–1	–1	69	1 1 1	$\bar{1}$ $\bar{1}$ 1	5 $\bar{5}$ $\bar{1}$
15	2 0 2 ; 4	3	8	19	–4	–1	0	12	1 1 1	$\bar{2}$ 2 0	$\bar{1}$ $\bar{3}$ 3
16	0 4 4 ; 4	4	4	27	–2	–2	0	139	2 0 0	0 2 0	$\bar{1}$ $\bar{1}$ 5
17	0 2 0 ; 4	4	11	11	1	2	2	87	2 0 0	1 $\bar{3}$ $\bar{1}$	1 1 $\bar{3}$
18	0 0 6 ; 4	8	8	11	4	4	4	166	2 2 0	0 2 $\bar{2}$	$\bar{1}$ 3 1
19	4 2 2 ; 5	3	3	72	0	0	–1	65	1 1 1	$\bar{1}$ $\bar{1}$ 1	6 $\bar{6}$ 0
20	2 0 2 ; 5	3	8	24	0	0	0	10	1 1 1	2 $\bar{2}$ 0	2 2 $\bar{4}$
21	2 0 0 ; 5	3	11	19	3	1	1	2	1 1 1	$\bar{1}$ $\bar{1}$ 3	3 $\bar{3}$ 1
22	0 4 4 ; 5	4	4	36	0	0	0	123	2 0 0	0 2 0	0 0 6
23	0 2 2 ; 5a	4	8	19	0	–2	0	65	2 0 0	0 $\bar{2}$ $\bar{2}$	$\bar{1}$ 3 $\bar{3}$
24	0 2 2 ; 5b	4	8	20	–4	0	0	65	2 0 0	0 $\bar{2}$ $\bar{2}$	0 4 $\bar{2}$
25	0 2 0 ; 5	4	11	16	–4	0	–2	12	2 0 0	$\bar{1}$ $\bar{3}$ $\bar{1}$	0 0 4
26	0 0 6 ; 5	8	8	12	0	0	–4	164	2 2 0	$\bar{2}$ 0 $\bar{2}$	$\bar{2}$ 2 2
27	0 0 4 ; 5	8	8	11	0	–4	0	65	2 2 0	$\bar{2}$ 2 0	$\bar{1}$ $\bar{1}$ 3
28	0 0 2 ; 5	8	11	11	5	4	4	12	2 2 0	$\bar{1}$ 3 1	1 1 3
29	4 2 2 ; 6	3	3	99	–1	–1	–1	69	1 1 1	$\bar{1}$ $\bar{1}$ 1	7 $\bar{7}$ $\bar{1}$
30	2 0 2 ; 6	3	8	35	–4	–1	0	12	1 1 1	$\bar{2}$ 0 2	3 $\bar{5}$ 1
31	2 0 0 ; 6	3	19	19	–9	–1	–1	148	1 1 1	$\bar{3}$ $\bar{1}$ 3	3 $\bar{3}$ $\bar{1}$
32	0 4 4 ; 6	4	4	51	–2	–2	0	139	2 0 0	0 2 0	$\bar{1}$ $\bar{1}$ 7
33	0 2 0 ; 6	4	11	20	–2	0	–2	12	2 0 0	$\bar{1}$ $\bar{3}$ $\bar{1}$	0 2 $\bar{4}$
34	0 0 6 ; 6	8	8	19	4	4	4	166	2 2 0	0 2 2	3 $\bar{1}$ 3
35	0 0 2 ; 6	8	11	11	–1	0	–4	12	2 2 0	$\bar{3}$ 1 1	1 $\bar{1}$ 3

Table 20c (continued)

#	T_i(M) ; y	a^2	b^2	c^2	bc	ac	ab	SG	a	b	c
36	4 2 2 ; 7	3	3	128	0	0	−1	65	1 1 1	$\bar{1}\,\bar{1}$ 1	8 $\bar{8}$ 0
37	2 0 2 ; 7	3	8	43	0	−1	0	10	1 1 1	$\bar{2}$ 2 0	$\bar{3}\,\bar{3}$ 5
38	2 0 0 2 ; 7a	3	11	32	0	0	−1	10	1 1 1	$\bar{3}$ 1 1	0 $\bar{4}$ 4
39	2 0 0 2 ; 7b	3	11	35	−5	−1	−1	12	1 1 1	$\bar{3}$ 1 1	1 $\bar{5}$ 3
40	2 0 0 0 ; 7	3	19	19	3	1	1	12	1 1 1	$\bar{3}$ 1 3	1 $\bar{3}$ 3
41	0 4 4 ; 7	4	4	64	0	0	0	123	2 0 0	0 2 0	0 0 8
42	0 2 2 ; 7a	4	8	32	0	0	0	47	2 0 0	0 2 2	0 4 $\bar{4}$
43	0 2 2 ; 7b	4	8	35	−4	−2	0	71	2 0 0	0 $\bar{2}$ $\bar{2}$	$\bar{1}$ 5 $\bar{3}$
44	0 2 0 4 ; 7	4	11	27	3	2	2	12	2 0 0	1 3 1	1 $\bar{1}$ 5
45	0 2 0 0 ; 7a	4	16	16	0	0	0	123	2 0 0	0 4 0	0 0 4
46	0 2 0 0 ; 7b	4	16	20	−8	0	0	65	2 0 0	0 4 0	0 $\bar{2}$ 4
47	0 0 6 ; 7	8	8	24	4	4	4	166	2 2 0	0 2 $\bar{2}$	$\bar{2}$ 4 2
48	0 0 4 ; 7a	8	8	16	0	0	0	123	2 2 0	$\bar{2}$ 2 0	0 0 4
49	0 0 4 ; 7b	8	8	20	−4	−4	0	139	2 2 0	$\bar{2}$ 2 0	0 $\bar{2}$ 4
50	0 0 2 4 ; 7	8	11	16	−4	0	−4	12	2 2 0	$\bar{3}$ 1 $\bar{1}$	0 0 4
51	0 0 2 2 ; 7	8	11	12	−2	0	0	10	2 2 0	$\bar{1}$ 1 $\bar{3}$	$\bar{2}$ 2 2
52	0 0 2 0 ; 7	8	12	12	−4	0	0	65	2 2 0	$\bar{2}$ 2 2	2 $\bar{2}$ 2
53	0 0 0 6 ; 7	11	11	11	−1	−1	−5	12	3 1 1	$\bar{1}$ $\bar{3}$ 1	1 $\bar{1}$ $\bar{3}$
54	0 0 0 4 ; 7	11	11	12	−2	−2	−5	12	3 1 1	$\bar{1}$ 1 $\bar{3}$	$\bar{2}$ 2 2
55	0 0 0 0 8 ; 7	12	12	12	−4	−4	−4	229	2 2 2	$\bar{2}\,\bar{2}$ 2	2 $\bar{2}$ $\bar{2}$
56	2 0 2 4 ; 8	3	8	56	−4	0	0	65	1 1 1	$\bar{2}$ 0 2	4 $\bar{6}$ 2
57	2 0 0 0 ; 8a	3	19	24	−4	0	−1	2	1 1 1	$\bar{3}$ 3 $\bar{1}$	$\bar{2}\,\bar{2}$ 4
58	2 0 0 0 ; 8b	3	24	24	−12	0	0	164	1 1 1	$\bar{4}$ 2 2	2 $\bar{4}$ 2
59	0 2 0 4 ; 8	4	11	35	5	2	2	12	2 0 0	1 $\bar{3}$ 1	1 $\bar{3}$ $\bar{5}$
60	0 2 0 0 ; 8a	4	19	19	1	2	2	139	2 0 0	1 $\bar{3}\,\bar{3}$	1 3 $\bar{3}$
61	0 2 0 0 ; 8b	4	19	20	−6	0	−2	12	2 0 0	$\bar{1}\,\bar{3}\,\bar{3}$	0 4 $\bar{2}$
62	0 0 2 4 ; 8a	8	11	19	−3	0	−4	12	2 2 0	$\bar{1}\,\bar{1}\,\bar{3}$	$\bar{3}$ 3 1
63	0 0 2 4 ; 8b	8	11	20	2	4	4	69	2 2 0	$\bar{1}$ 3 $\bar{1}$	0 2 4
64	0 0 6 0 ; 8	8	8	27	0	0	−4	164	2 2 0	$\bar{2}$ 0 $\bar{2}$	$\bar{3}$ 3 3
65	0 0 2 2 ; 8	8	11	19	−5	−4	0	12	2 2 0	$\bar{1}$ 1 $\bar{3}$	$\bar{3}$ 1 3
66	0 0 0 6 ; 8	11	11	11	−1	−1	−1	166	3 1 1	$\bar{1}\,\bar{1}$ 3	1 $\bar{3}$ $\bar{1}$

Table 20d: Reduced unit cells and space groups (SG) of all **pc** alloys MN_y (y = 1 – 8) with self-coordination numbers T_i(M) (i = 1 – 3) of M atoms. The cell parameters a^2, b^2, c^2, **bc**, **ac**, **ab** are in units of a_0 of the pc structure or $a_0/2$ of the F atoms of the CaF_2 structure. The Cartesian coordinates of **a**, **b** and **c** for a possible representation of the Bravais lattice in the same units.

#	T_i(M) ; y	a^2	b^2	c^2	**bc**	**ac**	**ab**	SG	**a**	**b**	**c**
1	6 12 8 ; (1)	1	1	1	0	0	0	221	1 0 0	0 1 0	0 0 1
2	4 4 0 ; 1	1	1	4	0	0	0	123	1 0 0	0 1 0	0 0 2
3	2 4 8 ; 1	1	2	2	0	0	0	123	1 0 0	0 1 1	0 $\bar{1}$ 1
4	0 12 0 ; 1	2	2	2	1	1	1	225	1 1 0	1 0 $\bar{1}$	0 1 $\bar{1}$
5	4 4 0 ; 2	1	1	9	0	0	0	123	1 0 0	0 1 0	0 0 3
6	2 2 4 ; 2	1	2	5	–1	0	0	65	1 0 0	0 1 1	0 $\bar{2}$ 1
7	0 6 2 ; 2	2	2	3	0	0	–1	164	1 1 0	0 $\bar{1}$ 1	1 $\bar{1}$ $\bar{1}$
8	4 4 0 ; 3	1	1	16	0	0	0	123	1 0 0	0 1 0	0 0 4
9	2 2 4 ; 3	1	2	8	0	0	0	47	1 0 0	0 1 1	0 $\bar{2}$ 2
10	2 0 0 6 ; 3	1	4	4	0	0	0	123	1 0 0	0 2 0	0 0 2
11	2 0 0 4 ; 3	1	4	5	–2	0	0	65	1 0 0	0 2 0	0 $\bar{1}$ 2
12	0 6 0 ; 3	2	2	6	1	1	1	166	1 1 0	1 0 1	2 $\bar{1}$ $\bar{1}$
13	0 4 0 6 ; 3	2	2	4	0	0	0	123	1 1 0	1 $\bar{1}$ 0	0 0 $\bar{2}$
14	0 4 0 4 ; 3	2	2	5	–1	–1	0	139	1 1 0	1 $\bar{1}$ 0	$\bar{1}$ 0 $\bar{2}$
15	0 2 4 ; 3	2	3	3	–1	0	0	65	1 1 0	1 $\bar{1}$ $\bar{1}$	$\bar{1}$ 1 $\bar{1}$
16	0 0 8 ; 3	3	3	3	–1	–1	–1	229	1 1 1	1 $\bar{1}$ $\bar{1}$	$\bar{1}$ 1 $\bar{1}$
17	4 4 0 ; 4	1	1	25	0	0	0	123	1 0 0	0 1 0	0 0 5
18	2 2 4 ; 4	1	2	13	–1	0	0	65	1 0 0	0 1 1	0 $\bar{3}$ 2
19	2 0 0 ; 4	1	5	5	0	0	0	83	1 0 0	0 2 1	0 $\bar{1}$ 2
20	0 6 0 ; 4	2	2	9	1	1	1	166	1 1 0	1 0 $\bar{1}$	$\bar{1}$ 2 $\bar{2}$
21	0 2 2 ; 4	2	3	5	–1	–1	0	12	1 1 0	1 $\bar{1}$ 1	0 $\bar{1}$ $\bar{2}$
22	4 4 0 ; 5	1	1	36	0	0	0	123	1 0 0	0 1 0	0 0 6
23	2 2 4 ; 5	1	2	18	0	0	0	47	1 0 0	0 1 1	0 $\bar{3}$ 3
24	2 0 0 4 ; 5a	1	4	9	0	0	0	47	1 0 0	0 2 0	0 0 3
25	2 0 0 4 ; 5b	1	4	10	–2	0	0	65	1 0 0	0 2 0	0 $\bar{1}$ 3
26	2 0 0 2 ; 5	1	5	8	–2	0	0	10	1 0 0	0 2 1	0 $\bar{2}$ 2
27	0 6 0 ; 5	2	2	12	0	0	–1	164	1 1 0	0 $\bar{1}$ 1	2 $\bar{2}$ $\bar{2}$
28	0 4 0 ; 5a	2	2	9	0	0	0	123	1 1 0	1 $\bar{1}$ 0	0 0 $\bar{3}$
29	0 4 0 ; 5b	2	2	10	–1	–1	0	139	1 1 0	1 $\bar{1}$ 0	$\bar{1}$ 0 $\bar{3}$
30	0 2 2 ; 5	2	3	6	0	0	0	10	1 1 0	1 $\bar{1}$ 1	1 $\bar{1}$ $\bar{2}$
31	0 2 0 2 ; 5a	2	4	5	0	–1	0	65	1 1 0	0 0 2	1 $\bar{2}$ 0
32	0 2 0 2 ; 5b	2	4	6	–2	–1	0	71	1 1 0	0 0 2	1 $\bar{2}$ $\bar{1}$
33	0 2 0 0 ; 5	2	5	5	2	1	1	12	1 1 0	2 $\bar{1}$ 0	1 0 $\bar{2}$
34	0 0 4 ; 5	3	3	5	1	1	1	12	1 1 1	1 1 $\bar{1}$	$\bar{1}$ 2 0
35	2 2 4 ; 6	1	2	25	–1	0	0	65	1 0 0	0 1 1	0 $\bar{4}$ 3
36	2 0 0 ; 6	1	5	10	–1	0	0	10	1 0 0	0 2 $\bar{1}$	0 1 3

Table 20d (continued)

#	T_i(M) ; y	a^2	b^2	c^2	bc	ac	ab	SG	a	b	c
37	0 6 0 ; 6	2	2	17	1	1	1	166	1 1 0	1 0 1	3 $\bar{2}$ $\bar{2}$
38	0 2 2 ; 6	2	3	9	−1	−1	0	12	1 1 0	1 $\bar{1}$ $\bar{1}$	$\bar{2}$ 1 $\bar{2}$
39	0 2 0 ; 6	2	5	6	1	1	1	12	1 1 0	1 0 $\bar{2}$	$\bar{1}$ 2 $\bar{1}$
40	0 0 2 ; 6	3	5	5	−2	−1	−1	148	1 1 1	1 0 $\bar{2}$	$\bar{2}$ 1 0
41	2 2 4 ; 7	1	2	32	0	0	0	47	1 0 0	0 1 1	0 $\bar{4}$ 4
42	2 0 0 4 ; 7a	1	4	16	0	0	0	47	1 0 0	0 2 0	0 0 4
43	2 0 0 4 ; 7b	1	4	17	−2	0	0	65	1 0 0	0 2 0	0 $\bar{1}$ 4
44	2 0 0 2 ; 7a	1	5	13	−1	0	0	10	1 0 0	0 2 1	0 $\bar{2}$ 3
45	2 0 0 2 ; 7b	1	8	8	0	0	0	123	1 0 0	0 2 2	0 $\bar{2}$ 2
46	2 0 0 2 ; 7c	1	8	10	−4	0	0	65	1 0 0	0 2 2	0 $\bar{3}$ 1
47	0 6 0 ; 7	2	2	22	1	1	1	166	1 1 0	1 0 $\bar{1}$	$\bar{2}$ 3 $\bar{3}$
48	0 4 0 ; 7a	2	2	16	0	0	0	123	1 1 0	1 $\bar{1}$ 0	0 0 $\bar{4}$
49	0 4 0 ; 7b	2	2	17	−1	−1	0	139	1 1 0	1 $\bar{1}$ 0	$\bar{1}$ 0 $\bar{4}$
50	0 2 2 ; 7	2	3	11	−1	0	0	10	1 1 0	1 $\bar{1}$ 1	1 $\bar{1}$ $\bar{3}$
51	0 2 0 2 ; 7a	2	4	8	0	0	0	47	1 1 0	0 0 2	2 $\bar{2}$ 0
52	0 2 0 2 ; 7b	2	4	9	−2	0	0	65	1 1 0	0 0 2	2 $\bar{2}$ $\bar{1}$
53	0 2 0 0 ; 7a	2	5	8	−2	0	−1	12	1 1 0	0 $\bar{1}$ $\bar{2}$	$\bar{2}$ 2 0
54	0 2 0 0 ; 7b	2	6	6	−2	0	0	65	1 1 0	1 $\bar{1}$ 2	1 $\bar{1}$ $\bar{2}$
55	0 2 0 0 ; 7c	2	6	6	−1	0	−1	12	1 1 0	1 $\bar{2}$ $\bar{1}$	$\bar{1}$ 1 $\bar{2}$
56	0 0 4 ; 7a	3	3	8	0	0	−1	65	1 1 1	1 $\bar{1}$ $\bar{1}$	0 2 $\bar{2}$
57	0 0 4 ; 7b	3	3	9	−1	−1	−1	69	1 1 1	1 $\bar{1}$ $\bar{1}$	$\bar{1}$ 2 $\bar{2}$
58	0 0 2 ; 7	3	5	5	1	1	1	12	1 1 1	2 0 $\bar{1}$	0 2 $\bar{1}$
59	0 0 0 6 ; 7	4	4	4	0	0	0	221	2 0 0	0 2 0	0 0 2
60	0 0 0 4 ; 7a	4	4	5	0	−2	0	65	2 0 0	0 2 0	$\bar{1}$ 0 2
61	0 0 0 4 ; 7b	4	4	6	−2	−2	0	139	2 0 0	0 2 0	$\bar{1}$ $\bar{1}$ 2
62	0 0 0 2 ; 7a	4	5	5	1	2	2	139	2 0 0	1 2 0	1 0 2
63	0 0 0 2 ; 7b	4	5	5	−2	0	−2	12	2 0 0	$\bar{1}$ 2 0	0 $\bar{1}$ 2
64	2 2 4 2 0 ; 8	1	2	41	−1	0	0	65	1 0 0	0 1 1	0 $\bar{5}$ 4
65	2 0 0 2 2 ; 8	1	5	17	−2	0	0	10	1 0 0	0 2 $\bar{1}$	0 1 4
66	2 0 0 2 0 ; 8a	1	9	10	−3	0	0	10	1 0 0	0 3 0	0 $\bar{1}$ 3
67	2 0 0 2 0 ; 8b	1	9	9	0	0	0	123	1 0 0	0 3 0	0 0 3
68	0 6 0 0 0 ; 8	2	2	27	0	0	−1	164	1 1 0	0 $\bar{1}$ 1	3 $\bar{3}$ $\bar{3}$
69	0 2 2 0 4 ; 8	2	3	14	0	−1	0	65	1 1 0	1 $\bar{1}$ 1	1 $\bar{2}$ $\bar{3}$
70	0 2 0 0 4 ; 8a	2	5	10	2	1	1	12	1 1 0	2 $\bar{1}$ 0	1 0 $\bar{3}$
71	0 2 0 0 4 ; 8b	2	5	9	0	0	−1	65	1 1 0	1 $\bar{2}$ 0	0 0 $\bar{3}$
72	0 2 0 0 0 ; 8	2	6	9	3	1	1	12	1 1 0	2 $\bar{1}$ 1	2 $\bar{1}$ $\bar{2}$
73	0 0 2 0 2 ; 8	3	5	6	−1	0	−1	2	1 1 1	1 $\bar{2}$ 0	1 1 $\bar{2}$
74	0 0 2 0 0 ; 8	3	6	6	−3	0	0	164	1 1 1	2 $\bar{1}$ $\bar{1}$	$\bar{1}$ 2 $\bar{1}$
75	0 0 0 0 6 ; 8	5	5	5	2	2	2	166	2 1 0	1 0 $\bar{2}$	0 2 $\bar{1}$
76	0 0 0 0 0 ; 15a	6	6	10	−2	−2	−2	69	2 1 1	$\bar{2}$ 1 1	0 $\bar{3}$ 1
77	0 0 0 0 0 ; 15b	8	8	8	4	4	4	225	2 2 0	0 2 2	2 0 2

Table 21a: Hexagonal close-packed structures with a single set of T_i(M) and T_i(N) values (homogeneous sphere packing with T_1(M) or T_1(N) contacts). Homometric structures a, b, ... with brackets, T_i values of hexagonal or square plane, space group (SG), Pearson symbol (PS), number of reduced unit cell from Table 20a–d and positions of M atoms in addition to M_1 at origin. (T_i;r) values are not at the borders of the structure map.

T_i(M);y/x hcp	T_i(M);r hex.plan.	SG	PS	#	M_2 M_5			M_3 M_6			M_4		
12 6 2; (1)	6 6 6; (1)	194	*hP*2	1	1/3	2/3	1/2						
9 3 0; 1	6 6 6; (1)	164	*hP*4	2	1/3	2/3	1/4						
(7 3 0; 1a)	4 2 2; 1	10	*mP*8	14	0	5/12	1/12	1/2	1/6	1/3	1/2	1/4	3/4
(7 3 0; 1b)	4 2 2; 1	11	*mP*8	14	0	5/12	1/12	1/2	3/4	1/4	1/2	1/6	1/3
(6 2 2; 1)*	2 4 2; 1	57	*oP*8	15	1/2	2/3	0	0	1/2	1/4	1/2	1/6	1/4
6 0 2; 1a	6 6 6; (1)	187	*hP*2	1									
6 0 2; 1b	2 2 6; 1	59	*oP*4	3	1/2	1/2	1/6						
(5 3 0; 1a)*	2 2 6; 1	12	*mC*8	4	3/4	1/12	1/2						
(5 3 0; 1b)*	2 2 6; 1	43	*oF*32	19	11/12	5/12	1/3	0	0	1/2	5/12	11/12	5/6
(5 3 0; 1d)*	2 4 2; 1	13	*mP*8	18	5/6	1/2	0	1/2	1/4	1/4	1/3	3/4	1/4
(5 3 0; 1e)*	2 4 2; 1	15	*mC*16	18	5/6	1/2	0	1/2	1/4	1/4	1/3	1/4	3/4
4 6 2; 1	2 2 6; 1	51	*oP*4	3	0	1/2	2/3						
4 4 2; 1	2 4 2; 1	62	*oP*8	15	1/2	1/6	1/4	1/2	2/3	1/2	0	1/2	3/4
6 0 0; 2	6 6 6; (1)	194	*hP*6	5	1/3	2/3	1/2						
2 2 2; 2	0 6 0; 2	63	*oC*12	8	1/2	2/3	0						
2 2 0; 2a	0 6 0; 2	15	*mC*12	9	1/2	1/6	1/2						
2 2 0; 2b	0 6 0; 2	178	*hP*18	76	1/3	0	1/6	2/3	1/3	1/3	2/3	2/3	1/2
					1/3	2/3	2/3	0	1/3	5/6			
0 6 2; 3	0 0 6; 3	194	*hP*8	16	1/2	2/3	1/3						

* on the borders of the T_1 T_2 T_3; y/x polyhedron

Table 21b: Same as Table 21a, except for ccp.

T_i(M) ; y/x ccp	T_i(M) ; y/x square	SG	PS	#	M_2	M_3	M_4
12 6 24 ; (1)	4 4 4 ; (1)	225	*cF*4	1			
9 3 12 ; 1	6 6 6 ; (1)**	166	*hR*4	7	1 0 1		
(8 4 8 ; 1)*	4 4 4 ; (1)	129	*tP*4	8	0 1 1		
(7 2 10 ; 1)*	3 2 2 ; 1	11	*mP*8	43	0 1 1	1 0 1	1 $\bar{1}$ 2
(6 2 12 ; 1a) }	2 0 4 ; 1	59	*oP*4	9	0 1 1		
(6 2 12 ; 1b) }	2 0 4 ; 1	131	*tP*8	47	0 $\bar{1}$ 1	1 0 1	1 1 2
(6 1 12 ; 1)	2 0 4 ; 1	11	*mP*8	41	0 1 1	1 0 3	0 0 2
6 0 12 ; 1a }	2 0 4 ; 1	166	*hR*2	2			
6 0 12 ; 1b }	2 0 4 ; 1	227	*cF*32	53	1 1 0	0 1 1	1 0 1
(5 4 10 ; 1)	1 2 2 ; 1	11	*mP*8	48	1 2 1	1 0 1	0 1 1
(5 3 12 ; 1a) }	3 2 2 ; 1	12	*mC*8	10	0 0 2		
(5 3 12 ; 1b) }	2 2 2 ; 1	15	*mC*16	52	2 0 0	3 $\bar{1}$ 0	1 0 $\bar{1}$
5 2 14 ; 1	1 2 2 ; 1	15	*mC*16	51	$\bar{1}$ $\bar{1}$ 2	$\bar{1}$ 0 1	0 $\bar{1}$ 1
4 6 8 ; 1	4 4 4 ; (1)	123	*tP*2	3			
4 5 12 ; 1a	0 4 4 ; 1	74	*oI*16	45	0 $\bar{1}$ 3	0 $\bar{1}$ 1	0 0 2
4 4 16 ; 1	0 4 4 ; 1	141	*tI*8	13	0 $\bar{1}$ 1		
4 2 12 ; 1.3a }	2 2 2 ; 1.3**	2	*aP*7	34	1 $\bar{1}$ 0	0 $\bar{1}$ 1	
4 2 12 ; 1.3b }	2 2 2 ; 1.3**	146	*hR*7	34	1 $\bar{2}$ 1	1 $\bar{1}$ 0	
3 3 12 ; 1.5	1 1 1 ; 1.5	12	*mC*10	18	1 0 1		
6 0 6 ; 2	6 6 6 ; (1)**	164	*hP*3	4			
(4 4 0 ; 2)*	4 4 4 ; (1)	139	*tI*6	5			
2 2 12 ; 2a }	2 0 2 ; 2	71	*oI*6	6			
2 2 12 ; 2b }	0 6 0 ; 2**	151	*hP*9	62	1 $\bar{1}$ 0	1 $\bar{2}$ $\bar{1}$	
2 2 12 ; 2c	0 6 0 ; 2**	2	*aP*6	63	3 $\bar{1}$ 0	2 $\bar{1}$ 1	
2 1 9 ; 2.5	1 1 1 ; 2.5**	2	*aP*7	34	0 $\bar{1}$ 1		
0 6 0 ; 3	0 4 4 ; 1	221	*cP*4	12			
0 2 8 ; 4a	0 0 0 4 ; 4	87	*tI*10	18			
0 0 6 ; 6	0 0 0 6 ; 6**	166	*hR*7	34			

* on the borders of the T_1 T_2 T_3 ; y/x polyhedron
** hexagonal planar

Table 21c: Same as Table 21a, except for bcc.

T_i(M) ; y/x bcc	T_i(M) ; y/x square	SG	PS	#	M_2	M_3	M_4
8 6 12; (1)	4 4 4; (1)	229	*cI*2	1			
(6 4 6; 1)*	2 2 0; 1	67	*oC*8	7	1 $\bar{1}$ 1		
(5 3 5; 1)*	1 2 4; 1	2	*aP*8	40	$\bar{1}$ 1 3	$\bar{2}$ 0 4	0 0 2
(4 4 4; 1a)* }	4 4 4; (1)	129	*tP*4	10	1 1 1		
(4 4 4; 1b)* }	2 0 4; 1	131	*tP*8	45	0 0 2	1 3 1	1 1 1
(4 3 4; 1)*	1 2 2; 1	11	*mP*8	46	1 $\bar{1}$ 3	1 1 1	0 0 2
(4 2 6; 1a) }	2 2 0; 1	11	*mP*4	8	0 $\bar{2}$ 2		
(4 2 6; 1b) }	2 2 0; 1	66	*oC*16	52	2 0 2	$\bar{1}$ 1 1	1 $\bar{1}$ 1
(4 2 5; 1)	1 2 4; 1	2	*aP*8	39	$\bar{2}$ 0 2	$\bar{1}$ $\bar{3}$ 3	0 $\bar{2}$ 2
(4 2 4; 1a)* }	2 0 4; 1	65	*oC*4	2			
(4 2 4; 1b)* }	2 0 4; 1	141	*tI*16	55	$\bar{1}$ $\bar{1}$ 1	1 $\bar{1}$ $\bar{1}$	2 0 0
(4 1 8; 1)*	0 4 4; 1	74	*oI*16	49	$\bar{1}$ 1 3	$\bar{1}$ 1 1	0 0 2
4 0 12; 1	0 4 4; 1	227	*cF*16	13	1 1 1		
(3 3 5; 1)*	1 2 4; 1	2	*aP*8	53	0 $\bar{2}$ 0	1 $\bar{3}$ $\bar{1}$	1 $\bar{1}$ $\bar{1}$
(2 4 6; 1)*	2 2 0; 1	74	*oI*8	12	0 0 $\bar{2}$		
0 6 12; 1	4 4 4; (1)	221	*cP*2	3			
(4 2 4; 1.3a) }	2 2 2; 1.3**	2	*aP*7	31	1 $\bar{1}$ 1	2 $\bar{2}$ 0	
(4 2 4; 1.3b) }	2 2 2; 1.3**	146	*hR*7	31	0 0 2	2 $\bar{2}$ 0	
(2 3 3; 1.5)	1 1 5; 1.5	12	*mC*10	17	1 $\bar{1}$ $\bar{1}$		
(4 2 2; 2a)* }	0 0 0; 2	69	*oF*12	4			
}	0 6 0; 2**						
(4 2 2; 2b)* }	0 6 0; 2**	151	*hP*9	58	0 0 2	1 $\bar{1}$ 1	
(2 2 2; 2)*	0 6 0; 2**	2	*aP*9	66	0 $\bar{2}$ 2	1 $\bar{3}$ 1	
2 0 6; 2	6 6 6; (1)**	164	*hP*3	5			
0 4 4; 2	4 4 4; (1)	139	*tI*6	6			
(3 1 2; 2.5)	1 1 1; 2.5**	2	*aP*7	31	2 $\bar{2}$ 0		
2 0 0; 3	0 0 6; 3**	166	*hR*4	9			
0 2 0; 4	0 0 0; 4	87	*tI*10	17			
2 0 0; 6	0 0 0; 6**	148	*hR*7	31			

* on the borders of the T_1 T_2 T_3 ; y/x polyhedron
** hexagonal planar

Table 21d: Same as Table 21a, except for pc.

T_i(M) ; y/x pc	T_i(M) ; y/x square	SG	PS	#	M_2 M_6	M_3 M_7	M_4 M_8	M_5
6 12 8 ; (1)	4 4 4 ; (1)	221	*cP*1	1				
5 8 4 ; 1	4 4 4 ; (1)	123	*tP*4	8	0 0 1			
(4 6 4 ; 1a)*	2 2 0 ; 1a	51	*oP*4	9	0 0 1			
(4 6 4 ; 1b)*	2 2 0 ; 1b	123	*tP*8	45	0 $\bar{1}$ 1	0 0 1	0 1 2	
(4 5 2 ; 1)*	2 1 2 ; 1	10	*mP*8	46	0 $\bar{1}$ 2	0 0 1	0 0 2	
4 4 0 ; 1	4 4 4 ; (1)	123	*tP*2	2				
(3 6 4 ; 1a)	6 6 6 ; (1)**	166	*hR*12	12	1 0 0			
(3 6 4 ; 1b)	2 2 0 ; 1a	63	*oC*16	54	1 $\bar{1}$ $\bar{1}$	1 0 0	1 0 1	
(3 6 4 ; 1c)	2 2 0 ; 1b	225	*cF*64	77	0 1 1	1 0 1	1 1 0	1 1 1
					1 2 2	2 1 2	2 2 1	
(3 6 4 ; 1d)	2 2 0 ; 1b	160	*hR*48	77	0 1 1	1 0 1	1 1 0	1 1 1
					1 2 2	2 1 2	2 2 3	
(3 6 4 ; 1e)	2 2 0 ; 1b	141	*tI*32	77	0 1 1	1 0 1	1 1 0	1 1 1
					1 2 2	2 2 3	2 3 2	
(3 5 4 ; 1a)	2 1 2 ; 1	2	*aP*8	58	1 1 0	1 2 $\bar{1}$	1 2 0	
(3 5 4 ; 1b)	2 1 2 ; 1	5	*mC*32	76	0 $\bar{1}$ 1	0 $\bar{1}$ 2	0 0 1	1 $\bar{1}$ 1
					1 $\bar{1}$ 2	1 0 1	1 1 1	
(3 5 4 ; 1c)	2 1 2 ; 1	2	*aP*16	76	0 $\bar{1}$ 2	0 0 2	0 1 2	1 $\bar{1}$ 1
					1 $\bar{1}$ 2	1 0 1	1 1 1	
(3 5 4 ; 1d)	2 1 2 ; 1	43	*oF*64	76	0 $\bar{1}$ 1	0 $\bar{1}$ 2	0 1 2	1 $\bar{1}$ 1
					1 $\bar{1}$ 2	1 0 1	1 1 1	
(3 5 4 ; 1e)	2 1 2 ; 1	15	*mC*32	76	0 $\bar{1}$ 2	0 0 1	0 0 2	1 $\bar{1}$ 1
					1 $\bar{1}$ 2	1 0 1	1 1 1	
(3 5 4 ; 1f)	2 1 2 ; 1	12	*mC*32	76	0 $\bar{2}$ 1	0 0 2	0 1 2	1 $\bar{1}$ 1
					1 $\bar{1}$ 2	1 0 1	1 1 1	
3 4 4 ; 1a	3 2 2 ; 1	65	*oC*8	11	0 0 1			
3 4 4 ; 1b	2 0 4 ; 1	141	*tI*16	61	0 0 1	0 1 0	1 0 1	
(2 6 4 ; 1a)*	2 2 0 ; 1a	63	*oC*8	15	0 1 $\bar{1}$			
(2 6 4 ; 1b)*	2 2 0 ; 1b	139	*tI*16	62	1 0 1	1 1 0	2 1 1	
(2 5 6 ; 1)	2 1 2 ; 1	12	*mC*16	57	0 1 $\bar{2}$	0 1 $\bar{1}$	1 0 $\bar{1}$	
2 4 8 ; 1	0 4 4 ; 1	123	*tP*2	3				
1 8 4 ; 1	0 4 4 ; 1	123	*tP*4	14	0 0 $\bar{1}$			
0 12 0 ; 1	0 4 4 ; 1	225	*cF*8	4				
(2 4 4 ; 1.3a)*	2 2 2 ; 1.3**	146	*hR*21	40	0 1 0	1 1 0		
(2 4 4 ; 1.3b)*	2 2 2 ; 1.3**	2	*aP*7	40	1 1 $\bar{1}$	1 1 0		
3 3 2 ; 1.5	1 1 1 ; 1.5	10	*mP*5	19	0 0 1			

Table 21d (continued)

T_i(M) ; y/x pc	T_i(M) ; y/x square	SG	PS	#	M_2 M_6	M_3 M_7	M_4 M_8	M_5
4 4 0 ; 2	2 0 2 ; 2	123	*tP*3	5				
2 2 4 ; 2a }	0 2 0 ; 2	51	*oP*3	6				
2 2 4 ; 2b }	0 6 0 ; 2**	151	*hP*9	74	0 1 0	1 1 0		
2 2 2 ; 2	0 6 0 ; 2**	2	*aP*9	75	1 1 $\bar{2}$	1 2 $\bar{2}$		
0 6 2 ; 2	6 6 6 ; (1)**	164	*hP*3	7				
(1 2 3 ; 2.5)*	1 1 1 ; 2.5**	2	*aP*7	40	0 1 0			
0 0 8 ; 3	0 0 4 ; 3	229	*cI*8	16				
2 0 0 ; 4	0 0 0 4 ; 4	83	*tP*5	19				
0 0 2 ; 6	0 0 0 6 ; 6**	148	*hR*21	40				

* on the borders of the T_1 T_2 T_3 ; y/x polyhedron
** hexagonal planar

Table 22: Group-subgroup relations of homogeneous sphere packings with s-CN values, space groups (SG) and Pearson symbols (PS) of the ccp, bcc and pc structures from Table 21b–d. Structures with underlined T_i; r values are stable sphere packings with contact numbers $k = T_1$ (or T_2, if $T_1 = 0$) (Koch and Fischer, 1992). All sphere packings with $k = T_1 \geq 4$ ($T_2 \geq 4$, if $T_1 = 0$) except 6 0 12; 1a, 9 3 12; 1 (ccp) are stable. Structures in double brackets have the same projection pattern, underlined T_i structures in square brackets are structures with a stable homogeneous packing of A or B atoms (only B atoms at y/x > 1).

SG	PS	T_i(M)$_{bcc}$	T_i(M)$_{fcc}$	T_i(M)$_{pc}$
229	*cI*2	8 6 12; (1)		
229	*cI*8			0 0 8; 3
227	*cF*32		6 0 12; 1b	
227	*cF*16	4 0 12; 1	((4 4 16; 1))	
225	*cF*64			3 6 4; 1c
225	*cF*8			0 12 0; 1
225	*cF*4		12 6 24; (1)	
221	*cP*4		0 6 0; 3	
221	*cP*2	0 6 12; 1	((4 6 8; 1))	
221	*cP*1			6 12 8; (1)
166	*hR*7		0 0 6; 6	
166	*hR*4	[2 0 0; 3]	9 3 12; 1	3 6 4; 1a
166	*hR*2		6 0 12; 1a	
164	*hP*3	[2 0 6; 2]	6 0 6; 2	0 6 2; 2
160	*hR*16			3 6 4; 1d
151	*hP*9	[4 2 2; 2b]	[2 2 12; 2b]	[2 2 4; 2b]
148	*hR*7	[2 0 0; 6]		[0 0 2; 6]
146	*hR*7	4 2 4; 1.33a	4 2 12; 1.33b	[2 4 4; 1.33a]
141	*tI*32			3 6 4; 1e
141	*tI*16	4 2 4; 1b		3 4 4; 1b
141	*tI*8		4 4 16; 1	
139	*tI*16			2 6 4; 1b
139	*tI*6	[0 4 4; 2]	4 4 0; 2	
131	*tP*8	4 4 4; 1b	6 2 12; 1b	
129	*tP*4	4 4 4; 1a	8 4 8; 1	
123	*tP*8			1 8 4; 1
				4 6 4; 1b
123	*tP*4		4 6 8; 1	5 8 4; 1
123	*tP*3			4 4 0; 2
123	*tP*2			4 4 0; 1

Table 22 (continued)

SG	PS	T_i(M)$_{bcc}$	T_i(M)$_{fcc}$	T_i(M)$_{pc}$
87	$tP2$			2 4 8 ; 1
87	$tI10$	[0 2 0 ; 4]	[0 2 8 ; 4a]	
83	$tP5$			[2 0 0 ; 4]
74	$oI16$	4 1 8 ; 1	4 5 12 ; 1a	
74	$oI8$	2 4 6 ; 1	((4 4 16 ; 1))	
71	$oI6$		[2 2 12 ; 2a]	
69	$oF12$	4 2 2 ; 2a		
67	$oC8$	6 4 6 ; 1	((8 4 8 ; 1))	
66	$oC16$	4 2 6 ; 1b		
65	$oC8$			3 4 4 ; 1a
65	$oC4$	4 2 4 ; 1a	((4 6 8 ; 1)) (in z) ((6 0 12 ; 1a)) (in x)	
63	$oC16$			3 6 4 ; 1b
63	$oC8$			2 6 4 ; 1a
59	$oP4$		6 2 12 ; 1a	
51	$oP6$			[2 2 4 ; 2a]
51	$oP4$			4 6 4 ; 1a
43	$oF64$			3 5 4 ; 1d
15	$mC32$			3 5 4 ; 1e
15	$mC16$		5 3 12 ; 1b	
			5 2 14 ; 1	
12	$mC32$			3 5 4 ; 1f
12	$mC16$			2 5 6 ; 1
12	$mC10$	[2 3 3 ; 1.5]	[3 3 12 ; 1.5]	
12	$mC8$		5 3 12 ; 1a	
11	$mP8$	4 3 4 ; 1	7 2 10 ; 1	
			6 1 12 ; 1	
			5 4 10 ; 1	
11	$mP4$	4 2 6 ; 1a		
10	$mP8$			4 5 2 ; 1
10	$mP5$			3 3 2 ; 1.5
3	$mP16$			3 5 4 ; 1b
2	$aP16$			3 5 4 ; 1c
2	$aP9$	[2 2 2 ; 2]		2 2 2 ; 2
2	$aP8$	3 3 5 ; 1		3 5 4 ; 1a
		4 2 5 ; 1		
		5 3 5 ; 1		
2	$aP7$	4 2 4 ; 1.33b	4 2 12 ; 1.33a	[2 4 4 ; 1.33b]
		[3 1 2 ; 2.5]	[2 1 9 ; 2.5]	[1 2 3 ; 2.5]
2	$aP6$		[2 2 12 ; 2c]	

Table 23a: Self-coordination numbers T_i^M ($i = 1 - I$) of M particles in the hcp lattice with identical values of all M (in the bulk), neutral clusters M_xN_y with closed shells and theoretical structures of isotopes with closed shells T_i. Structures with T_i in brackets are not at the border of the structure maps (Fig.9). Structures with T_i and an asterisk (*) are on the border of the $T_1\ T_2\ T_3$; y/x polyhedron. In the last column clusters without central atom are in brackets.

T_1	T_2	T_3	T_4	T_5	T_6	T_7	T_8	T_9	T_{10}	T_{11}	T_{12}	T_{13}	T_{14}	T_{15}	T_{16}	T_{17}	T_{18} ; r	Isotopes	x + y neutr. clust.
12	6	2	18	12	6	12	12	6	6	12	24	6	12	12	24	12	12 ; 0		
9	3	0	12	0	6	6	0	3	3	0	18	3	6	9	0	6	6 ; 1	^{51}Mn,^{81}Rb,^{87}Zr,^{93}Tc,^{105}Tc ^{183}Au	
(7	3	0	8	4	2	6	8	3	3	8	10	3	6	7	16	6	6 ; 1a,b)	^{13}O,^{21}Na,^{39}K,^{51}V,^{57}Mn, ^{69}Ga	(20,104)
(6	2	2	8	4	2	8	8	6	4	4	12	2	4	6	16	4	8 ; 1)*	^{13}N,^{19}F,^{21}Na,^{39}K,^{51}V, ^{57}Mn,^{69}As	(12,20,80)
6	0	2	6	12	6	0	12	0	0	12	12	0	0	6	24	0	0 ; 1	^{13}N,^{19}N,^{21}F,^{69}As	(12)
6	0	2	10	4	6	8	4	0	4	12	12	0	8	6	8	0	8 ; 1	^{13}N,^{19}N,^{21}F,^{39}K,^{51}V,^{87}Nb	(12,56,80)
(5	3	0	8	8	6	6	8	3	3	0	10	3	6	5	16	6	6 ; 1a,b)*	^{13}C,^{19}F,^{21}F,^{39}Cl,^{51}Mn	
(5	3	0	10	8	2	6	4	3	3	8	14	3	6	5	8	6	6 ; 1d,e)*	^{13}C,^{19}F,^{21}F,^{39}K	(56,68,104)
4	6	2	6	4	6	4	4	6	2	12	8	6	4	4	8	12	4 ; 1	^{13}B,^{39}K,^{51}V,^{69}As,^{81}Rb	(56,128)
4	4	2	12	4	2	4	8	0	2	4	16	4	8	4	16	8	4 ; 1	^{13}B,^{19}F,^{21}Na,^{69}As,^{87}Nb, ^{93}Tc,^{105}Ag	(20,56,80)
6	0	0	6	0	6	0	0	0	6	0	12	6	12	6	0	0	12 ; 2	^{13}N,^{19}N,^{21}N	21,39,57,183
2	2	2	10	0	0	4	12	2	2	0	4	2	4	8	0	4	4 ; 2	^{21}N,^{39}Cl,^{81}As,^{87}Br,^{93}Rb	21,51
2	2	0	10	6	0	4	0	2	2	6	4	2	4	8	12	4	4 ; 2a,b	^{51}Sc	105,159
0	6	2	0	0	6	0	0	6	0	12	0	6	0	0	0	12	0 ; 3	^{19}N,^{21}F	

Table 23b: Same as Table 23a, except for ccp.

T_1 T_2 T_3 T_4 T_5 T_6 T_7 T_8 T_9 T_{10} T_{11} ; r	Isotopes	x + y neutr. clust.
12 6 24 12 24 8 48 6 36 24 24 ; 0		
9 3 12 6 6 4 24 0 15 12 12 ; 1	^{79}Rb,^{87}Nb	
(8 4 8 4 16 0 16 6 24 16 8 ; 1)*	^{43}Sc,^{55}Mn,^{87}Nb,^{135}La, ^{141}Eu	
(7 2 10 6 10 4 28 2 21 16 10 ; 1)*	^{13}O,^{19}Ne,^{43}Ca,^{55}Fe, ^{79}Kr, ^{87}Zr	(18,134)
(6 2 12 4 12 8 24 6 18 8 12 ; 1a,b)	^{13}N,^{19}F,^{43}Sc,^{55}Mn, ^{79}Rb	(12,200,224)
(6 1 12 8 12 4 24 4 18 12 12 ; 1)	^{13}N,^{19}O,^{43}Ca	(12,54,78,86,134)
6 0 12 12 12 0 24 6 18 0 12 ; 1a,b	^{13}N,^{19}N,^{43}K	(12)
(5 4 10 6 14 4 28 2 15 8 10 ; 1)	^{13}C,^{19}Ne,^{43}Ca,^{55}Fe	(18,78,86,176)
(5 3 12 6 14 4 24 0 19 12 12 ; 1a,b)	^{13}C,^{19}F,^{43}Sc,^{55}Co	
5 2 14 6 14 4 20 2 15 16 14 ; 1	^{13}C,^{19}O,^{43}Ti	(42,54,224)
4 6 8 12 8 8 16 6 12 24 8 ; 1	^{13}B,^{43}K	(224)
4 5 12 8 8 4 24 4 20 12 12 ; 1	^{13}B,^{19}Ne,^{43}Ti,^{79}Sr	(18,42)
4 4 16 4 8 0 32 6 12 16 16 ; 1	^{13}B,^{19}F,^{79}Rb,^{87}Rb	
4 2 12 4 12 4 20 2 12 12 8 ; 1.33a,b	^{13}B,^{19}N,^{43}K,^{79}Br, ^{87}Y,^{135}Pr,^{141}Pm,^{177}Ta, ^{201}At	
3 3 12 3 9 2 24 3 9 9 6 ; 1.5	^{19}N,^{43}K,^{79}Ga,^{87}As, ^{135}La,^{141}Nd,^{201}Pt	55
6 0 6 6 0 2 24 0 18 12 0 ; 2	^{13}N,^{19}N	135,225
(4 4 0 4 16 0 16 4 12 8 16 ; 2)*	^{13}B,^{19}F	87,135
2 2 12 2 8 4 8 2 24 4 8 ; 2a,b		
2 2 12 2 8 2 14 2 12 10 8 ; 2c		201,225
2 1 9 2 9 3 13 1 6 9 4 ; 2.5		
0 6 0 12 0 8 0 6 0 24 0 ; 3	^{19}N	
0 2 8 0 4 0 16 2 0 4 0 ; 4		55
0 0 6 0 6 2 6 0 0 6 0 ; 6		

Table 23c: Same as Table 23a, except for bcc.

T_1	T_2	T_3	T_4	T_5	T_6	T_7	T_8	T_9	T_{10}	T_{11}	T_{12} ; r	Isotopes	x + y neutr. clust.
8	6	12	24	8	6	24	24	24	32	12	48; 0		
(6	4	6	10	4	2	10	8	12	16	4	20; 1)*	^{113}Sb	(64)
(5	3	5	9	4	2	13	12	14	18	6	26; 1)*	^{9}C,^{27}Si,^{51}V,^{59}Co, ^{65}Cu,^{113}Xe	
(4	4	4	12	0	6	12	16	8	16	12	24; 1a,b)*	^{9}B,^{27}Al,^{51}Mn,^{65}Ga	(8)
(4	3	4	12	4	4	12	12	16	16	4	24; 1)*	^{9}B,^{15}O,^{27}Mg,^{51}Cr, ^{59}Ni,^{65}Ge	(8,14)
(4	2	6	12	4	2	12	16	12	16	4	24; 1a,b)	^{9}B,^{15}N,^{27}Al,^{51}Mn, ^{59}Cu,^{65}Ga	(8,180,228)
(4	2	5	12	6	4	12	12	10	16	6	24; 1)	^{9}B,^{15}N,^{27}Mg,^{51}Cr	(8,58)
(4	2	4	12	8	6	12	8	8	16	12	24; 1a,b)*	^{9}B,^{15}N,^{27}Na,^{51}V	(8,112)
(4	1	8	12	4	4	12	12	8	16	4	24; 1)*	^{9}B,^{15}C,^{27}Si	(8,50,58)
4	0	12	12	0	6	12	0	24	16	12	24; 1	^{9}B,^{15}B,^{59}Cu,^{113}Ag	(8)
(3	3	5	15	4	2	11	12	14	14	6	22; 1)*	^{9}Be,^{15}N,^{27}Mg	(64)
(2	4	6	14	4	2	14	8	12	16	4	28; 1)*	^{9}Li,^{15}N,^{27}Al	(64,228)
0	6	12	0	8	6	0	24	24	0	12	0; 1	^{15}N,^{59}Co	(36,64,112)
(4	2	4	8	4	2	12	12	12	16	4	20; 1.33a,b)	^{9}B,^{15}N,^{27}Na,^{89}Rb, ^{113}In,^{137}Pm	
(2	3	3	12	2	3	12	9	12	8	3	18; 1.5)	^{9}Li,^{15}C,^{51}Sc,^{89}Sr, ^{113}Ag,^{137}Pr,^{169}Ho, ^{229}Ra	15,65
(4	2	2	4	4	2	8	4	12	20	2	8; 2a,b)*	^{9}B,^{15}N	27
(2	2	2	10	2	2	8	10	12	8	2	14; 2)*	^{9}Li,^{15}B	9,15,51
2	0	6	12	2	0	0	12	6	14	6	24; 2	^{9}Li,^{51}Sc	9,27
0	4	4	8	0	4	16	8	0	8	4	16; 2	^{15}B,^{89}Rb,^{113}Rh	27,51
(3	1	2	4	3	1	9	9	9	12	2	13; 2.5)	^{9}Be,^{15}B	
2	0	0	6	8	6	6	0	0	8	12	12; 3	^{9}Li	
0	2	0	8	0	2	8	4	8	0	0	8; 4		15,65
2	0	0	0	2	0	6	6	6	8	0	6; 6	^{9}Li	

Table 23d: Same as Table 23a, except for pc.

T_1	T_2	T_3	T_4	T_5	T_6	T_7	T_8	T_9	T_{10}	T_{11}	T_{12} ; r	Isotopes	x + y neutr. clust.
6	12	8	6	24	24	12	30	24	24	8	24; 0		
5	8	4	4	12	8	4	9	16	12	0	12; 1	^{123}Cs	
(4	6	4	2	8	12	4	20	12	12	8	8; 1a,b)*	^{33}Cl,^{57}Mn,^{81}Rb,^{93}Nb	(32)
(4	5	2	4	12	10	6	16	14	14	4	12; 1)*	^{19}Ne,^{27}Mg,^{33}S,^{57}Ni, ^{81}Sr,^{93}Ru	(18,146)
4	4	0	6	16	8	12	20	8	0	8	16; 1	^{19}F,^{33}P	
(3	6	4	0	12	12	12	15	12	12	0	12; 1a–e)	^{7}Be,^{19}Ne,^{27}Si,^{33}Si,^{57}Fe, ^{81}Sr	(6,18,26)
(3	5	4	2	12	14	6	15	14	12	4	12; 1a–f)	^{7}Be,^{19}F,^{27}Al,^{33}P,^{57}Co	(6,80,92,122)
3	4	4	4	12	16	4	15	8	12	0	12; 1a,b	^{7}Be,^{19}O,^{27}Mg,^{33}S,^{57}Ni	(6)
(2	6	4	2	16	12	4	10	12	12	8	16; 1a,b)*	^{7}Li,^{19}F,^{27}Al,^{33}P	(92)
(2	5	6	4	12	10	6	14	14	10	4	12; 1)	^{7}Li,^{19}O,^{27}Si,^{33}Ar,^{81}Zr	(26,146)
2	4	8	6	8	8	12	10	8	24	8	8; 1	^{7}Li,^{19}N,^{81}Rb	(56)
1	8	4	4	12	8	4	21	16	12	0	12; 1	^{7}He,^{19}Ne,^{27}Si,^{33}Ar, ^{81}Sr,^{93}Mo	(18,26)
0	12	0	6	0	24	12	0	24	0	8	0; 1	^{27}Al,^{123}Cs,^{203}Fr	
(2	4	4	2	12	12	4	10	12	8	4	12; 1.33a,b)*	^{7}Li,^{19}N,^{27}Na,^{33}Al, ^{57}Mn,^{81}Rb,^{93}Nb,^{123}Sb, ^{147}Eu,^{171}Lu,^{179}Re,^{203}Fr	7,147
3	3	2	3	9	12	3	15	9	12	2	6; 1.5	^{7}Be,^{19}N,^{81}As,^{93}Kr,^{123}Sb, ^{147}Nd,^{171}Hf,^{179}W,^{203}Hg	
4	4	0	4	8	0	4	6	16	8	0	16; 2	^{19}F,^{33}Al	27
2	2	4	2	4	12	2	18	8	4	4	8; 2a,b	^{7}Li,^{33}Na	171
2	2	2	2	10	12	2	6	8	10	2	8; 2	^{7}Li	57,171
0	6	2	0	12	6	6	12	0	12	2	0; 2	^{19}N	27,81,171
(1	2	3	1	9	9	2	5	9	4	3	9; 2.5)		7,147,203
0	0	8	6	0	0	12	0	0	24	8	0; 3	^{33}P	
2	0	0	2	4	8	0	10	4	8	0	0; 4	^{7}Li	
0	0	2	0	6	6	0	0	6	0	2	6; 6		7,147

Table 24: Characterization of nucleic acids by the number of adenine (**A**), thymine or uracyl (**T**), cytosine (**C**) and guanine (**G**) units (first number), the clusters per mill (second number) and the location on the structure map (Fig.16).

nucleic acid		A			T			C			G		
secA 7	*S.carnosus*	1308	154	IIIa	990	75	IIIa	564	7	Ia	727	21	Ia
secA 10	*O.lutens* chloroplast	1212	207	IIIa,IVb	980	169	IIIa	359	25	IIIa,IVb	508	24	IIIa
enolase 3	*S.cerevisiae*	523	98	IIIa	634	120	IIIa	443	29	Ia,IIIb	413	24	Ia
enolase 59	*A.glutinosa* mRNA	473	99	IIIa	438	71	IVb	329	33	Ia	415	39	Ia,IIIb
enolase 249	*Schisosoma mansoni* mRNA	12731	125	IVb	12776	127	IVb	8117	35	IIIb	8040	37	IIIb
enolase 2	*N.fontalis*	691	188	IVb	613	90	IIIb	303	36	IVb	361	19	IIIb
enolase 100	*Streptococcus thermophilus*	2323	195	IVb	1933	153	IVb	1021	36	IIIa	1222	46	IIIa,IVb
enolase 1	*M.musculus* mRNA	363	72	IIIa	285	28	IIa	378	56	IIIb	407	91	IIIa
enolase 8	*H.sapiens* mRNA	340	50	IIIa	271	22	Ib	367	68	IIIa	420	114	IIIa
enolase 15	*Rattus norvegicus* mRNA	396	61	IIIa	378	40	IIa	490	84	IIIb	461	61	IIIb
enolase 13	Peking duck tan.cryst.	439	71	IIIa,IVb	415	58	Ib,IIa	417	96	IIIa	444	43	Ia
enolase 25	*Xenopus laevis* mRNA	461	93	IVb	448	54	Ib,IIa	370	62	IIIb	441	50	Ia,IIIb
secA 21	*Synechococcus* sp.	905	70	IIIa	777	51	IIIb	989	39	Ia	1121	40	Ib
secA 6	*P.sativum* mRNA	1120	124	IIIa,IVb	996	94	IVb	688	28	Ia,IIIb	804	50	IIb,IVa
secA 11	*S.oleracea* chloroplast	1084	101	IIIa,IVb	1043	82	IVb	689	45	IVa,b	923	53	Ib,IIa
secA 15	*Mycobacterium bovis*	782	35	IIIb	667	21	Ia,IIIb	1286	38	Ia,b	1310	45	Ib
secA 8	*Escherichia coli*	1061	121	IIIa	853	74	IIIa	938	29	Ib	1004	27	Ia,b
secA 4	*Streptomyces lividans*	709	4	Ia	509	10	Ib	1351	53	Ia	1437	76	Ib

Table 25a: Lattices with highest density (lowest r values) from different positions *a* – *f* of the cubic space groups (SG) 195 – 230 without variable *x*, *y*, *z* parameters and a selection of structure types R_nM_x or $R_nM_xN_y$ with T_i(M) of M atoms or T_i(N) of N atoms. The majority positions are occupied for $\underline{T_i}$; r values.

SG	*a*	*b*	*c*	*d*	*e*	*f*	further SG
195	pc	pc	fcc 1	fcc 1			200,207,215,219,221,226
196	fcc	fcc	fcc	fcc			216
197	bcc	pc 1					
201	bcc	fcc	fcc	pc 1			
202	fcc	fcc	pc	fcc 1			209,225
203	bcc 1	bcc 1	fcc 2	fcc 2			210,227
204	bcc	pc 1	pc				
205	fcc	fcc					
206	pc	pc					
208	bcc	fcc	fcc	pc 1	fcc 5	fcc 5	
211	bcc	pc 1	pc	fcc 3			222,229
212	fcc 6	fcc 6					213
214	fcc 4	fcc 4	fcc 8	fcc 8			
217	bcc	pc 1	–	fcc 3			
218	bcc	pc 1	fcc 5	fcc 5			
220	fcc 9	fcc 9					
223	bcc	pc 1	fcc 5	fcc 5	pc		
224	bcc	fcc	fcc	pc 1	–	fcc 3	
228	bcc	fcc	fcc	bcc			
230	bcc	pc 2	fcc 7a	fcc 7b			

pc (6 12 8; (1)): Po α, $\underline{ClCs}$, Cu_3Au, O_3Re, Fe_4C, O_3CaTi, B_6Ca, Cu_3S_4V, $NaPt_3O_4$, $Pr_3Sn_{13}Rh_4$, $PtHg_4$, Pt_3O_4, As_3Co, $P_{12}LaFe_4$, $Re_7Si_6U_4$, CaF_2, D_6RuSr_2, S_4Cu_3Sb, $Zn_{13}Na$, $B_{198}Th_3O$, $Cu_{6.5}Al_{6.5}Ca$, $B_{66}ThO_{0.33}$, $PdGa_{12}Y_4$, $(Si,Re)_{13}U_4$, $Ce_3Ni_6Si_2$, $Tb_3Ni_6H_{0.5}Al_2$, NiD_4Mg_2, $(FeCu_5)S_4$, $Ni_{2.67}Sn_{5.44}Gd$, $Pt_{12}Sn_{25}Ce_4$, $LaSn_3Ru$, $Yb_3Sn_{13}Rh_4$, $Y_3Ge_{13}Co_4$, $AlMnCu_2$, $MnGa_6Gd_2$, Ni_3Ga_4, Ga_4Ni_3

pc 1 ($\underline{0\ 0\ 8}$; 3): Ag_2O_3, Bi_2O_3, La_2O_3, O_4Pt_3, S_4VTl_3, $Ge_4Pt_4Na_3$, P_2Mg_3, $B_{14}Fe_{62}Y_3$

pc 2 (0 3 2; 3)

pc 3 (2.7 2.7 0; 2.55) (229*b*+*d*): SAg_2

pc 4a (0 3.43 0; 3.57) (229*a*+*d*): $U_4Si_6Re_7$

pc 4b (0 0 0 1.5; 7) (218*a*+*d*): $(Al,Ge)_{23}Na_4$, As_4Ba_4Si, Li_7N_4Mn, H_3U, $RuSn_3La$, $Al_8Ga_{15}Ba_4$, $Ge_{11}K$, $Si_{23}K_4$

Table 25a (continued)

fcc (12 6 24;(1)): OAg_2, O_3Ag_2, O_3Bi_2 δ, S_2Fe, $S_9Pb_4Sb_2Sn$, Cu, SZn, ClNa, LiSiAl, AsMgAg, F_2Ca, Hg_2TiCu, F_3Bi, Be_5Au, Cu_3Te_2, Ca_7Ge, C_2La, D_6Sr_2Ru, D_3Ce, Cu_9Se_5, S_8Mo_4Ga, $B_{12}U$, S_4Zr_3, S_6Cu_9Bi, $Sb_4Co_5Mn_4$, S_4Cu_7, Se_6Ag_9Ga, Te_6Ag_8Ge, Mg_2D_4Ni, $CuFe_5S_4$ HT, $Cl_{14}Mo_6Hg$, Rb_7Ge_8Na, $S_9(Pb_{0.67}Sb_{0.33})_6Sn$, Li_2AgSb, LiMgPdSn, Cu_4SnMg, S_8Mo_4Ga HT, S_6Ag_7Ta, OCu_2, Cu_2MnAl, S_6Cu_9Bi, $Sc_{11}Ir_4$, S_4Zr_3, CoSbMn, NF_4, Mo_3N_2, C_3Nb_4, N_2Mo_3, S_3U_4, $Pt_7Cu \mathrel{\widehat{=}} Ca_7Ge$, Cl_6K_2Pt, O_8Mg_6Mn, $Fe_7C_{0.45}Cr$, $S_8(Fe,Ni)_8Ag$

fcc 1 (0 6 0;3): $AuCu_3$, ReO_3, $CaTiO_3 \mathrel{\widehat{=}} AlCMn_3$, ONb, U_4S_3, Nb_4C_3, S_4VCu_3, $Hg_{11}Ba$, S_4SbCu_3, $Bi_4Cu_4Mn_3$, Rb_6O, Ag_4Al_7Ca, $S_{26}ClK_6Fe_{23}Li$, $Ca_4Mg_4H_{22}Fe_3$, NCu_3, Ga_3TmRu

fcc 2 (6 0 12;1b): $MgCu_2$, Ti_2C, O_4MgAl_2, $C_4N_4ZnK_2$, Fe_3W_3C, $D_7Zr_2Cr_4$, Ge_2S_5Ba, $D_9Zr_2V_4$, HCa_2N, $Al_{10}V$, $Al_{18}Mg_3Cr_2$, W_4Co_2C, $Ni_7Zn_6Ge_2$, $H_{3.7}ZrV_2$ HT, $CeAl_{20}Cr_2$, $Al_{11}V$, $Ca_2(Ca,Ge) \mathrel{\widehat{=}} Ti_2C$, O_2LiTi, $S_4CuLi_2Ti_2$, H_7ThZr_2, Mn_3Ni_2Si

fcc 2b (0 0 0 12;7) (225*b*+*d*): $GeCa_7 \mathrel{\widehat{=}} CuPt_7$, $Zr_6Cu_{16}H_9Al_7$, $Mg_6Cu_{16}Si_7$

fcc 3 (4 2 8;1.67): V_2D α, $As_7S_{12}Hg_4$, $P_{17}La_6Ni_6$, $S_{12}(Cs,Tl)_2As_4Hg_5$, $P_{17}La_6Ni_6$

fcc 4 (3 0 6;3): Te_2AuAg_3 *LT*

fcc 5 (0 2 8;4.33): $SiCr_3$, $HSnNb_2$, O_4NaPt_3, $Rh_4Sn_{13}Pr_3$, $HSnNb_3$, $Ge_{20}Ni_3Ba_4$, $Co_4Ge_{13}Y_3$

fcc 6 (0 0 6;7): Si_2Sr, Al_2Mo_3C, $Te_{10}Al_6Ca$, $O_{23}P_8Na_3Fe$

fcc 7a (0 0 4;9.67a): Bi_4Rh α, $O_{12}Al_2Si_3Ca_3$

fcc 7b (0 0 4;9.67b): $O_{12}Al_2Ca_3Si_3$

fcc 8 (0 0 4;20.33)

fcc 9 (T_7=8;20.33): P_4Th_3, Ga II HP, $Sb_4Au_3Y_3$, $Li_{12}Si_4Mg_3$, $S_8Ba_3Sn_2Cd$

bcc (8 6 12;(1)): Ag_2O, Cr_3Si, HNb_2Sn, O_4Pt_3Na, W, O_3La_2, Hg_4Pt, DV_2 α, S_4Tl_3V, Ag_2S, $Al_{12}W$, $P_{12}Fe_4La$, $Y_4Ga_{12}Pd$, Ni_3Ga_3Zn, $O_{12}Ca_3Si_3Al_2$, $Gd_4Ni_{12}Sn_{24}(Gd,Sn)$, F_4Si, $Hg_5As_4S_{12}$, Nb_3HSn, O_4Pt_3Na

bcc 1 (4 0 12;1): C, $CuTiHg_2$, NaTl, Cu_2Mg, O_4Al_2Mg, S_4Yb_2Fe, $C_4K_2N_4Zn$, Mo_6Ni_6C, $Cr_4D_7Zr_2$, $D_9V_4Zr_2$, $Al_{20}Cr_2Ce$, $Zn_{22}Zr$, O_2Si (cristoballite), Na_8Sb_4Sn, W_6Fe_6C, N_2CsTa, W_3Fe_3C, $V_2H_{3.7}Zr$ HT, $S_4Li_2Ti_2Cu$, H_7Zr_2Th, $Mo_2S_4Al_{0.55}$, $AgSbLi_2$, S_8Mo_4Al

bcc 2 (0 0 12;3) (225*b*+*c*): BiF_3, $AlFe_3$, $P_{11}Cs_3$ HT, $Co_{20}B_6Al_3$, $GePd_2Mn$, $C_{60}K_3$

bcc 3a (2 0 3;3) (227*a*+*b*+*d*): Ti_2NiH

bcc 3b (0 0 4;4.33) (227*a*+*d*): S_4Co_3, $Li_{13}In_3$, $Si_{17}Na_{1.25}$, $Si_{94}Na$, Pd_7Te_2

bcc 3c (2.7 0 4;4.33) (227*a*+*c*): $S_4(Cr,Sn)_2Cu_3$, $Nb_8Zn_4C_3$, $Cr_2Al_{18}Mg_3$

Table 25b: Same as Table 25a, except for trigonal and hexag. space groups 143 – 194

SG	*a*	*b*	*c*	*d*	*e*	*f*	*g*	further SG
147	ph	ph	–	–	ph 2a	ph 2a		164
148	ph 1f	ph 1f	–	ph 3c	ph 3c			166
149	ph	ph	ph	ph	ph	ph		174,187,188
150	ph	ph						
155	ph 1f	ph 1f						
162	ph	ph	ph 1b	ph 1b	–	ph 2a	ph 2a	175,177,191,192
163	ph	ph	ph 1e	ph 1e	–	–	ph 2a	176,194
165	ph	ph	–	–	ph 2a			
167	ph 1f	ph 1f	–	ph 3c				
180	ph	ph	ph 2d	ph 2d				181
182	ph	ph	ph 1e	ph 1e				190
189	ph	ph	ph 1b	ph 1b				
193	ph	ph	ph 1b	ph 1b	–	ph 2a		

ph (2 6 12 2 6 24 6;(1)) (147*a*): LiRh, CW, Cd_2Ce, I_2Cd, Zn_2Cu, BaLiSi, B_2Al, Fe_2N, S_2CuSc, O_3U, Li_3N, AsNi, Se_2CuEr, Be_2H_2Zr, $Zn_{1.7}Pt$, S_2Cu_3Cs, Cu_5Ca, SFe, In_2Ca, S_2Nb, S_4Ga_2Fe, C_6Li, Cu_7Tb, P_2NiMo, B_3Re, S_2TaSn, $AlCr_2C$, O_6As_2Ca, Zr_6Al_2Co, D_3Zr_4N, $Mn_{12}Pt_4N$, BaS_3V, Se_6AlNb_3, $S_6Zn_3In_2$, Ru_3Si_2La, Al_9Co_2Sr, BCo_4Ce, B_2Pt_3Ba, Fe_6Ge_6, Mg, Co_5Y, C_6Eu, Nb_6Se_8Tl, $S_{12}Ti_9K$, $Cu_{13}Yb_2$, Se_8Nb_4Cr, S_8Nb_4Mn, $Zn_{11}Sm$, Fe_8Ho, $Ni_{19}Th_2$, $Co_{17}Ho_2$, $O_{27}Fe_{18}Ba$, Se_2Ta, C_8Cs, $Al_3Fe_{14}Tb_2$, B_2Ru_3U, $Si_3Ce_5Ni_2$, D_7Ni_5La

ph 1a (0 0 6 2 6 0 0;2) (194*b*+*d*): C, BaCu, $Ni_{17}Th_2$, Ti_3O, $Se_{24}Zr_{12}Fe_5$, B_4W, H_9K_2Re, $Zn_{17}U_2$

ph 1b (2 0 0 2 6 12 0;2) (162*c*): AlB_2, ZrH_2Be_2, $NdRh_3B_2$, $NaPd_3Sn_2$, O_6CaAs_2, $S_6Na_{35}Sn_2$, Zr_6CoAl_2, Al_9SrCo_2, $CeCo_4B$, S_3PLi

ph 1c (0 0 0 2 6 0 0;5) (191*a*+*c*+*d*): $Zn_{10}U$, $W_{12}C_5$

ph 1d (0 2 8 2 6 4 2;1) (191*b*+*c*): NLi_3, NTa, CoSn, V_2N, Fe_2P, $Ga_5Ni_5Ho_2$, Fe_6Ge_6Li, La

ph 1e (0 0 6 2 6 0 0;2) (194*c*) (hcp): Mg, $CuZn_2$, NFe_2, ZnS, NiAs, Ni_2Si, Ni_7Ge_4, B_3Re, S_2Mo, Ni_2In, S_2InTl, $Se_6Nb_3K_2$, Ni_3Sn, S_2SnTa, CCr_2Al, Na_3As, $Mn_{12}NPt_4$, S_3VBa, Se_4CuNb_2, C_6Ba, Fe_3Te_3Tl, Cu_2S, B_4Ir_3Zr, $Fe_4Si_9Y_2$, S_6Nb_3Co, $S_{12}Ti_9K$

ph 1f (0 0 6 0 6 6 0;2) (166*a*/195*a*, 196*a*, 197*a*) (pc, fcc, bcc): Hg, Po, OBi, HgIn, PtCu, S_2Mo, N_2W, S_4NaTi_2, N_3Na, S_2NaV, $S_2NaCr \cong O_2NaFe \cong Cu_2SrGa$, S_2CuCr, Se_2AgCr, Ni_3C, S_8Mo_8Pb, $S_{16}Mo_{12}FeSn_2$, Rh_3Si_7Sc, $S_2Ni_3Pb_2$, $B_6Ni_{12}Sr$, Mg_2Ni_3Si, K_5Sb_2Cu, $Se_3Ga_2Na_2$, Te_4Sb_2Ge, Au_5Sn, S_2Ta_2C, Bi_2Te_2S, Cl_2Cd, F_2HNa, $CuSe_{1-x}$, SSc_{1-x}, Bi_2Te_2S, S_2Ta_2CFe, P_2K_4Cd, P_2Cu_4Ca, Se_4Al_2Mg, Fe_6Ge_4Zr, S_3KPt_2, Mn_3Bi, $B_6Ni_{12}Sr$

Table 25b (continued)

ph 1g (0 0 6 1 6 3 0;2) (194*a*+*c*): TiAs, Ni_3Ti, $SiNi_2$, $InNi_2$, Be_3N_2, Se_4Nb_2Cr
ph 1h (0 0 4 0 6 4 0;3) (225*b*+*c*) (bcc 2):
ph 1i (0 0 3 0 6 0 0;5) (203*a*) (bcc 1):

ph 2a (2 0 0 2 0 0 6;3) (164*e*): S_2CsCu_3, SnCo, $NaSn_2Pd_3$, $S_8P_2Pd_3$, $Si_{16}U_{20}C_3$
ph 2b (0 3 6 2 3 12 6;1) (164*a*+*f*): Se_6Ti_3Fe, Ge_6Ni_6Sc
ph 2c (1 2 6 1 2 12 6;1) (180*b*+*d*): Mg_2Ni
ph 2d (0 0 4 0 0 8 6;3) (180*c*): O_2Si (high quartz), Si_2Cr, Si_2Nb

ph 3a (0 0 4.8 2 2.4 0 1.2;1.4) (191*c*+*g*): $CaCu_5$, $DLaNi_5$
ph 3b (0 0 5.1 0 5.1 5.1 0;2.43) (225*b*+*d*) (fcc 2b):
ph 3c (0 0 4 0 4 4 0;3) (166*e*/197*b*, 195*c*) (pc 1, fcc 1): $S_2Pb_2Ni_3$, $P_2K_3Cu_3$, Se_8Rh_3, $SiMg_2Ni_3$, B_2ThC
ph 3d (0 0 2.4 0 4.8 4.8 0;3.8) (166*a*+*b*+*d*): Ti_8C_5
ph 3e (0 0 3 0 3 3 0;5) (203*c*, 166*b*+*e*) (fcc 2): $TbFe_2$
ph 3f (0 0 3 1.5 3 0 0;5) (194*c*+*g*): SiO_2, $W_{20}Co_6C_7$
ph 3g (0 0 1.5 0 0 1.5 0;11) (227*a*+*b*+*d*) (bcc 3a):
ph 3h (0 0 0 0 2 0 0;15) (227*a*+*d*) (bcc 3b): $S_2Ni_3Pb_2$
ph 3i (0 0 2 0 2 0 0;15) (227*a*+*c*) (bcc 3c):

ph 4a (0 0 2 0 2 2 0;7) (211*d*) (fcc 3):
ph 4b (0 0 2.7 0 1.3 1.3 0;9.67) (229*b*+*d*) (pc 3):
ph 4c (0 0 1.5 0 1.5 1.5 0;11) (214*a*) (fcc 4):
ph 4d (0 0 0 0 1.5 1.5 0;11) (230*b*) (pc 2):
ph 4e (0 0 0 0 1.7 1.7 0;12.71) (229*a*+*d*) (pc 4a):
ph 4f (0 0 0 0 0 2 0;15) (218*c*) (fcc 5):
ph 4g (0 0 0 0 0 2 0;23) (212*a*) (fcc 6):
ph 4h (T_{11}=1.5;23) (218*a*+*d*) (pc 4b):

ph 5a (0 0 0 0 0 1 0;31a) (230*c*) (fcc 7a):
ph 5b (0 0 0 0 0 1 0;31b) (230*d*) (fcc 7b):
ph 5c (0 0 0 0 0 1 0;63) (214*c*) (fcc 8):
ph 5d (T_{14}=2;63) (220*a*) (fcc 9):

Table 25c: Same as Table 25a, except for tetragonal space groups 75 – 142

SG	*a*	*b*	*c*	*d*	*e*	*f*	further SG
81	pc′	pc′	pc′	pc′			115,116,120,127,135
82	bcc′	bcc′	bcc′	bcc′			86,118,119
83	pc′	pc′	pc′	pc′	pc′	pc′	89,111,123,124,125,132
84	pc′	pc′	bcc′	bcc′	pc′	pc′	93,131
85	pc′	pc′	–	pc′	pc′		129
87	bcc′	bcc′	pc′	pc′	–	pc′	126,139
88	bcc 1	bcc 1	fcc 2	fcc 2			141
90	pc′	pc′					113
94	bcc′	bcc′					114
97	bcc′	bcc′	pc′	pc′			117,121,128,136
98	bcc 1	bcc 1					122
112	pc′	bcc′	pc′	bcc′	pc′	bcc′	
130	pc′	pc′	–	pc′			
133	pc′	pc′	pc′	pc′	pc′		140
134	bcc′	bcc′	pc′	pc′	bcc′	bcc′	
137	bcc′	bcc′	–	–	pc′		
138	pc′	pc′	bcc′	bcc′			
142	bcc′	bcc′	bcc′				

pc′ (4 2 4 8 4 20; (1)): S_6P_2Zr, Te_3Ga, S_4BaFe_2 β, $Se_4\underline{In_2Cd}$ α, Se_8In_5Ag LT, Cl_4AlCu, Se_2FeCu, $ClO_2(NH_4)$, S_3Ba, Cr_3GeN, $O_7Si_2Ca_2Mg$, $S_8\underline{Cu_6SnFe_2}$, $B_{25}AlCu_{0.79}$, Sn_2Au_4K, I_4HgCu_2 β, $S_4SnFeCu_2$, $\underline{TiCu}$ δ, $\underline{CuAu}$, $\underline{Hg_2Pt}$, Si_2Fe α, $\underline{NFeNi}$, Pb_3Sr, Ti_3Cu, $Pt_2\underline{ZnCd}$, $\underline{Si_2Mg_2Ce}$, $\underline{Mn_2Co_2C}$, $Cl_4\underline{K_2Pt}$, $Ga_5\underline{CoHo}$, $Pd_5\underline{AsTl}$, $Ga_6\underline{CuCe}$, S_3Cu_4K, $H_5Sr_2\underline{LiPd}$, $Ga_8\underline{Ho_2Co}$, Ga_6LaNi, Te_4Nb HT, $Nb_4\underline{SiCo}$, Pb_4Pt, $Se_4\underline{KCe}$, Ga_6Pu, $Te_4\underline{Al_2Ba}$, $S_4\underline{SrFe_2}$, B_2Mo_2Fe, F_5Rb_3Pd, $Mg_2Ir_5B_2Si$, Ni_9In_2Y, Mn_6Ni_5Ce, I_6TeRb_2 LT, PbO, PbClF, AlGeMn, $P\underline{LiMn}$, C_2ScCo, Si_2HfCu, $AsZr\underline{SiCu}$, PtS, $C\underline{YCo}$, C_2B_2Y, Te_2Cu_3Tl, $VSnRh_2$, Se_2TlCu_2, TeUGe, H_4PtNa_2 LT, Al_4YbMo_2, Bi_2SrZn, H_5IrSr_2 LT, S_2Sr, Al_2Cu θ, Ir_3Si, U_3Si, SeTl, $Te\underline{InNa}$, Cu_2CeIn_2, D_5CoMg_2, $N_2CoLiSr_2$, D_4PtK_2, D_3K_3Pd, ThH_2, Ga_2CeAl_2, $Te_4\underline{Al_2Sr}$, N_3K, Se_2InGa, NCr_3As, Ga_5Pd, U_6Mn, H_4Th_2Al, Nb_5Sn_2Si, La_2NiGe, Mo_5B_2Si, Te_3Tl_4Pb, Te_5Tl_2Sn, $C_{15}Cs_3Co$, Ge_4Co_9Pr, $Si_4(Ni,Si)Ni_8Ce$, Nb_9Co_4Ge, H_3Zr_2Ni, $Pr_6Fe_{13}Ge$, $La_6Co_9(Co,Ga)_4Ga$, Tb_6Al_3Si, $H_{4.8}Zr_2Ni$ HT, S_4PPr

pc 1 (0 0 8; 3) (126*a*+*c*): Se_4Al_2Ba

fcc 1 (0 6 0; 3 $\widehat{=}$ bcc 0 2 4; 3) (123*c*+*e*): $SrPb_3$, $CuTi_3$, Mn_3Au

fcc 2 (6 0 12; 1b $\widehat{=}$ bcc 4 2 4; 1) (88*c*): H_4HfV_2 LT, S_4UPd_2, N_3Cu, $H_{3.6}ZrV_2$ LT, O_4CdMn_2, $Mn_{11}LaC_2$

Table 25c (continued)

bcc′ (8 4 2 4 8; (1)): S_4InP, $S_4(NH_4)(Mo,Cu)$, S_4Ga_2Cd, S_4Cu_2ZnSn, $S_4Cu_7(NH_4)$, C_4W_4U, $S_4(Pt,Ni)_3Pd$, B_4Co_4Nd, Ni_4Mo, S_4Fe_2Ba β, H_4Li_4Rh, C_4Cr_4U, Br_6Rb_2Te LT, Br_6TeRb_2 LT, P_4Cu_8Ba, Cu_2S, GeP HP, $B_{25}N$, Cl_4CuAl, Pd_4Se, S_4Na_4Sn, $H_{1.33}Pd$, $(Ga,Ag)Te$, Te_2AgTl, I_4Cu_2Hg β, S_4Cu_2SnFe, S_4Cu_3Sb, Sn_6Ru_4Y, I_6Rb_2Te LT, $B_{13}Er_4Ni$, $S_{11}(H_2O)_2(NH_4)_2Pd$, Al_4Ba, Ga_2Al_2Ce, Se_2Cu_2Tl, F_4K_2Ni, H_4Na_2Pt LT, Al_4Mo_2Yb, $(Mn,Cu)_6Ce$, Ni_2Al_5Zr, Pt_8Ti, H_5Sr_2Ir LT, Fe_8N, SPt, C_2Th HT, YCoC, $B_{24}TiC$, $B_{25}Ti$, O_2Ti (rutile), Li_3N_2B α, N_2Sr_2LiCo, Si_2Fe_4Zr, D_4K_2Pt LT, V_8N, I_2Hg β, B_4Co_4Ce, N_4Li_6Mo, In, Pa LT, Mn γ, $C_{0.05}Fe$, OCo, H_2Th, C_2Ca, Si_2Mo, Zr_2Cu, Rh_2SnV, Al_3Ti, Al_2UCu, O_2Na_2Hg, S_4Cu_6Tl, $Ga_{10}Ce_2Ni$, Al_8Mn_4Ca, $Fe_{10}Mo_2Nd$, $Mn_{12}Th$, $P_4Eu_2Pt_7Al$, $S_4(Cu,Fe,Ag)_{6.35}(Tl,K)_2Sb$, $Fe_{11}TiN_{0.5}Y$, $Ga_{17}Ce_4Ni_2$, $S_{16}Ni_{18}Bi_3As$, B_4Ru_4Lu, $Sb_{11}Ca_{14}Al$

bcc 1 (4 0 12; 1): Cl_4Th β, O_4SiZr, Ca_4In_2N, Li_4N_2Sr, O_4Mn_2Cd, $Cd_{11}Ba$, $Si_{2.4}Ni_{8.6}Ce$, Cl_2Zn α, N_2CaGe, S_2CuFe, $Se_4(Sn,Ga)Ag$, Sn β, UPb, Si_2Sr, Si_2Th α, Mo_2N β, O_2Ti, anatase Ti_2N, $C_{0.5}SiFe_{10}Nd$, $Mn_{11}C_2La$

bcc 2 (0 0 12; 3 $\widehat{=}$ fcc 0 4 8; 3) (139*b*+*d*): N_2BLi_3 α, $TiAl_3$, NbN γ

bcc 3b (0 0 4; 4.33 $\widehat{=}$ fcc 0 1.33 8; 4.33) (88*b*+*c*): $SrPb_3$, $CuTi_3$, Mn_3Au

Forschungszentrum Jülich

Jül-3732
January 2000
ISSN 0944-2952